University of Strathclyde

Department of Mechanical & Aerospace Engineering

MICRO-TRIGENERATION FOR ENERGY-EFFICIENT RESIDENTIAL BUILDINGS IN SOUTHERN EUROPE

Simon Paul Borg B. Eng (Hons.), M.Sc.

A thesis presented in fulfilment of the requirements

for the degree of Doctor of Philosophy

2012

COPYRIGHT DECLARATION

Signed: _____ Date: _____

ACKNOWLEDGEMENTS

It has been a long but rewarding three years, which has not only enriched me as a scholar but also a person.

During the course of these three years, a number of people have been influential in completing this research task which has eventually led to this doctoral publication.

Primarily, I would like to thank my supervisor, Dr. Nick Kelly. His dedication, guidance and encouragement for me to find an answer to the various research questions encountered during the process of completing this thesis have been a determining factor in its successful completion. Thanks go to Prof. Joe Clarke for the fruitful discussions we had during specific aspects of completing this thesis. Acknowledgments are also due to the academics, researchers and student colleagues at ESRU. It has been a privilege working within such an esteemed energy systems research group and the help I found from the various members of this group during the completion of this research, has been instrumental.

Special thanks also go to members of the IEA Solar Heating and Cooling Programme Task 38 for providing the necessary data to calibrate the absorption chiller model and for the help and guidance provided by members of IEA Energy Conservation in Buildings and Community Systems Annex 54 and the Supergen Highly Distributed Power Consortium.

Finally, but definitely not least, I would like to thank my wife Denise for being constantly there to support me during the whole process leading to the completion of this thesis.

The research work disclosed in this publication is partially funded by the Strategic Educational Pathways Scholarship (Malta). The scholarship is part-financed by the European Union – European Social Fund (ESF) under Operational Programme II – Cohesion Policy 2007-2013, "Empowering People for More Jobs and a Better Quality of Life".

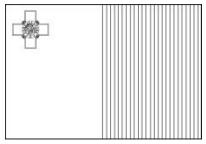

Operational Programme II – Cohesion Policy 2007-2013
Empowering People for more Jobs and a Better Quality of Life
Advert part-financed by the European Union
European Social Fund (ESF)
Co-financing rate: 85% EU Funds; 15% National Funds

Investing in your future

ABSTRACT

The domestic sector accounts for a substantial 25% of the total energy consumption within the EU. Although a number of measures aimed at reducing this energy consumption have successfully been implemented, in southern Europe this reduction has been partly offset by the increased penetration of residential air conditioning relying on vapour compression packaged split units. A more concrete action is therefore needed. One method which is being proposed is to use micro-trigeneration systems to provide combined heating, cooling and electrical power. By recycling the waste heat produced from a small energy conversion system and utilise it to run a thermally activated cooling device, micro-trigeneration has the potential to improve the energy-efficiency of dwellings, hence reducing consumption.

An important aspect in evaluating micro-trigeneration and its potential effect on improving energy-efficiency in buildings is the formulation of a detailed assessment of its energetic, environmental and economic performance. This should not be limited only to the present operating conditions but should also include possible future ones. In this context, a lot of research still needs to be done to understand the potential impact that externally imposed conditions, such as those caused by additional measures meant at reducing the overall energy demands of a building, might have on the system. The research presented in this thesis makes use of a combined deterministic and sensitivity analysis methodology in conjunction with data obtained from simulations performed using a whole building simulation tool run at high temporal resolution to model, simulate and assess micro-trigeneration performance under varying conditions. The research in this thesis presents the methodology used to create the different scenarios and the resulting results obtained.

The outcomes from this PhD work include a new method and tool to generate high resolution electrical demand data incorporating the effect of future energy efficiency savings; a dynamic model of an absorption chiller designed to be easy-to-calibrate and; detailed, integrated models of a trigeneration system along with the Maltese apartment building which it serves.

Performance simulation of the trigeneration system for the island of Malta indicated that considering the current local electricity grid network, a residentially installed micro-trigeneration system fed by an internal combustion engine and using an absorption chiller as the thermally activated cooling device, would produce primary energy savings of up to 44% along with CO_2 savings of approximately 10,000 kg/yr.

TABLE OF CONTENTS

LIST OF FIGURES

LIST OF TABLES

ACRONYMS & ABBREVATIONS

BMS	Building Management System
CF	Cash Flow
CFL	Compact Fluorescent Lamp
CHP	Combined Heat and Power
CCHP	Combined Cooling, Heat and Power
CO_2	Carbon Dioxide
COP	Coefficient of Performance
DEFRA	Department for Environment, Food and Rural Affairs (UK)
DHW	Domestic Hot Water
ECBCS	Energy Conservation in Buildings and Community Systems (IEA Programme)
EEA	European Environmental Agency
EPBD	Energy Performance of Buildings Directive (Directive 2002/91/EC)
ES	Emission Savings
EU	European Union
FIT	Feed-in Tariff
GF	Ground Floor
HVAC	Heating, Ventilation and Air Conditioning
IC	Internal Combustion Engine
IEA	International Energy Agency
IR	Investment Rate
IRR	Internal Rate of Return
LPG	Liquefied Petroleum Gas
MARR	Minimum Attractive Rate of Return
MC	Maintenance Cost
MF	Middle Floor
MTP	Market Transformation Program (DEFRA, UK - Energy-Efficiency Program)
NPV	Net Present Value
NVF	Normalised Verification Factor
PDF	Probability Density Function

PE	Primary Energy
PES	Primary Energy Savings
PP	Payback Period
PW	Present Worth
REMODECE	Residential Monitoring to Decrease Energy Use and Carbon Emissions in Europe (IEEA Program Funded Project)
RES	Renewable Energy Systems
SWH	Solar Water Heater
TAC	Thermally Activated Cooling
TF	Top Floor

CHAPTER 1
INTRODUCTION

Chapter overview

The scope of this first chapter is primarily that of giving an overview of the whole thesis; its scope, objectives and the methodology used to answer the specific research questions posed. The chapter starts by explaining the concept behind micro-trigeneration, specifically describing what kind of research has been done on micro-trigeneration so far and highlighting the gaps which this research addresses in order to fully assess the technology's performance in dwellings, including energy-efficient ones. The chapter finally also explains the layout of this thesis by briefly giving a short description of the work done in each subsequent chapter.

1.1 Energy use in dwellings

The domestic sector accounts for a considerable portion of the final energy consumption of most developed countries. Within the European Union (EU), approximately 25% of the total annual final energy consumption is used in dwellings [1]. A precise breakdown of how this energy is consumed on a country by country basis is difficult to ascertain, especially considering that such a breakdown is highly dependent on factors such as climate, technology used and other conditions which are variable from country to country [2]. However, an approximate breakdown is given by the European Environmental Agency (EEA) in [3], which indicates that a substantial amount of this energy, about 69%, goes into space heating with the remaining balance accounted for by water heating (15%), providing electricity for appliances and lighting equipment (11%) and cooking activities (5%). In warm climates such as that present in southern European countries, space cooling is the predominant load [4]. Ensuring the efficient provision and use of energy in dwellings is therefore an essential aspect in attaining the overall 20% improvement in energy-efficiency target set out by the Presidency Conclusions of the European Council [5] for 2020.

1.1.1 Current measures aimed at improving the energy-efficiency in buildings

Governments and organisations worldwide have realised the potential benefits in reducing domestic energy demands and have implemented various measures to aid in reducing residential energy demand. The measures can be typically grouped into:

- Measures aimed at reducing energy demand by increasing efficiency; and

- Measures aimed at offsetting fossil-fuel sourced energy through the use of renewable energy sources, including solar water heating, photovoltaic and micro-wind systems.

Measures aimed at reducing energy demand typically rely on improving the way energy is used. Directive 2002/91/EC *on the Energy Performance of Buildings* (EPBD) [6], considered to be the main tool in promoting energy-efficiency in

buildings, and Directive 2006/32/EC *on energy end-use efficiency* [7] requiring EU countries to improve their energy end-use efficiency by 9% by 2016, are prime examples of legislation designed to encourage implementation of energy-efficiency measures in the EU. Using renewable energy sources to displace fossil fuel use relies on providing incentives favouring systems making use of renewable energy sources.

The efficacy of these measures is heavily dependent on local conditions such as climate, cost of conventionally sourced energy, the existence of financial incentives, public acceptance, access to renewable energy sources *etc*. In northern Europe for example, several countries have managed to control their overall energy consumption by lowering the demand for space heating through the use of improved building techniques and insulation [3]. Countries in southern Europe, on the other hand, have been particularly successful in harvesting solar energy for domestic hot water [8].

Electricity consumption in domestic households is still on the increase [9]. This is partially attributable to larger penetration of certain appliances (such as microwave ovens, set-top boxes and other audiovisual equipment), electrification of certain activities (*e.g.* to the introduction of a number of '*gadgets*' automating manual activities), improved expectations of comfort and an ageing population. These are all factors which are contributing to such an increase. In warm climates all this has been compounded by the significant increase in the use of residential air conditioning relying on vapour compressor packaged split units [2, 9]. Over the period 2006 and 2009, the 7 EU countries bordering the Mediterranean sea: Greece, Malta, Italy, Slovenia, France, Cyprus and Spain have seen an annual increase in electricity consumption of 1.35%, compared to the 0.31% increase reported in the other EU countries [10] over the same period.

1.1.2 Aiming at more ambitious targets

In order to reach the energy-efficiency improvement targets set by the EU, a more concrete and perhaps active approach is therefore required [11]. Most of the energy-efficiency measures which have been implemented so far are considered to be a first step towards decreasing energy demand in the domestic sector; a step in the right

direction but still far away from achieving the desired target. One way in which the individual targets can be achieved is through policy measures specifically aimed at achieving higher penetrations of renewable energy technologies or efficient micro-generation technologies in dwellings [12].

1.2 The potential role of micro-trigeneration in improving residential energy-efficiency

1.2.1 Cogeneration and micro-cogeneration

A particular solution which is being considered by many researchers [13-15] and institutions [16] as a possible means to increase energy-efficiency in the residential sector is micro-cogeneration, also known as micro-CHP (*Combined Heat and Power*).

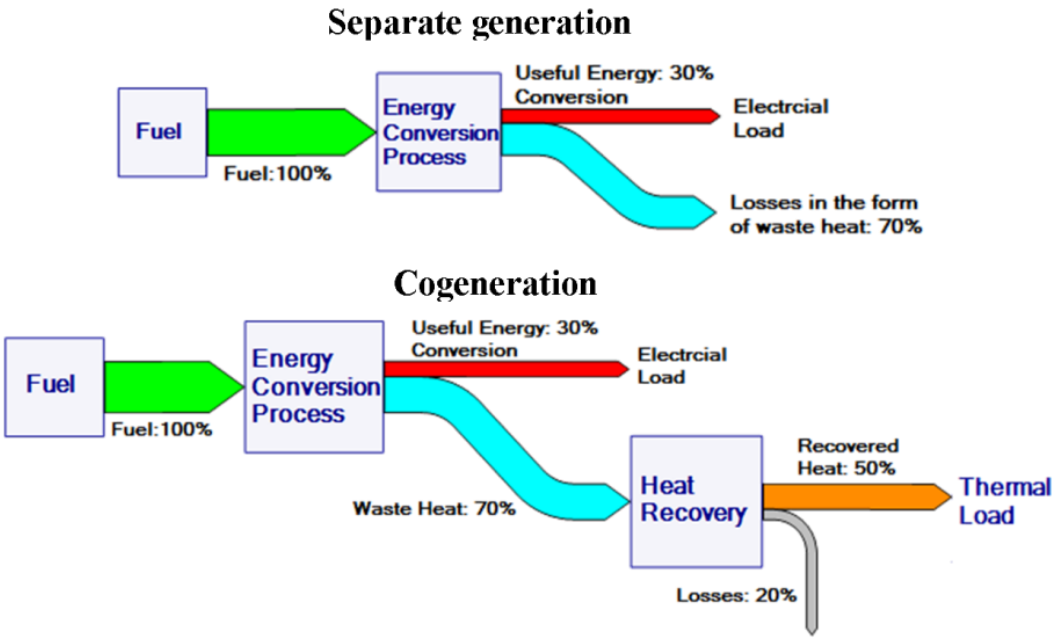

Fig. 1.1 - Separate generation *vs.* cogeneration (efficiency values are indicative)

Unlike conventional heat and power supplies to buildings in which each is satisfied separately by two distinct energy flow processes, micro-cogeneration, as shown in Figure 1.1, makes use of a single process whereby the 'waste heat' from electricity generation is recovered and re-utilised to satisfy a heating demand [17], hence improving the fuel usage efficiency.

Micro-cogeneration can make use of the 'waste heat' exhausted from practically any energy conversion system including the traditional internal combustion (IC) engines, stirling engines, to the more advanced technologies such as micro-gas turbines and fuel cells [18].

The idea of re-utilising waste heat from an electricity producing process is not a new concept. In 1882, Thomas Edison's first commercial power station in Pearl Street used to supply both power and heat [19] to a neighbouring block in Manhattan. Similarly, district heating in northern and central Europe has been successfully implemented for many years, with the result that an average 13% of the gross electricity generation in the EU is currently produced by cogeneration as shown in Figure 1.2 (data published by Eurostat for 2009 [10]).

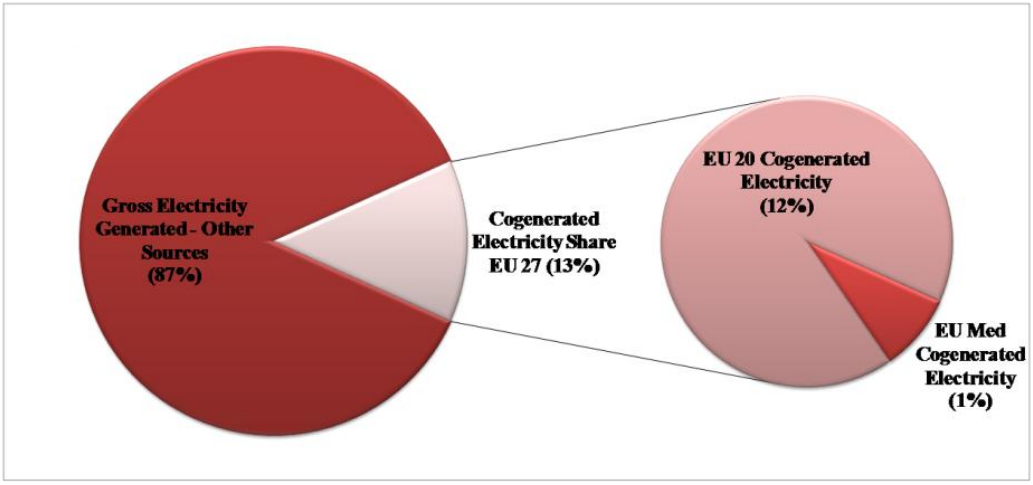

Fig. 1.2 - Share of electricity produced by cogeneration in the EU

Given the proven experience in the technology and its substantial use in large parts of Scandinavia [20], it is by no means surprising that cogeneration already plays an important role in ensuring an efficient energy supply in these countries. Further increase in the use of cogeneration in such countries or indeed introducing large scale cogeneration in countries with no prior experience of district heating is however hindered by the fact that district heating requires huge investments costs and implementing such a scheme requires appropriate location conditions (*e.g.* dense population) and extensive infrastructural work [20].

One way how these limitations can be overcome is by extending cogeneration to include micro-scale cogeneration. The idea of micro-scale cogeneration or micro-cogeneration differs from district heating or centralised cogeneration, in that, micro-scale cogeneration typically refers to single systems capable of supplying heat and power to individual buildings such as households, small commercial premises, hotels *etc*. which may or may not be connected to the centralised grid network [18]. Sizes for micro-cogeneration are considerably smaller than typical cogeneration or district heating systems, running into only few kW_{el}. Although the official definition given in Directive 2004/8/EC *on the promotion of cogeneration based on a useful heat demand in the internal energy market*, the relevant EU directive on cogeneration [16], qualifies micro-cogeneration as systems with an electrical power output of less than 50 kW_{el}, the definition supplied by Pehnt *et al.* in [18] better explains and qualifies micro-cogeneration for the kind of research conducted in this thesis. Pehnt *et al.* discuss how given the type of load thresholds found in the domestic environment, a limit of 15 kW_{el} is more adequate to qualify systems specifically meant for use in residential single and multi-family households. For the scope of this thesis this lower limit is therefore used as the basis for system sizing.

In terms of market penetration, micro-cogeneration in residential buildings is still considered to be at an early stage of market development [21]. A full country by country analysis is outside the scope of this research, however in general it has been observed that micro-cogeneration penetration rates have shown a steady growth in countries where the market forces and local legislation have proved to be adequate to support micro-cogeneration, examples of which are Germany and Japan (for an example outside the EU) [18]. The problem with micro-cogeneration is that although the energy flow process concept is similar to large scale cogeneration, the associated scaling down required to accommodate the highly intermittent and variable energy demands of residential buildings, presents new and challenging design problems.

In terms of technology numerous books (*e.g.* [17, 18, 21]), journal papers (*e.g.* [22, 23]) and research studies (*e.g.* [24]) have analysed at length the advantages and

disadvantages of each individual micro-cogeneration technology. Being the most mature and well proven technology (with the lowest costs amongst micro-cogeneration packages) [23], only IC engines fed micro-cogeneration are currently considered as commercially viable. All other micro-cogeneration technologies are considered to be in a status ranging from advanced research phase to pilot demonstration phase/early commercialisation stage, still addressing issues such reliability, electrical efficiency, fuel flexibility and costs [18]. Examples of IC engine-based micro-cogeneration packages include the 1 kW_{el} package by Ecowill [25] and the 5.5 kW_{el} system by Senertec Dachs [25, 26], offering electrical efficiencies ranging from 20% to 26% and overall efficiencies following heat recovery in the range of 85% to 89%.

1.2.2 Micro-cogeneration - Specific problems in warm climates

An important issue with micro-cogeneration systems is that contrary to the fairly constant electrical and thermal supply-demand environment in which large to medium scale cogeneration systems work, micro-cogeneration systems are exposed to highly varying energy demands over short periods of time [27, 28]. This creates a problem as to the appropriate sizing of micro-cogeneration, leading to potential undersizing or oversizing of a system resulting in inefficient dumping of energy (waste heat) or disproportionate payback periods [24]. Also if not properly designed (and controlled) such intermittent loads may lead to problems related to the CHP unit having high cycling rates (switching 'On'/'Off'), resulting in increased maintenance. In warmer climates, the problem is further aggravated by the absence of a prolonged heating season

Recalling Figure 1.2, it can be observed how the average share of electricity produced from cogeneration in the 7 countries which border the Mediterranean Sea and which have a predominant warm climate with short mild winters is still a small part of the overall cogenerated electricity produced in the EU. Like any other technology the feasibility and market interest in cogeneration depends on the payback period. When assessing the payback period an important role is played by the operational or usage time, as this has a direct affect on the ability of a system to

offer reasonable and adequate return on investments. Although plant configuration schemes such as additional storage can be used to introduce a degree of flexibility in micro-cogeneration operation [29], the operational or usage time is still a function of the electrical and thermal demand. In warm climates with the exception of the provision of hot water, the thermal demand is very low due to the low number of heating days. Consequently, the investment required for the installation of a micro-cogeneration system is difficult to justify [30].

1.2.3 Micro-trigeneration as a potential way forward

A solution to this problem is to extend the concept of cogeneration to trigeneration by including a thermally driven cooling load. Unlike cogeneration, trigeneration also known as *Combined Cooling, Heat and Power* (CCHP), is the process whereby the 'waste heat' recovered from an energy conversion process is used either to supply a heating demand such as in a normal cogeneration system or to supply a thermally activated cooling (TAC) device [23] capable of satisfying a cooling demand as shown in Figure 1.3.

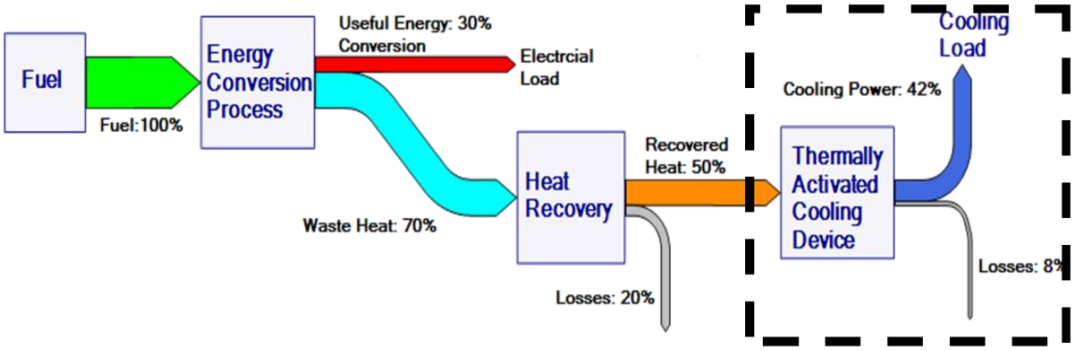

Fig. 1.3 - Extending cogeneration to include for trigeneration (efficiency values are indicative)

In warm climates this provides a more consistent requirement for heat, thus increasing the system utilisation time [31]. This renders the trigeneration process particularly suitable for use in warm climates given that it can be used both during the summer and the winter period [30, 32]. Trigeneration offers an interesting avenue for efficiently delivering power, heating and cooling to residential buildings in warmer climates.

As shown in Figure 1.3 an important component in trigeneration is the thermally activated cooling device. There are various types of TAC devices which can be used in a trigeneration system [23] including absorption chillers [33], adsorption chillers [34], ejector type chillers [35] and rotor based desiccant systems [36]. Given the low temperature heat source at which 'waste heat' is exhausted from CHP units used in micro-cogeneration systems (stirling engine-based CHP *approx.* 90ºC, IC engine-based CHP *approx.* 80ºC, proton exchange membrane (PEM) fuel cell *approx.* 60ºC [23]), single-effect absorption chillers are the preferred type [37].

1.3 Assessing the performance of micro-trigeneration in residential buildings

An important aspect in addressing micro-trigeneration development in residential buildings is the assessment of the system's energetic, environmental and economic performance. Various studies reporting either on the basis of real-life installed systems or computer generated simulations have already shown the feasibility of trigeneration systems in excess of 50 kW_{el}. These studies, which include trigeneration projects in factories [38], hotels [39], educational buildings [40] and supermarkets [41], have shown that for such projects the fairly constant demand for energy in these buildings and the associated lengthy utilization times ensure advantageous rates of return on investment. Micro-trigeneration in residential buildings, on the other hand, can be considered quite a novelty with very few applications outside laboratories [42].

Research into using micro-scale trigeneration in the residential sector has mainly focused on the documentation of results obtained from experimental test rig systems [42-44]. Whereas the results obtained from these experimental systems give a clear indication of what the expected micro-trigeneration system performance should be for specific conditions, these studies stop short of indicating how a micro-trigeneration system would respond to changes in the surrounding environmental conditions. Overall system performance is largely dictated by the surrounding environment and therefore when assessing the performance of a micro-trigeneration

system in a residential building, it is of paramount importance that due consideration is given to the environment the system is working in.

Similarly, other operating conditions such as building size and occupancy may also affect the system's performance. The system has also to contend with the possibility of having different plant configurations, including the existence (and size) of storage tanks and additional renewable energy systems working in tandem with the CHP unit. A final complication in the implementation of trigeneration in future buildings is that measures aimed at reducing residential energy demand by (for example) improving the building fabric to reduce the heating (or cooling) demand or increasing the household appliances' electrical efficiency to reduce the electrical demand, although beneficial on their own merits, may result in a situation where the energy demand required to be satisfied by the micro-trigeneration decreases to such an extent that the system is no longer feasible.

Before implementing any measures (including installing the micro-trigeneration itself) it is therefore of the utmost importance that a thorough understanding is obtained not only of the performance of the micro-trigeneration system itself but also of the system in combination with the surrounding environment including the building within which it operates.

Depending on the type of assessment required, micro-trigeneration system performance can be modelled and analysed either through the use of real-life experimental models or dedicated modelling-simulation techniques. The latter of course can take the shape and form of varying degrees of complexity, from simple mathematical equations to complex modelling tools [45]. In both cases the end result would be a series of performance metrics (*e.g.* fuel consumption, system efficiency, emission savings *etc.*) which describe the viability of the system. The following two sections, Section 1.3.1 and Section 1.3.2 respectively, describe the use of real-life experimental models and the use of optimisation modelling (in literature this is the most common example of simulation technique used in cogeneration and trigeneration modelling) as research methods used to assess residential micro-

trigeneration performance. The sections discuss the advantages and disadvantages of each method in assessing micro-trigeneration performance and explain why neither technique can be used to fully assess micro-trigeneration performance in dwellings. Section 1.3.3 then explains why, considering the limitations of these two research techniques and based on the type of research required in this thesis, the most effective way to model and assess the impact of varying operating conditions on the performance of a residential micro-trigeneration system is through the use of a combined deterministic and sensitivity analysis methodology based on data obtained from simulations carried out using a whole building simulation tool.

1.3.1 Assessing the performance of micro-trigeneration through real-life experimental models

Over the last decade real-life experimental models in the area of micro-trigeneration have mainly taken the form of either laboratory built test-rigs such as those described by Khatri *et al.* in [42], Kong *et al.* in [46], Angrisani *et al.* in [43] and Rocha *et al.* in [47] or purposely built building demonstration projects such as that described by Henning *et al.* in [36]. Typically although the physical arrangement is different comprising different combinations of CHP unit types and thermally activated chillers (a 3.7 kW_{el} converted agricultural IC engine and vapour absorption chiller in [42], a 8.7 kW_{el} IC engine and vapour absorption chiller in [46], a 6 kW_{el} IC engine and thermal chemical accumulator in [43], a 30 kW_{el} micro-turbine and a 26 kW_{el} IC engine fed absorption chiller in [47] and a cogeneration plant and a desiccant air handling unit in [36]), the primary scope of such a research technique is to acquire data on the setup being investigated from which data on the performance metrics of the micro-trigeneration system can be eventually evaluated.

Typically the analysis of such systems concentrates on calculating the overall system efficiency and other metrics related to the system's energetic and environmental performance compared to separate generation. Although such type of experimental techniques presents the researcher with reliable data and is therefore a very important and useful tool for assessing micro-trigeneration systems, this method of investigation is limited in terms of simulating the impact external operating

conditions have on the performance of a micro-trigeneration system.

1.3.2 Assessing the performance of micro-trigeneration through optimisation modelling techniques

A second route in assessing the performance of micro-trigeneration in buildings is to use optimization modelling techniques [48] whereby a particular 'cost function' (*e.g.* CHP size, storage size, operation methodology *etc.*) needs to be optimised under various boundary conditions. Although optimisation modelling may be considered more of a design tool rather than a means to analyse performance, such a technique can be extended to and is particularly useful when, the focus is expanded to include the environment in which the micro-trigeneration system is operating. Unlike experimentation this approach permits the inclusion of external operating conditions in performance assessment.

Various examples of the use of this technique in understanding the effect certain operating conditions may have on small and medium scale trigeneration (50 kW_{el} to 1 MW_{el}) can be found in literature. These studies have mainly focused on trigeneration projects in commercial, health care, educational or hospitality buildings. Wang *et al.* in [48] and Carvalho *et al.* in [30] are examples whereby the performance of small scale trigeneration under different climatic conditions and in different building establishments (hotels, hospitals and offices) was studied using such an optimization process. Kavvadias *et al.* in [49] use an optimization process to understand the influence of CHP sizing and other parameters on the project investment. Napolitano *et al.* in [40, 50] present the results of an optimization study aimed at understanding small scale trigeneration systems coupled with solar collectors on an educational building.

A common aspect of all these studies is that, the number of variables investigated is commonly limited to a selected few (*e.g.* the CHP electrical power rating, control strategy *etc.*); typically those variables which are of specific interest for that particular study. The application of an optimisation technique to holistically model a micro-trigeneration system under a number of varying external conditions such as

those experienced in the residential sector is therefore not suited in this case, as the complexities involved in fully modelling such a setup using an optimisation modelling technique would be considerable.

1.3.3 Assessing the performance of micro-trigeneration through the use of a combined deterministic and sensitivity analysis approach

Dorer and Weber in [51] mention deterministic methods coupled with sensitivity analysis as possible techniques that can be used in the performance assessment of residential micro-cogeneration. Dorer and Weber explain that in a deterministic approach, different scenarios and configurations may be assessed through detailed comparisons with other scenarios, including base case scenarios. Sensitivity analysis, on the other hand, relies on assessing the effect a parameter has on a specific case through the incremental change of the parameter in question.

Compared to optimisation techniques, this combined approach permits a higher degree of flexibility vis-à-vis the type and number of operating conditions being analysed. This permits a more holistic approach as multiple factors can be analysed with relative ease both independently and in aggregated form. Based on the data obtained from the analysis and the type of operating condition being investigated either method can be used, depending on, whether the results obtained are being compared to a base case scenario or if the sensitivity of the system to a specific operating condition is being investigated.

1.3.3.1 Use of a whole building simulation tool

The previous section highlighted the fact that when considering a large number of variables, deterministic methods and sensitivity analysis are the most appropriate methodologies. However, this is only the process used to assess a system and an important aspect in using these two methods is the method or means by which the primary data is obtained. Dorer and Weber in [45] explain that in cogeneration applications the complexities arising from the strong relationship between the CHP unit, the ventilation system, the ancillary equipment and the building requires whole building simulation tools to fully simulate the behaviour of such a system in an

effective manner. The research in this thesis therefore makes use of data derived from simulations performed using a similar whole building simulation tool.

1.4 Scope of research and methodology adopted

1.4.1 Scope of research

The scope of this research can be summarised as to better understand the impact of operating conditions on micro-trigeneration performance in residential buildings in warm climates. More specifically this thesis has two particular research aims.

To extend previous work done on micro-cogeneration and trigeneration in residential buildings (*e.g.* IEA ECBCS Annex 42 [52],and Beausoleil-Morrison *et al.* in [53]), to include detailed analysis of residential cooling through the following:

(i) The development of a detailed yet easy-to-calibrate model of an absorption chiller capable of capturing the dynamic behaviour. When modelling a chiller within a trigeneration system, the dynamic conditions due to (for example) 'On'/'Off' or modulating behaviour, start-up and shut down or other temporal fluctuations in operating conditions experienced by the chiller results in a situation where although intrinsically more complex to develop compared to steady-state models, dynamic models are by far the more appropriate means to assess the actual performance of an absorption chiller model [37, 54]. Existing attempts at dynamic absorption chiller modelling however have resulted in the creation of detailed models of specific chillers [55] or detailed models of specific cycles and system configurations [56] which with, difficulty can be adapted to represent other chiller models or included in plant configurations other than those for which they were originally designed. Also, although an emerging approach of developing models [37, 57] capable of being customised through calibration with data obtained for different units is slowly becoming significant, such models still require the user to define the characteristics of the components comprising the desired absorption chiller (*e.g.* the individual components' heat exchange surface area, individual internal component dimensions, solution composition and internal mass flow

rates), a non-trivial task often requiring invasive experimental measurements. The model developed in this research and which is described in detail in Chapter 3 relies on a novel approach whereby, it can be easily calibrated as a single unit using measured data of the inlet and outlet temperatures of the three water circuits flowing in and out of the chiller, without the need for invasive measurements.

The model calibrated using data obtained for a chiller sized to cater for residential loads (the 10 kW_{th} absorption chiller developed by SK SonnenKlima GmbH [58, 59]) was used extensively throughout the research as an integral part of simulations aimed at analysing the technical performance (in a realistic operational context) of very detailed trigeneration plant configurations.

(ii) Improving the modelling of the electrical loads served by trigeneration through providing the means to generate high resolution residential electrical demand profiles including the effect of future energy-efficiency improvement measures. Compared to the relatively stable electrical and thermal demands typical of large buildings, residential buildings have a very variable and time-dependent demand. Simulations performed at low resolutions (*e.g.* hours) are therefore not suitable in this case and higher temporal resolutions down to 1 minute are appropriate [60]. Furthermore, for systems where electricity is being produced, such as this case, higher time resolutions are required to give an accurate depiction of electrical import/export characteristics [28]. In this context, Chapter 2 builds upon the work done by Stokes in [60] to provide a 3 stage transformation process which first creates seasonal variations of individual monthly data using low-resolution electrical hourly demand datasets, then converts the low-resolution into high-resolution minute data and finally projects the data into a future scenario reflecting improved appliance energy-efficiency.

The second aim of the research was to make use of the developed models and data to

investigate how a residential micro-trigeneration system would perform under realistic dynamic operating conditions and subject to different operational scenarios including increased residential energy-efficiency, different occupancy levels and different plant configurations. Finally, the analysis in addition to including a thorough analysis of the energetic and environmental performance of the different scenarios being proposed also includes an in-depth analysis of different financial scenarios.

1.4.2 The methodology adopted - An overview

The research presented in this thesis makes use of the whole building simulation tool ESP-r [61] to simulate the performance of a grid-connected micro-trigeneration system under a number of varying operating conditions. The system was modelled to represent a micro-trigeneration system supplying both the electrical and the HVAC (heating, ventilation and air conditioning) demand of a multi-family residential building in the Mediterranean island of Malta. Given its location in the middle of the Mediterranean sea, Malta is a good example of a sub-tropical *Csa Köppen Climate Classification* (moderate rainy winters and hot dry summers) [62], typical not only of substantial parts of southern Europe, but also parts of North Africa and parts of the middle-east overlooking the Mediterranean, where micro-trigeneration could possibly have a large impact.

A number of operating conditions were selected (this is explained in further detail in Section 1.4.2.1) and for each of these, a number of scenarios were created, either by directly changing the specific parameters of the ESP-r model or else through post-processing of the data obtained from the simulations. The combined deterministic/sensitivity approach discussed previously was then used to assess the performance of the trigeneration system.

Each individual scenario was simulated for a whole year, however to better understand the seasonal performance of the micro-trigeneration system, the simulations were sub-divided into three distinct seasons, the heating season (mid-December to mid-March), the cooling season (June to September) and the remaining

shoulder months.

All simulations performed were run at a high temporal resolution of 1 minute. The use of a high temporal resolution in this case ensures that the simulations were modelled with enough temporal precision to characterise the highly varying nature typical of residential energy demands as discussed by Stokes in [60].

1.4.2.1 Selecting the operating conditions to be investigated

The number of operating conditions which can potentially influence the performance of a residential micro-trigeneration system is considerable. These range from those conditions that have a direct effect on the system by affecting its usage time (such as reduced thermal demand from the use of insulated building fabric), to those factors which have an indirect effect but which would still impact the performance of a micro-trigeneration system compared to separate generation (such as improvements carried out on the grid network). These operating conditions may also be classified into other categories such as whether they are the result of additional regulations, a cost-benefit opportunity or a system addition.

In the context of a time-limited research such as this it is very difficult to analyse all possible operating conditions which could have an impact on micro-trigeneration system performance. For this reason, given that the main theme of this research was to analyse the effect energy-efficiency improvements would have on residential buildings and micro-trigeneration systems, the operating conditions chosen for this investigation were those currently considered to be the most promising in terms of improving energy-efficiency [63]. These conditions are shown in Table 1.1.

Needless to say other aspects such as, building management systems and improved use (and control) of natural ventilation, additional plant configurations, thermal storage and use of phase change materials could also have been included as examples of energy-efficiency measures. In this thesis these additional operating conditions were however not considered any further, but could possibly provide interesting research aspects for future work as discussed in Chapter 6. Importantly however,

Table 1.1 also includes additional aspects (*e.g.* building size and occupancy, sensitivity to fuel prices and electricity tariffs) which, although are not directly related to energy-efficiency improvements, play an important part in assessing micro-trigeneration system performance in residential buildings.

Table 1.1 - Operating conditions investigated

Operating condition	Direct / Indirect effect	Possible effect on micro-trigeneration system	Driver
Improvement in building fabric	Direct	Changes the thermal demand	Regulation/Cost-benefit opportunity
Building size and number of occupants	Direct	Changes the thermal demand	-
Addition of a chilled water storage tank	Direct	Changes operating mode	System addition
Improvement in household appliances' electrical efficiency	Direct	Changes the electrical demand	Regulation/Cost-benefit opportunity
Addition of a solar water heating system in tandem with micro-trigeneration system	Direct	Changes the thermal demand	Regulation/Cost-benefit opportunity
Sensitivity to grid network improvements	Indirect	Changes the comparison with separate generation	Regulation/Cost-benefit opportunity
Sensitivity to fuel prices	Direct	Changes the system's running costs	-
Sensitivity to electricity tariffs	Indirect	Changes the comparison with separate generation	-

Finally, although a certain degree of interaction exits between the different operating conditions (*e.g.* increased occupancy leads to an increase in the electrical demand – the two are therefore dependent), the study's primary focus was to analyse the impact each individual operating condition had on micro-trigeneration system performance. A detailed analysis of the interaction between the aggregated effect of different operating conditions and the impact on micro-trigeneration system performance was therefore outside the scope of this research although, again, such an analysis would provide interesting research material for future work.

1.5 Summary of Chapter 1

This chapter has introduced the concept of micro-trigeneration as a means to increase

the energy-efficiency in residential buildings. The use of thermally activated chillers may provide a means to increase the operational time of cogeneration systems in warm climates, rendering them a feasible solution to increase the energy-efficiency of residential buildings. Although trigeneration has been the subject of previous studies (*e.g.* [36, 41, 50]), a lot of research still needs to be done to understand the potential impact externally imposed conditions, such as those caused by additional measures meant at reducing the overall energy demands of a building, might have on the system. Given the limitations inherent to other research techniques, the research presented in this thesis makes use of a combined deterministic and sensitivity analysis methodology in conjunction with data obtained from simulations performed using a whole building simulation tool run at high temporal resolution to model, simulate and assess micro-trigeneration performance under varying conditions. The research in this thesis presents the methodology used to create the different scenarios and the resulting results obtained.

1.6 Subsequent chapters

Chapter 2 addresses the demand side and explains the procedure adopted in modelling the building used in the simulation and its energy (electrical and thermal) demands. In particular Chapter 2 considers existing buildings and their energy demands and explains the methodology used to model the impact energy-efficiency measures will have on the buildings and their associated energy demand. In doing so, different scenarios for both low and high electrical and building fabric efficiencies were modelled. Chapter 3 examines the supply side, mainly the micro-trigeneration plant and associated HVAC system modelled in ESP-r. Apart from explaining in detail how a new dynamic absorption chiller model was developed, this chapter also explains possible alternative plant configuration solutions. Chapter 4 describes in detail the various scenarios modelled, giving specific details of how each scenario was modelled and simulated. This chapter also explains the performance metrics used to quantify and assess the system performance. Chapter 5 reviews and discusses the results obtained for the different scenarios simulated. Finally, Chapter 6 concludes the thesis by providing an overview of the work carried out in this research listing also possible future work.

1.7 Chapter References

[1] DG for Energy and Transport (2009). "*EU energy and transport in figures*" - Luxembourg: Office for the Official Publications of the European communities. European Commission. Luxembourg. Available from: http://ec.europa.eu/energy/publications/statistics/doc/2009_energy_transport_figures.pdf [Accessed 01/09/2011]

[2] REMODECE Project Members (2008). "*Report with the results of the surveys based on questionnaires for all countries in REMODECE - Residential Monitoring to Decrease Energy Use and Carbon Emissions in Europe (IEEA Program Funded Project)*". Available from: http://www.isr.uc.pt/~remodece/downloads/REMODECE_D9_Nov2008_Final.pdf [Accessed 01/12/2009]

[3] European Environmental Agency (2001). Chapter "*Households*" in *"Indicator Fact Sheet Signals 2001"* - European Environmental Agency. Available from: http://www.eea.europa.eu/data-and-maps/indicators/household-energy-consumption [Accessed 10/01/2011]

[4] *de* Almeida, A. and Fonseca, P. "*Residential monitoring to Decrease Energy use and Carbon Emissions in Europe"* in *European Council for an Energy Efficient Economy, ECEEE Conference 2007 Summer Study*. 2007. Côte d´Azur, France

[5] *"Presidency Conclusions - Council of the European Union 8/9 March 2007"* - European Parliament and European Council - Doc No. 7224/1/07 REV 1

[6] *"Directive 2002/91/EC of the European Parliament and of the Council of 16 December 2002 on the energy performance of buildings"* - European Parliament and European Council

[7] *"Directive 2006/32/EC of the European Parliament and of the Council of 5 April 2006 on energy end-use efficiency and energy services"* - European Parliament and European Council

[8] Menanteau, P. (2007). "*Policy measures to support solar water heating: information, incentives and regulations"* - Université de Grenoble, Grenoble, France. Available from: www.worldenergy.org/documents/solar_synthesis.pdf [Accessed: 08/06/2012]

[9] Bertoldi, P. and Atanasiu, B. (2007). "*Electricity Consumption and Efficiency Trends in the Enlarged European Union - Status Report 2006"* - EUR 22753EN. Institute for Environment and Sustainability. JRC European Commission

[10] Eurostat. "*Eurostat Web Portal"*. Main Database - Environment and Energy [Accessed: 30/11/2010]; Available from: http://epp.eurostat.ec.europa.eu/portal/page/portal/eurostat/home

[11] The World Bank (2010). *"Part II-7Accelerating innovation and technology diffusion*" in "*World Development Report 2010"* - The International Bank for Reconstruction and Development / The World Bank. Washington, USA. [Accessed: 30/11/2011]; Available from: http://siteresources.worldbank.org/INTWDRS/Resources/477365-1327504426766/8389626-1327510418796/Chapter-7.pdf

[12] *"Directive 2009/28/EC of the European Parliament and of the Council of 23 April 2009 on the promotion of the use of energy from renewable sources"* - European Parliament and European Council

[13] Paepe, M.D., D'Herdt, P. and Mertens, D. "*Micro-CHP systems for residential applications"* Energy Conversion and Management 2006. 47: pgs. 3425-3446

[14] Gigliucci, G., Petruzzi, L., Cerelli, E., Garzisi, A. and La Mendola, A. "*Demonstration of a residential CHP system based on PEM fuel cells"* Journal of Power Sources 2004. 131: pgs. 62-68

[15] Sattari, S. and TeymouriHamzehkolaei, F. "*Technical and economic feasibility study of using Micro CHP in the different climate zones of Iran"* Energy, 2011. 36: pgs. 4790-4798

[16] *"Directive 2004/8/EC of the European Parliament and of the Council of 11 February 2004 on the promotion of cogeneration based on a useful heat demand in the internal energy market and amending Directive 92/42/EEC"* - European Parliament and European Council

[17] Macchi, E., Campanari, S. and Silva, P. La Microcogenerazione a gas naturale, ed. Polipress. Vol. Scienza e tecnologia per l'energetica. 2005, Milano: Polipress

[18] Pehnt, M., Cames, M., Fischer, C., Praetorius, B., Schneider, L., Schumacher, K. and Voß, J.-P. "*Micro-Cogeneration: Towards Decentralized Energy Systems "*, ed. Springer. 2006, The Netherlands: Springer

[19] Josephson, M. "*Edison; a biography"*. 1959, New York, USA: McGraw-Hill

[20] Rezaie, B. and Rosen, M.A. "*District heating and cooling: Review of technology and potential enhance*ments" Applied Energy, 2012. 93: pgs. 2-10

[21] Boehnke, J., "*Buisness Models for Micro-CHP in residential buildings"*, ed. SVH. 2008, Saarbruchen: Sudwestdeutscher verlag fur Hochschulschriften Aktiengesellschaft & Co. KG, Saarbrucken, Germany

[22] Chicco, G. and Mancarella, P. "*Distributed multi-generation: A comprehensive view"* Renewable and Sustainable Energy Reviews 2009. 13: pgs. 535-551

[23] Wu, D.W. and Wang, R.Z. "*Combined cooling, heating and power: A review"* Progress in Energy and Combustion Science 2006. 32: pgs. 459-495

[24] Knight, I. and Ugursal, I. (2007). "*Residential Cogeneration Systems: A Review of the Current Technologies"* - A Report of Subtask A of FC+COGEN+SIM The Simulation of Building-Integrated Fuel Cell and Other Cogeneration Systems: Annex 42 of the International Energy Agency's Conservation in Buildings and Community Systems Programme. International Energy Agency

[25] Macchi, E., Campanari, S. and Silva, P. "*Cap.3 - Motori Alternativi"*, in *La Microcogenerazione a gas naturale*, Polipress, Editor. 2005, Polipress: Milano

[26] Baxi-SenerTec UK (2010). DACHS Mini-CHP - Online Brochure. [Accessed: 28/03/2011]; Available from: http://www.baxi-senertec.co.uk/documents/Sales_brochure_July_2010.pdf

[27] Hawkes, A. and Leach, M. "*Impacts of temporal precision in optimising modelling of micro-Combined Heat and Power"* Energy, 2005. 30: pgs. 1759-1779

[28] Wright, A. and Firth, S. "*The nature of domestic electricity-loads and effects of time averaging on statistics and on-site generation calculations"* Applied Energy, 2007. 84(2007): pgs. 389-403

[29] Lai, S.M. and Hui, C.W. "*Feasibility and flexibility for a trigeneration system"* Energy, 2009. 34: pgs. 1693-1704

[30] Carvalho, M., Serra, L.M. and Lozano, M.A. "*Geographic evaluation of trigeneration systems in the tertiary sector. Effect of climatic and electricity supply conditions"* Energy, 2010. 36(4): pgs. 1931-1939

[31] Macchi, E., Campanari, S. and Silva, P. "*Cap.7 - La Trigenerazione"*, in *La Microcogenerazione a gas naturale*, Polipress, Editor. 2005, Polipress: Milano

[32] Lozano, M.A., Carvalho, M. and Serra, L.M. "*Operational strategy and marginal costs in simple trigeneration systems"* Energy, 2009. 34: pgs. 2001-2008

[33] Khatri, K.K., Sharma, D., Soni, S.L. and Tanwar, D. "*Experimental investigation of CI engine operated micro-trigeneration system"* Applied Thermal Engineering, 2010. 30: pgs. 1505-1509

[34] Wu, J.Y., Huangfu, Y., Wang, R.Z., Kong, X.Q. and Wei, B.H. "*Evaluation and analysis of novel micro-scale combined cooling, heating and power (MCCHP) system"* Energy Conversion and Management 2007. 48: pgs. 1703-1709

[35] Godefroy, J., Boukhanouf, R. and Riffat, S. "*Design, testing and mathematical modelling of a small-scale CHP and cooling system (small CHP-ejector trigeneration)"* Applied Thermal Engineering 2007. 27: pgs. 68-77

[36] Henning, H-M., Pagano, T., Mola, S. and Wiemken, E. "*Micro trigeneration system for indoor air conditioning in the Mediterranean climate"* Applied Thermal Engineering, 2007. 27: pgs. 2188-2194

[37] Fujii, T., Komatsu, T., Nishiguchi, A. and Matsushima, H. "*Dynamic simulation program with object-oriented formulation for absorption chillers (modelling, verification, and application to triple-effect absorption chiller)"* International Journal of Refrigeration 2010. 33: pgs. 259-268

[38] Biezma, M.V. and San Cristóbal, J.R. "*Investment criteria for the selection of cogeneration plants - A state of the art review"* Applied Thermal Engineering, 2006. 26(5-6): pgs. 583-588

[39] Cardona, E. and Piacentino, A. "*A methodology for sizing a trigeneration plant in Mediterranean areas"* Applied Thermal Engineering, 2003. 23: pgs. 1665-1680

[40] Napolitano, A., (2009) "*Trigeneration Systems Assisted by Solar Energy Design Criteria and Off Design Simulations."* Doctoral Thesis in Energy and Environmental Technologies - Faculty of Engineering, Department of Industrial Engineering, University of Bergamo, Bergamo, Italy

[41] Polonara, F., Arteconi, A. and Brandoni, C. "*Distributed generation and trigeneration: Energy saving opportunities in Italian supermarket sector"* Applied Thermal Engineering 2009. 29: pgs. 1735-1743

[42] Khatri, K.K., Sharma, D., Soni, S.L. and Tanwar, D. "*Experimental investigation of CI engine operated Micro-Trigeneration system"* Applied Thermal Engineering, 2010. 30(11-12): pgs. 1505-1509

[43] Angrisani, G., Rosato, A., Roselli, C., Sasso, M. and Sibilio, S. "*Experimental results of a micro-trigeneration installation"* Applied Thermal Engineering, 2012. 38: pgs. 78-90

[44] Lin, L., Wang, Y., Al-Shemmeri, T., Ruxton, T., Turner, S., Zeng, S., Huang, J., He, Y. and Huang, X. "*An experimental investigation of a household size trigeneration"* Applied Thermal Engineering, 2007. 27: pgs. 576-585

[45] Dorer, V. and Weber, A. "*Energy and CO_2 emissions performance assessment of residential micro-cogeneration systems with dynamic whole-building simulation programs"* Energy Conversion and Management, 2009. 50: pgs. 648-657

[46] Kong, X.Q., Wang, R.Z., Wu, J.Y., Huang, X.H., Huangfu, Y., Wu, D.W. and Xu, Y.X. "*Experimental investigation of a micro-combined cooling, heating and power system driven by a gas engine"* International Journal of Refrigeration, 2005. 28: pgs. 977-987

[47] Rocha, M.S., Andreos, R. and Simões-Moreira, J.R. "*Performance tests of two small trigeneration pilot plants"* Applied Thermal Engineering, 2012. 41: pgs. 84-91

[48] Wang, J., Zhai, Z., Jing, Y. and Zhang, C. "*Influence analysis of building types and climate zones on energetic, economic and environmental*

performances of BCHP systems" Applied Energy, 2011. 88(9): pgs. 3097-3112

[49] Kavvadias, K.C., Tosios, A.P., and Maroulis, Z.B. "*Design of a combined heating, cooling and power system: Sizing, operation strategy selection and parametric analysis"* Energy Conversion and Management, 2010. 51: pgs. 833-845

[50] Napolitano, A., Franchini, G., Perdichizzi, A. and Sparber, W. *"Design Criteria for trigeneration systems coupled with solar thermal collectors"*, in *64° Congresso Nazionale ATI*. 2009: L'Aquila, Italy

[51] Dorer, V. and Weber, A. (2007). "*Methodologies for the Performance Assessment of Residential Cogeneration Systems"* - A Report of Subtask C of FC+COGEN+SIM The Simulation of Building-Integrated Fuel Cell and Other Cogeneration Systems: Annex 42 of the International Energy Agency's Conservation in Buildings and Community Systems Programme. International Energy Agency

[52] Beausoleil-Morrison, I. (2008). "*An Experimental and Simulation-Based Investigation of the Performance of Small-Scale Fuel Cell and Combustion-Based Cogeneration Devices Serving Residential Buildings"* - Final Report of FC+COGEN+SIM The Simulation of Building-Integrated Fuel Cell and Other Cogeneration Systems: Annex 42 of the International Energy Agency's Conservation in Buildings and Community Systems Programme. International Energy Agency

[53] Beausoleil-Morrison, I., Mottillo, M., Brandon, R., Sears, P. and Ferguson, A. "*The simulation of a residential space-cooling system powered by the thermal output of a cogeneration system"* in *Proceedings of esim 2004*. Vancouver, Canada

[54] Jeong, S., Kang, B.H. and Karngt, S.W. "*Dynamic simulation of an absorption heat pump for recovering low grade heat"* Applied Thermal Engineering, 1998. 18(1-2): pgs. 1-12

[55] Kim, B. and Park, J. "*Dynamic simulation of a single-effect ammonia-water absorption chiller"* International Journal of Refrigeration, 2007. 30: pgs. 535-545

[56] Shin, Y., Seo, J.A., Cho, H.C, Nam, S.C. and Jeong, J.H. "*Simulation of dynamics and control of a double-effect LiBr–H2O absorption chiller"* Applied Thermal Engineering, 2009. 29: pgs. 2718-2725

[57] Fu, D.G., Poncia G., and Lu, Z. "*Implementation of an object-oriented dynamic modelling library for absorption refrigeration systems"* Applied Thermal Engineering, 2006. 26: pgs. 217-225

[58] *SONNENKLIMA* package solution description - Online Brochure. [Accessed: 15/07/2010]; Available from: http://www.solarcombiplus.eu/docs/D46_SonnenKlima_v02_English.pdf

[59] Volker, C. "*Sonnenklima Suninverse - Solar cooling product information and experience"* in *Derbi Conference*. 2009. Perpignan, France

[60] Stokes, M., (2004) "*Removing barriers to embedded generation: a fine-grained load model to support low voltage network performance analysis."* Doctoral Thesis - Institute of Energy and Sustainable Development, De Montfort University, Leicester, UK

[61] *"ESP-r"*, 2005, Energy Systems Research Unit, Department of Mechanical and Aerospace Engineering, University of Strathclyde Glasgow, UK

[62] McKnight, T.L. and Hess, D. "*Climate Zones and Types: Mediterranean Climate (Csa, Csb)"*, in *Physical Geography: A Landscape Appreciation*. 2007, Prentice Hall: Upper Saddle River, NJ. pgs. 221-223

[63] Malta Resources Authority (2011). "*Malta 2nd National Energy Efficiency Action Plan"* - Malta Resources Authority, Marsa, Malta. [Accessed 17/12/2011]; Available from: http://ec.europa.eu/energy/efficiency/doc/mt_-_energy_efficiency_action_plan_en.pdf

CHAPTER 2
MODELLING OF HEAT AND POWER DEMANDS

Chapter overview

This chapter explains the methodology used to model the thermal and electrical energy demands of a building. Specifically, this chapter serves to (1) explain some basic aspects of the building simulation tool ESP-r; (2) provide a short explanation of how the demand side was modelled using ESP-r; and, (3) explain how the different operating conditions which affect the demand side of the system were factored into the modelling.

2.1 Modelling residential demand - Characterisation of a building through its energy requirements

The energy demand of a residential building can be divided into two basic categories, the electrical and thermal demands. The electrical demand relates to the aggregated electrical load of appliances and lighting, whilst the thermal demand accounts for the energy demand for water heating and space conditioning. In the latter case, the energy required for space heating and/or cooling is the result of multiple drivers (*e.g.* climate, building characteristics, shading, internal heat gains, solar gains *etc*.), some of which are interrelated and dependent on one another.

The use of a whole building, dynamic simulation tool such as ESP-r [1] is an appropriate means to calculate these energy demands, in that, it can be used to generate demand data whilst accounting for the temporal interactions between climate, the building fabric, the building occupants and the energy systems (both thermal and electrical). Before going into detail explaining how demand data is obtained, the next section briefly explains the modelling process adopted when using ESP-r [1]. The section also gives specific details as to how the various inputs and outputs required for analysis of trigeneration systems were obtained.

2.2 The building simulation tool ESP-r

As discussed in Chapter 1, the building simulation tool used in this research is the energy modelling tool ESP-r. Various studies (*e.g.* [2-4]) explain the concepts underpinning ESP-r, including more in-depth explanations of the control volume principle used by the tool to model building and plant systems. Hence, what follows is a brief overview of the basic concepts and fundamental principles, which will enable the reader to follow the model development and modelling activities described in subsequent sections.

2.2.1 A quick user guide to modelling combined building and plant systems using ESP-r

Figure 2.1 shows a simplified ESP-r input and output process. Similarly to other building simulation tools, ESP-r permits the modelling of complex buildings and the

associated plant systems by simply defining a series of design aspects such as climate, model location (latitude and longitude), building characteristics (geometry, fabric, shading and internal heat gains), HVAC plant networks, plant system control schemes *etc*.

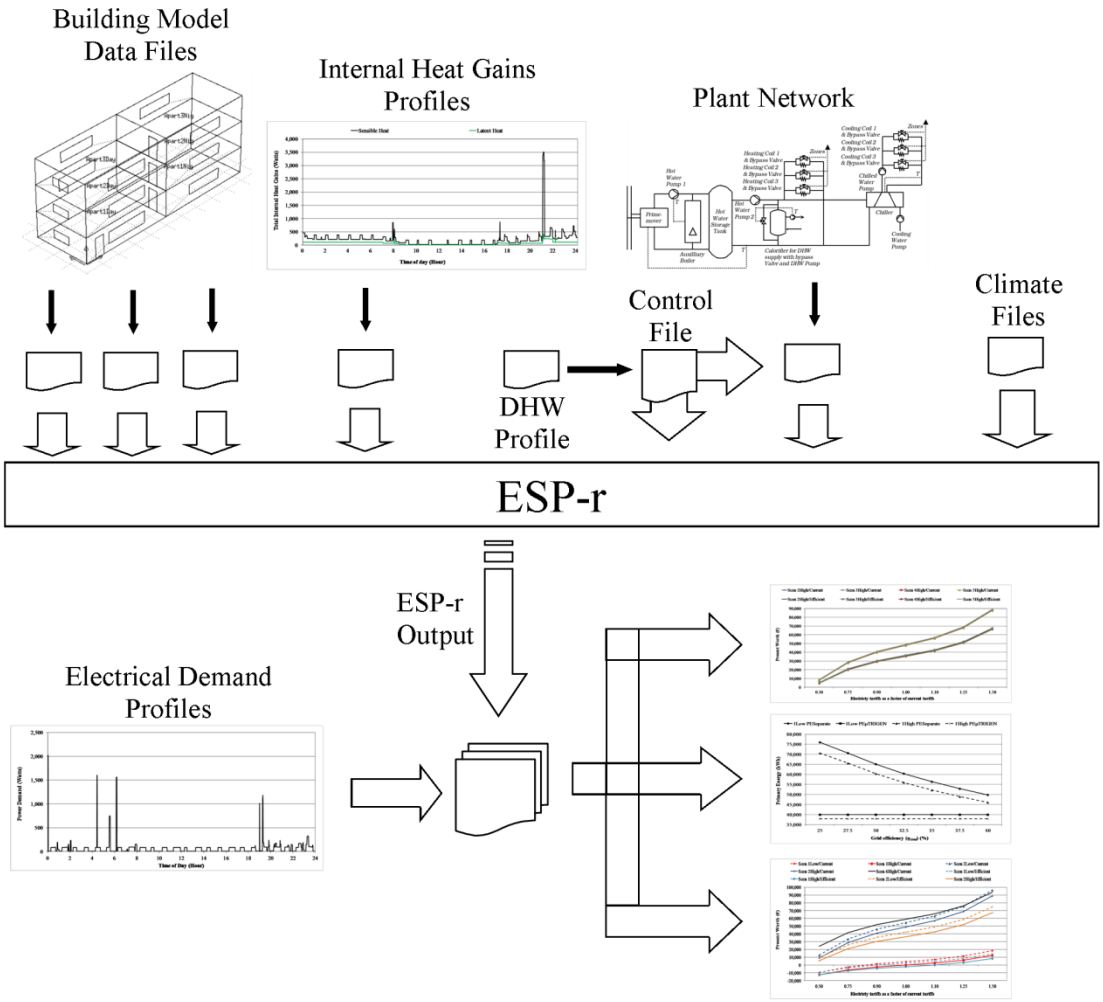

Fig. 2.1 - ESP-r input and output process

The first aspect in modelling using ESP-r involves modelling the building structure by supplying details regarding the building geometry, location, orientation, surrounding environment, building fabric and shading. Once the building structure is fully defined the user is then required to characterize the internal heat gains inside the building. This can be done either through a coarse hourly pre-set template or else through a more elaborate system which requires ESP-r to access external data containing information on the internal heat gains; this permits the use of finer 1

minute resolution data. The research in this thesis uses this latter approach as explained in Section 2.5.4.

If the building simulation is to be complemented, as it is in this case, with an integrated HVAC model, then the user is also required to describe the HVAC plant system. This is done in a similar fashion as if this was being done in real-life that is, by specifying the duct work for ventilation and pipe work for cooling and heating systems, listing plant components *etc*. The plant network description apart from containing data and specifications about the individual plant components selected also includes details of how these are linked together and to the building. In order to control the HVAC plant, a user is also required to impose a control scheme which controls the individual HVAC components. A more detailed description of modelling plant networks in ESP-r can be found in Chapter 3.

Other inputs (not shown in Figure 2.1) such as the detailed modelling of infiltration and ventilation through the building apertures can also be included in ESP-r to simulate for natural ventilation processes. In this thesis this aspect was not modelled explicitly as the source of ventilation inside the building was through a mechanically driven air conditioning system. Especially during summer when the outside mean temperature is predominantly at (or exceeds) 25ºC [5], the use of natural ventilation for cooling is not enough and temperature controlled forced means of ventilation becomes necessary. As briefly mentioned in Chapter 1, and as later on explained in Chapter 6, the introduction of future intelligent building management systems might bring a change in this context, with air conditioning systems working in tandem with natural ventilation becoming a popular option.

Once all the data required to represent the desired model is prepared, different simulations may be run using a desired time-step for a pre-determined time duration. As discussed in Chapter 1, for residential building modelling, especially those involving electrical imports/exports, typically a high resolution time-step of 1 minute is required. Each simulation period was run for a period of 1 week during representative weeks of the year as explained in Chapter 4.

On completion of a simulation, the output data from that simulation can either be viewed using a dedicated ESP-r module or else exported as a text file for further post-processing and analysis. In this research this latter method was used as some of the simulation output data was used together with the electrical demand profiles modelled to provide the resulting micro-trigeneration performance metrics.

2.3 Modelling the building

When modelling a building in ESP-r, a user is required to define a number of characteristics. The first task is that of defining the building geometry; this is typically defined as a number of zones or spaces, with each zone representing a single or multiple rooms. For each zone, walls and windows are defined in ESP-r as a series of linked vertices and surfaces based on a Cartesian co-ordinate system. The surrounding environment of each wall and window is specified by declaring whether that surface (wall or window) is an external surface, or an internal surface linking two zones *etc.* Finally the building model is completed by denoting the building fabric. Modelling building fabric using ESP-r relies on specifying the individual characteristics of the different materials making up a construction. Each construction can be modelled and represented using multiple layers. An insulated double leaf wall for example is modelled by defining the characteristics (thickness, density, thermal conductivity *etc*.) of the three material layers (the external wall, the internal wall and the insulation) making up the wall component. The basic geometry can be augmented with additional details where applicable such as adding external shading.

The process is demonstrated below, where a Maltese multi-family residence to be used in later simulations is defined. Although figures published in the latest available national Census [6] show that terraced houses still constitute a large part of the residential buildings in Malta (35.7% of the total), in recent years this figure has experienced a declining trend in favour of maisonettes, flats and penthouses. The building shown in Figure 2.2 therefore tries to capture features of the latter more modern types of dwellings.

2.3.1 Example: specifying the building geometrical features for a typical Maltese multi-family residence

Figure 2.2 shows the basic geometrical features of a Maltese building [7] modelled in ESP-r. The building has a total living floor space of about 360m^2, 120m^2 per floor, slightly higher than the average household size in Malta of 103m^2 reported by Abela *et al.* in [8]. The building is representative of new residential building complexes currently being built and in this case was modelled to represent a building abutting an adjacent building on the east side and extensive parts of the north side (shown in bold in Figure 2.2). Compared to more traditional buildings in Malta (where vapour compression split packaged units would be the preferred choice), these type of buildings would be more apt to include a micro-trigeneration system, especially considering the high occupancy of the building (large number of apartments) and the fact that some of the buildings would already have a centralised HVAC system.

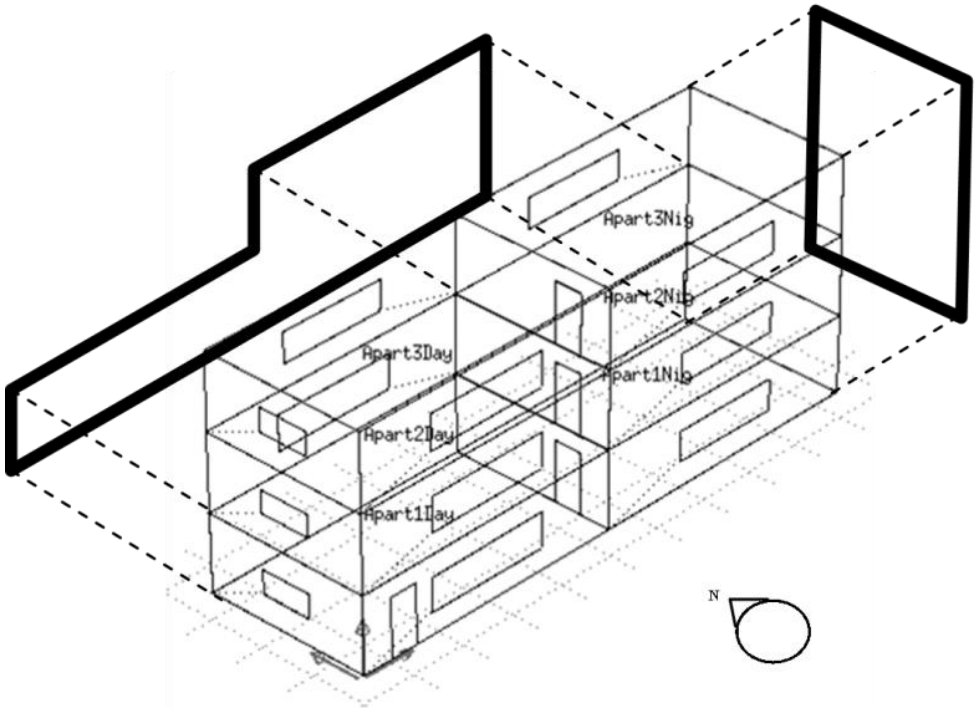

Fig. 2.2 - External view of the building model [7]

Windows sizes used in the building were based on the recommendations listed in the *Technical Guidance - Conservation of Fuel, Energy and Natural Resources* [9], the minimum requirements set for energy performance of buildings in Malta - the

maximum allowable size of glazing for west facing sides is of 9% of the total side, 20% for south facing sides and 25% for north facing sides.

Each floor was modelled to constitute (in terms of its electrical and thermal demand) an individual apartment housing a single household. The ground floor apartment housed a 2 person household, the middle floor housed a 3 person household and the top floor housed a 4 person household; with just under 70% of the total number of private households in Malta, the three sizes of household selected are the most common type of households in Malta [10]. Details of how the electrical demand and the internal heat gains were represented for the differently sized households are given in Section 2.4 and Section 2.5.

To facilitate the modelling procedure, each apartment was modelled using a two zone representation, such that each zone represented the aggregated internal space of a particular set of rooms. For all floors, the south/west facing zone represented the living area zone, grouping together the living room and kitchen for that particular apartment. Conversely, facing south/east was the bedroom area zone, grouping together the bedrooms of each respective apartment. As discussed by ASHRAE in [11] it is customary that when considering space conditioning in residential buildings, multiple rooms are grouped as a single zone. This facilitates not only the modelling side but also the thermal control of the building.

Table 2.1 gives the individual dimensions of the different zones, showing also which sides had externally exposed faces and glazing. Also shown is the number of occupants per floor. Length and width were chosen arbitrarily (based on the floor space) whilst the height is the minimum height for habitable conditions set by the Maltese Environment and Planning Authority [12].

For the summer simulations the building was modified to include for shading in the form of external louvers. The louvers were modelled so as to cover about 70% of the aperture. This is typical of shading devices used in Mediterranean climates [13].

Table 2.1 - Dimensions of the modelled building

Total floor dimensions: length 20m; width 6m; height 2.75m

Zone (Floor)	Number of Occupants	Externally exposed walls area (m^2)					Glazed area (m^2)				
		South	West	North	East	Total	South	West	North	East	Total
Ground Floor (GF)	2										
Living Area		22.0	15.0	0.0	0.0	37.0	5.5	1.5	0.0	0.0	7.0
Bedroom Area		22.0	0.0	0.0	0.0	22.0	5.5	0.0	0.0	0.0	5.5
Middle Floor (MF)	3										
Living Area		22.0	15.0	20.6	0.0	57.6	5.5	1.5	6.9	0.0	13.9
Bedroom Area		22.0	0.0	0.0	0.0	22.0	5.5	0.0	0.0	0.0	5.5
Top Floor (TF)	4										
Living Area		22.0	15.0	20.6	0.0	57.6	5.5	1.5	6.9	0.0	13.9
Bedroom Area		22.0	0.0	20.6	0.0	42.6	5.5	0.0	6.9	0.0	12.4
Total Building	9	132.0	45.0	61.9	0.0	238.9	66.0	8.9	41.3	0.0	58.1

2.3.2 Enlarged three storey building to represent 6 household building

One of the operating conditions mentioned in Chapter 1 as having a potential impact on micro-trigeneration performance is building size and occupancy. An increased dwelling size and a larger number of occupants directly effects the operational time of a residentially installed micro-trigeneration system and therefore may have an important influence on its performance and feasibility.

To address these two operating conditions and help assess their impact on the micro-trigeneration system performance, a second larger building housing 6 households was modelled. Rather than going through the whole process of adding additional zones, a more pragmatic approach was adopted were, the height of each floor in this enlarged building model was doubled (the spatial volume for each floor was hence doubled from $330m^3$ to $660m^3$) to represent the volume taken by two apartments rather than one. Each floor of the enlarged building was thus modelled to represent two apartments rather than one, with intervening floors modelled as an additional thermal mass. The length and width of the building and the glazing-to-wall ratio

were not modified. Figure 2.3 shows the enlarged 6 household building model.

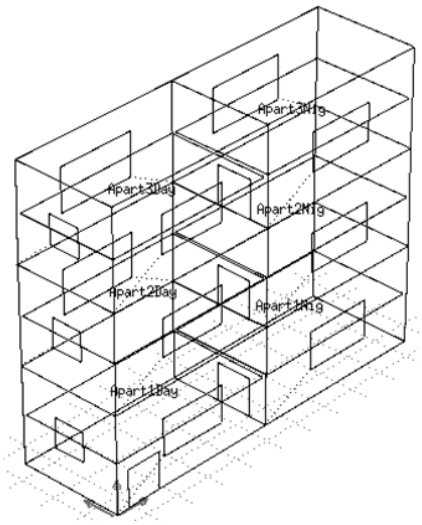

Fig. 2.3 - The enlarged 6 household building model

Table 2.2 summarises the individual dimensions of the different zones of the enlarged 6 household building, as well as the increased occupancy for each floor.

Table 2.2 - Dimensions of the enlarged modelled building

Total floor dimensions: 20m; width 6m; height 5.5m

Zone (Floor)	Number of Occupants	Externally exposed walls area (m^2)					Glazed area (m^2)				
		South	West	North	East	Total	South	West	North	East	Total
Ground Floor (GF)	5										
Living Area		44.0	30.0	0.0	0.0	74.0	11.0	3.0	0.0	0.0	14.0
Bedroom Area		44.0	0.0	0.0	0.0	77.0	11.0	0.0	0.0	0.0	11.0
Middle Floor (MF)	7										
Living Area		44.0	30.0	41.3	0.0	115.3	11.0	3.0	13.8	0.0	27.7
Bedroom Area		44.0	0.0	0.0	0.0	44.0	11.0	0.0	0.0	0.0	11.0
Top Floor (TF)	6										
Living Area		44.0	30.0	41.3	0.0	115.3	11.0	3.0	13.8	0.0	27.7
Bedroom Area		44.0	0.0	41.3	0.0	85.3	11.0	0.0	13.8	0.0	24.8
Total Building	18	264.0	90.0	123.8	0.0	477.8	66.0	8.9	41.3	0.0	116.2

In this second enlarged building, the number of occupants doubled from 9 to 18. The ground floor apartment was in this case adapted to represent the 2 person household modelled in the 3 household building plus an additional 3 person household. The middle floor apartment was modified to represent the 3 person household modelled in the 3 household building plus an additional 4 person household. Finally, the top floor apartment was altered to represent the 4 person household modelled in the 3 household building plus an additional 2 person household.

The internal heat gains and the electrical demand load profiles of each floor were similarly transformed in such a way as to represent the profiles of two households rather than one household. This was done by aggregating the individual profile of two households into one profile. A more detailed analysis of the method used to aggregate the electrical demand load profile and the internal heat gains is given in Section 2.4 and Section 2.5, respectively.

2.3.3 Building fabric

As discussed in various studies including those by Tejedor *et al.* in [14], Anastaselos *et al.* in [15], D'Orazio *et al.* in [16], Nikolaidis *et al.* in [17], the type of building fabric used in a building plays an important part in improving its energy-efficiency. For this reason another important operating condition which needs to be considered when assessing micro-trigeneration performance in residential buildings is the type of building fabric.

Section 2.3.3.1 and Section 2.3.3.2 describe the two sets of building fabric scenarios modelled in order to assess the influence of such an operating condition on residential micro-trigeneration performance, specifically in relation to energy performance improvements.

Section 2.3.3.1 describes a *low efficiency building fabric scenario* representative of poorly insulated fabric. As discussed by Buhagiar in [18] and Tejedor *et al.* in [14] this can be considered as representative of most of the existing Maltese housing stock.

Section 2.3.3.2, on the other hand, describes a *high efficiency building fabric scenario* representative of well insulated fabric, satisfying the minimum local legal requirements set by the *Technical Guidance - Conservation of Fuel, Energy and Natural Resources* [9], and which applies to all new buildings and buildings with a floor space area in excess of 1,000m^2 undergoing major renovation as required by the EPBD [19].

2.3.3.1 Modelling the low efficiency fabric scenario

The high premium for living space in Malta, the scarcity and cost of natural building resources [18] and a perceived mild climate [8] has unfortunately led to a situation where for a long period of time the efficient use of energy in space heating and cooling was not a priority compared to providing relatively cheap accommodation. It is important to stress that when most of the existing building stock was built, enforcement of the minimum building requirements was scarce [18] and it is therefore very difficult to state with certainty what type of fabric was used for most of the existing housing stock.

Nonetheless Buhagiar in [18] and Tejedor *et al.* in [14] give a reasonably detailed account of what were the typical building standards used with regards to building materials in Malta. Table 2.3 lists the main features of the building fabric used to model the low efficiency fabric scenario used in the simulations. The list includes material thickness, thermal conductivity, physical layout description and the total calculated U-Value of the construction fabric.

External walls are distinguished between south facing and other external exposed walls on the basis that, although all external walls should have been built with double walls, anecdotally only the primary external façade was typically constructed using double walls.

The recommended maximum U-Value set by the *Technical Guidance - Conservation of Fuel, Energy and Natural Resources* [9] are listed for comparison.

Table 2.3 - Main characteristics of the low efficiency building fabric scenario

Item	Features and characteristics	Comments
South façade exposed external walls	Double skinned wall with external 230mm thickness soft limestone block (1.1 W/mK) and internal 150mm thickness concrete block (1.13 W/mK) with interstitial 10mm cavity between blocks. Internally finished with a 12.5mm gypsum plaster board (0.19 W/mK). **Total U-Value - 1.194 W/m^{2}K**	Recommended maximum U-Value 1.57 W/m^{2}K.
Exposed external walls facing other directions	Single skinned 230mm thickness external concrete block (1.13 W/mK) with internal 12.5mm gypsum plaster board (0.19 W/mK). **Total U-Value - 1.889 W/m^{2}K**	Recommended maximum U-Value 1.57 W/m^{2}K.
Adjacent bounded walls	Single skinned 230mm thickness external concrete block (1.13 W/mK) with internal 12.5mm gypsum plaster board (0.19 W/mK). **Total U-Value - 1.889 W/m^{2}K**	Recommended maximum U-Value 1.57 W/m^{2}K.
Internal dividing walls	Single skinned 150mm thickness concrete block (1.13 W/mK) in between two layers of 12.5mm gypsum plaster board (0.19 W/mK). **Total U-Value - 1.907 W/m^{2}K**	Not specified
Roof	150mm thickness 2% steel reinforced concrete (2.5 W/mK). Externally covered with a 100mm thickness layer of crushed limestone (0.8 W/mK) and a 75mm thickness lean concrete mix (0.38 W/mK). Externally finished with a 4mm thickness dark coloured roof felt (0.23 W/mK) having solar absorption of 0.9. Internally finished with a 12.5mm thickness ceiling gypsum board (0.21 W/mK). **Total U-Value - 1.390 W/m^{2}K**	Recommended maximum U-Value 0.59 W/m^{2}K.
Intermediate ceilings	150mm thickness 2% steel reinforced concrete (2.5 W/mK) covered on one side with a 50mm thickness layer of crushed limestone (0.8 W/mK), a 50mm thickness lean concrete mix (0.38 W/mK) and a 6mm tile (0.85 W/mK). On the other side finished with a 12.5mm thickness ceiling gypsum board (0.21 W/mK). **Total U-Value - 1.722 W/m^{2}K**	Recommended maximum U-Value 1.57 W/m^{2}K.
Glazing	6mm single glass pane. **Total U-Value - 3.733 W/m^{2}K**	Recommended maximum U-Value 5.8 W/m^{2}K.

2.3.3.2 Modelling the high efficiency fabric scenario

A standard model of high efficiency building fabric for Maltese residential buildings does not exist. A good starting point is as already discussed the *Technical Guidance - Conservation of Fuel, Energy and Natural Resources* [9], which lists the minimum requirements with respect to the individual U-Values of the different building parts, roof, walls, glazing *etc*.

Another good source of information is Buhagiar [20, 21] who addressed different aspects of improving the thermal envelope of Maltese buildings. However, a particularly relevant piece of work was that done by Buhagiar and Yousif in [22] who provide a post occupancy evaluation of the energy-efficiency measures in a prototype low-carbon building in Malta, shown in Figure 2.4, with integrated building fabric improvement measures and renewable energy systems.

Fig. 2.4 - Energy efficient housing project discussed by Buhagiar and Yousif in [22]

The study examined the measures deployed (*e.g.* roof installed photovoltaic and solar water heating systems, insulated double walls, external louvers for shading, insulated roof *etc.*) and gave preliminary results in terms of quantified energy savings of the individual measures for the whole building.

Based on the recommendations listed in these sources, Table 2.4 lists the main features of the building fabric used to model the high efficiency fabric used in the simulations.

Table 2.4 - Main characteristics of the high efficiency building fabric scenario

Item	Features and characteristics	Comments
South façade exposed external walls	Double skinned wall with external 230mm thickness soft limestone block (1.1 W/mK) and internal 150mm thickness concrete block (1.13 W/mK) with interstitial 50mm Expanded Polystyrene Board (0.03 W/mK) between blocks. Internally finished with a 12.5mm gypsum plaster board (0.19 W/mK). **Total U-Value - 0.428 W/m^{2}K**	Recommended maximum U-Value 1.57 W/m^{2}K.
Exposed external walls facing other directions	Double skinned wall with external 230mm thickness soft limestone block (1.1 W/mK) and internal 150mm thickness concrete block (1.13 W/mK) with interstitial 50mm Expanded Polystyrene Board (0.03 W/mK) between blocks. Internally finished with a 12.5mm gypsum plaster board (0.19 W/mK). **Total U-Value - 0.428 W/m^{2}K**	Recommended maximum U-Value 1.57 W/m^{2}K.
Adjacent bounded walls	Single skinned 230mm thickness external concrete block (1.13 W/mK) with and internal 12.5mm gypsum plaster board (0.19 W/mK) with interstitial 10mm Expanded Polystyrene Board (0.03 W/mK) between layers. **Total U-Value - 1.159 W/m^{2}K**	Recommended maximum U-Value 1.57 W/m^{2}K.
Internal dividing walls	Single skinned 150mm thickness concrete block (1.13 W/mK) in between two layers of 12.5mm gypsum plaster board (0.19 W/mK). **Total U-Value - 1.907 W/m^{2}K**	Not specified
Roof	150mm thickness 2% steel reinforced concrete (2.5 W/mK). Externally covered with 180mm thickness roof insulation board (0.19 W/mK), a 100mm thickness layer of crushed limestone (0.8 W/mK) and a 75mm thickness lean concrete mix (0.38 W/mK). Externally finished with a 12mm thickness white coloured roof felt (0.23 W/mK) having solar absorption of 0.5. Internally finished with a 12.5mm thickness ceiling gypsum board (0.21 W/mK). **Total U-Value - 0.588 W/m^{2}K**	Recommended maximum U-Value 0.59 W/m^{2}K.
Intermediate ceilings	150mm thickness 2% steel reinforced concrete (2.5 W/mK) covered on one side with a 50mm thickness roof insulation board (0.19 W/mK), a 50mm thickness layer of crushed limestone (0.8 W/mK), a 50mm thickness lean concrete mix (0.38 W/mK) and a 6mm tile (0.85 W/mK). On the other side finished with a 12.5mm thickness ceiling gypsum board (0.21 W/mK). **Total U-Value - 1.185 W/m^{2}K**	Recommended maximum U-Value 1.57 W/m^{2}K.
Glazing	12mm thick air filled double glazing with 6mm glass having low emissivity properties. **Total U-Value - 2.265 W/m^{2}K**	Recommended maximum U-Value 5.8 W/m^{2}K.

2.3.4 Use of the building models developed

The various combinations considered were developed in ESP-r to create a number of

thermal scenarios (*e.g.* 3 household building with low efficiency building fabric, 3 household building with high efficiency building fabric, 6 household building with low efficiency building fabric *etc.*). These were then linked with the plant network and used together with the other design elements (*e.g.* electrical efficiency of household appliances *etc.*) to assess the individual effects of each parameter on micro-trigeneration performance.

2.4 Modelling the electrical demand

It has already been discussed how the electrical demand in residential households is of a very variable nature with short instantaneous peak demands separated by periods of very little demand. In studies relating to micro-trigeneration in residential buildings high temporal resolution is therefore an important requirement [23, 24]. It has also already been mentioned that increased energy-efficiency caused by an increased penetration of high efficiency appliances, could lead to a lower demand impacting the performance of a micro-trigeneration system.

In order to address these issues, this chapter aims to explain the tool and method developed to generate high resolution seasonal daily electrical demand profiles for differently occupied households accounting for different electrical appliances (and lighting) efficiency scenarios: a *current efficiency electrical scenario* based on current appliances' efficiencies and a future *high efficiency electrical scenario* based on the expected best future available technology. The approach is also described in more details by Borg and Kelly in [25].

Electrical demand was treated separately from the main ESP-r analysis, with the profiles used as part of a post-simulation process aimed at calculating the micro-trigeneration performance metrics. A more detailed explanation of the method used is given in Chapter 4.

2.4.1 Method of profile generation - Overview

The modelling of domestic electrical demands uses a combination of appliance data, end-use energy surveys and a customised stochastic model to generate high

resolution demand data for individual appliances. The model is calibrated using data from the REMODECE energy end-use measuring campaign [26], which was an EU funded project conducted in a number of European countries between 2006 and 2008. The data consisted of both real field measurements and questionnaires returns.

The approach adopted for the generation of electrical demand profiles in this thesis is similar to that described by Stokes [27], Richardson *et al.* [28] and Widen and Wäckelgård [29, 30]. For example, Richardson *et al.* utilise demand data generated using UK 'time-use' survey data [31]; 'time-use surveys' are detailed diaries kept by individuals recording their activities on a daily basis at 10 minute intervals. This data is then manipulated to produce minute resolution electrical demand profiles [28]. The approach adopted in this thesis uses one-hour resolution electrical demand data derived from field monitoring as the starting point. Additionally, the calculation of the detailed demand profile is augmented with a means to adapt the high-resolution profile based on future estimations of improvements in appliances' energy-efficiency; this allows detailed profiles to be generated for future high efficiency scenarios. The generation of these future high efficiency demand profiles is done on an appliance-by-appliance basis; a profile for each appliance is generated and the population of appliance profiles can then be aggregated to give a high-resolution electrical demand profile for the dwelling. An important clarification is that although reference is being made to appliances, in a broader sense the term also encompasses lighting.

The REMODECE Italian dataset consists of measurements done in 60 households. No similar Maltese dataset exists and although the REMODECE study contains more populous datasets from other countries, the Italian dataset was chosen as being the most relevant and representative for the study, given Italy's geographical proximity and cultural influence to Malta. Data was collected for the most energy intensive appliances and the 10 most used lamps [32]. In total, 778 different one-day appliance profiles were available from the REMODECE project at one-hour resolution as described in Section 2.4.2.1. Additional measurements were also taken across the main switchboard to measure the overall household electrical energy consumption. The energy consumption for each appliance and each hour was then averaged over

the measuring period (2 weeks) to create one representative daily profile of energy demand at an hourly time resolution representative of the whole month for each appliance monitored; these are the base profiles to which the transformation process described below is applied.

2.4.2 Explaining the methodology – A three stage-process

The generation of synthetic, high resolution electrical demand data profiles for a particular appliance type consists of a 3-stage transformation process, shown schematically in Figure 2.5.

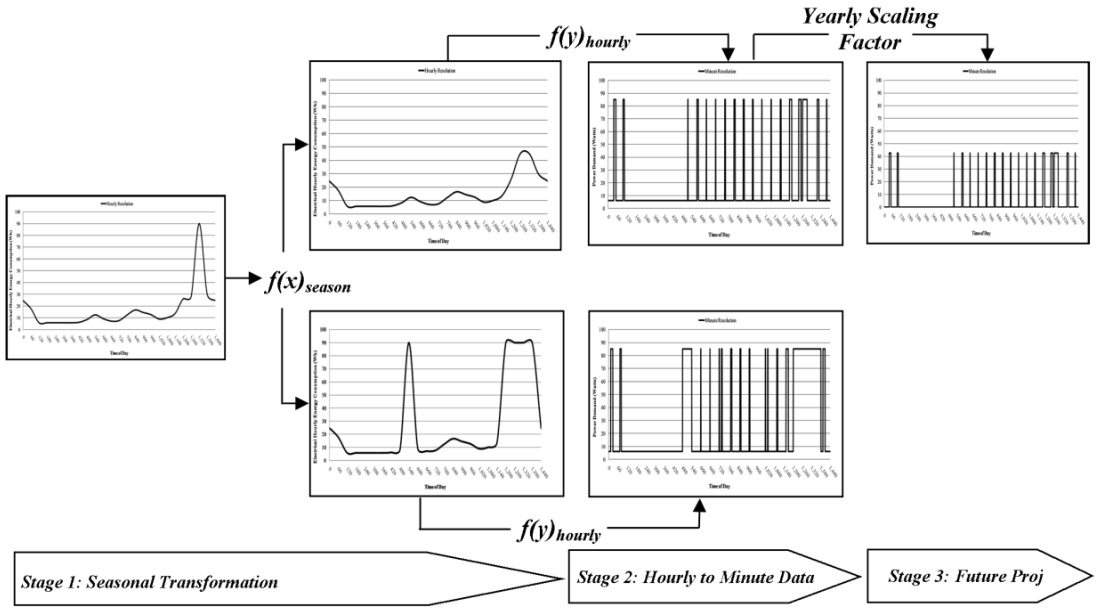

Fig. 2.5 - The three stage approach

Using a single REMODECE 1-day, hourly resolution appliance profile as a starting point, 12 day-long profiles (one for each month of the year) at 1-minute resolution are generated, that can also incorporate the effects of future appliances' energy-efficiency improvements. The specifics of the three stage process are as follows:

- ***Stage 1*** – using one of the REMODECE datasets of a single appliance (comprising 1-day hourly resolution demand data for a single month of the year) as a starting point, the first transformation generates 12, 1-day hourly resolution profiles, one for each month. This is achieved by applying a modifier function to

the original data (see equation 2.1); this modifier is partly a time-dependent sinusoidal function and partly a random number. The equation's constant, amplitude, phase and standard deviation of the modifier function are calibrated from a statistical analysis of all of the available REMODECE data for the specific appliance type. Therefore, stage 1 extrapolates a 1-day dataset representative of one month of the year, to 12 1-day datasets spanning the full calendar year.

- ***Stage 2*** – the 12 datasets from stage 1 are then used to produce 12 day-long 1-minute resolution datasets for the appliance type; this creates finer resolution and a more variable profile that better represents the variability inherent in real electrical demands.

- ***Stage 3*** – applies the effects due to appliance energy-efficient improvements to the profiles. Stage 3 can be applied either to Stage 1 (hourly resolution) or Stage 2 (1-minute resolution) results as discussed later in Section 2.4.2.3.

The overall result of the three transformation process is therefore to obtain high-resolution minute long profiles representative of the changes brought about by the change-over to more energy-efficient appliances from coarse resolution appliance hourly datasets. An in-depth analysis of the individual stages follows in sections 2.4.2.1 to 2.4.2.3.

2.4.2.1 Stage 1 - Introducing monthly variation

Similar to other end-use measurement campaigns, one limitation of the REMODECE datasets was that only two weeks' worth of demand data was collected for each household [33] and in most cases only data for one specific month was available per household. In order to obtain a full set of monthly variation in electrical energy consumption for each individual appliance in the analysed households, a procedure similar to that adopted by Stokes in [27] was used. The procedure relies on scaling a single appliance's representative monthly profile using a seasonally-dependent modifier; enabling the generation of a whole-year dataset that incorporates seasonal variations in electrical energy consumption. The coefficients of the modifier which,

as described by Stokes, follows a sinusoidal trend coupled with some random 'noise' were obtained using the following procedure.

The original REMODECE Italian datasets for each appliance were first grouped by appliance type and then sorted on a per month basis as represented by the left hand side matrix shown in Figure 2.6. Given the different appliances' ownership rates, frequency of use and operating behaviour (repetitive/cyclic, such as in the case of refrigerators or single events, such as washing machines), multiple sets of hourly data were available for each month for the most commonly owned, frequently used or repetitive/cyclic behaviour appliances such as refrigerators (32 datasets), electronic equipment (27 datasets), televisions (32 datasets), lighting (600 datasets) and water heaters (17 datasets). Conversely, for the other less commonly owned, less used single event appliances such as dish washers (12 datasets), microwave ovens (12 datasets), electric ovens (12 datasets) and washing machines (34 datasets) the data available was mostly enough to produce just one single data entry for each individual month. This effectively resulted in a situation whereby, as discussed in the verification process, the results derived from the methodology described in Stage 1 were most accurate for the former type of appliances.

$$\begin{bmatrix} Hour_1, Month_1 & Hour_2, Month_1 & \dots & Hour_{24}, Month_1 \\ Hour_1, Month_2 & Hour_2, Month_2 & \dots & Hour_{24}, Month_2 \\ \vdots & \vdots & & \vdots \\ Hour_1, Month_{11} & Hour_2, Month_{11} & \dots & Hour_{24}, Month_{11} \\ Hour_1, Month_{12} & Hour_2, Month_{12} & \dots & Hour_{24}, Month_{12} \end{bmatrix}_{App(z)} \rightarrow \begin{bmatrix} \frac{Hour_1, Month_1}{Max(Hour_1, Month_n)} & \frac{Hour_2, Month_1}{Max(Hour_2, Month_n)} & \dots & \frac{Hour_{24}, Month_1}{Max(Hour_{24}, Month_n)} \\ \frac{Hour_1, Month_2}{Max(Hour_1, Month_n)} & \frac{Hour_2, Month_2}{Max(Hour_2, Month_n)} & \dots & \frac{Hour_{24}, Month_2}{Max(Hour_{24}, Month_n)} \\ \vdots & \vdots & & \vdots \\ \frac{Hour_1, Month_{11}}{Max(Hour_1, Month_n)} & \frac{Hour_2, Month_{11}}{Max(Hour_2, Month_n)} & \dots & \frac{Hour_{24}, Month_{11}}{Max(Hour_{24}, Month_n)} \\ \frac{Hour_1, Month_{12}}{Max(Hour_1, Month_n)} & \frac{Hour_2, Month_{12}}{Max(Hour_2, Month_n)} & \dots & \frac{Hour_{24}, Month_{12}}{Max(Hour_{24}, Month_n)} \end{bmatrix}_{App(z)}$$

Fig. 2.6 - Grouping and normalisation of the original datasets

For each grouped appliance dataset, each column in the left hand side matrix was then divided by the highest occurring row value in that column, effectively normalising the hourly electrical energy consumption values by the maximum consumption value recorded during that hour (contained in the original dataset). As discussed by Stokes in [27], the maximum rather than the average is used as this is the common practice in the electrical industry. Normalising gives a flexible, dimensionless hourly value that can be scaled to represent variations in demand over

the course of a year. The end result of this normalisation process, are the columns present in the right hand side matrix in Figure 2.6, which represent the normalised hourly consumption values.

Once calculated, each column in the right hand side matrix was then used to find the coefficients of the general trend described in equation (2.1) for each individual $Hour_{(ho)}$. Having been normalised all terms in equation (2.1) are dimensionless.

$$\boldsymbol{e_{App(z),Month(mo),Hour(ho)}} = \boldsymbol{\psi_{ho} + Amp_{ho} \sin\left(2\pi * \left(\frac{Month_{(mo)}}{12}\right) + \varphi_{ho}\right) + Rand(-\sigma_{STDEVho}, \sigma_{STDEVho})} \quad \text{- (2.1)}$$

Equation (2.1) describes the normalised electrical energy consumption, $\boldsymbol{e_{App(z),Month(mo),Hour(ho)}}$, for a specific domestic appliance ***App(z)*** during $\boldsymbol{Hour_{(ho)}}$ of $\boldsymbol{Month_{(mo)}}$. As discussed by Stokes [27], this is made up of three parts. A constant $\boldsymbol{\psi_{ho}}$; a sinusoidally varying component with amplitude $\boldsymbol{Amp_{ho}}$ and phase angle $\boldsymbol{\varphi_{ho}}$ and a third part made up of a random 'noise' value. The constant ψ_{ho}, amplitude A_{ho} and phase angle φ_{ho} for each individual $Hour_{(ho)}$ were obtained by applying a simplified curve fitting algorithm to the values contained in each individual column present in the right hand matrix of Figure 2.6 (normalised values of each hour set $Hour_{(ho)}$,$Month_{(1)}$, $Hour_{(ho)}$,$Month_{(2)}$,…., $Hour_{(ho)}$,$Month_{(12)}$ *etc.*) [34], effectively calibrating equation (2.1) for each individual $Hour_{(ho)}$. The random value added in the third part of the equation was obtained by using a uniformly distributed selection to select a value from a range comprising $\boldsymbol{\sigma_{STDEVho}}$ and $\boldsymbol{-\sigma_{STDEVho}}$, the standard deviation value calculated for the values contained in each column present in the right hand side matrix of Figure 2.6 (normalised values of each hour set $Hour_{(ho)}$,$Month_{(1)}$, $Hour_{(ho)}$,$Month_{(2)}$,…., $Hour_{(ho)}$,$Month_{(12)}$ *etc*.).

Equation (2.1) differs from that proposed by Stokes in [27] in two ways. Firstly, given that the monitored data was only available as a profile representing one day of each month, the variations in appliance hourly electrical energy consumption were calculated on a monthly basis (Stokes applies the calculation on a daily basis).

However, this can be changed if more than one daily profile is available for each appliance for each month. Secondly, given that the standard deviation was being calculated from a relatively small dataset, choosing a random value using a normal distribution as suggested by Stokes from such a small sample might not have given representative results. For this reason in this particular case the random 'noise' was selected using a uniform distribution. Nonetheless, the results obtained and the subsequent verification of the approach discussed in Section 2.4.3 confirm that such minor differences do not invalidate the method or the results obtained.

For each appliance, the end result was an hourly list of dimensionless factors which when applied in equation (2.1) give the trend in demand followed by that particular appliance for each of the 24 hours at any time of the year. Table 2.5, shows some of the factors calculated for a refrigerator. Appendix 'A' lists the factors calculated for all investigated appliances.

Table 2.5 - Factors for seasonal variation equation for a refrigerator (Dimensionless)

$Hour_{(ho)}$	**Constant** (ψ_{ho})	**Amplitude** (Amp_{ho})	**Sine Phase** (φ_{ho})	**Standard Deviation** ($\sigma_{STDEVho}$)
[0,1]	0.264	-0.072	0.818	0.079
[1,2]	0.288	-0.071	0.540	0.069
:	:	:	:	:
[22,23]	0.230	-0.064	0.816	0.079
[23,24]	0.218	-0.068	1.020	0.086

Once the factors were obtained for each individual appliance, the original datasets could be scaled to include for seasonal variation. The original dataset containing the hourly electrical energy consumption of a particular appliance for a known month was first divided by the corresponding normalised electrical energy consumption calculated for that month using equation (2.1). Assuming that the electrical consumption for the month of January was known, $e_{App(z),Month(Jan),Hour(ho)}$ would be used. The resulting value was then multiplied by $e_{App(z),Month(mo),Hour(ho)}$ (again calculated using equation (2.1)) for the desired month in order to obtain $E_{App(z),Month(mo),Hour(ho)}$, the electrical energy consumption in Watt-Hours (Wh) for that

specific appliance at a particular hour in that month. In this case assuming that the desired month was February, $e_{App(z),Month(Feb),Hour(ho)}$ would be used to obtain $E_{App(z),Month(Feb),Hour(ho)}$. Using this approach two sets of appliance data are available for the whole year: the original averaged measured dataset based on all the appliances' data collected in the REMODECE database and a modelled dataset based on the calculated sinusoidal trend which can be used to seasonally scale individual appliances. This same procedure was used for all appliances for which datasets were available including television sets, water heaters, lighting, microwave ovens and washing machines.

The aggregation of the appliances' energy demand available from the original dataset does not, however, add up to the total electrical energy demand of a household. As discussed by Widen and Wäckelgård in [29] end-measurement campaigns are usually unsuccessful in measuring and recording all of a household's electrical energy consumption by monitoring individual appliances, and some of the household's consumption remains unspecified. This unspecified demand may be roughly divided into two categories - a continuous base load demand as suggested by Widen and Wäckelgård [29] and a number of miscellaneous loads as suggested by Stokes [27]. In order to calculate the amount of unspecified demand attributable to each category, a similar procedure to that adopted in finding the monthly variation of individual appliances was applied to the general electrical energy consumption values, which were also measured in the REMODECE campaign for each individual household. Based on the values calculated for the electrical energy consumption for each household deduced using this method, the minimum value obtained, that is the minimum hourly electrical energy consumption, was aggregated to the entire profile as a continuous daily base demand. Any difference between the aggregated appliance demand (now including the base demand) and the general electric energy consumption calculated on an hourly basis was awarded to a miscellaneous load occurring during that hour.

The Stage 1 methodology can be adapted to discriminate between weekdays and weekends in that two individual sets of trends can be calculated separately for both

days; one reflecting the monthly hourly variation on weekdays and the other the monthly hourly variation on weekends. This is however only possible if suitable data is available. A limitation of this research is that the original data used does not distinguish between weekdays and weekends, hence differences between weekdays and weekends are not taken into account.

2.4.2.2 Stage 2 - Converting to 1-min time resolution

Stage 2 takes on from the work done in Stage 1 to produce 1-minute time resolution load profiles for each hour of each individual appliance. The assumptions behind this process were that:

- Most appliances (including television sets, entertainment appliances, water heaters, fridges, cooking and lighting) can be assumed to follow a simple 'On'/'Off' square pulse pattern varying between zero power during its 'Off' state and the steady-state operating power during its 'On' state [29]; and

- Certain appliances such as washing machines, a finite amount of energy consumed by that particular appliance over one complete utilisation cycle can be re-modelled using a known energy utilisation pattern.

In both cases switching-on transients are ignored as these are for the most part only seconds long [35].

For an appliance ***App(z)*** with an 'On'/'Off' pattern having a steady-state operating power $\boldsymbol{P_{On\text{-}App(z)}}$ in Watts (W), whose electrical energy consumption during $Hour_{(ho)}$ was $\boldsymbol{E_{App(z),Hour(ho)}}$ in Watt-Hours (Wh), the active time in minutes, $\boldsymbol{min_{On(Hour(ho))}}$, can be calculated using equation (2.2) below.

$$min_{On(Hour(ho))} = \frac{E_{App(z),Hour(ho)}\ x\ 3600}{P_{On-App(z)} x\ 60} \qquad \text{- (2.2)}$$

If the appliance has a stand-by power, $\boldsymbol{P_{Stand\text{-}By}}$, in W, then, assuming that the appliance is continuously on stand-by when not 'On' and that the electrical energy

consumption during this period is equal to $\boldsymbol{E_{Stand\text{-}By}}$ in Wh, equation (2.2) becomes:

$$min_{On(Hour(ho))} = \frac{(E_{App(z),Hour(ho)} - E_{Stand-By})x\ 3600}{(P_{On-App(z)} - P_{Stand-By})x60} \quad \text{- (2.3)}$$

In selecting the appropriate operating steady-state power, $\boldsymbol{P_{On\text{-}App(z)}}$, of an appliance a review of typical steady-state power ratings was undertaken. The results of this review are summarised in Table 2.6.

Table 2.6 - Range of steady-state power ratings for selected 'On'/'Off' appliances

Appliance	**Range of steady-state operating power ratings ($P_{On\text{-}App(z)}$) (Watts)**	**Comment**
Refrigerator, fridge freezers and freezers [36]	80 - 250	
Television (CRT) [37]	32 - 185	Active stand-by may account to a maximum of 12 Watts.
Television (LCD) [37]	31 - 421	Active stand-by may account to a maximum of 18 Watts.
Microwave oven (Defrost) [27]	200 - 300	
Microwave oven (Cooking) [27]	700 - 1,300	Typical peak power is of 900 Watts. Variations including other accessories account for the variable power range.
Electric oven [27, 29]	1,000 - 3,000	
Electric water heater [30]	1,000 - 3,000	
Hi-Fi [37]	4 - 40	
Laptop [37]	40 - 100	Different active stand-by and hibernation modes make it difficult to establish a single stand-by power demand. Indicative figures for the two modes of stand-by mentioned are 20 - 40 Watts for laptops and 20 - 70 Watts for desktops.
Desktops [37]	50 - 175	
Set-top boxes [37]	20	During stand-by periods, which can account to 80% of the active time a continuous demand in the range of 9 Watts is drawn.

In the generation of the high-resolution profile, the start of the appliance's power use during the hour is assigned on a random basis using a uniform distribution. Currently,

the transformation process models the electrical energy consumption during any single hour as a single 'On'/'Off' occurrence. Future work will be aimed at improving this modelling process, by producing a system whereby electrical energy consumption can be sub-divided into multiple 'On'/'Off' occurrences. Figure 2.7 shows the resulting 1-minute profile when applying the Stage 2 transformation method to the hourly consumption data of an 85 Watts CRT TV.

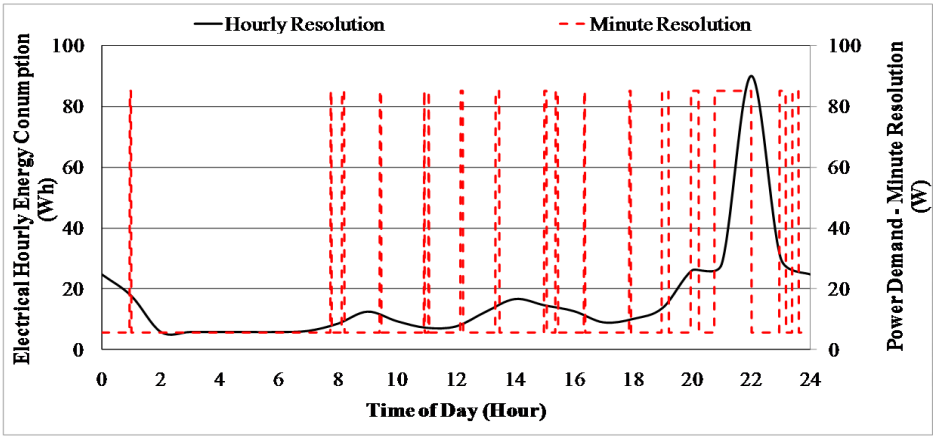

Fig. 2.7 - Minute resolution for the power demand of an 85 Watts CRT TV

For those appliances with complex demand patterns, such as dishwashers and washing machines, appliance cycle patterns presented by Stokes in [27] were employed. The data presented by Stokes provides the minutely power demand over the duration of a whole cycle for different appliances and for different cycles. In order to decide which particular cycle was to be selected, the electrical energy consumption derived from Stage 1 was matched to the total electrical energy consumption per cycle calculated using Stoke's patterns with the closest match yielding the selected pattern. Again the start of the cycle is awarded on a random basis following a uniform distribution. This time however since the cycle can be longer than one hour, a single cycle may continue over to the following hour.

Finally, the demand which in Stage 1 was awarded to an unspecified miscellaneous electrical demand is assumed to follow an 'On'/'Off' pattern with $\boldsymbol{P_{On\text{-}App(z)}}$ chosen at random from a range of 50 Watts and 2,000 Watts which roughly covers the steady-state power demand of most domestic appliances [27]. Again the start of the cycle is

awarded on a random basis following a uniform distribution.

2.4.2.3 Stage 3 - Accounting for improvements in energy-efficiency

In order to obtain the yearly scaling factors by which the individual appliance profiles could be transformed to reflect changes due to efficiency improvements, data from the UK's DEFRA (Department for Environment, Food and Rural Affairs) Market Transformation Program (MTP) [38] was used. Although the data is based on a UK program and the profiles under investigation are those of Italian households (as representative of Mediterranean households), the fact that the assumptions and policy instruments used in the MTP are mostly based on the EU wide energy-efficiency labelling program [39] ensures the intra-country validity and hence that the assumptions contained in them can be extended to this study as well. The MTP sets out the envisaged improvements due to energy-efficiency in specific appliances up to 2020. In practice, these improvements mimic what would happen to appliance energy consumption, should households change their existing appliances to more energy efficient ones. The data used, effectively comes from a database used within the MTP program, namely, the "*What If?Tool"* [40]. The database presents future energy consumption for a number of commercial and residential appliances under different policy scenarios. One of these scenarios named the *Earliest Best Practice Scenario* specifies what would happen to various appliances' electrical energy consumption should the market adopt the best available technologies ignoring financial or other market barriers.

Based on the "*What If?Tool" Earliest Best Practice Scenario*'s data, the scaling factors for each appliance were obtained by dividing the electrical energy consumption used in 2008 (the reference year for the REMODECE datasets), by the expected consumption in 2020. In most cases the scaling factor is simply a result of the technology's development and so it applies to the device average power draw. For example, for appliances such as lighting and television, the scaling factor reflects the fact that the time period during which such appliances will be active will remain unchanged, and the change will only be due to changes in the electrical power demand of that appliance. However, in some cases the scaling factor is the result of

changes in human requirements and behaviour, such as the expected shift from cooking using traditional ovens in favour of microwave ready-cooked meals [41]. The scaling factor in this case will have an effect on the time the appliance is active. The scaling factors are therefore applied to either the average steady-state power demand of the device keeping the active time calculated in Stage 2 constant, or to the time of use of the device keeping the steady-state power demand assumed in Stage 2. Table 2.7 gives the calculated scaling factors used in this study for the most common household appliances and whether these should be applied to the steady-state power demand or the time-of-use.

Table 2.7 - Scaling factors for the future *Earliest Best Practice Scenario*

Appliance	2020 Scaling factor compared to 2008	Application of scaling factor	Rationale behind assumed change
Refrigerator	0.467	reduced power demand	Shift towards A^{++} technology [42].
Fridge Freezer	0.650	reduced power demand	
Electric Oven	0.690	reduced time-in-use	Reduction in cooking time, driven by technology improvements and aptitude towards more ready-made meals [41].
Microwave Oven	1.016	increased time-in-use	More frequent use [41].
Electric Water Heater	0.943	reduced time-in-use	Slight improvement brought about by better insulation [43, 44].
Television	0.782	reduced power demand and standby	Envisaged that new technologies will be mature and efficient by 2020 with additional energy-efficiency features such as automatic switching off during prolonged stand-by periods [45].
Domestic Lighting	0.502	reduced power demand	Increased use of Compact Fluorescent Lamps (CFLs) and LEDs, with direct replacement of tungsten filament lamps [46]. Given that a range of power ratings is equivalent to an incandescent bulb the scaling factor represents a conservative average of the future demand.
Computer	0.364	reduced power demand	Improvement in energy-efficiency [47].
Set-Top Boxes	1.050	increased power demand	Set-top boxes to become more elaborate and energy consuming, but slightly more efficient [48].

Table 2.7 - Scaling factors for the future *Earliest Best Practice Scenario* (cont.)

Appliance	2020 Scaling factor compared to 2008	Application of scaling factor	Rationale behind assumed change
Dishwasher			
(65 Deg^{o}C cycle)	0.845	reduced power demand	Improved technology and better detergents [49].
(55 Deg^{o}C cycle)	0.902		
Fridge Freezer			
(90 Deg^{o}C cycle)	0.958	reduced power demand	Improved technology with better laundry load management [50].
(60 Deg^{o}C cycle)	0.895		
(40 Deg^{o}C cycle)	0.902		

Given that the end result of using the scaling factor in Stage 3 is a change in the electrical energy consumption, the scaling factor can also be applied directly to Stage 1 in order to project the effect of energy-efficiency onto the future electrical energy demand.

2.4.3 Verification of the electrical demand modelling process

Before proceeding with explaining the process of creating the current and high electrical efficiency profiles for the 3 household and the 6 household building models used in the simulations, it is important to verify the correctness and accuracy of this transformation process.

The use of a sinusoidal function coupled with random 'noise' to describe the seasonal variation of an appliance's hourly energy demand, used in the Stage 1 transformation has already been validated by Stokes [27]. The verification of the approach techniques used in this particular research therefore revolves around ensuring that the original profiles created using Stage 1 and Stage 2 of the process are comparable to the results conducted by other research studies.

2.4.3.1 Normalised verification factor

One method to compare modelled to measured data is to use the dimensionless *Normalised Verification Factor, NVF,* suggested by both Capasso in [51] and Widen in [30]. The *NVF* is the squared sum of the error between the modelled ($\boldsymbol{e_{modelled}}$) and

the measured ($e_{measured}$) data of every time step *t*, normalised by the product of the mean squared average of the measured data and the total number of time steps, t_o. Mathematically this is shown in equation (2.4). The smaller the resulting *NVF* value the more accurate is the predicted modelled data.

$$\frac{\sum_{t=1}^{t_0}(e_{modelled(t)}-e_{measured(t)})^2}{t_0\,(e_{measured(Average)})^2} \qquad \text{- (2.4)}$$

$e_{measured}$ is the normalised original data used to calculate the parameters in equation (2.1), that is, the actual data derived from the REMODECE database for all appliances, whilst $e_{modelled}$ is the output data after Stage 1 has been applied to $e_{measured}$, that is, the data derived from the assumed sinusoidal trend equation used in Stage 1. Although the *NVF* should be used to compare two independent datasets, in this case the *NVF* is being used as a measure to quantify how closely the modelled data follows the measured data. Using equation (2.4) the hourly *NVF*, that is, the measure of how each single modelled hour value compares to the measure data on a 12 month period, was deduced. Table 2.8 shows the hourly *NVF* averaged over all 24 hours for all appliances, the maximum hourly *NVF* value for each appliance under investigation and the hour during which this maximum error value occurs.

Table 2.8 - Hourly *NVF* for all appliances

Appliance	**Hourly *NVF* averaged over all hours**	**Maximum Hourly *NVF*; (Hour occurring)**
Refrigerator	0.111	0.247; (23-24)
Television	1.648	9.736; (4-5)
Water Heater	0.677	2.548; (6-7)
Lighting	0.507	1.066; (5-6)
Electric Oven	3.580	18.917; (1-2)
Microwave Oven	3.135	10.869; (0-1)
Washing Machine	10.773	87.683; (5-6)
Dish Washer	2.757	12.406; (5-6)
Total General Consumption	0.282	0.648; (7-8)

The low *NVF* values for refrigerators, lighting and electronic appliances and the high

NVF values for washing machines, electric ovens and dish washers suggests that the methodology is most accurate for cyclic or relatively repetitive appliances rather than single event appliances, mainly due to the availability of data. The results also indicate that the maximum error is during the night period, when hourly variations between the modelled and measured data are highest. This is comparable with results from Widen in [30].

2.4.3.2 Comparison with other end-measurement campaigns and research

Another method of verification relies on comparing the annual electrical energy consumption calculated using the output data from the transformation process in Stage 1, with other analogous studies. For this reason the individual appliance data of 8 households contained in the REMODECE Italian dataset were modelled using the transformation process. Table 2.9 lists the characteristics of the analysed households: the occupancy and the appliances/lights monitored during the REMODECE campaign for that particular household.

Table 2.9 - Characteristics and appliance ownership of the 8 modelled households

Household code	Number of occupants	Appliances monitored in the REMODECE campaign	Lights monitored in the REMODECE campaign (values are in Watts)
1A	1	Hi-Fi, Refrigerator, Laptop, Microwave oven, Washing machine	2x60, 2x75, 1x15, 1x40
1B	1	Refrigerator, Water heater, PC, Washing machine,	2x17, 1x41, 1x26, 1x37
2A	2	Television, Refrigerator, Laptop, Electric oven, Washing machine	2x7, 2x140, 1x60, 1x40
2B	2	Refrigerator, Laptop, Electric oven, Water heater, Microwave oven, Dish washer, Washing machine	2x75, 2x25, 1x60, 1x30, 1x11, 1x33, 1x80, 1x100, 1x70
3A	3	Hi-Fi, Refrigerator, Laptop, Water heater, Electric oven, microwave, Dish washer Washing machine	2x11, 2x25, 2x75, 1x70, 1x80, 1x60, 1x30, 1x33
3B	3	Television, Hi-Fi, Refrigerator, Set-top box, Electric oven, Coffee machine, Microwave oven, Washing machine	2x25, 1x20, 1x7, 1x120, 1x100
4A	4	2 x Television, Hi-Fi, Refrigerator, Microwave oven, Washing machine	4x25, 2x40, 1x120, 1x35, 1x80
4B	4	2 x Television, Refrigerator, Microwave oven, Dish washer, Washing machine	1x225, 1x40, 1x50, 1x36, 1x8, 1x15, 1x22, 1x16

For each appliance in each household, Stage 1 of the transformation was used to calculate the total energy consumption of a characteristic day for each of the 12 months. Given the limitations in the original dataset described previously, using the approach presented previously only a single representative day could be generated for each month, giving a possible 12 characteristic days covering the entire year. Nonetheless, this was enough to capture the salient features of the demand.

Figure 2.8 (for example) shows how the modelled daily electrical energy consumption for the individual appliances in household 2A varies over the course of a calendar year. The impact of seasonality on the daily electrical energy consumption of appliances such as refrigerators and lighting fixtures is very clear; high electrical energy consumption in the former case and low electrical energy consumption in the latter case during the summer months, and *vice versa* during the winter months.

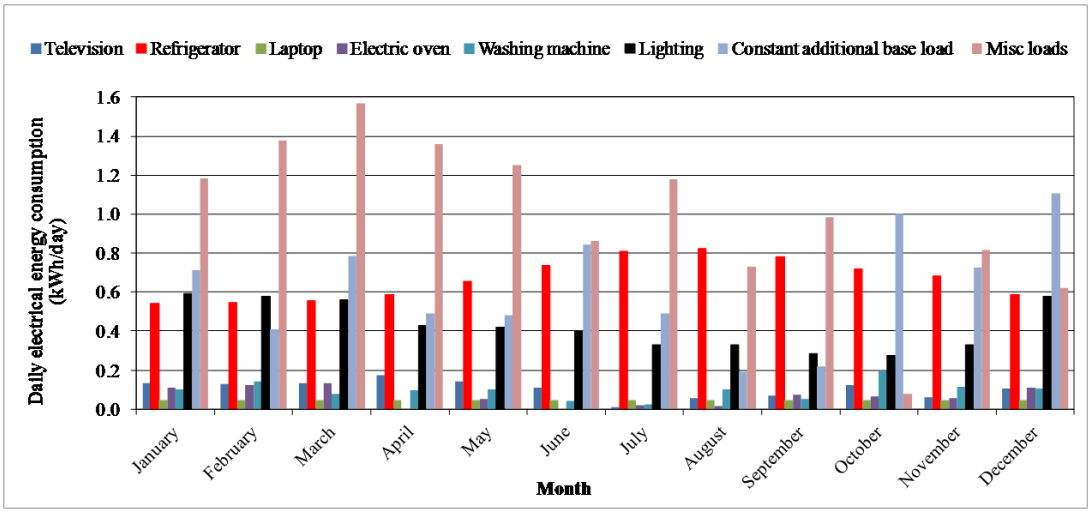

Fig. 2.8 - Daily electrical energy consumption for household 2A by appliance type

The annual electric energy consumption is the total addition of the individual results of the product of the daily electrical energy consumption, calculated for each characteristic day of each month and the number of days present in each month.

Table 2.10 lists down the results obtained for each individual household.

Table 2.10 - Annual electrical energy consumption for the households investigated

Household code	Annual electrical consumption (kWh)	Annual electrical consumption per person (kWh/person)
1A	1,370	1,370
1B	2,079	2,079
2A	1,149	575
2B	3,359	1,680
3A	4,075	1,358
3B	2,219	740
4A	2,827	707
4B	3,175	794

The annual consumption of six out of eight households (75%) was between 2,000 and 5,000 kWh per *annum* - a similar result to that obtained by another research campaign conducted in Italy, the MICENE project [52]. The MICENE project reported that the electrical consumption of 80% of the households analysed during a similar research had an annual electrical energy consumption of a similar magnitude.

2.4.3.3 Aggregated loads frequency distribution

One final method used to verify the profiles created was to compare the statistical frequency distribution of the 1-minute temporal electrical load of the aggregated 8 households created using the transformation process, with statistical frequency distributions known to be followed by aggregated household load profiles. Individual domestic load profiles such as that shown in Figure 2.9 for household 4A (for a characteristics day in February), created using Stage 2 of the transformation process, do not follow any particular frequency distribution [24].

Low voltage aggregated load profiles such as that shown in Figure 2.10 for all 8 households for the same day in February however follow skewed statistical distributions such as ***Weibull*** or ***Beta*** distributions [53, 54]. Figure 2.11 shows the fit obtained when the 3 Probability Density Functions (PDF), namely Beta, Weibull and Gamma, suggested in literature [53, 54] are superimposed on the demand frequency histogram created using the aggregated 1-minute resolution electrical demand of all 8 households shown in Figure 2.10. The level of significance calculated using the

Kolmogorof-Smirnov test exceeds the minimum accepted threshold of 0.05. In Figure 2.11 values are normalised using the highest daily occurring load.

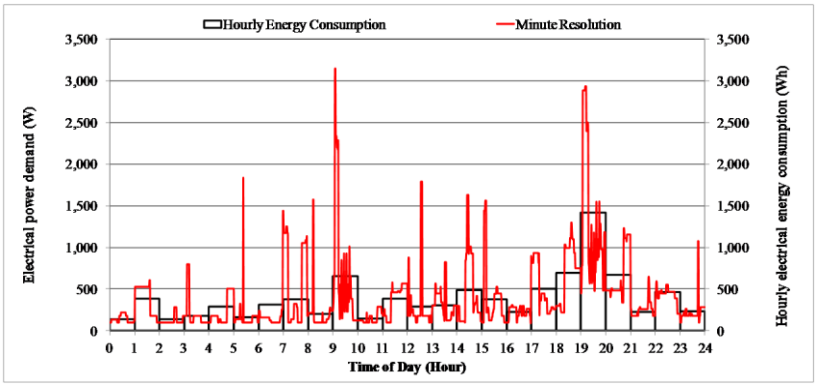

Fig. 2.9 - Electrical demand profile for household 4A for a day in February

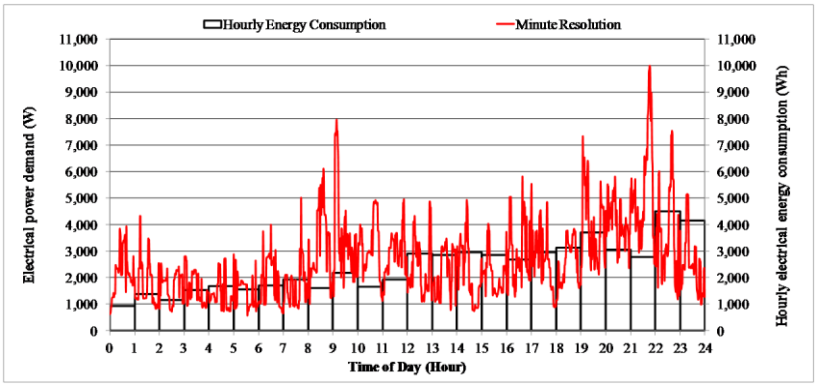

Fig. 2.10 - Aggregated electrical demand profile for all 8 households

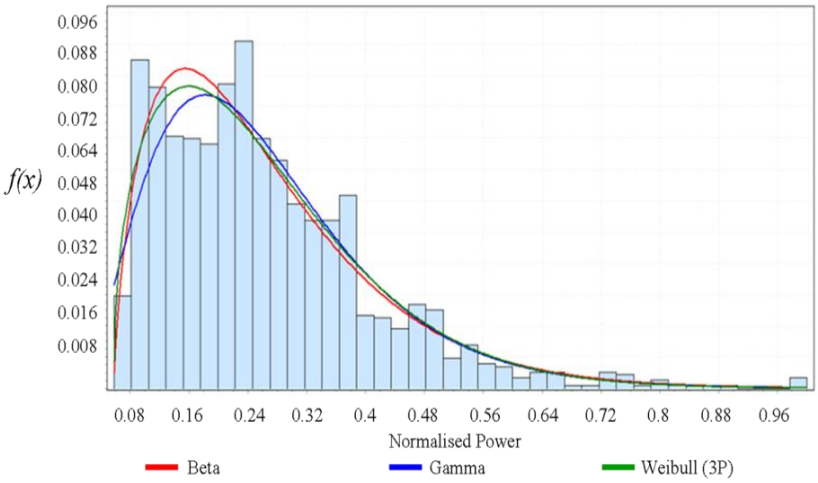

Fig. 2.11 - Demand frequency histogram with the PDF superimposed

2.4.4 Creating the profiles used in the simulation

The transformation process explained was used to model the current and high efficiency demand profiles for the selected households in the 3 household and the 6 household buildings, as described in the following sections.

2.4.4.1 3 Household building - Seasonal electrical profiles

Three of the households described in Table 2.9, namely households 2A, 3B and 4B were selected as those used to simulate the electrical demand in the 3 household building model. Household 2A was used to model the demand of the ground floor (GF) apartment, whilst household 3B and household 4B were used to model the demand of the middle floor (MF) and the top floor (TF) apartments respectively.

Figure 2.12, Figure 2.13 and Figure 2.14 show the minute resolution demand profile for three of the days (one each as a representative of the shoulder (transition) [May], summer [August] and winter [February] months) created for household 3B using Stage 2 of the transformation process. The profiles shown are based on the current appliance efficiency and are therefore representative of the *current efficiency electrical scenario*. Appendix 'B' shows similar figures for the other two households.

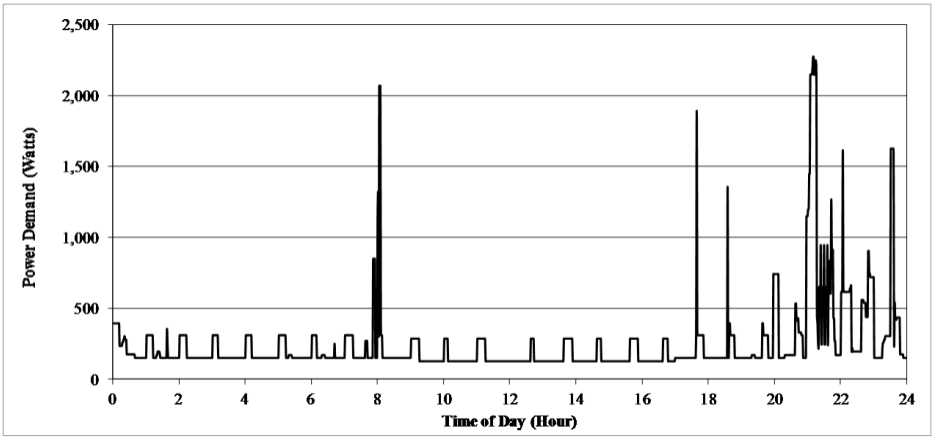

Fig. 2.12 - Electrical demand profile for household 3B (May)

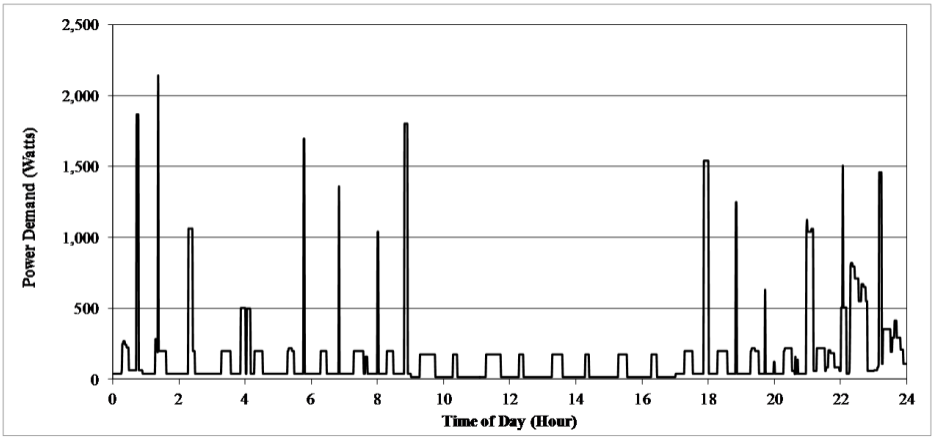

Fig. 2.13 - Electrical demand profile for household 3B (August)

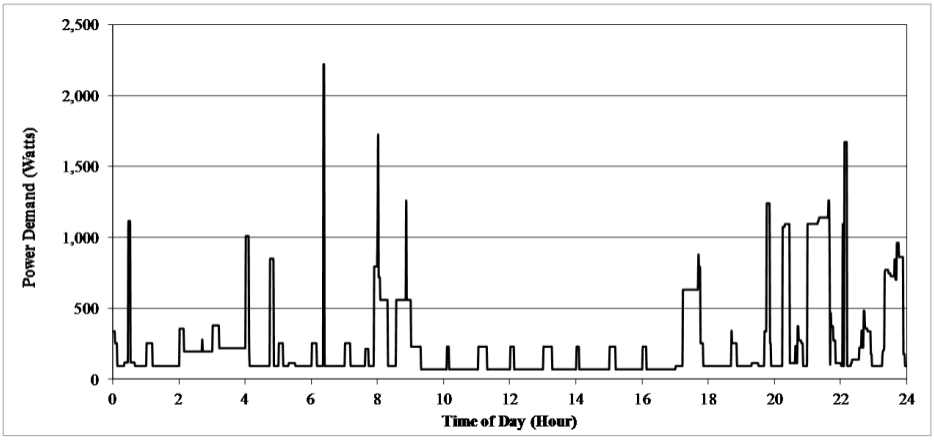

Fig. 2.14 - Electrical demand profile for household 3B (February)

Figure 2.15, Figure 2.16 and Figure 2.17 show the aggregated electrical demand profile for all 3 households for the same days in May, August and February.

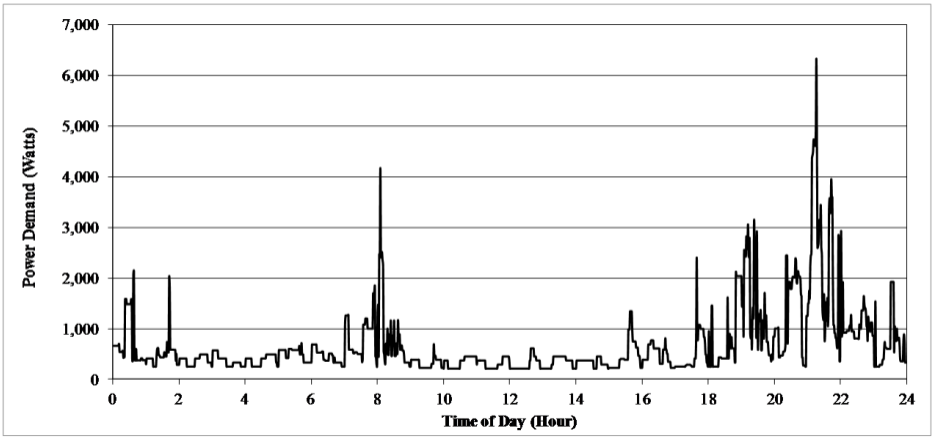

Fig. 2.15 - Electrical demand profile for all households (May)

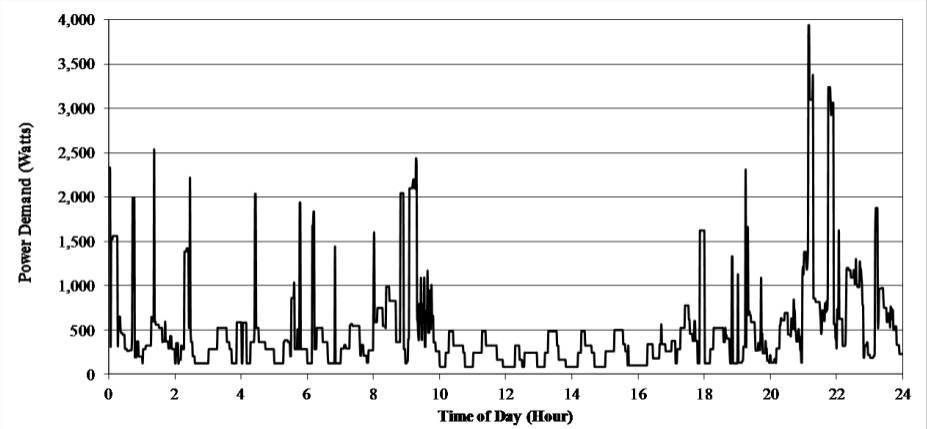

Fig. 2.16 - Electrical demand profile for all households (August)

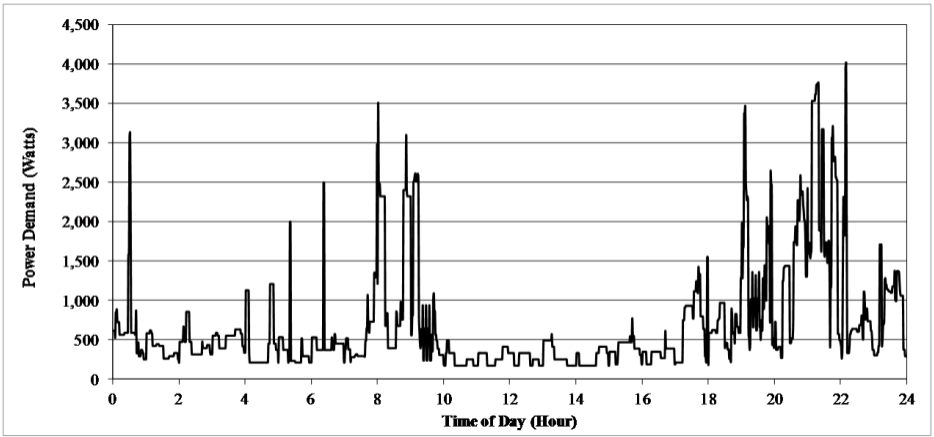

Fig. 2.17 - Electrical demand profile for all households (February)

As can be observed from the two sets of figures, the daily electrical demand profile varies on a seasonal basis. Similarly to Figure 2.8, where the effect of seasonal variability was shown for different appliances for the same household, Figure 2.18 shows the daily electrical energy consumption calculated for the three households on a monthly basis. Excluding HVAC loads (in this analysis HVAC loads are being treated as a separate load which is catered for by the 'waste heat' recovered from the micro-trigeneration system), it can be observed that the annual electrical energy consumption modelled to represent demand in residential buildings in southern European countries is not particularly different from the annual consumption modelled for other European residential buildings; a high winter demand, a low summer demand and an intermediate demand during the shoulder months [27].

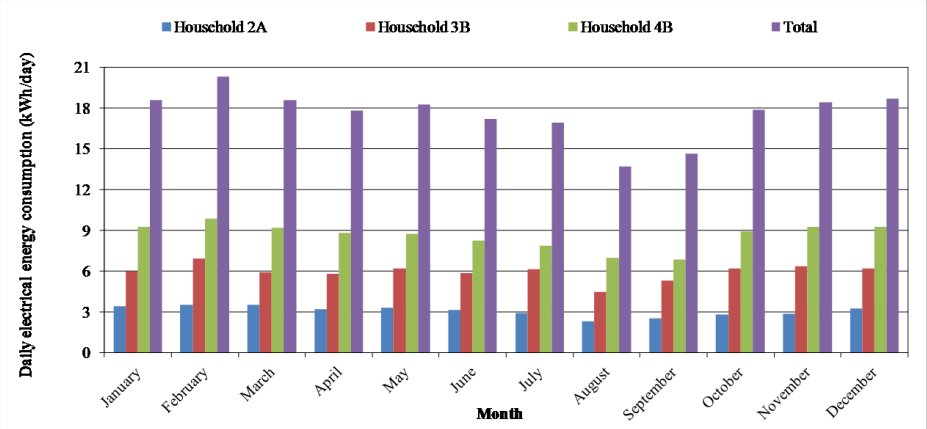

Fig. 2.18 - Daily electrical energy consumption for the three households

On the other hand, at this low level of aggregation peak demands appear not to be effected by seasonality (although a slight time shift in the evening peak demand can be picked up between February and August), but rather to the sum of the different appliances which are active during any specific time. Chapter 5 further explores this.

2.4.4.2 3 Household building - Current efficiency vs. high efficiency electrical demand scenarios

In order to create the demand profiles required in the *high efficiency electrical scenario*, Stage 3 of the transformation process was applied to the current efficiency electrical scenario demand profiles of the 3 households modelled in the previous section.

Figure 2.19, Figure 2.20 and Figure 2.21 show the transformed demand profiles for household 3B for the same characteristic days shown in Figure 2.12, Figure 2.13 and Figure 2.14. For comparative purposes the high efficiency electrical demand profile is superimposed on the current efficiency electrical demand profile (dotted black line in the background).

Appendix ‘B’ shows similar figures for the other two households.

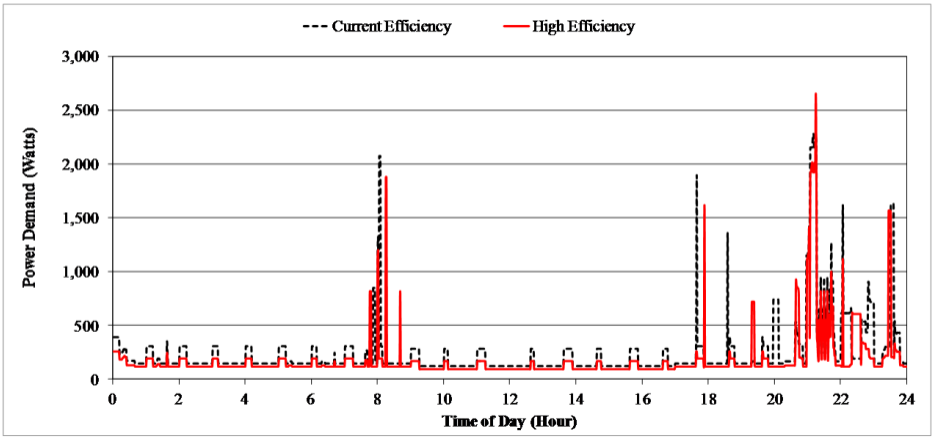

Fig. 2.19 - High efficiency electrical demand profile for household 3B (May)

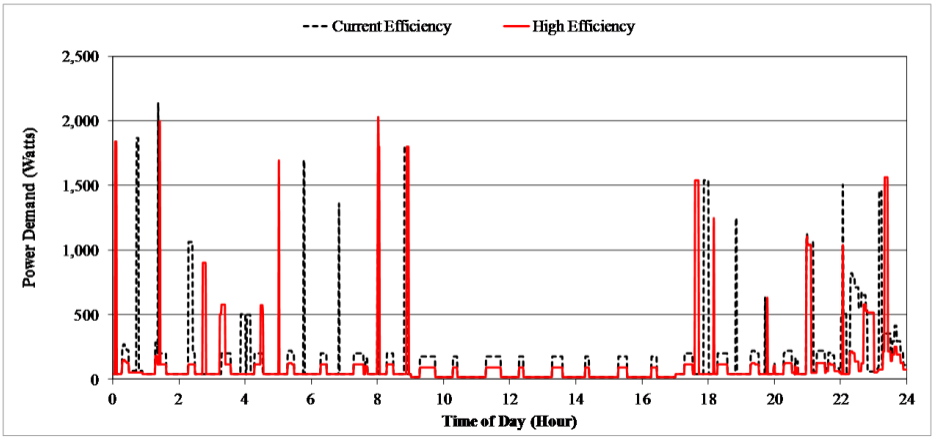

Fig. 2.20 - High efficiency electrical demand profile for household 3B (August)

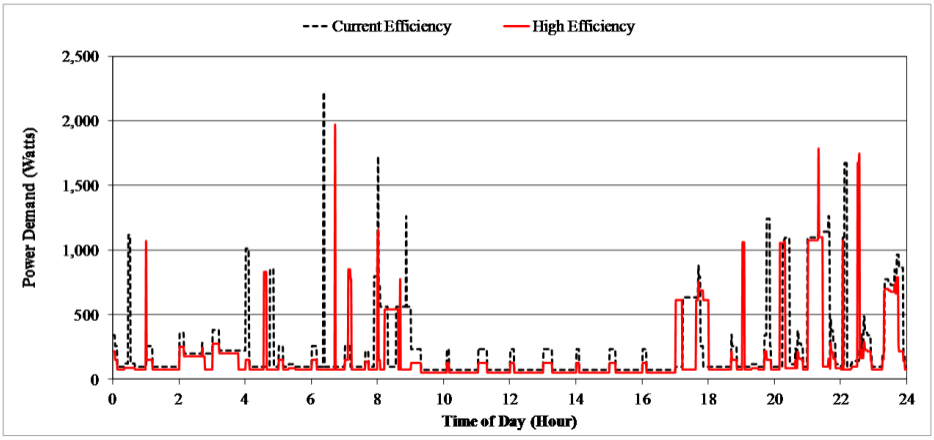

Fig. 2.21 - High efficiency electrical demand profile for household 3B (February)

The total aggregated demand profiles for all 3 households for the same characteristic days in May, August and February are similarly shown in Figures 2.22, 2.23 and 2.24.

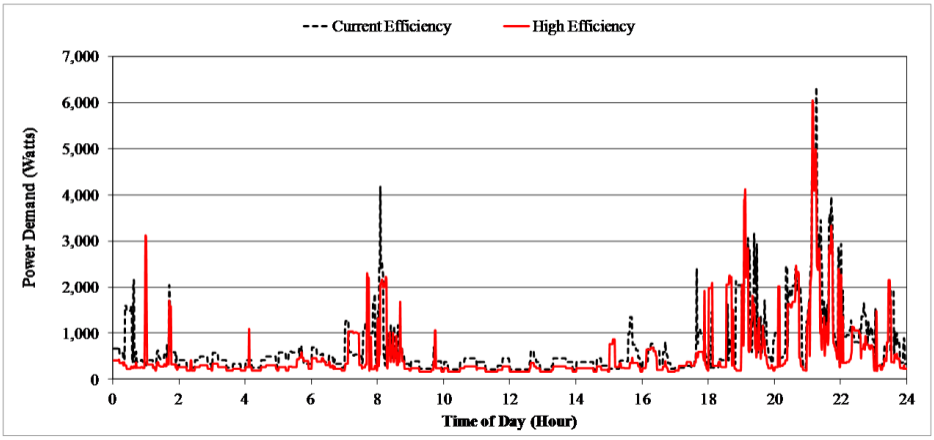

Fig. 2.22 - High efficiency electrical demand profile for all households (May)

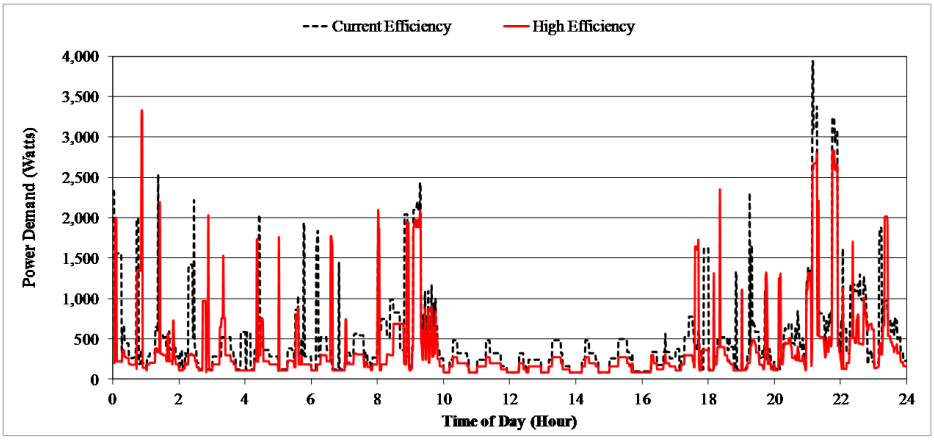

Fig. 2.23 - High efficiency electrical demand profile for all households (August)

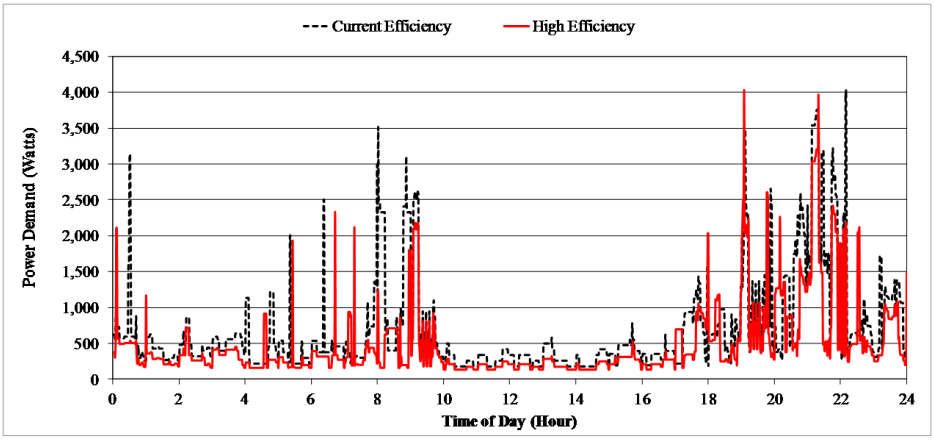

Fig. 2.24 - High efficiency electrical demand profile for all households (February)

2.4.4.3 6 Household building

As mentioned in Section 2.3.2 in order to analyse the effect of building size and occupancy, a second enlarged building was modelled with each floor representing the internal space taken by two storeys. The electrical demand of each floor in this case was modelled to represent the electrical demand profile of two households.

To model the demand profile of this 6 household building, the demand profiles of households 2B, 3A and 4A (whose characteristics are shown in Table 2.9) were individually added to the profiles of the households used to model the electrical demand profiles of the 3 household building. The electrical demand profile of household 2B was added to that of household 4B to represent the electrical demand of the enlarged top floor. The electrical demand profile of household 3A was added to that of household 2B to represent the electrical demand of the enlarged ground floor and the electrical demand profile of household 4A was added to household 3B to represent the electrical demand of the enlarged middle floor.

Apart from increasing the electrical energy demand, aggregating the load profiles of the different households also creates a temporally different load, (slightly) levels out the load demand, increases the average demand and shifts peak demands. Figure 2.25 shows one such aggregation between household 2B and household 3A for a characteristic day in May. The resulting demand profile is that of the 2-household ground floor in the 6 household building.

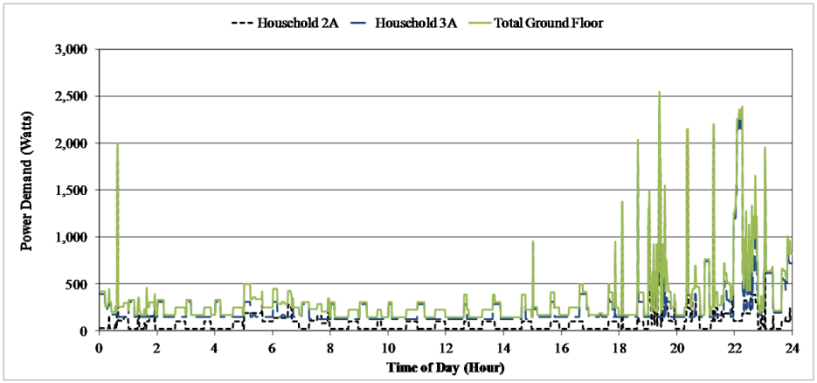

Fig. 2.25 - Aggregation used to generate the electrical demand profile for the 2-household ground floor for a characteristic day in May

Note that the domestic hot water profile was modelled separately from the electrical demand profile (since this was directly satisfied by the micro-trigeneration system), and therefore even though Table 2.9 lists an electric water heater as an appliance owned by households 2B, 3A and 4A, in the modelling process this was omitted.

Figure 2.26 and Figure 2.27 show the electrical demand for the 2-household ground floor in August and February as representative of the summer and winter months respectively.

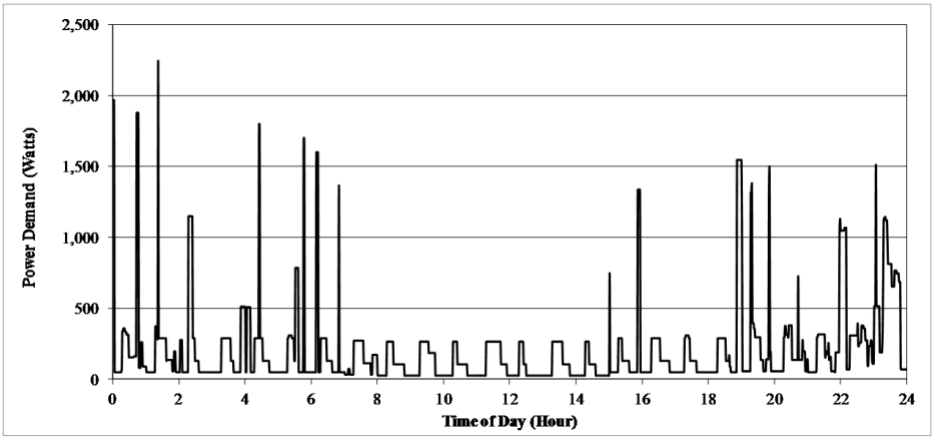

Fig. 2.26 - Electrical demand profile for the 2-household ground floor (August)

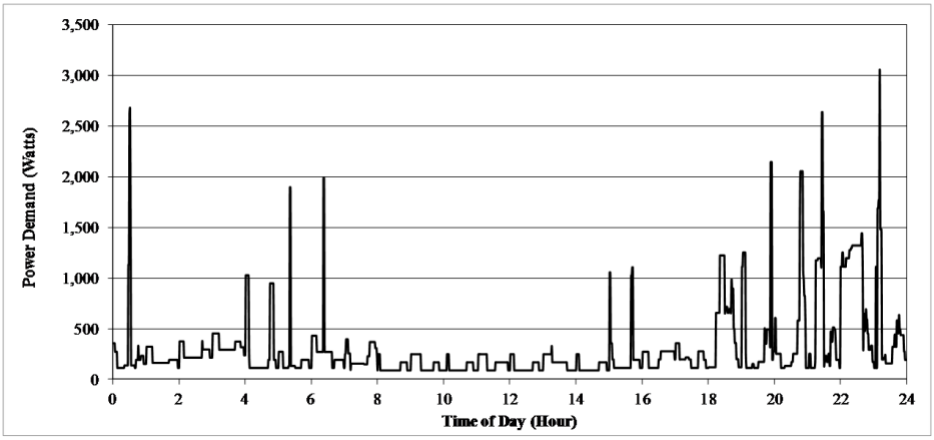

Fig. 2.27 - Electrical demand profile for the 2-household ground floor (February)

Also, in the same way to the procedure used in modelling the demand profiles for the 3 household building, Stage 3 was again adopted to transform the current efficiency demand profiles into high efficiency electrical demand profiles. Figure 2.28, Figure

2.29 and Figure 2.30 show the resulting high efficiency profiles for the 2-household ground floor for May, August and February respectively.

Appendix 'B' shows the other profiles for the other floors and the aggregated demand load for the whole building.

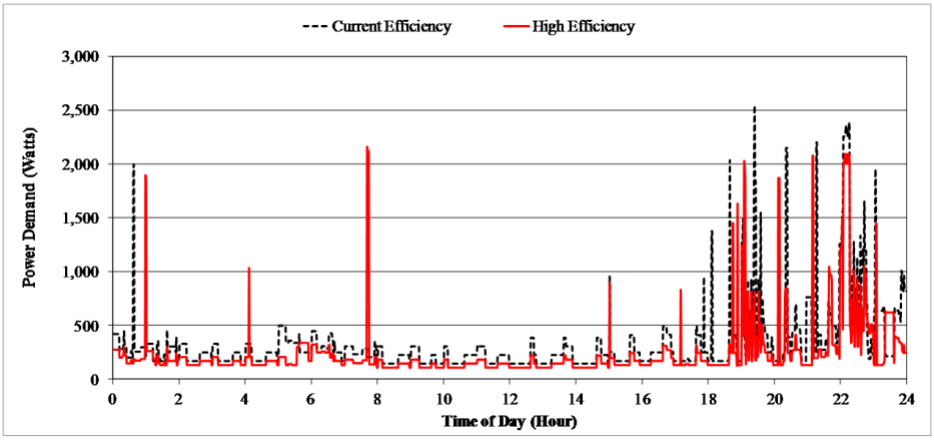

Fig. 2.28 - High efficiency electrical demand profile for the 2-household ground floor (May)

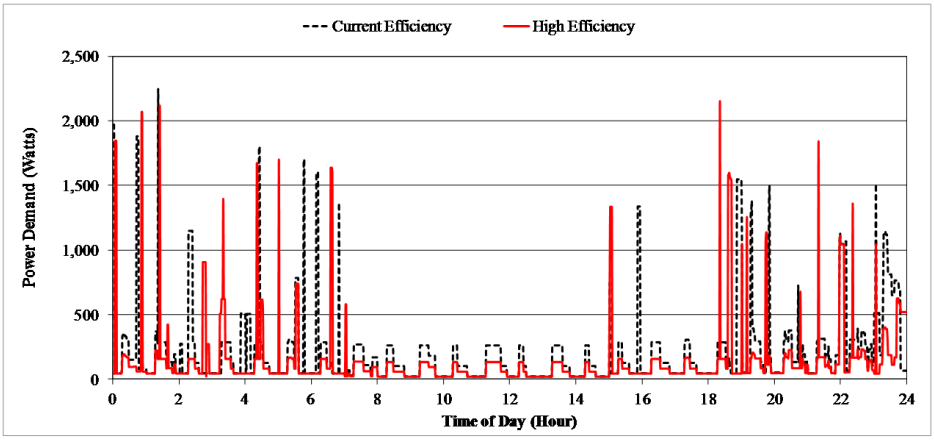

Fig. 2.29 - High efficiency electrical demand profile for the 2-household ground floor (August)

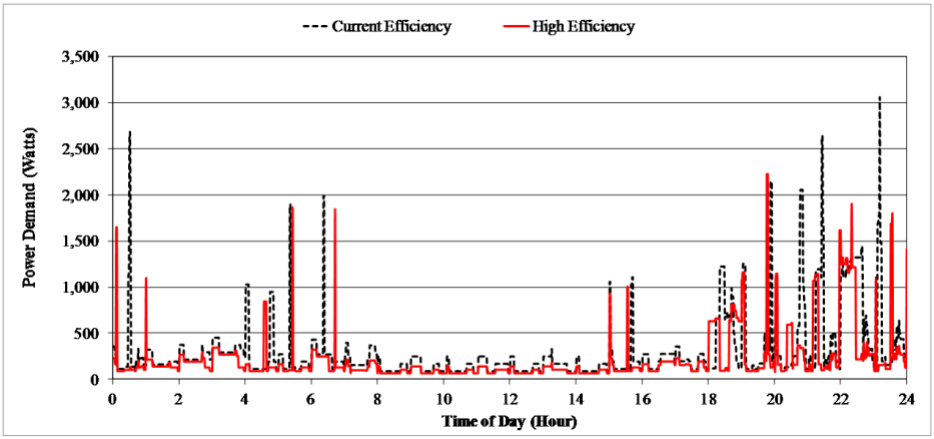

Fig. 2.30 - High efficiency electrical demand profile for the 2-household ground floor (February)

2.5 Modelling the internal heat gains

In Section 2.1 it was explained how the thermal demand arising from the heating or cooling energy demand required for space conditioning in a building is a factor of multiple aspects such as climate, building characteristics, internal heat gains *etc*. In this context, the third aspect discussed in this chapter as part of modelling the demand side is the modelling of the internal heat gains.

As discussed by Hodges [55] when modelling space heating for residential units, internal heat gains must be included in the modelling procedure. Hodges explains that failure to do so could lead to potentially oversizing a system, as the calculations would not be taking into consideration the effect internal heat gains have on the indoor temperature. In summer the inverse is true; internal heat gains emitted into a space increase the internal temperature, potentially increasing the demand for space cooling.

2.5.1 Internal heat gains - An overview

Internal heat gains in residential buildings are caused by two sources; the heat emitted by the occupants and the heat emitted from the household appliances (including lighting) [11]. Generally in sizing HVAC systems for residential households, both the internal heat gains due to occupants and those due to appliances are modelled as lumped sensible and latent heat loads awarded for a continuous

period [11].

In order to improve on the resolution currently employed for residential buildings, a new method is being used in this thesis to enable high resolution modelling of internal heat gains. The methodology is an extension to the transformation process developed to model electrical demand profiles. The methodology approach makes use of the electrical demand profiles created in Section 2.4 to model two distinct internal heat gains profiles, one due to occupants and the other due to appliances, which when combined form an aggregated internal heat gains profile for a particular household. The following two sections, Section 2.5.2 and Section 2.5.3, explain in detail the methodology by giving a step by step account of how the internal heat gains profile of household 3B (middle floor - 3 household building) for a characteristic day in May was modelled (the equivalent electrical demand profile is shown in Section 2.4.4.1 [Figure 2.12]).

2.5.2 Internal heat gains due to occupancy

The method used to simulate the internal heat gains due to the occupants relies on allocating internal heat gains (sensible and latent) for each occupant present in the apartment at any particular time (occupancy timing is discussed later). Although, occupants emit sensible or latent heat depending on their current activity (*e.g.* sleeping, cooking, standing, *etc.*), for domestic environments ASHRAE in [11] suggest that a practical approximation for the internal heat gains emitted by occupants is to use average default values of 67 Watts of sensible heat and 35 Watts of latent heat emitted for every occupant present.

To model occupancy for any single household, use was made of research done by Richardson *et al.* in [56] who present a methodology complemented by an interactive tool which permits the creation of stochastic 10 minute resolution active (active in this case means not asleep) occupancy profiles for different sized household such as that shown in Figure 2.31 for a 3 person household, based on data extracted from the UK's 'time-use survey' [31] (the applicability of using such data is discussed later).

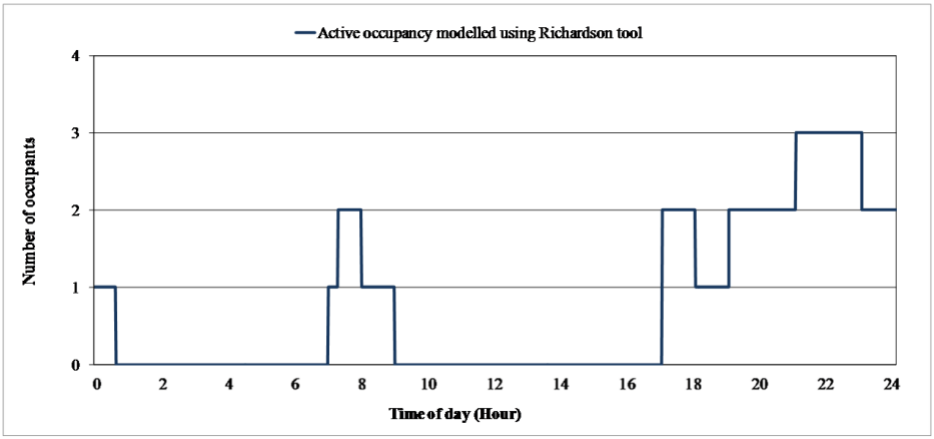

Fig. 2.31 - Occupancy model for a 3 person household created using the method described by Richardson *et al.* in [56]

By superimposing the electrical demand profiles modelled in Section 2.4 with the closest matching occupancy profile created using the interactive tool by Richardson, an occupancy profile can be assumed for any household based on the known electrical demand profile for that household. Figure 2.32 shows one such case where the occupancy profile shown in Figure 2.31 was matched with the electrical demand profile of household 3B for a characteristic day in May.

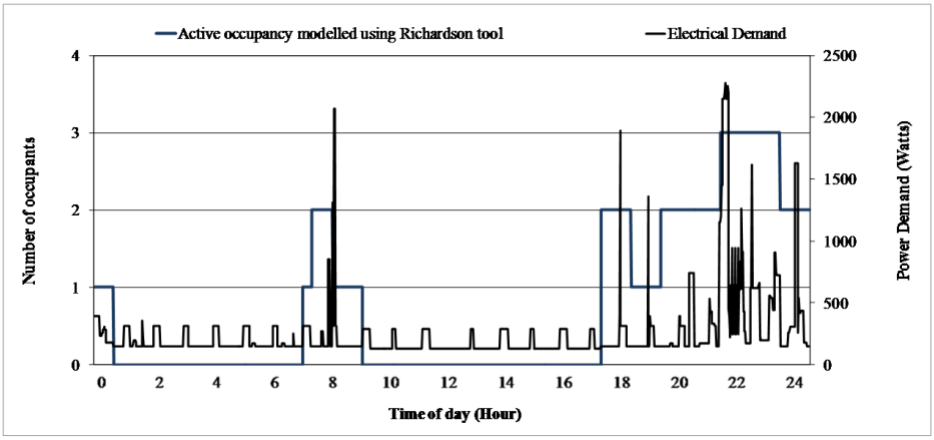

Fig. 2.32 - Electrical demand profile superimposed on the active occupancy profile for household 3B for a characteristic day in May

The electrical demand profile and the active occupancy profile being matched belong to two different datasets (the REMODECE Italian dataset and the UK 'time-use survey'), however, the occupancy profile can be considered a plausible match in that

(as discussed by Richardson *et al.* in [28]) most of the variations in electrical demand take place when occupants are indoors and active. In Figure 2.32 the large variations in demand after 17.00 Hours and the stable demand between 09.00 and 17.00 Hours (the only loads present are the constant base load and the cyclic demand of the refrigerator) concur with this conclusion, suggesting that effectively between 09.00 and 17.00 Hours the apartment is vacant whilst most of the occupants are actively present after 17.00 Hours.

The occupancy profile modelled using Richardson's interactive tool was extended to account for heat emissions when people are not active (i.e. asleep). By using Richardson's approach [56], there is no way in which one can distinguish the difference between an apartment being empty or the apartment's inhabitants being asleep. Therefore, a reasonable assumption, based on the 'time-use survey' used by Richardson *et al.* is to assume that during the night all occupants of a particular household are inside the building. Figure 2.33 shows the adjusted occupancy profile to account for when people are asleep.

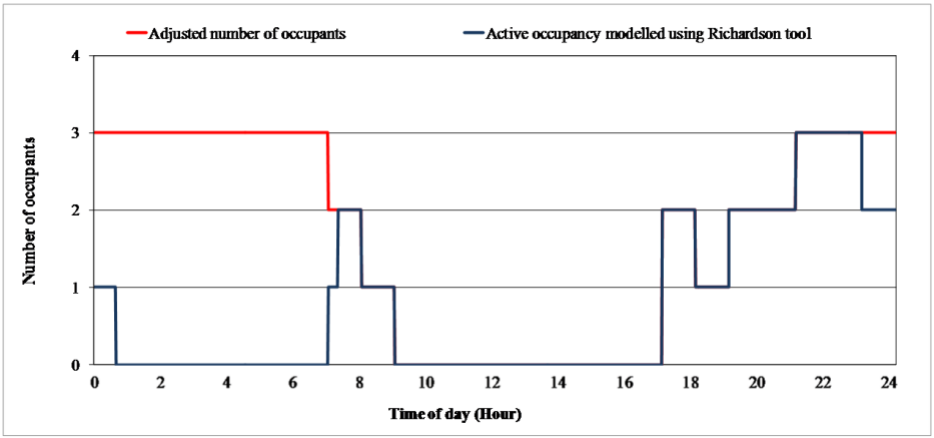

Fig. 2.33 - Adjusted occupancy profile

Based on the modelled occupancy pattern the internal heat gains profile for each individual household can therefore be modelled by awarding default values for sensible and latent heat gain set by ASHRAE in [11] based on the number of occupants present during any specific time. This resulting internal heat gain profile due to occupants is shown in Figure 2.34.

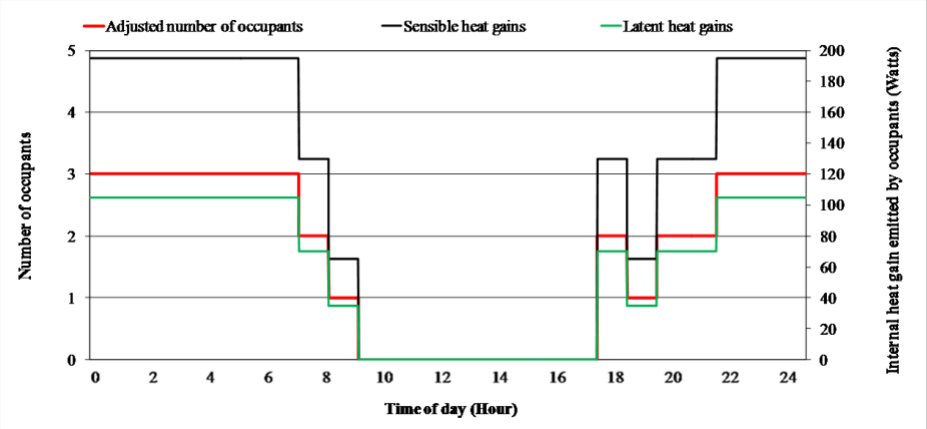

Fig. 2.34 - Internal heat gains emitted due to occupants

2.5.3 Internal heat gains due to appliances

2.5.3.1 Electrical appliances

Internal heat gains due to appliances are much more complex to model. Similarly to their electrical demand different appliances have different heat emission values. However, contrary to electrical loads, which can be considered as instantaneous loads, which go 'On' or 'Off' instantaneously, heat gains emitted from appliances show what is termed a time delay effect [57].

An important aspect of appliance related internal heat gains is that appliances would continue to emit heat even after being switched 'Off'. Likewise after switching 'On', an appliance would take some time to warm up before reaching its steady-state working temperature. One presumption which is therefore being made in this modelling is that both the heating up and cooling down periods are of such a short duration in comparison to the time the appliance is considered to being emitting heat at its working temperature, that they can be neglected. For appliances whose thermal mass is small (*e.g.* small electronic equipment *etc*.), this is a reasonable assumption as the heat is gained and dissipated quickly. For other appliances such as electric ovens this is a coarse approximation which merits further analysis as part of possible future work annexed to this research.

Assuming a low thermal inertia, appliance internal heat gains can be modelled in a

similar fashion to the modelling of the electrical demands. Whenever an appliance is electrically 'On' (as represented by its corresponding electrical demand profile) a value for the sensible and latent internal heat gain due to that appliance is allocated.

Table 2.11 lists the typical values of heat emission for the various appliance groups. The heat gains were assumed to be equally split between convective and radiative gains.

Table 2.11 - Internal heat gains due to various electrical appliance groups

Appliance group	Default values	Comment
Lighting	Based on light source type and rating. Typical range for household units is of 10-200 Watts [58]	Incandescent bulbs emit the equivalent of 90% of their power rating directly as sensible heat. CFLs emit only the equivalent of 50% of their power rating [58, 59]. Nonetheless 100% of the power eventually becomes heat.
Audiovisual and IT equipment	Based on type of technology. Typical range for household units is of 4-400 Watts [57]	If the actual power demand of an IT appliance is known this can be considered to be directly equivalent to the total sensible heat gain emitted by that appliance [57].
Wet appliances	Typical values - 56 Watts sensible heat and 123 Watts latent heat	Depending on size and technology, dish washers and washing machines are typically assumed to emit a sensible and latent heat gain in the range of between 40 - 60 Watts and 90 - 130 Watts respectively [57]. It is assumed that the heat emitted in the surrounding environment is for the whole duration of the cycle.
Cold appliances	Based on type of technology	Similarly to IT equipment, the sensible heat gain due to cold appliances such as refrigerators is equal to the electrical power demand [60].
Cooking appliances	Based on type of technology. Typical range for household units is of 500-1,500 Watts [57]	For electric ovens the heat emitted into the environment may be assumed to be equal to 50% of the electrical power demand sub-divided into 34% latent and 66% sensible heat. Heat gain due to the use of microwave ovens is equivalent to their electrical power demand [57].

Table 2.11 presents two important aspects with regards to modelling internal heat gains due to electrical appliances. The first is that depending on the type of appliance group there is a distinctive divide between the internal heat gains emitted as sensible heat and those emitted as latent heat. Appliance groups which involve handling water, such as cold, wet or cooking appliances, typically have shares of both sensible and latent heat. The internal heat emission for other appliances is only sensible.

The second aspect is that the internal heat gains emitted can be considered to be a factor of the electrical power demand of the appliance. It is important to note that the average power demand is different from the nameplate value found on most appliances, as the latter can only be considered as an upper bound to the actual power demand [57]. The electrical power demand in this case refers to the *measured* electrical demand. Given that typically all electrical consumption is eventually degraded to heat, this measured demand is therefore the same as the total heat emission (both sensible and latent) from the appliance. This also implies that improvements in energy-efficiency will correspond to changes in both the electrical demand and the heat gains emitted by a particular appliance.

In real life the difference in internal heat gains emitted due to technology changes for most household appliances is too small to be actually perceived and the main thermal loads will remain the heat loss or gain due to the heat transfer through the building fabric and ventilation [11]. Brunner *et al.* in [61] provide evidence, using natural gas billing data, that a changeover from incandescent bulbs to CFL did not result in a higher consumption of natural gas for use as space heating fuel, suggesting that the two are not correlated. In future zero or very low energy buildings this changeover in technology may result in a situation where the internal conditions are much more sensitive and a change in heat gain emitted is actually perceivable. In the context of this thesis however, preliminary simulations showed that the change in internal heat gains due to the appliance energy-efficiency improvements assumed had such a small effect on the internal conditions of the building, it could be neglected.

2.5.3.2 Non-electrical appliances

The final part of the methodology concerns the modelling of heat gains which are emitted from non-electrical appliances. In a household typically these are limited mainly to cooking gas hobs [11]. This is an important heat emitting activity which cannot be associated with any electrical demand. In order to model such an event, research done by Stokes in [27] is used. Stokes in [27] reports on work done by Mansouri *et al.* [62] on energy consumption in UK households whereby, based on

observed measurements from a number of households a statistical distribution was calculated to determine the probability of how many gas hobs would be used during a particular cooking event and for how long these would be 'On'. Mansouri *et al.* [62] specify data for electrical cooking hobs but in this case their research is being extended to include gas hobs as well. Also, given that the data relates to the duration of the event rather than the occurrence, the intra-country variability is negligible.

Based on the process which is shown schematically in Figure 2.35 the number of hobs used and the duration of each event can be calculated using a stochastic modelling process.

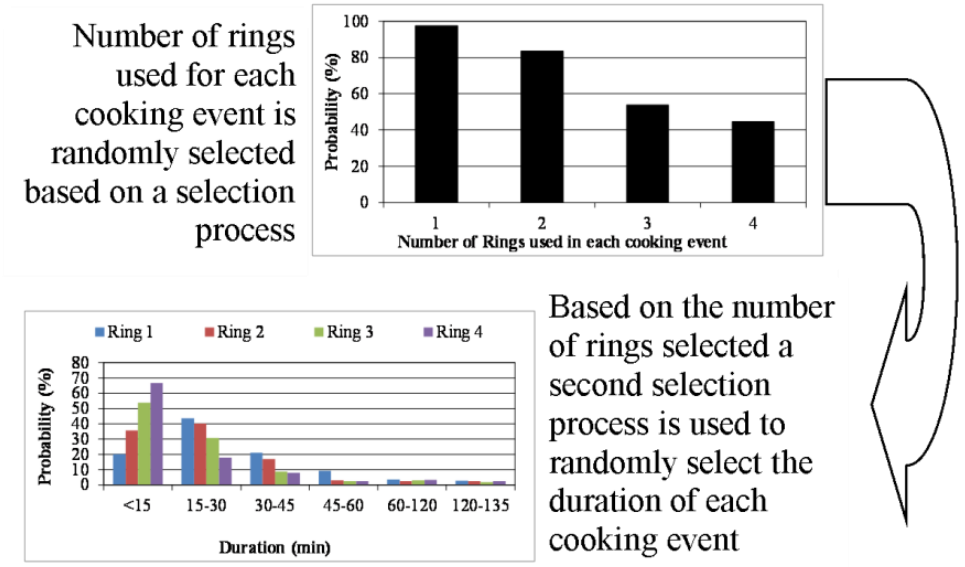

Fig. 2.35 - Stochastic process used to determine number of hobs used during a cooking event and duration of each event

The number of hobs used for a cooking event is selected using a random selection process making use of the statistical probability distribution calculated using data from Mansouri *et al*. Once the number of rings used during a particular cooking event is chosen a second selection process is used to randomly select the duration of that cooking event. The starting time of each cooking event is awarded on the basis of the probability that a cooking event is taking place.

Similarly to occupancy such a probability distribution can typically be extracted from

'time-use surveys'. In this case the 'time-use surveys' conducted by the National Statistics Office in Malta was used [63]. Following this selection process each lit burner is allocated a sensible heat gain value of 965 Watts.

2.5.3.3 Aggregated internal heat gains due to appliances

Figure 2.36 shows the aggregated internal heat gains due to the appliances for household 3B for a characteristic day in May.

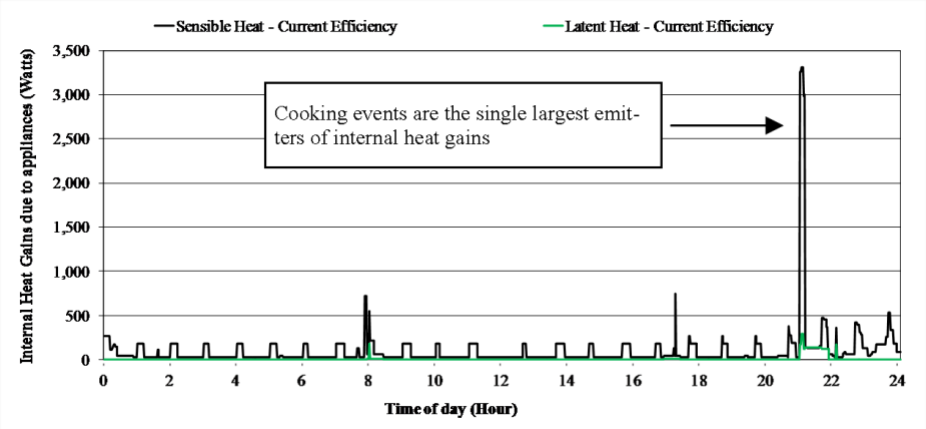

Fig. 2.36 - Aggregated internal heat gains due to appliances

It can be observed that a considerable part of the internal heat gains due to appliances in residential households is due to relatively short duration cooking events. Other appliances such as lighting or audiovisual equipment have a lower but more prolonged effect reflecting their use and electrical demand. Also, typically latent heat output from appliances is considerably lower or negligible compared to their sensible heat output.

2.5.4 Aggregated internal heat gains and use in simulations

Once the individual internal heat gain profiles for each of the appliances and the occupants were created, these were aggregated together into one profile, representing the total internal heat gains of a particular apartment. Figure 2.37 shows the aggregated internal heat gain profile due to occupants and appliances for household 3B for a characteristic day in May. The resulting profile could be exported to ESP-r for use in simulations.

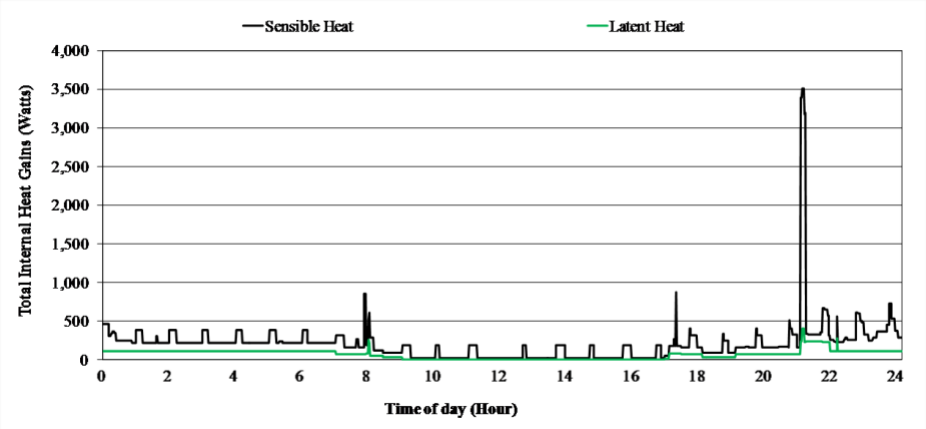

Fig. 2.37 - Total internal heat gains profile for household 3B

The same process was used to model the internal heat gains for each of the 3 households in the 3 household building and the 6 households in the 6 household building for the other months. The end result was that each individual floor/apartment was represented by its own distinctive and consistent electrical demand and internal heat gains profile.

2.6 Domestic Hot Water (DHW) demand

The last part of modelling the demand side described in the chapter relates to the modelling of the domestic hot water demand. A lot of research on this subject has already been conducted in other studies such as the IEA ECBCS Annex 42 [64] and IEA SHC Annex 26 [65]. The main activity was therefore to adapt this research in the context of Mediterranean climates based on the conditions present in the households being investigated.

2.6.1 Modelling the DHW demand in Mediterranean climates

Domestic hot water usage varies from country to country depending on the availability of the resource and its associated cost [64]. Compared to countries where water is not a scarce resource *e.g.* Canada (94 litres/day/person), Germany (64 litres/day/person) and Finland (43 litres/day/person), countries in the Mediterranean region, given the high premium paid, have a lower daily consumption in the region of 30 litres/day/person [64]. Related literature by Borg *et al.* in [66] suggests that the

annual average daily hot water usage for each individual occupant in Malta is also in this range, a consumption comparable to another Mediterranean island, Cyprus [67].

Based on this assumption, the interactive tool created by Jordan and Vajen [68] was used to model the domestic hot water profile for both the 3 household building equivalent to 9 persons and for the 6 household building equivalent to 18 persons. The tool permits the creation of realistic domestic hot water profiles in different time-scales, which are based on a number of user set assumptions on the way and time hot water is used in a specific household. The resolution used in this case is that of 1 minute. Table 2.12 shows the basic assumptions used to create the DHW profiles for each of the three households in the 3 household building.

Table 2.12 - Assumptions used to create DHW profile for 3 household building

Household / Floor	**2A / Ground floor**	**3B / Middle floor**	**4B / Top floor**
Number of Persons	2	3	4
Notes	Place vacant - No DHW draw between 08.00-18.00 Hours	Place vacant - No DHW draw between 09.00-17.00 Hours	Place vacant - No DHW draw between 10.00-15.00 Hours
Daily Draw	60ltr/day annual average	90ltr/day annual average	120ltr/day annual average
Mean DHW-volume tapped during 6 time periods (Time period / ratio of daily DHW drawn during time segment)	24:00-06:30 / 6.2 %	22:00-06:30 / 6.6 %	22:00-06:30 / 5.4 %
	06:30-07:30 / 23.9 %	06:30-08:30 / 20.8 %	06:30-09:30 / 37.8 %
	07:30-18:30 / 0.0 %	08:30-17:30 / 0.0 %	09:30-15:30 / 0.0 %
	18:30-19:30 / 11.9 %	17:30-19:00 / 26.0 %	15:30-17:00 / 10.4 %
	19:30-22:00 / 10.2 %	19:00-21:30 / 29.9 %	17:00-18:00 / 12.6 %
	22:00-24:00 / 47.8 %	21:30-22:00 / 16.8 %	18:00-22:00 / 33.8 %

In order to maintain consistency with the occupancy and heat gain profiles, during time periods in which the apartment is assumed to be vacant (based on the related occupancy profile created for the internal heat gains), the DHW draw was assumed to be 0%. The percentages for the remaining time segments were divided based on

comparing water consumption related activities in dwellings reported in the 'time-use survey' conducted for the Maltese Islands by the National Statistics Office [63] in Malta with the likelihood of a hot water draw.

Figure 2.38 shows the aggregated DHW profile for all three households over a 6 day period with a time resolution of 1 minute.

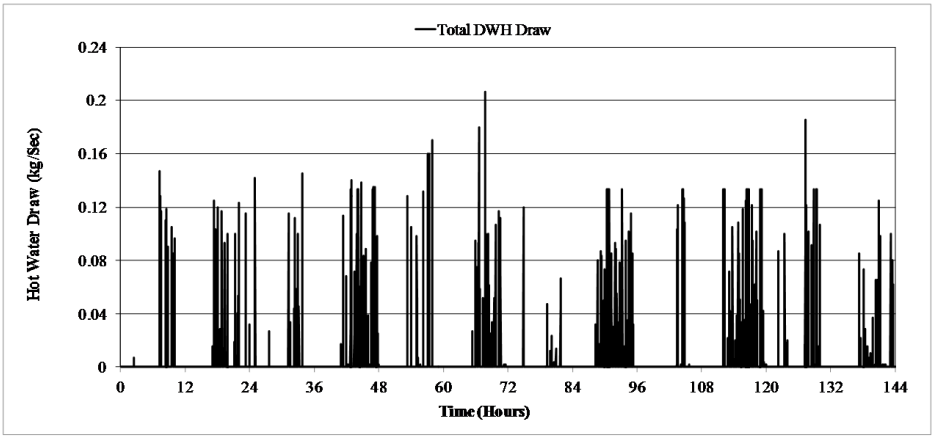

Fig. 2.38 - Aggregated DHW draw profile for the 3 household building

In this case only the aggregated DHW profile for the three households is required, as the hot water demand (in kg/s) is associated with one single draw off by the DHW supply pump from the domestic hot water storage tank fed by the micro-trigeneration system (as shown in Figure 3.2). In a similar fashion to the case of internal heat gains, the minutely DHW profile can be used by the ESP-r tool whilst performing the simulation. Also, during the simulations the inlet temperature was set at the seasonal mains temperature, whilst the nominal outlet temperature was set at 60/65ºC.

The 30 litres/day/person annual average assumed in this research is already a conservative amount and so no further reductions were envisaged in this thesis. The only variable which is therefore being considered is the different draw volumes associated with the 3 household and the 6 household building models. In this context, in the case of the 6 household building, again the assumptions used to represent the profiles of the added households, and which are shown in Table 2.13, are based on the occupancy profiles modelled using the methodology discussed in Section 2.5.

Figure 2.39 shows the resulting aggregated DHW profile for all six households over a 6 day period with a time resolution of 1 minute.

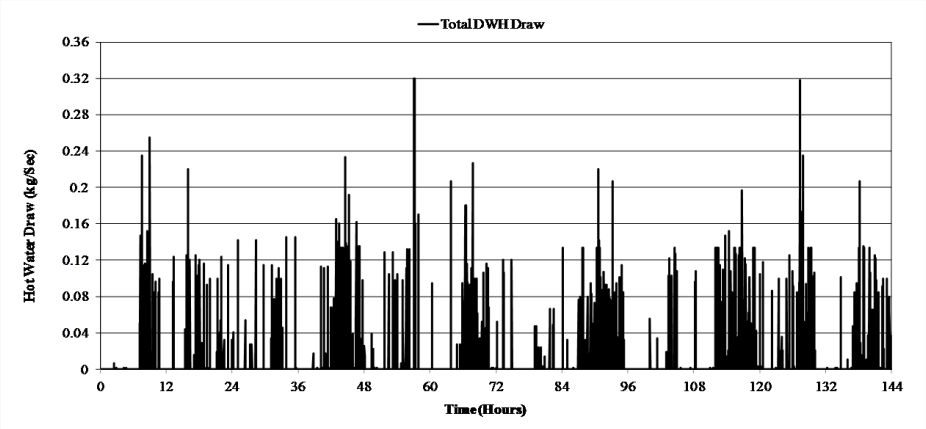

Fig. 2.39 - Aggregated DHW draw profile for the 6 household building

Table 2.13 - Assumptions used to create additional DHW profile for 6 household building

Household / Floor	**3A / Added to 2A to represent 2-household ground floor**	**4A / Added to 3B to represent 2-household middle floor**	**2B / Added to 4B to represent 2-household top floor**
Number of Persons	3	4	2
Notes	Place vacant - No DHW draw between 07.00-15.00 Hours	Place never vacant	Place vacant - No DHW draw between 08.00-13.00 Hours
Daily Draw	90ltr/day annual average	120ltr/day annual average	60ltr/day annual average
Mean DHW-volume tapped during 6 time periods (Time period / ratio of daily DHW drawn during time segment)	22:00-06:30 / 20.6 %	22:00-06:30 / 16.6 %	22:00-06:30 / 24.9 %
	06:30-07:30 / 10.6 %	06:30-07:30 / 20.1 %	06:30-07:30 / 14.7 %
	07:30-12:00 / 0.0 %	07:30-12:00 / 15.1 %	07:30-10:00 / 0.0 %
	12:00-15:30 / 0.0 %	12:00-13:00 / 2.8 %	10:00-13:30 / 0.0 %
	15:30-18:00 / 19.3 %	13:00-18:00 / 15.3 %	13:30-18:00 / 31.0 %
	18:00-22:00 / 49.6 %	18:00-22:00 / 30.1 %	18:00-22:00 / 29.3 %

2.7 Summary of Chapter 2

The aim of this chapter was primarily to explain the methodology used to model the

various aspects which make up the heat and power demands of the building, and explain how the various factors being investigated were factored in the modelling process.

In the case of the electrical demand, a method has been developed whereby low-resolution electrical demand datasets can be used to create high-resolution demand data reflecting the effects of appliance energy-efficiency improvements. The method makes use of a three stage transformation process which first creates seasonal variations of individual monthly data, then converts the low-resolution hourly data into high-resolution minute data and finally projects the data into a high efficiency scenario reflecting improved appliance energy-efficiency. Such a method therefore permits the creation of two high resolution electrical efficiency scenarios, a current efficiency and a high efficiency.

In the case of the thermal demand, it was discussed how this can be broadly divided into two parts, the domestic hot water demand and the heating and cooling energy demand arising from space conditioning. The modelling of the domestic hot water demand makes use of established research to create minute resolution hot water demand profiles. The former demand is more complex, as it is the result of a number of factors, including climate, building characteristics, solar gains and internal heat gains and requires the use of a building simulation tool to calculate. This chapter therefore focused on two critical aspects that affect the heat load: the modelling of the building characteristics and the internal heat gains. The chapter elaborates on how the building fabric and the geometry were modified to include for operating conditions which could possibly impact micro-trigeneration system performance. With regards to the internal heat gains, this chapter presents a process leading to the modelling of high resolution internal heat gains due to occupants and appliances which was eventually used in the simulations.

2.8 Chapter References

[1] *"ESP-r"*, 2005, Energy Systems Research Unit, Department of Mechanical and Aerospace Engineering, University of Strathclyde Glasgow, UK

[2] Kelly, N.J., (1998) "*Towards a design environment for building integrated energy systems: The Integration of electrical power flow modelling with building simulation."* Doctoral Thesis - Department of Mechanical and Aerospace Engineering, University of Strathclyde, Glasgow, UK

[3] Aasem, E.O., (1993) "*Practical simulation of buildings and air-conditioning in the transient domain."* Doctoral Thesis - Department of Mechanical and Aerospace Engineering, University of Strathclyde, Glasgow, UK

[4] Hensen, J.L.M., (1991) "*On the thermal interaction of building structure and heating and ventilation system."* Doctoral Thesis - Technische Universiteit Eindhoven, The Netherlands

[5] "*Temperature records for the Maltese Islands"*. Online Database held at www.maltaweather.com [Accessed: 08/02/2011]; Available from: http://www.maltaweather.com/archives.shtml

[6] National Statistics Office (2007). "*Census of Population and Housing 2005, Volume 2: Dwellings."* - National Statistics Office, Valletta, Malta.

[7] Borg, S.P., Kelly, N.J. and Rizzo, K. "*Modelling and simulating the effects of the use of insulated building fabric in a multi-story Maltese residential building"* in *Sustainable Energy 2012: The ISE Annual Conference*. 2012. Qawra, Malta

[8] Abela, A., Hoxley, M., McGrath, P. and Goodhew, S. (2011). "*A comparative study of the implementation of the energy certification of residential properties in Malta in compliance with the Energy Performance of Buildings Directive"* - School of Architecture, Design and the Built Environment, Nottingham Trent University. Nottingham, UK. Available from: http://nottinghamtrent.academia.edu/AlanAbela/Papers/1123894/A_comparative_study_of_the_implementation_of_the_energy_certification_of_residential_properties_in_Malta_in_compliance_with_the_Energy_Performance_of_Buildings_Directive [Accessed: 28/12/2011]

[9] *"Malta Building Regulations, Part F - Conservation of Fuel, Energy and*

natural Resources" - (LN 238 of 2006). Building Regulations Office, Malta

[10] National Statistics Office (2007). "*Census of Population and Housing 2005, Volume 1: Population."* - National Statistics Office, Valletta, Malta.

[11] ASHRAE, *"Chapter 17 - Residential Cooling and Heating Load Calculations"* in *"The 2009 ASHRAE Handbook - Fundamentals"*, Mark Owen, Editor. 2009, American Society of Heating Refrigerating and Air Conditioning Engineers

[12] "*Development Control Policy and Design Guidance 2007"* - Malta Environment and Planning Authority, Floriana, Malta. Available from: www.mepa.org.mt/file.aspx?f=965 [Accessed: 08/06/11]

[13] Jorge, J., Puigdoemench, J. and Cusiodo, A. "*A practical tool for sizing optimal shading devices"* Building and Environment, 1993. 28(1): pgs. 69-72

[14] Tejedor, M.V., Farrugia, R.N. and Yousif, C. *"Energy Study in a Maltese Household"*, in *World Renewable Energy Congress*, A. Sayigh, Editor. 2008. pgs. 757-762

[15] Giama, E., Papadopoulos, A.M. and Anastaselos, D. "*An assessment tool for the energy, economic and environmental evaluation of thermal insulation solutions"* Energy and Buildings 2009. 41: pgs. 1165-1171

[16] D'Orazio, M., Di Perna, C. and Di Giuseppe, E. "*The effects of roof covering on the thermal performance of highly insulated roofs in Mediterranean climates"* Energy and Buildings, 2010. 42: pgs. 1619-1627

[17] Pilavachi, P.A., Nikolaidis, Y. and Chletsis, A. "*Economic evaluation of energy saving measures in a common type of Greek building"* Applied Energy, 2009. 86: pgs. 2250-2559

[18] Buhagiar, V. "*Technical Improvement of Housing Envelopes in Malta"*. 2007 [Accessed: 30/11/2010]; Available from: www.costc16.org/downloads/FACADES_AND_ROOFS/Boek_04-09.pdf

[19] *"Directive 2002/91/EC of the European Parliament and of the Council of 16 December 2002 on the energy performance of buildings"* - European Parliament and European Council

[20] Buhagiar, V. (2002). "*Energy efficiency in building design"* - BICC, Valletta, Malta. [Accessed: 30/10/2010]; Available from:

http://www.bicc.gov.mt/bicc/files_folder/Energy%20efficiency%20in%20Building%20Design%20by%20VB.pdf

[21] Buhagiar, V. "*Sustainable Development and Building Design in Malta"* in *BEPIC - Built Environment Professions in the Commonwealth*. 2005. Valletta, Malta: Commonwealth Association of Architects

[22] Buhagiar, V. and Yousif, C. "*A post occupancy evaluation of energy efficient measures in the housing sector: A case study for Malta"*. 2008 [Accessed: 30/10/2010]; Available from: http://www.buildup.eu/system/files/content/Energy%20Efficient%20Social%20Housing%20in%20Malta%20-%20Birkirkara%20Tal-Ftieh,%20a%20Pilot%20Study.pdf

[23] Hawkes, A. and Leach, M. "*Impacts of temporal precision in optimising modelling of micro-Combined Heat and Power"* Energy, 2005. 30: pgs. 1759-1779

[24] Wright, A. and Firth, S. "*The nature of domestic electricity-loads and effects of time averaging on statistics and on-site generation calculations"* Applied Energy, 2007. 84(2007): pgs. 389-403

[25] Borg, S.P. and Kelly, N.J. "*The effect of appliance energy efficiency improvements on domestic electric loads in European households"* Energy and Buildings, 2011. 43(9): pgs. 2240-2250

[26] REMODECE Project Members (2008). "*REMODECE Database - Residential Monitoring to Decrease Energy Use and Carbon Emissions in Europe (IEEA Program Funded Project)"*. [Database] 2008 [Accessed: 01/12/2009]; Available from: http://www.isr.uc.pt/~remodece/database/login.htm

[27] Stokes, M., (2004) "*Removing barriers to embedded generation: a fine-grained load model to support low voltage network performance analysis."* Doctoral Thesis - Institute of Energy and Sustainable Development, De Montfort University, Leicester, UK

[28] Richardson, I., Hodgson, G., Thomson, M., Infield, D. and Delahunty, A. *"Simulation of high-resolution domestic electricity demand based on a building occupancy model and its applicability to the study of demand side management"*, in *5th EEDAL - International Conference on Energy Efficiency*

in Domestic Appliances and Lighting. 2009: Berlin

[29] Widén, J. and Wäckelgård, E. "*A high-resolution stochastic model of domestic activity patterns and electricity demand*" Applied Energy, 2010. 87(6): pgs. 1880-1892

[30] Widén, J., Lundh, M., Vassileva, I., Dahlquist, E., Ellegård, K. and Wäckelgård, E. "*Constructing load profiles for household electricity and hot water from time-use data-Modelling approach and validation*" Energy and Buildings, 2009. 41(7): pgs. 753-768

[31] Ipsos-RSL and Office for National Statistics, UK Data Archive (distributor), United Kingdom Time Use Survey, 2000 (Computer File), 3rd ed., Colchester, Essex, UK,

[32] Larsonneur, P. (2006). "*Establishment of the samples for the monitoring and survey campaigns*" - ADEME. Paris, France. Available from: http://www.isr.uc.pt/~remodece/downloads/REMODECE_D9_Nov2008_Final.pdf [Accessed 01/12/2009];

[33] REMODECE Project Members (2008). "*Final Report REMODECE - Residential monitoring to Decrease Energy use and Carbon Emissions in Europe (IEEA Program Funded Project)*". Available from: http://www.isr.uc.pt/~remodece/downloads/REMODECE_D9_Nov2008_Final.pdf [Accessed 01/12/2009]

[34] John, E.G., "*Simplified Curve Fitting using Spreadsheet Add-ins*" International Journal of Engineering Education 1998. 14(5): pgs. 375-380

[35] Zmeureanu, R. and Farinaccio, L. "*Using a pattern recognition approach to disaggregate the total electricity consumption in a house into the major end-uses*" Energy and Buildings 1999. 30: pgs. 245-259

[36] EURECO Partners (2002). "*Final Report*" - EURECO Project - End-use metering campaign in 400 households of the European Community, SAVE Programme Contract N° 4.1031/Z/98-267. EURECO Project - End-use metering campaign in 400 households of the European Community

[37] *de* Almeida, A., Fonseca, P., Schlomann, B., Feilberg, N. and Ferreira, C. "*Residential monitoring to Decrease Energy use and Carbon Emissions in Europe*" in *Energy Efficiency in Domestic Appliances and Lighting (EEDAL)*

Conference 2006. 2006. London

[38] DEFRA. "*Market Transformation Programme"* - DEFRA, UK [Accessed: 08/04/2010]; Available from: http://efficient-products.defra.gov.uk/cms/market-transformation-programme/

[39] *"Directive 92/75/EEC of 22 September 1992 on the indication by labelling and standard product information of the consumption of energy and other resources by household appliances"* - European Parliament and European Council

[40] DEFRA, *"What if? Tool "*, 2008, [Accessed 01/03/2010]; Available from: http://whatif.mtprog.com/

[41] DEFRA (2008). "*Assumptions underlying the energy projections of cooking appliances"* - Volume in Series *"Market Transformation Programme"*. DEFRA, UK

[42] DEFRA (2008). "*Assumptions underlying the energy projections for domestic cold appliances"* - Volume in Series *"Market Transformation Programme"*. DEFRA, UK

[43] DEFRA (2008). "*Policy Brief: Improving the energy performance of domestic heating and hot water systems"* - Volume in Series *"Market Transformation Programme"*. DEFRA, UK

[44] DEFRA (2008). "*Water heaters: proposed energy labelling directives"* - Volume in Series *"Market Transformation Programme"*. DEFRA, UK

[45] DEFRA (2009). "*Televisions (TVs) Government Standards Evidence Base 2009: Best Available Technology Scenario"* - Volume in Series *"Market Transformation Programme"*. DEFRA, UK

[46] DEFRA (2010). "*Domestic Lighting Government Standards Evidence Base 2009: Best Available Technology Scenario"* - Volume in Series *"Market Transformation Programme"*. DEFRA, UK

[47] DEFRA (2008). "*ENERGY STAR® specification for computers"* - Volume in Series *"Market Transformation Programme"*. DEFRA, UK

[48] DEFRA (2010). "*Set Top Boxes Government Standards Evidence Base 2009: Best Available Technology Scenario"* - Volume in Series *"Market Transformation Programme"*. DEFRA, UK

[49] DEFRA (2010). "*Dishwashers Government Standards Evidence Base 2009: Best Available Technology Scenario"* - Volume in Series *"Market Transformation Programme"*. DEFRA, UK

[50] DEFRA (2010). "*Combined Laundry: Government Standards Evidence Base 2009: Best Available Technology Scenario"* - Volume in Series *"Market Transformation Programme"*. DEFRA, UK

[51] Capasso, A., Grattieri, W., Lamedica, R. and Prudenzi, R. "*A Bottom-Up approach to residential load modelling"* IEEE Transactions on Power Systems, 1994. 9(2): pgs. 957-964

[52] eERG. "*MICENE - MIsure Dei Consumi di ENergia Elettrica nel settore domestico"*. [Database Files & Reports] 2006 [Accessed: 01/12/09]; Available from: http://www.eerg.polimi.it/micene.php

[53] Herman, R. and Kritzinger, J.J. "*The statistical description of grouped domestic electrical load currents"* Electric Power Systems Research 1999. 27: pgs. 43-48

[54] Herman, R. and Trevor Gaunt, C. "*A Practical Probabilistic Design Procedure for LV Residential Distribution Systems"* IEEE Transactions on Power Delivery, 2008. 23(4): pgs. 2247-2254

[55] Hodges, L., "*The effects of internal gains on residential space heating analysis"* Energy, 1985. 10(12): pgs. 1273-1276

[56] Richardson, I., Thomson, M. and Infield, D. "*A high-resolution domestic building occupancy model for energy demand simulations"* Energy and Buildings, 2008. 40(8): pgs. 1560-1566

[57] ASHRAE, *"Chapter 18 - Non-Residential Cooling and Heating Load Calculations"* in *"The 2009 ASHRAE Handbook - Fundamentals"*, Mark Owen, Editor. 2009, American Society of Heating Refrigerating and Air Conditioning Engineers

[58] CCHT (2008). "*Benchmarking Home Energy Savings from Energy-Efficient Lighting"* - Technical Series 08-101. Canada Mortgage and Housing Corporation

[59] General Electric. *"Compact Fluorescent Light Bulb (CFL) FAQs"*. [Accessed: 30/04/2010]; Available from:

http://www.gelighting.com/na/home_lighting/ask_us/faq_compact.htm

[60] Hosni, M.H., Jones, B.W. and Xu, H. "*Experimental Results for Heat Gain and Radiant/Convective Split from Equipment in Buildings*" ASHRAE Transactions, 1999. 105(1): pgs. 527-539

[61] Brunner, E.J., Ford, P.S., McNulty, M.A. and Thayer, M.A. "*Compact fluorescent lighting and residential natural gas consumption: Testing for interactive effects*" Energy Policy 38, 2010. 38: pgs. 1288-1296

[62] Mansouri, I., Newborough, M. and Probert, D. "*Energy Consumption in UK Households Impact of Domestic Electrical Appliances*" Applied Energy, 1996. 54(3): pgs. 211-285

[63] National Statistics Office (2007). "*Time Use-Survey 2002*" - National Statistics Office, Valletta, Malta.

[64] Knight, I., Kreutzer, N., Swinton, M., Manning, M. and Ribberink, H. (2007). "*European and Canadian non-HVAC Electric and DHW Load Profiles for use in Simulating the Performance of Residential Cogeneration Systems*" - A Report of Subtask A of FC+COGEN+SIM The Simulation of Building-Integrated Fuel Cell and Other Cogeneration Systems: Annex 42 of the International Energy Agency's Conservation in Buildings and Community Systems Programme. International Energy Agency

[65] Jordan, U. and Vajen K. (2001). "*Realistic Domestic Hot-Water Profiles in Different Time Scales*" - Solar Heating and Cooling Program of the International Energy Agency (IEA SHC), Task 26: Solar Combisystems. International Energy Agency

[66] Borg, S.P., Yousif, C. and Farrugia, R.N. *"Investigation of domestic Solar Water Heating installations in Malta"*, in *Renewable Energies in Malta and beyond*. 2005: Salina, Malta

[67] Kalogirou, S.A. "*Use of TRNSYS for modelling and simulation of a hybrid pv–thermal solar system for Cyprus*" Renewable Energy, 2001. 23 pgs. 247-260

[68] Jordan, U. and Vajen, K. *"DHWcalc: Program to generate domestic hot water profiles with statistical means for user defined conditions"*, in *ISES Solar World Congress*. 2005: Orlando, USA

CHAPTER 3
MODELLING MICRO-TRIGENERATION

Following on from the description of building modelling in Chapter 2, Chapter 3 focuses on the micro-trigeneration plant, providing a detailed description of the system modelled and the associated control strategies; the control used to maintain adequate indoor temperatures in each of the individual apartments/floors and the control strategy used to control the individual plant components. The chapter also highlights the main aspects of modelling plant systems in ESP-r along with the development of a new dynamic absorption chiller model for use in trigeneration system modelling. Finally, the chapter introduces a number of possible trigeneration system variants which are analysed in later chapters.

3.1 Control strategies for the indoor air temperatures

Chapter 2 explained that in order to ensure better temperature control of the individual apartments, each apartment in the two buildings modelled (the 3 and the 6 household building) was divided into two zones, a living area and a bedroom area zone. For each individual zone a different control strategy was adopted for both the heating and cooling season, based on whether that particular zone was occupied or not. The temperature controlled periods during which the indoor temperature in each zone was controlled, was based on the occupancy. Living area zones were assumed to be occupied between 7 in the morning and midnight (except when the occupancy profile dictated that the apartment was vacant), whilst bedroom area zones were considered to be occupied from midnight till 7 in the morning. This is typical of a 'working family' profile in Malta [1].

3.1.1 Heating season set control temperatures

The thermally controlled time periods and (heating season) temperature limits for the individual zones in the 3 household building were set as shown in Table 3.1. The heating season was assumed to start on the 17th of December and finish on the 19th of March, a 92 day period chosen on the basis of similar heating season durations used for other Mediterranean countries [2].

Determining with exact precision when heating is required in residential buildings is difficult given that, in their own domestic environment occupants tend to have much better control of both the surrounding environment and the way they adjust to it, compared to being in public places [3]. Their adaptability is therefore much higher. For example, although people might be inside and according to comfort theory (Fanger [4]) heating may be required, heating may still not be used, as the occupants would adjust (*e.g.* by changing clothes, drinking warm beverages *etc*.). Based on the fact that the daily mean temperatures tend to be lowest during the evening, in this research it was assumed that heating was needed predominantly around this time of the day, with the start time being when the apartment would become occupied after being left vacant during the day. Although as reported by Peeters *et al.* in [3], the World Health Organisation recommends a minimum bedroom temperature of 16°C,

the same research also suggests that bedrooms which do not double as study rooms or extended living areas (for watching television) are typically not heated during the night. It is argued in [3] that people tend to use thick sheets and warmer clothing to keep warm during the night rather than switching on heating. In this study it was therefore assumed that during the heating season, for a typical Maltese climate, only the living areas are heated (during preset times of the day) and all bedroom area zones are thermally uncontrolled.

Table 3.1 - Control settings for heating season; 3 Household building

Floor level / Apartment	**Zone**	**Household No.**	**Occupancy (No. of persons)**	**Control time periods (Temperature limits) ('Off' - 'On')**	**Comment**
Ground Floor	Living Area	2A	2	18.00-24.00 Hours (21.5°C - 18.5°C) Remaining hours were uncontrolled	Ground floor is vacant between 08.00-18.00 Hours
	Bedroom Area			24.00-07.00 Hours Uncontrolled	
Middle Floor	Living Area	3B	3	17.00-24.00 Hours (21.5°C - 18.5°C) Remaining hours were uncontrolled	Middle floor is vacant between 09.00-17.00 Hours
	Bedroom Area			24.00-07.00 Hours Uncontrolled	
Top Floor	Living Area	4B	4	15.00-24.00 Hours (21.5°C - 18.5°C) Remaining hours were uncontrolled	Top floor is vacant between 10.00-15.00 Hours
	Bedroom Area			24.00-07.00 Hours Uncontrolled	

Setting an acceptable temperature controlled range depends on an individual's age, how active they are, type of clothing they are wearing, physiological and psychological disposition to be adaptable to the temperature *etc.* [3]. Similarly, different guidelines such as ASHRAE [5] and CIBSE [6] offer slightly dissimilar interpretations of what constitutes the optimum indoor temperature range [7]. As shown in Table 3.1, in this study an indoor air temperature range of 18.5°C-21.5°C was chosen as a reasonable compromise between the various guidelines. The HVAC system therefore was set to control the indoor air temperature inside the different

floors within a ‘dead band’ of 3ºC. During controlled time periods, if the air temperature inside any zone fluctuates outside the defined temperature range, the HVAC system would supply hot (or cold air depending on the season) air to adjust the indoor air temperature back into the defined range. In this case the HVAC system would switch ‘On’ when the indoor temperature falls below 18.5°C and would switch ‘Off’ if the indoor air temperature rises beyond 21.5°C.

The same procedure was adopted to determine the control parameters for the individual zones in the 6 household building as shown in Table 3.2. The control temperature range is the same used for the 3 household building. The thermally controlled periods were however adjusted to reflect the (time-sensitive) occupancy profiles of the two household units present on each floor.

Table 3.2 - Control settings for heating season; 6 Household building

Floor level / Apartment	**Zone**	**Household No.**	**Occupancy (No. of persons)**	**Control time periods (Temperature limits) (‘Off’ - ‘On’)**	**Comment**
Ground Floor	Living Area	2A + 3A	5	15.00-24.00 Hours (21.5°C - 18.5°C) Remaining hours were uncontrolled	Ground floor is vacant between 08.00-15.00 Hours
	Bedroom Area			24.00-07.00 Hours Uncontrolled	
Middle Floor	Living Area	3B + 4A	7	17.00-24.00 Hours (21.5°C - 18.5°C) Remaining hours were uncontrolled	Middle floor is never vacant
	Bedroom Area			24.00-07.00 Hours Uncontrolled	
Top Floor	Living Area	4B + 2B	6	16.00-24.00 Hours (21.5°C - 18.5°C) Remaining hours were uncontrolled	Top floor is vacant between 10.00-13.00 Hours
	Bedroom Area			24.00-07.00 Hours Uncontrolled	

3.1.2 Cooling season set control temperatures

As discussed in Chapter 1, most regions in Mediterranean countries have a considerable demand for cooling which could justify the use of a thermally activated

cooling device in conjunction with a micro-cogeneration unit. The cooling season in this thesis was assumed to span four months, from the beginning of June to the end of September, a calendar period of 122 days during which the mean outside temperature is at or above 25°C. Table 3.3 shows the temperature control settings adopted in the case of the individual apartments in the 3 household building.

Table 3.3 - Control settings for cooling season; 3 Household building

Floor level / Apartment	**Zone**	**Household No.**	**Occupancy (No. of persons)**	**Control time periods (Temperature limits) ('On' - 'Off')**	**Comment**
Ground Floor	Living Area	2A	2	07.00-08.00 Hours 18.00-24.00 Hours (24°C - 21°C)	Ground floor is vacant between 08.00-18.00 Hours
	Bedroom Area			00.00-07.00 Hours (24°C - 21°C)	
Middle Floor	Living Area	3B	3	07.00-09.00 Hours 17.00-24.00 Hours (24°C - 21°C)	Middle floor is vacant between 09.00-17.00 Hours
	Bedroom Area			00.00-07.00 Hours (24°C - 21°C)	
Top Floor	Living Area	4B	4	07.00-10.00 Hours 15.00-24.00 Hours (24°C - 21°C)	Top floor is vacant between 10.00-15.00 Hours
	Bedroom Area			00.00-07.00 Hours (24°C - 21°C)	

A major difference between the cooling and heating season thermal controls is the fact that during the night the temperature in the bedroom area zones was continuously controlled. In summer, especially during the night, adaptive measures may be limited, as even opening windows may prove worthless if the outside temperature is high and there is a lack of natural ventilation. To ensure optimum temperature conditions throughout day and night, the temperature inside the apartments is hence always thermally controlled, except for time periods when an individual apartment was assumed to be vacant.

The temperature settings were selected on the basis of a three degree temperature range, below the 24°C temperature suggested by Humphreys in [8] as being the maximum temperature limit beyond which sleep may become uncomfortable and

below the maximum comfortable temperature of around 26°C recommended by both CIBSE in [6] and ASHRAE in [5]. For the 6 household building, similar settings were adopted as shown in Table 3.4.

Table 3.4 - Control settings for cooling season; 6 Household building

Floor level / Apartment	Zone	Household No.	Occupancy (No. of persons)	Control time periods (Temperature limits) ('On' - 'Off')	Comment
Ground Floor	Living Area	2A + 3A	5	07.00-08.00 Hours 15.00-24.00 Hours (24°C - 21°C)	Ground floor is vacant between 08.00-15.00 Hours
	Bedroom Area			00.00-07.00 Hours (24°C - 21°C)	
Middle Floor	Living Area	3B + 4A	7	07.00-24.00 Hours (24°C - 21°C)	Middle floor is never vacant
	Bedroom Area			00.00-07.00 Hours (24°C - 21°C)	
Top Floor	Living Area	4B + 2B	6	07.00-10.00 Hours 13.00-24.00 Hours (24°C - 21°C)	Top floor is vacant between 10.00-13.00 Hours
	Bedroom Area			00.00-07.00 Hours (24°C - 21°C)	

3.1.3 Intermediate season

The indoor temperature of all apartment zones during the intermediate season, which covers the calendar period between the 20th of March and the end of May and the beginning of October and the 18th of December, was uncontrolled for the entire duration of the period. Although during this calendar period daily morning and afternoon temperatures tend to be in the low 20s [9], temperatures are still comfortable enough that no cooling is required. Similarly temperatures during the evening are high enough that no heating is required. No form of indoor temperature control was assumed for any of the apartments during this period. The thermal demand in this case was therefore exclusively due to the hot water demand.

3.2 Satisfying the energy demand - The micro-trigeneration plant configuration

Before describing how the micro-trigeneration plant was modelled and controlled to satisfy the energy demands of the building, Section 3.2.1 elaborates on the building

simulation tool ESP-r by explaining important principles in ESP-r plant modelling.

3.2.1 Modelling a plant network in ESP-r

ESP-r offers the facility of creating complex plant system models comprising groups of components linked together in a "network" which can represent a building energy sub-system such as a ventilation system or in this case a detailed trigeneration fed HVAC system. This plant network can be integrated with the building model to form a complete representation of the building and its attendant energy systems.

In creating plant networks, the first aspect is to select the required components through an existing database of components library (*e.g.* ductwork, pipework, cooling coils, heating coils, ventilation fans, pumps, air flow diverters *etc*.) included in the tool. Recalling that the main underlying concept of ESP-r is that a complex system such as a building or a plant system can be reduced to series of discrete control volumes or nodes onto which the basic rules of conservation of energy and mass can be applied [10], a plant network can therefore be considered as a node or a set of nodes (each describing a particular plant component) linked together. For each component, the user can indicate specific features related to its physical characteristics (*e.g.* in the case of a duct these would be mass, length *etc*.) and operating characteristics (*e.g.* in the case of a pump these would be the efficiency, rated flow rate *etc*.). Once all the components have been selected the user then proceeds to link the different components.

In ESP-r plant networks, plant components are connected on the basis of what type of node is specified. In the ventilation part of a plant network, for example, only plant components whose nodes have been specified to represent an air control volume can be connected together, such as the case of a duct and ventilation fan. Similarly, for components whose nodes represent a control volume which is liquid (typically water). In the case of plant components with multiple node types, such as cooling coils, heating coils or CHP units each node has to be connected to a plant component having that same type of node. Figure 3.1 shows the case of a cooling coil. The air flow in this case is sent from the node in Air duct 1 to the node in Air

duct 2 via the air node in the cooling coil. The water flow, on the other hand, is sent from the node in Water pipe 1 to the node in Water pipe 2 via the water node in the cooling coil. The interaction between the air and water node of the cooling coil accounts for the energy transfer between the air and the water flow.

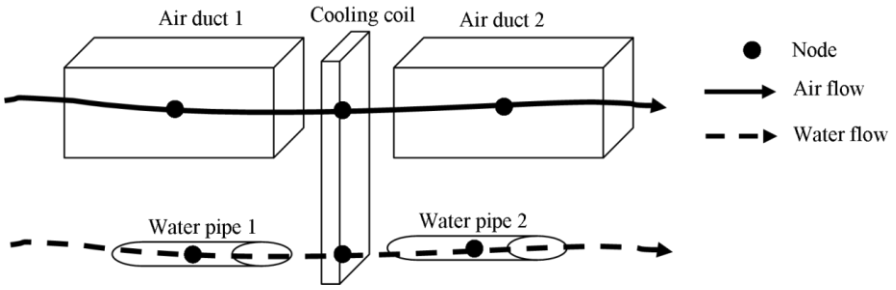

Fig. 3.1 - Plant system connections in ESP-r

Once all the links between the different components have been established, the surrounding conditions in terms of air temperature (outside air temperature or zone temperature) can be selected for each individual plant component. This is particularly important in terms of describing any potential heat loses from plant components. The final part requires the user to specify which components inside the plant network are linked to the individual building zones, *e.g.* supply and exhaust ducts, radiators, *etc*.

In order to control the output of the plant system and hence match it with the energy demands of the individual zones, a control scheme is associated with the plant network. For each component which needs to be controlled, a control scheme is defined featuring a sensor (*e.g.* a temperature sensor sensing the temperature of a particular zone in a building model), an associated actuator which responds to a signal from a controller (*e.g.* a centrifugal fan) and a control loop (*e.g.* a simple 'On'/'Off' or a more complex Proportional/Integral/Derivative [PID] control).

3.2.2 Basic plant configuration

The base case plant configuration used in the simulations (described in Chapter 5) is shown in Figure 3.2. All of the components shown, except for the absorption chiller, were already present in the ESP-r plant library. As will be explained in Section 3.3 a new dynamic absorption chiller model had to be developed for this thesis.

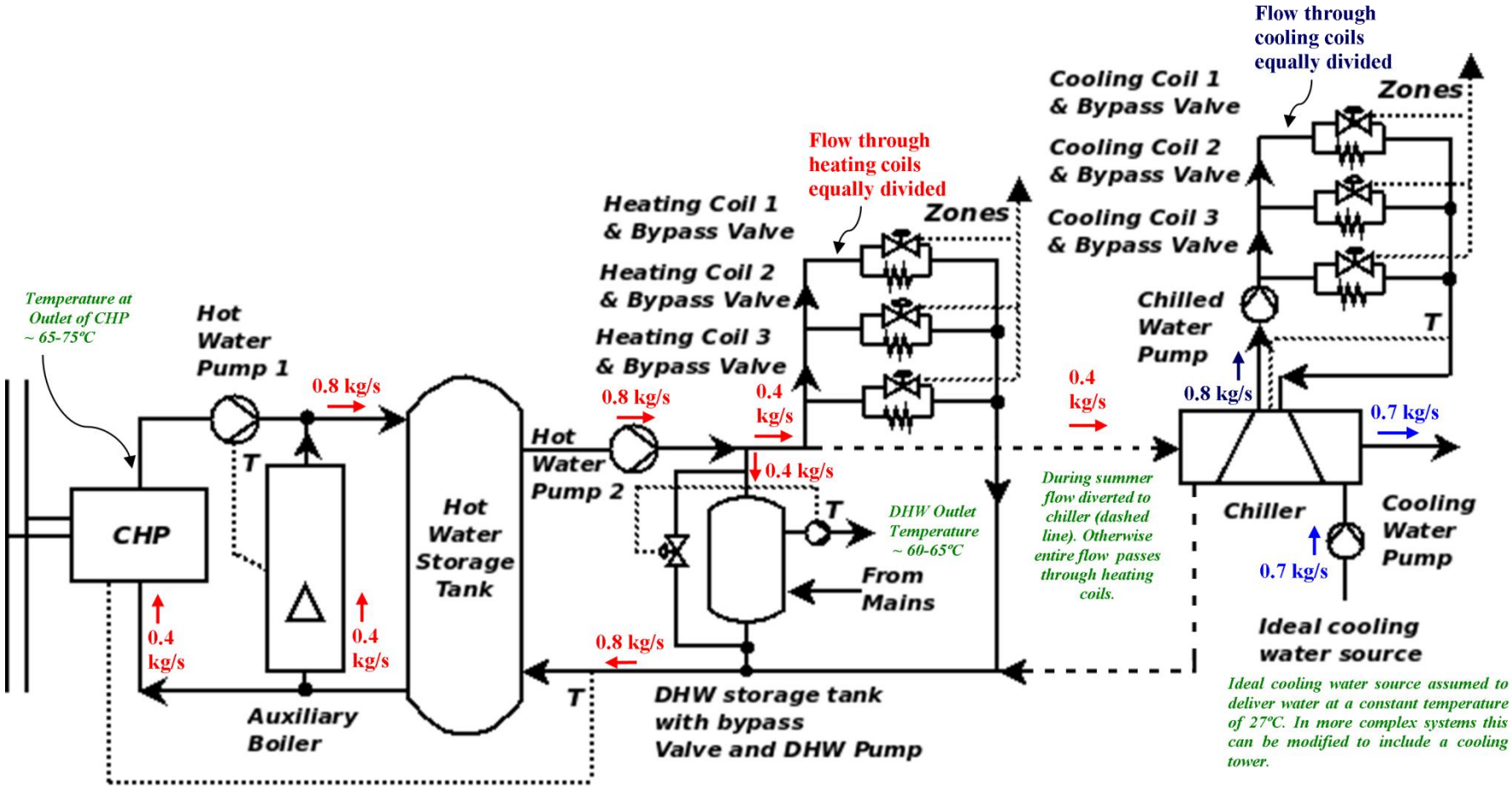

Fig 3.2 - Basic micro-trigeneration plant configuration

The dotted lines in Figure 3.2 represent the location of the controlling sensors. The control strategies adopted for the whole building and individually on each component are explained in more detail in Section 3.2.3.

The CHP component model used in the plant network to provide heating and electrical power is the one calibrated in the IEA Annex 42 project [11], and represents a 5.5 kW_{el} / 12.5 kW_{th} IC engine by Senertec Dachs [12, 13]. Although the unit is intended to run on Natural Gas, in this research the unit was assumed to run on Liquefied Petroleum Gas (LPG) as Natural Gas is absent from the Maltese fuel mix. The system was assumed to be grid connected, enabling both export and import of electricity. The recycled 'waste heat' stored in the hot water storage tank, was recovered from the engine's cooling system and the combustion exhaust gases. To cover for any shortfalls in the heat supply, an auxiliary boiler with 'On'/'Off' control (developed by Hensen in [14]) was connected in parallel to the CHP unit.

The hot water storage tank was connected via a water pump to both the domestic hot water storage tank feeding the hot water supply of the entire building, and the ventilation system. In case of the ventilation system, depending on the type of space conditioning demand required, the hot water was fed either to the absorption chiller or directly to the heating coils. Separate ventilation supply ducts were used to supply each individual apartment, with each duct containing its own cooling and heating coil. The flow could be manipulated so as to permit control of the individual apartment temperatures. For further details, Appendix 'C' shows the physical and thermal characteristics of the main components used in the plant network.

The plant network topology used was the same for both the 3 household and the 6 household models. Preliminary simulations performed showed that the same plant network topology (including cooling coils, heating coils and ancillaries sizing) could be used satisfactory for both building models provided that, the plant controls were adjusted to take into consideration the different (time-sensitive) thermal demands of the two buildings. Considering the higher demand in terms of hot water, the hot water storage tank in the 6 household building was however enlarged to 0.5m^3.

3.2.3 Control strategies for the plant

The control philosophy used to control the micro-trigeneration system during the simulations was based on matching the thermal demand. Each individual component within the system therefore responded to thermal based controls. In ESP-r a plant can be controlled by creating a dedicated control scheme. Table 3.5 describes the controls used on the plant system components feeding the 3 household building model.

Table 3.5 - Control scheme used to control the plant in the 3 household building

Control Loop 1	**CHP control**		
Description	Control scheme used to control (actuate) CHP. Control is based on feedback received from temperature sensor sensing the temperature of the water return to the hot water storage tank.		
Time – based control scheme	00.00-10.00 Hours	65°C / 75°C	'On'/'Off' Control with 10ºC dead band
	10.00-14.00 Hours	40°C / 50°C	'On'/'Off' Control with 10ºC dead band
	14.00-24.00 Hours	65°C / 75°C	'On'/'Off' Control with 10ºC dead band
Control Loop 2	**Auxiliary boiler control**		
Description	Control scheme used to control (actuate) auxiliary boiler. Control is based on feedback received from temperature sensor sensing the temperature of the water flowing through hot water pump 1.		
Time – based control scheme	00.00-10.00 Hours	60°C / 65°C	'On'/'Off' Control with 5ºC dead band
	10.00-15.00 Hours	-	Boiler 'Off'
	15.00-24.00 Hours	60°C / 65°C	'On'/'Off' Control with 5ºC dead band
Control Loop 3	**Bypass valve calorifier control**		
Description	Control scheme used to control the amount of hot water passing through or bypassing calorifier. Based on a proportional control which senses the temperature of the water flowing through the DHW supply pump the valve varies between fully open (F.O) and fully closed (F.C.).		
Time – based control scheme	00.00-24.00 Hours	Fully Open 65°C Fully Closed 60°C	Proportional Control
Control Loop 4	**Chiller**		
Description	Control scheme used to control (actuate) chiller. Control is based on feedback received from temperature sensor sensing the temperature of the water return from the cooling coils.		
Time – based control scheme	00.00-10.00 Hours	12°C / 6°C	'On'/'Off' Control with 6ºC dead band
	10.00-15.00 Hours	-	Chiller 'Off'
	15.00-24.00 Hours	12°C / 6°C	'On'/'Off' Control with 6ºC dead band
Control Loop 5	**DHW pump**		
Description	Responds to external file created using DWH profile modelled in Chapter 2		

Control Loop 6	Bypass valve cooling coil 1 control	
Description	Control scheme used to control the amount of chilled water passing through or bypassing cooling coil 1. Based on a proportional control which senses the temperature of the air return from the ground floor apartment the valve varies between fully open (F.O) and fully closed (F.C.).	
Time – based control scheme	00.00-08.00 Hours	Valve varies between fully open and fully closed when air temperature varies between 24ºC-21ºC respectively.
	08.00-18.00 Hours	No control
	18.00-24.00 Hours	Valve varies between fully open and fully closed when air temperature varies between 24ºC-21ºC respectively.

Controls 1 to 4 are used to ensure that the system works within user defined specifications. Sensors and actuators were all positioned within the plant system; sensing a parameter within a part of the plant network and sending feedback to an actuator in another part of the plant. For example, control loop 1 operates the CHP unit via an 'On'/'Off' control strategy featuring a 10ºC 'dead band' which ensured that the contents within the hot water storage tank were continuously within a controlled 10°C temperature range. Set back control is employed during the afternoon (between 10.00 and 14.00 Hours) when demand is low. In parallel the auxiliary boiler was controlled (using loop 2) in such a way that if a shortfall in the supply hot water temperature was detected, the boiler would switch 'On' to supplement the heating energy provided by the CHP Unit.

In addition to mimicking the classical control seen in buildings and systems, control in building simulation can also be used for more abstract purposes. Control loop 5 for example was used to mimic the draw on the hot water tank using one-minute profiles generated using the approach described in Chapter 2. In this case the controller sets the flow from the tank (modelled using a pump) to be equal to the flow rate in the profile (refer to Figures 2.38 and 2.39).

Finally loop 6 is an example of a control loop which creates an interaction between a plant system component and the building. In this case the sensor is positioned in the exhaust duct of the ground floor apartment, sensing the return air temperature from the ground floor apartment and sending feedback to the bypass valve of the cooling coil. Based on the temperature sensed, the bypass valve of the cooling coil increases

or decrease the flow rate of the cooling water through the cooling coil. Based on the operating times listed in Table 3.1 and Table 3.3 similar control schemes were imposed on the other heating and cooling coils.

For the 6 household building plant system a similar scheme shown in Table 3.6 was used.

Table 3.6 - Control scheme used to control the plant in the 6 household building

Control Loop 1	**CHP control**		
Description	Control scheme used to control (actuate) CHP. Control is based on feedback received from temperature sensor sensing the temperature of the water return to the hot water storage tank.		
Time – based control scheme	00.00-24.00 Hours	65°C / 75°C	'On'/'Off' Control with 10ºC dead band
Control Loop 2	**Auxiliary boiler control**		
Description	Control scheme used to control (actuate) auxiliary boiler. Control is based on feedback received from temperature sensor sensing the temperature of the water flowing through hot water pump 1.		
Time – based control scheme	00.00-24.00 Hours	60°C / 65°C	'On'/'Off' Control with 5ºC dead band
Control Loop 3	**Bypass valve calorifier control**		
Description	Control scheme used to control the amount of hot water passing through or bypassing calorifier. Based on a proportional control which senses the temperature of the water flowing through the DHW supply pump the valve varies between fully open (F.O) and fully closed (F.C.).		
Time – based control scheme	00.00-24.00 Hours	Fully Open 65°C Fully Closed 60°C	Proportional Control
Control Loop 4	**Chiller**		
Description	Control scheme used to control (actuate) chiller. Control is based on feedback received from temperature sensor sensing the temperature of the water return from the cooling coils.		
Time – based control scheme	00.00-10.00 Hours	12°C / 6°C	'On'/'Off' Control with 6ºC dead band
	10.00-15.00 Hours	-	Chiller 'Off'
	15.00-24.00 Hours	12°C / 6°C	'On'/'Off' Control with 6ºC dead band
Control Loop 5	**DHW pump**		
Description	Responds to external file created using DWH profile modelled in Chapter 2		
Control Loop 6	**Bypass valve cooling coil 1 control**		
Description	Control scheme used to control the amount of chilled water passing through or bypassing cooling coil 1. Based on a proportional control which senses the temperature of the air return from the ground floor apartment the valve varies between fully open (F.O) and fully closed (F.C.).		

Time – based control scheme	00.00-08.00 Hours	Valve varies between fully open and fully closed when air temperature varies between 24ºC-21ºC respectively.
	08.00-15.00 Hours	No control
	15.00-24.00 Hours	Valve varies between fully open and fully closed when air temperature varies between 24ºC-21ºC respectively.

In general, the control scheme used for the 6 household building is similar to the control scheme used for the 3 household building, however the operating times of the controls actuating the chiller, the CHP and the bypass valves of the cooling and heating coils were adjusted to reflect the different operating periods imposed by the different (time-sensitive) thermal demands of the 6 household building.

3.3 The absorption chiller model

To facilitate the dynamic modelling of trigeneration systems, a dedicated dynamic chiller model had to be developed for ESP-r. The chiller model described represents a single-effect hot water fed lithium bromide-water absorption chiller, the most apt [15] for use in CCHP trigeneration systems, however the same rationale can be extended to other chiller setups. The pragmatic, yet fully-dynamic model described was designed to be easily calibrated using data that can be obtained by measurements of inflows and outflows to a chiller, without resorting to intrusive measurements, thus greatly reducing the complexities involved and simultaneously increasing the model's flexibility. The model described here builds upon the work done by Beausoleil-Morrison *et al*. [16] who developed a steady state chiller model for the tool.

3.3.1 The absorption chiller cycle

Contrary to a vapour compression cycle which relies on an energy-intensive process of compressing the refrigerant vapour exiting the evaporator through the use of a compressor, an absorption refrigeration cycle relies on the affinity between two liquids to dissolve the refrigerant inside a liquid solution which can then be pumped, in a less energy-intensive process. Figure 3.3 shows a schematic of a single-effect hot water fed chiller showing the associated external (dashed lines) and internal (solid lines) flows inside the chiller. The external flows constitute the feed flows, that is, the hot, chilled and cooling water circuits, whilst the internal flow is the cycle

refrigerant, which in this case is water.

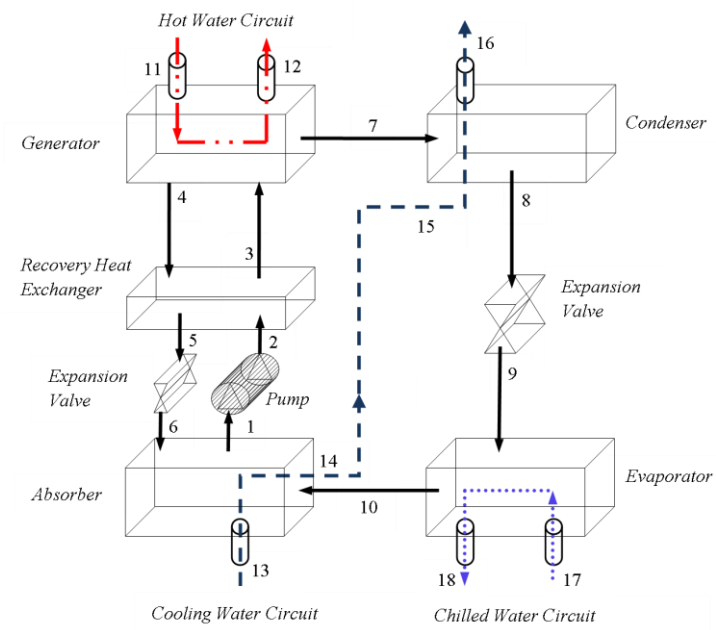

Fig 3.3 - Internal and external flows inside an absorption chiller

Considering the thermodynamic process as starting from the evaporator and moving in a clockwise rotation, the operation of the chiller is as follows:

- After having absorbed thermal energy from the surrounding environment through the chilled water circuit (Points 17-18), the refrigerant exiting the evaporator in gas form (Point 10) is absorbed by a solvent (a liquid which has a high affinity with the refrigerant) inside the absorber.

- The solution which then consists of the solvent and the refrigerant is passed through a pump (Points 1-2) to raise the pressure of the solution to the high system pressure present inside the condenser-generator setup.

- On exiting the pump and after passing through the heat recovery heat exchanger (Point 3), the solution is heated up inside the generator by absorbing heat from the external hot water circuit (Points 11-12). The difference in boiling temperature distils the refrigerant from the solution.

- The refrigerant continues its thermodynamic cycle by condensing inside the condenser (Points 7-8), thus releasing the heat previously absorbed in the evaporator. On the other hand the now strong solution (weak in refrigerant) is returned back to the absorber hence closing up the cycle (Point 6). The cooling water circuit (Points 13-16), cools the absorber (Points 13-14) to keep it working at optimum conditions and extracts heat from the condenser (Points 15-16).

3.3.2 Steady-state vs. dynamic modelling

Plant components can be modelled using one of two approaches; a steady-state approach or a dynamic approach. Steady-state models are used to predict model performance under fixed operating conditions [15]. A number of steady-state models have been developed [17-20], mostly as design aids. Chiller systems, especially those used in trigeneration systems, however will typically operate under dynamic conditions, due to 'On'/'Off' or modulating behaviour, start-up and shut down or other temporal fluctuations in operating conditions, as discussed by Jeong *et al.* [21] and Fujii *et al.* [15]. Dynamic models [21-25], whilst intrinsically more complex, are therefore a more appropriate means to assess the actual performance of absorption chillers.

3.3.2.1 Existing dynamic models

Most of the existing attempts at dynamic absorption chiller modelling have resulted in the creation of detailed models of specific chillers [26] or detailed models of specific cycles and system configurations [27]. An alternative approach is to develop a model capable of being easily customised through calibration with data obtained for different units. Fu *et al.* [24] and Fujii *et al.* [15] both present studies aimed at flexible and customisable models. Fu *et al.* [24] created an extension to the idea of the ABSIM modular program [20] to offer ABSLM, an object-oriented dynamic library, built using the language Modelica, which provides a component list (*e.g.* pumps, condenser, evaporator *etc.*) enabling the creation of different types of absorption chiller configurations. Fujii *et al.* [15] developed an object-oriented model capable of predicting the transient behaviour of absorption refrigerators with an

arbitrary cycle configuration, using a triple-effect system as an example. Other examples of dynamic models of absorption chillers include work carried out by Takagi *et al.* [23] which simulate the behaviour of a single effect absorption chiller using HVACSIM^{+}, and Nurzia [28] which uses the transient simulation code TRNSYS [29] to model a similar single-stage absorption chiller.

3.3.3 Requirement for a new dynamic model

The models described typically require the user to define the characteristics of the internal components making up the absorption chiller such as the components' heat exchange surface area, dimensions, solution composition and internal mass flow rates. This is a non-trivial task often requiring invasive experimental investigation which is difficult to perform and very time-consuming; potentially limiting the flexibility and adaptability of these models.

Hence, for this thesis there was a need to create a functional dynamic model, which could be adapted to represent different chillers using easily obtainable data. The model concept is similar to that developed by the IEA ECBCS Annex 42 in [30] where the model of a generic, dynamic engine-based CHP system (the same as used in the micro-trigeneration plant presented in this research), was developed comprising performance maps linking key input and output parameters, coupled with lumped thermal masses that enabled transient thermal performance to be captured. The Annex 42 model was complemented by a calibration approach using non-invasive tests and measurements.

3.3.4 Development of the proposed model

3.3.4.1 The control volume concept

As discussed in other studies [10, 14, 31, 32], the development of a new plant component in ESP-r follows a well established procedure. The proposed model is modelled as a series of nodes or discrete control volumes to which the laws of conservation of energy and mass are applied [10].

Considering the example discussed by Kelly in [31] and shown in Figure 3.4, where

a hypothetical control volume represented by Node *k* having a total mass M_k (in kg), temperature T_k (in ºC) and averaged mass weighted specific heat $\bar{c}_k$(in kJ/kgK), is:

- receiving a fluid at a mass flow rate of $\dot{m}_{k-1}$ (in kg/s) from an adjacent Node *k-1* having temperature T_{k-1} (in ºC) and a specific heat c_{k-1} (in kJ/kgK); and is,

- exchanging energy with a heat flux Φ (in Watts) and an adjacent surface *s* at temperature T_s (in ºC) having an overall heat transfer coefficient U_s (in W/m^{2}K).

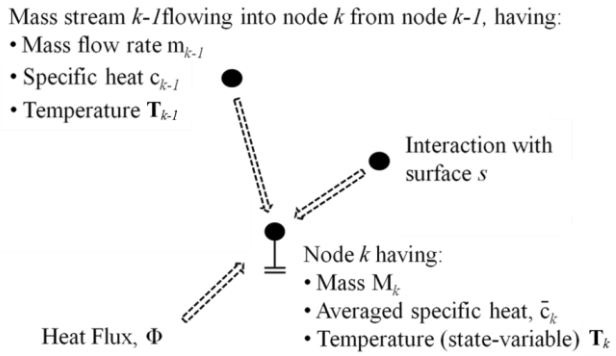

Fig. 3.4 - A simple representation of the energy and mass balance used in ESP-r

Applying the laws of conservation of energy, the partial differential equation shown in equation (3.1) is obtained for the node described above.

$$\frac{M_k \bar{c}_k \partial T_k}{\partial t} = \dot{m}_{k-1} c_{k-1}(T_{k-1} - T_k) + U_s A_s (T_s - T_k) + \Phi \qquad \text{- (3.1)}$$

The term on the left hand side of equation (3.1) serves as the thermal capacitance of the node [31] representative of the node's time-dependent dynamic behaviour, whilst the right hand side of the equation represents all the heat exchanges going on between the node and the surrounding environment. For each node making up a plant component, a full description entails creating a similar equation as that described in equation (3.1). Irrespective of the number of heat flows terms related to any particular node, the solution adopted in ESP-r is always the same. The partial differential equations describing the individual nodes are solved using a numerical approximation with a time interval Δ*t* as described in [10, 14, 31, 32], from which

coefficients for the future and present terms of the state-variable of each node are obtained. The term state-variable, which in equation (3.1) would be T_k, refers to the condition which is being investigated for that particular node, and which in real-life would be representative of (for example) the temperature of a particular volume of fluid such as the exit temperature of a fluid from a plant component. The coefficients are then solved by the solver within ESP-r.

3.3.4.2 The control volume concept used to model the thermal transients inside the chiller

Using the same control volume concept, a single-effect absorption chiller such as that described in Section 3.3.1 can be modelled using a system of three nodes as shown in Figure 3.5. In this three node system each individual node represents the thermal mass corresponding to one of the water circuits associated with the absorption chiller, specifically the chilled water, cooling water and hot water circuits. As mentioned, this concept is an evolution of the one outlined by Beausoleil-Morrison *et al.* in [16] who develop a steady-state chiller model for ESP-r.

Figure 3.5 shows the same chiller shown in Figure 3.3 represented by a series of three control volumes and the respective energy flows within each node.

- **Node *i*** represents the chilled water circuit, incorporating the evaporator casing and the mass of refrigerant and chilled water. Q_i is the net energy process occurring internally within the control volume which affects the incoming chilled water circuit.

- **Node *j*** represents the cooling water circuit, comprising the condenser, absorber and heat exchanger casing and the mass of refrigerant, cooling water and solution contained within them. Q_j, in this case is the net energy process occurring internally within Node *j* which affects the cooling water circuit.

- Finally, in the upper part of the diagram **Node *g*** represents the hot water circuit including the generator casing and the mass of solution and water

contained within it. Similarly as for Q_i and Q_j, Q_g is the net energy process occurring in the control volume affecting the hot water circuit.

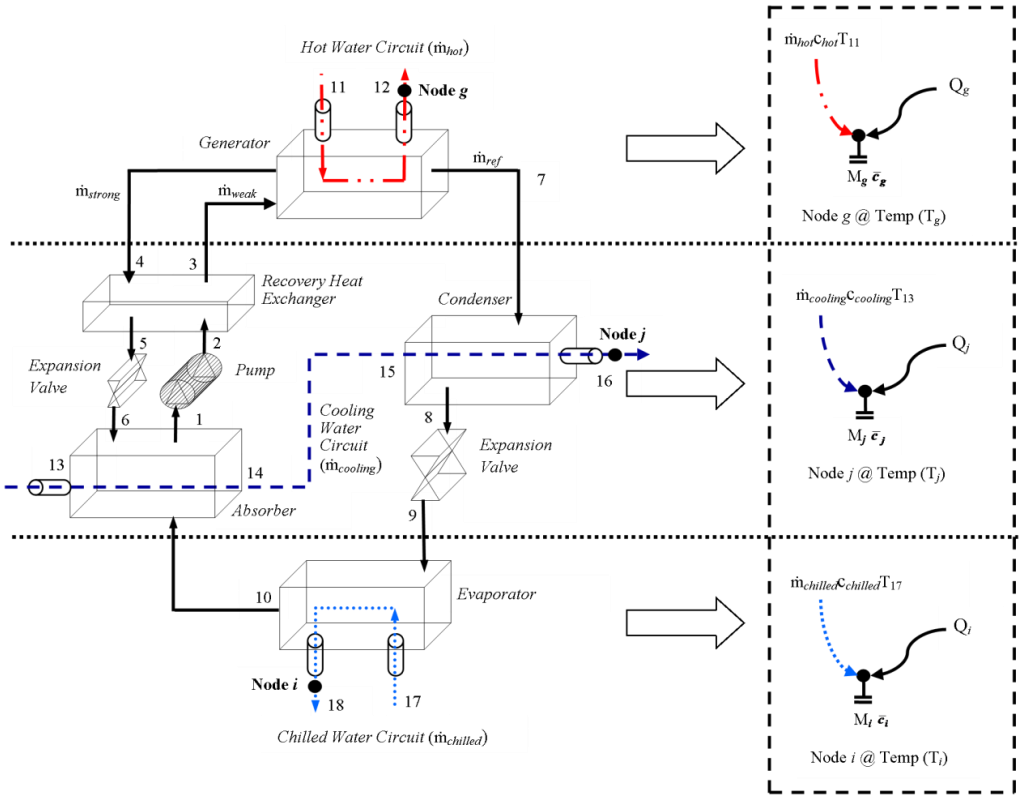

Fig. 3.5 - The absorption chiller system represented by a system of three nodes

Although not explicitly mentioned in the above definitions, Node *j* and Node *g*, in different proportions, also represent the masses of the pump and the recovery heat exchanger. As discussed later in Section 3.3.5.3, one advantage of the modelling procedure adopted in the development of this chiller is that the thermal capacities of the control volumes (which dictate the chiller's dynamic behaviour) are calibrated using empirical data rather than by using measurements of the internal components. For the purpose of establishing the thermal capacitance of a node an accurate sub-division of the internal component masses is therefore unnecessary as the calibration itself establishes the parameters which best represent the dynamic behaviour of the chiller. For simplification purposes and for establishing the energy conservation equation for each node in Figure 3.5 the pump and the recovery heat exchanger are however assumed to be within the control volume represented by Node *j*.

Applying basic energy and mass conservation individually on the three nodes, three partial differential equations, one for each node are obtained as follows:

For **Node *i*** (having Mass M_i in kg and an average mass weighted specific heat $\bar{c}_i$ in kJ/kgK), for an incoming chilled water mass flow rate $\dot{m}_{chilled}$ in kg/s and heat capacity $c_{chilled}$ in kJ/kgK:

$$\frac{M_i \bar{c}_i \partial T_i}{\partial t} = \dot{m}_{chilled} c_{chilled} (T_{17} - T_i) + \mathrm{Q}_i, \text{ where} \quad \text{- (3.2)}$$

$$\mathrm{Q}_i = \dot{m}_{ref} (h_9 - h_{10}) \quad \text{- (3.3)}$$

For **Node *j*** (having Mass M_j in kg and an average mass weighted specific heat $\bar{c}_j$ in kJ/kgK), for an incoming cooling water mass flow rate $\dot{m}_{cooling}$ in kg/s and heat capacity $c_{cooling}$ in kJ/kgK:

$$\frac{M_j \bar{c}_j \partial T_j}{\partial t} = \dot{m}_{cooling} c_{cooling} (T_{13} - T_j) + \mathrm{Q}_j, \text{ where} \quad \text{- (3.4)}$$

$$\mathrm{Q}_j = \dot{m}_{ref} (h_7 - h_8) + (\dot{m}_{ref} h_{10} + \dot{m}_6 h_6 - \dot{m}_1 h_1) \quad \text{- (3.5)}$$

For **Node *g*** (having Mass M_g in kg and an average mass weighted specific heat $\bar{c}_g$ in kJ/kgK), for an incoming hot water mass flow rate of $\dot{m}_{hot}$ in kg/s and heat capacity c_{hot} in kJ/kgK:

$$\frac{M_g \bar{c}_g \partial T_g}{\partial t} = \dot{m}_{hot} c_{hot} (T_{11} - T_g) + UA(T_{env} - T_g) + \mathrm{Q}_g, \text{ where} \quad \text{- (3.6)}$$

$$\mathrm{Q}_g = (\dot{m}_3 h_3 - \dot{m}_4 h_4 - \dot{m}_{ref} h_7) \quad \text{- (3.7)}$$

The numbers in subscript refer to the individual state points within the chiller cycle shown in Figure 3.3 and Figure 3.5. The term $UA(T_{env} - T_g)$ associated with the analysis of Node g represents the heat transfer to and from the environment and h is the specific enthalpy in kJ/kg.

Solving equations (3.2), (3.4) and (3.6) yields the temperatures of the three nodes, T_i, T_j, and T_g - the outlet temperatures of the three water circuits, the chilled water (T_{18}), the cooling water (T_{16}) and hot water circuits (T_{12}), respectively. For the interested reader, Appendix 'D' provides full detail of the mathematical process used to solve

equation (3.2), (3.4) and (3.6), the partial differential equations of the modelled chiller, using the numerical approximation process mentioned in Section 3.3.4.1.

3.3.4.3 Finding the state points within the chiller

In order to obtain Q_i, Q_j and Q_g, the net energy flows into and out of Node *i*, Node *j* and Node *g* respectively, the individual state points within the chiller's thermodynamic cycle are calculated as follows:

Equations and assumptions used to find Q_i

Recall from equation (3.3) that:

$$Q_i = \dot{m}_{ref}(h_9 - h_{10})$$

Assuming that the refrigerant exits the evaporator as saturated vapour (the amount of superheating in the evaporator of an absorption chiller is insignificant [28]), h_{10} can be considered to be the specific enthalpy (in kJ/kg) at dry conditions of p_{low}, the low pressure inside the evaporator-absorber. Also, assuming adiabatic expansion in the expansion valve implies that h_9 is equal to h_8, the specific enthalpy (in kJ/kg) at wet vapour conditions of p_{high} (the amount of sub-cooling in the condenser of an absorption chiller is insignificant [28]), the high pressure inside the condenser-generator. The low pressure, p_{low}, and the high pressure, p_{high}, are calculated using empirically calibrated data as explained in Section 3.3.5.1.

Considering the fact that in most chillers the condenser-generator and the evaporator-absorber assembly are built into two separate shells, a reasonable assumption is that no pressure loss occurs between the condenser and the generator and between the evaporator and absorber, and that pressure changes are only due to the pump and expansion valve [28].

The refrigerant mass flow rate, $\dot{m}_{ref}$ in kg/s, is found using equation (3.8).

$$\dot{m}_{ref} = \frac{CH_{Power}}{1000(h_{10} - h_9)} \quad \text{- (3.8)}$$

CH_{Power}, the chiller's refrigerating power output in Watts (W) is calculated using empirically calibrated data as described in Section 3.3.5.2.

Equations and assumptions used to find Q_i

Recall from equation (3.5) that:

$$Q_j = \dot{m}_{ref}(h_7 - h_8) + \left(\dot{m}_{ref}h_{10} + \dot{m}_6 h_6 - \dot{m}_1 h_1\right)$$

Now, considering that the addition of the refrigerant mass flow rate, $\dot{m}_{ref}$, and the strong solution branch mass flow rate, $\dot{m}_{strong}$ in kg/s, is equal to the weak solution branch mass flow rate, $\dot{m}_{weak}$ in kg/s, the following relation equation (3.9) can be obtained:

$$\dot{m}_{ref} + \dot{m}_{strong} = \dot{m}_{weak} \quad \text{- (3.9)}$$

Assuming that all solution concentration (X, in percentage concentration lithium bromide in water) changes occur only in the absorber and generator, the concentration in the weak and strong solution branches are constant such that $X_1 = X_2 = X_3 = X_{weak}$ and $X_4 = X_5 = X_6 = X_{strong}$, from which the circulation factor f results as shown in equation (3.10).

$$f = \frac{X_{strong}}{X_{strong} - X_{weak}} = \frac{\dot{m}_{weak}}{\dot{m}_{ref}} \quad \text{- (3.10)}$$

The solution concentrations inside the two branches, X_{strong}, and X_{weak} are found using a Gauss-Seidel iterative process which make use of a series of equations described by Kaita in [33]. In this iterative process use is made of T_1, which is assumed to be slightly higher than the arithmetic mean between the inlet and outlet temperature of the cooling water circuit temperatures [17], T_{13} and T_{16} respectively, and T_4 which is assumed to be slightly lower than the inlet temperature of the hot water circuit [17], T_{11}. T_1 and T_4 are calculated using equation (3.11) and (3.12) respectively.

$$T_1 = T_{13} + 1.275(T_{16} - T_{13})/2 \quad \text{- (3.11)}$$

$$T_4 = 0.95T_{11} \quad \text{- (3.12)}$$

Assuming solution saturation and considering the case of X_{weak}, the iterative process relies on comparing p_{low} (the low cycle pressure calculated using the empirical method explained in Section 3.3.5.1) with p_{weak} [the low cycle pressure, in kPa, calculated as a function of solution concentration and temperature as shown in equations (3.13), (3.14) and (3.15)] until the two values converge. The coefficients N_{vw} in equation (3.15) are given in Table 3.7 as described by Kaita in [33].

$$p_{weak} = 10^{LgP} \quad \text{- (3.13)}$$

$$\text{where } LgP = (7.05) - \left(\frac{1603.54}{273.15+D}\right) - \left(\frac{1.040955x10^5}{(273.15+D)^2}\right) \quad \text{- (3.14)}$$

$$\text{where D, the dew point temperature is } D = \sum_{v=0}^{2}\sum_{w=0}^{3} N_{vw}(X-40)^v T^w \quad \text{- (3.15)}$$

Table 3.7 - Coefficients to calculate the dew point temperature

w	N_{0w}	N_{1w}	N_{2W}
0	-9.133128	9.439697 x 10^{-1}	-7.324352 x 10^{-5}
1	-4.759724 x 10^{-1}	-2.882015 x 10^{-3}	-1.556533 x 10^{-5}
2	-5.638571 x 10^{-2}	-1.345453 x 10^{-4}	1.992657 x 10^{-6}
3	1.018418 x 10^{-3}	5.852133 x 10^{-7}	-3.924205 x 10^{-8}

For equation (3.15), T is T_1 derived from equation (3.11), whilst X_{weak} is varied from an initial concentration of X being equal to 40% up to a point where p_{weak} is equal to p_{low}. Equation (3.15) is valid for a concentration X in the range of 40% to 65% [33], a wide enough range to include typical working concentrations for absorption cycle chillers and ensuring no crystallisation problems occur above 65% [34]. Similarly for X_{strong}, the same iterative process is repeated this time using T_4, p_{high} and p_{strong}.

Considering the solution at Point 1 and Point 6, respectively the weak solution exiting the absorber and the strong solution entering the absorber, to be saturated, the specific enthalpy (in kJ/kg) of Point 1 and Point 6, h_1 and h_6, are calculated using the

general form of equation (3.16) [33].

$$h = [3.462023 - 2.679895\text{x}10^{-2}(\text{X})]T + 0.5[1.3499\text{x}10^{-3} - 6.55\text{x}10^{-6}(\text{X})][T^2] + [162.81 - 6.0418(\text{X}) - 4.5348\text{x}10^{-3}(\text{X})^2 + 1.2053\text{x}10^{-3}(\text{X})^3] \quad \text{- (3.16)}$$

In the case of h_1, the temperature is T_1 and the solution concentration is X_1. On the other hand, assuming again that the expansion process in the expansion valve is completely adiabatic, h_6 is equal to h_5. T_5 which is used to find h_5 is in this case calculated using equation (3.17). T_5 is assumed to be slightly lower than the mid-point temperature between the generator and the absorber [17]. η is the recovery heat exchanger efficiency.

$$T_5 = 0.95T_{11} - \eta(0.95T_{11} - T_1) \quad \text{- (3.17)}$$

The specific enthalpy (in kJ/kg) at Point 7, h_7, the exit point of the refrigerant from the generator assumed to be superheated at temperature T_7 and pressure p_{high}, is calculated using equation (3.18) (from Florides *et al.* [35]).

$$h_7 = \left(\frac{\left(\left[1\text{x}10^{-5}p_{high}^2 - 1.193\text{x}10^{-1}p_{high} + 2689\right] - \left[32.508\text{Ln}(p_{high}) + 2513.2\right]\right)}{100}\right)(T_7 - T_8) + 32.508\text{Ln}(p_{high}) + 2513.2 \quad \text{- (3.18)}$$

In equation (3.18) T_8 is the saturation temperature at the high cycle pressure p_{high}, whilst T_7 is calculated using equation (3.19); the mean temperature of the solution flows in and out of the generator [17].

$$T_7 = 0.5(T_4 + T_3) = 0.5(T_4 + h_3/c_{weak}) \quad \text{- (3.19)}$$

c_{weak} is the specific heat (in kJ/kgK) of the lithium bromide-water solution inside the

weak solution branch calculated using equation (3.20) (from Florides *et al.* [35]).

$$c_{weak} = 9.76x10^{-5}{X_{weak}}^{2} - 3.751x10^{-2}X_{weak} + 3.8254 \quad \text{- (3.20)}$$

Equations and assumptions used to find Q_g

Recall from equation (3.7) that:

$$\mathrm{Q}_g = \left(\dot{m}_3 h_3 - \dot{m}_4 h_4 - \dot{m}_{ref} h_7\right)$$

The specific enthalpy of point 4, h_4, the strong solution at the exit of the generator is again found using equation (3.16); h_3, is calculated as shown in equation (3.21).

$$h_3 = h_2 + \left(1 - \left(\frac{1}{f}\right)\right)(h_4 - h_5) \quad \text{- (3.21)}$$

The specific enthalpy (in kJ/kg) of point 2, h_2, the weak solution at the exit of the pump is calculated using equation (3.22) – h_1 plus the pressure difference across the pump divided by the density of the solution (Florides *et al.* [35]).

$$h_2 = h_1 + Work\ done\ by\ pump$$
$$= h_1 + \frac{\left(p_{high} - p_{low}\right)}{[(1145.36 + 470.84\mathrm{X}_2 + 1374.79\mathrm{X}_2^2) - (0.333393 + 0.571749\mathrm{X}_2^2)(273 + T_1)]} \quad \text{- (3.22)}$$

The algorithm describing the operation of the component is shown in Appendix 'E'.

3.3.5 Model calibration

A three-stage model calibration process is used to obtain the data needed to run the model. Stage 1 and stage 2 develop the chiller *'performance map'*, whilst stage 3 identifies the dynamic characteristics. Specifically, in:

- ***Stage 1*** - Expressions for the high and low operating pressures are derived as

functions of hot water circuit inlet temperatures;

- ***Stage 2*** - An expression for the chiller's refrigerating power output is derived as a function of all of the water circuit inlet temperatures; and

- ***Stage 3*** - The thermal capacities of the chiller model constituents are identified.

The data required to calibrate the chiller (see Table 3.8) is derived from two sources:

- Some of the parameters such as the highest and lowest permissible high and low pressure, the minimum chilled water protection temperature and the working minimum hot water outlet temperature can be extracted directly from manufacturer's data sheets as these are typically listed to avoid any damage being caused to the chiller.

- The high (p_{high}) and low (p_{low}) pressure curve coefficients (a_0, a_1, b_0 and b_1), the chiller's refrigerating power output function (CH_{Power}) curve coefficients (d_0, d_1, d_2 and d_3), the thermal masses (M_i, M_j and M_g) and the mass weighted average specific heat values ($\overline{c_i}$, $\overline{c_j}$ and $\overline{c}_g$) all require empirical data, obtained from a three stage calibration process. Details on how these values can be obtained are given in Sections 3.3.5.1, 3.3.5.2 and 3.3.5.3.

Table 3.8 lists the parameters that require calibration together with the respective values obtained after calibrating the model with experimentally measured data acquired for a 10 kW_{th} absorption chiller developed by SK SonnenKlima GmbH [36, 37]. The chiller is adequately sized to cater for a broad spectrum of residential thermal loads.

For the nodal parameters, alternative values obtained from a more pragmatic calibration process are shown and compared to measured values later.

Table 3.8 - Component coefficients and data making up the absorption chiller

Nodal parameters:	
Node *i*	**Value**
1 M_i - Evaporator total mass (kg)	47.000
2 $\bar{c}_i$ - Mass weighted average specific heat of evaporator (kJ/kgK)	1.7180
Node *j*	
3 M_j - Condenser and absorber total mass (kg)	122.40
4 $\bar{c}_j$ - Mass weighted average specific heat of condenser and absorber (kJ/kgK)	1.7670
Node *g*	
5 M_g - Generator total mass (kg)	79.700
6 $\bar{c}_g$ - Mass weighted average specific heat of generator (kJ/kgK)	1.8070
Whole device parameters:	
1 Recovery heat exchanger efficiency (η)	0.6400
2 UA Modulus (W/K)	3.5000
3 p_{High} - High pressure curve coefficient (a_0)	0.0735
4 p_{High} - High pressure curve coefficient (a_1)	0.3429
5 Highest permissible high pressure (kPa)	8.0000
6 Lowest permissible high pressure (kPa)	4.0000
7 p_{low} - Low pressure curve coefficient (b_0)	-0.0137
8 p_{low} - Low pressure curve coefficient (b_1)	2.4019
9 Highest permissible low pressure (kPa)	2.0000
10 Lowest permissible low pressure (kPa)	1.0000
11 Working maximum outlet temp cooling water (ºC)	40.000
12 Working minimum outlet temp hot water (ºC)	42.000
13 CH_{Power} - Power function coefficient (d_0)	-6370.0
14 CH_{Power} - Power function coefficient (d_1)	304.90
15 CH_{Power} - Power function coefficient (d_2)	168.30
16 CH_{Power} - Power function coefficient (d_3)	-76.520
17 Minimum chilled water temp protection (ºC)	2.5000
18 Circulation pump electrical efficiency (-)	0.9000
Control variables:	
1 ON/OFF control signal (-)	1/0

3.3.5.1 Calibration stage 1: Obtaining the cycle high and low pressures in terms of the hot water circuit inlet temperature

This section explains how the general relationships between the internal high (p_{high}) and low (p_{low}) cycle pressures and the incoming inlet temperature of the hot water

circuit were obtained and how the pressure curve coefficients (a_0, a_1, b_0 and b_1) were eventually calibrated.

Experimental data obtained from the IEA Task 38 Solar Heating and Cooling Programme (personal communication, October 29, 2010) for the mentioned 10 kW_{th} absorption chiller shows that, over the working range of inlet water circuit temperatures [Lowest-Highest inlet temperature (Working Range)] specified by the manufacturer data sheet in [36] (lowest and highest hot water inlet temperature and working range [55-95°C (40°C)], lowest and highest cooling water inlet temperature and working range [27-35°C (7°C)] and lowest and highest chilled water inlet temperature and working range [6-20°C (14°C)], both the high pressure inside the condenser-generator and the low pressure inside the evaporator-absorber are predominantly effected by the hot water circuit inlet temperature, and that the inlet temperatures of the cooling and chilled water flow circuits have only a marginal effect on the cycle pressures. Also, considering that the control scheme employed by most chillers is to use constant water circuit flow rates and vary the hot or cooling water inlet circuit temperature to control the output power of the absorption chiller [38], a reasonable assumption is that the cycle pressures can be expressed as a function of hot water circuit inlet temperature. In this context, the experimental data of Figure 3.6 shows how the high pressure inside the condenser-generator and the low pressure inside the evaporator-absorber vary over the whole range of hot water circuit inlet temperatures.

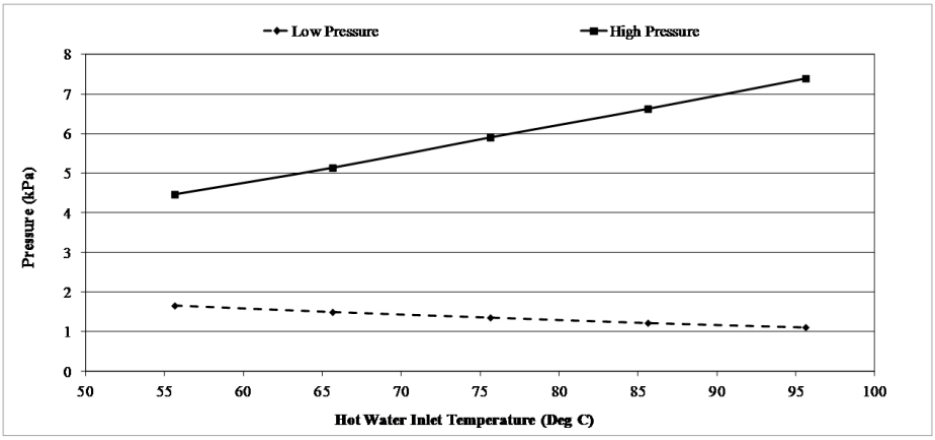

Fig. 3.6 - Internal low and high cycle pressures *vs.* hot water inlet temperature

Both the high pressure inside the condenser-generator and the low pressure inside the evaporator-absorber vary linearly with change in hot water circuit inlet temperature. However, whereas the pressure inside the condenser-generator increases with increasing temperature, the pressure inside the evaporator-absorber decreases with increasing temperature.

The high and low cycle pressure curves coefficients (a_0, a_1, b_0 and b_1) can therefore be derived by varying the hot water circuit inlet temperature to the generator and recording the resulting part-load cycle pressures. The relationships describing the behaviour of the two system pressures with a corresponding change in T_{11}, the hot water circuit inlet temperature in °C, were then obtained using a linear regression analysis on the test data shown in Figure 3.6. A similar calibration exercise can be repeated to obtain the characteristics of any other chiller. Table 3.9 shows the general and specific equations for the calibrated chiller together with the corresponding correlation coefficients.

Table 3.9 - Relationships between hot water inlet temperature and the high and low pressure

	General equation form	**Specific equation for calibrated chiller**	**Correlation coefficient with measured data (R)**
Low pressure inside Evaporator-Absorber (p_{low}) (kPa)	$a_0+a_1(T_{11})$ (3.23)	$0.0735(T_{11}) + 0.3429$	0.9953
High pressure inside Condenser-Generator (p_{high}) (kPa)	$b_0+b_1(T_{11})$ (3.24)	$-0.0137(T_{11}) + 2.4019$	0.9995

3.3.5.2 Calibration stage 2: Obtaining the chiller's refrigerating power output as a function of the water circuits' inlet temperatures

This part of the calibration process obtains an expression for the chiller's refrigerating power output function (CH_{Power}) in terms of the three water circuits' inlet temperatures. It is this calculated power output which serves as the "*performance map*" described earlier in Section 3.3.3 and which in conjunction with

the internal high and low pressures values is used to calculate the internal state points within the refrigeration cycle and the refrigerant mass flow rate ($\dot{m}_{ref}$) from which all other internal mass flow rates are calculated. Similarly to the calibration process in stage 1, the expression describing the chiller's refrigerating power output considers the case that the flow rates of all three incoming water circuits (hot, chilled and cooling water circuits) remain constant, whilst their temperature is varied to control the chiller's refrigerating output power. As discussed by Kohlenbach in [38] this state of affairs is common in absorption cooling refrigeration plant control.

Stage 2 calibration used a time-series dataset compiled from three non-consecutive days during which the absorption chiller was being field tested together with a solar water heating system. This is similar to the approach employed by Ferguson and Kelly in [39] where efficiency correlations for a combustion based cogeneration device obtained from measured data of cooling water flow rates and temperatures, and the unit's electrical loading were used to create performance maps of the system behaviour under varying loading degrees. Data was supplied in the form of 1-minute averaged recordings of the three water circuits' individual inlet and outlet temperatures and their respective mass flow rates. The chiller's refrigerating power output can be expressed in terms of the three water circuits' inlet temperatures - the best fit being a simple linear relation having the general form of equation (3.25) shown in Table 3.10. T_{11} is the hot water circuit inlet temperature, T_{13} is the cooling water circuit inlet temperature and T_{17} is the chilled water circuit inlet temperature. The coefficient values (d_0, d_1, d_2 and d_3) can be calibrated for any kind of single-effect lithium bromide-water chiller using a similar dataset obtained from experimental measurements.

Table 3.10 - Relationship between chiller's refrigerating power output and the water circuits' inlet temperatures

	General equation form	**Specific equation for calibrated chiller**
Chiller's refrigerating power output (CH_{Power}) (Watts)	$d_0+d_1(T_{17})+d_2(T_{11})+d_3(T_{13})$ (3.25)	$-6370.7+304.9(T_{17})+168.3(T_{11})-76.52(T_{13})$

3.3.5.3 *Calibration stage 3: Obtaining the total mass and the mass weighted average specific heat capacity of each individual node*

Once the internal state points of the chiller have been defined, the third and final part of the calibration process is needed to calibrate the total mass (M_{node} - M_i, M_j and M_g in kg) and the mass weighted average specific heat capacity ($\bar{c}_{node}$ - $\bar{c}_i$, $\bar{c}_j$ and $\bar{c}_g$in kJ/kgK) of the individual nodes. These define the dynamic characteristics of the chiller.

There are two methods which can be used to calibrate the total mass and the mass weighted average specific heat capacity. The first uses a *'traditional'* approach and can be used if enough information on the individual internal components is available. In this case the total mass (M_{node}) of each individual node can be considered as the addition of all the masses (m_1, m_2, …, m_n) represented by the node as shown in equation (3.26). The nodal mass weighted average specific heat capacity ($\bar{c}_{node}$) is calculated using the specific heat values of the individual masses making up an individual node (c_1, c_2, …, c_n) as shown in equation (3.27).

$$M_{node} = m_1 + m_2 + \cdots + m_n \quad \text{- (3.26)}$$

$$\bar{c}_{node} = \frac{(m_1 c_1 + m_2 c_2 + \cdots + m_n c_n)}{(m_1 + m_2 + \cdots + m_n)} \quad \text{- (3.27)}$$

For this specific 10 kW_{th} chiller, Kohlenbach in [38] gives a detailed breakdown of the masses and characteristics of the individual internal components from which M_{node} and $\bar{c}_{node}$ can be calculated as shown in Table 3.11.

Using such a method however suffers from two major limitations. As discussed previously, detailed data is required for the internal components of the chiller. This data may not be available or require intrusive measurements to obtain. Secondly, in such a complex system, made up of multiple parts, it is relatively difficult to clearly identify which mass may be associated with each node. The thermal capacitance of a node may be (even if partly) influenced by an internal component which is outside

the imaginary boundary constituting that control volume or components (or liquids *e.g.* water or lithium bromide solution) may be shared.

To address these two limitations the proposed model permits a second, more pragmatic method of calibration which relies on an iterative parametric identification process, which makes use of an optimization tool; this drives the simulation over multiple runs, comparing the modelled outlet temperatures of the three water circuits with the measured outlet water data for the same feed conditions. For each run the thermal masses (M_i, M_j and M_g) and the mass weighted average specific heat values ($\overline{c_i}$, $\overline{c_j}$ and $\overline{c}_g$) are varied individually and the resulting error between the modelled and the measured outlet water temperatures computed. The values of the thermal masses and the mass weighted average specific heat values which best represent the internal dynamics of the chiller are obtained once the error, which in this case is the objective function, is minimised. This is derived from the parametric identification technique described by Ferguson and Kelly in [40].

Table 3.11 shows the calculated results for the thermal masses (M_i, M_j and M_g) and the mass weighted average specific heat values ($\overline{c_i}$, $\overline{c_j}$ and $\overline{c}_g$) obtained using the two methods:

- Method 1 using the known characteristics of the internal components; and
- Method 2 using the iterative process.

Table 3.11 - M_{node} and $\bar{c}_{node}$ calculated using method 1 and method 2

Node	***Method***	***i***	***j***	***g***
Total mass M_{node} (kg)	Method 1	47.0	122.4	79.7
	Method 2	100.0	128.7	66.6
Mass weighted average specific heat capacity $\bar{c}_{node}$ (kJ/kgK)	Method 1	1.718	1.767	1.807
	Method 2	2.743	2.161	1.991

Although the two sets of results show a considerable discrepancy between one another[1], in practice when modelling the dynamic output of the proposed chiller, the difference is negligible. In this context, Figure 3.7 shows the resulting temperature profile for the chilled water circuit using the thermal masses and the mass weighted average specific heat values calculated using both methods. The two sets give very similar results with an average error calculated over the investigated period shown in Figure 3.7, between the modelled and measured data of 0.27°C in the case of Method 1, and 0.21°C in the case of Method 2.

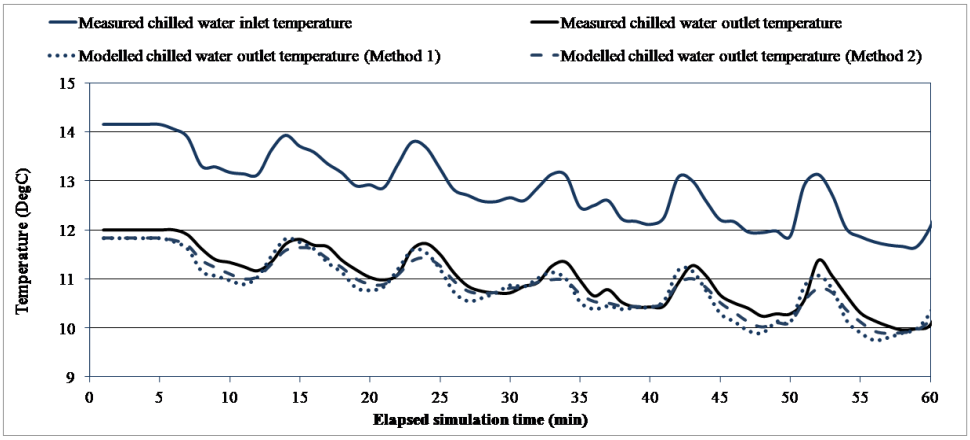

Fig. 3.7 - Chilled water circuit outlet temperature response

3.3.6 Verification of the proposed model

The model was verified using two techniques:

- an inter-model comparative exercise where the results obtained for the proposed chiller were compared to results obtained from the model presented by Kohlenbach and Ziegler in [22, 25], which was calibrated against the same 10 kW_{th} chiller; and

[1] One reason for the discrepancy between the two sets of values calculated using the two methods could be fact that the temperature range used for calibration is relatively small and that hence the dynamic behaviour of the chiller model could have been not fully captured. In this sense as will be discussed later the relatively limited amount of data points used to calibrate the model was a limitation in the calibration process.

- the model was then compared to a separate set of experimental results from that used for calibration purposes.

3.3.6.1 Inter-model comparison

Kohlenbach and Ziegler in [22, 25] performed a dynamic test on their model whereby it was first run at steady-state conditions at rated inlet temperatures and mass flow rates and then subjected to a 10°C step increase in hot water circuit inlet temperature. The results obtained in this experiment indicated that it took around 10-minutes for the hot water temperature to stabilise at the new state, and approximately 15-minutes for the remaining chiller parameters to reach steady-state, depending on the thermal mass involved in each internal component. Replicating this test using the dynamic model, the chiller was supplied at steady, rated conditions (hot water circuit inlet temperature of 75°C with a mass flow rate of 0.4 kg/s, chilled water circuit inlet temperature of 18°C with a mass flow rate of 0.8 kg/s and the cooling water circuit inlet temperature of 27°C with a mass flow rate of 0.7 kg/s). A step increase of 10°C was then applied to the hot water circuit inlet temperature. The simulation was run at a resolution of 1 second. The results obtained for the proposed model are very close to those reported by Kohlenbach and Ziegler, with the simulated hot water circuit outlet temperature modelled stabilising in 620 seconds. The Kohlenbach and Ziegler model reached a stable state at around 600 seconds; this is a difference of around 3%.

3.3.6.2 Comparison with experimental data

The chiller model was supplied with minute by minute inlet temperature measurements of the three water circuits entering the chiller from an empirical data set. The model's output was then compared to the measured data. Figure 3.8 shows how the results obtained for the chilled water outlet temperature data modelled at 1-minute time resolution compare with the measured chilled water outlet temperature data.

The modelled data closely follows the measured data with identical time response patterns, yielding a maximum and mean error of 0.35°C and 0.09°C between the modelled and measured datasets, respectively. The standard deviation is 0.10°C.

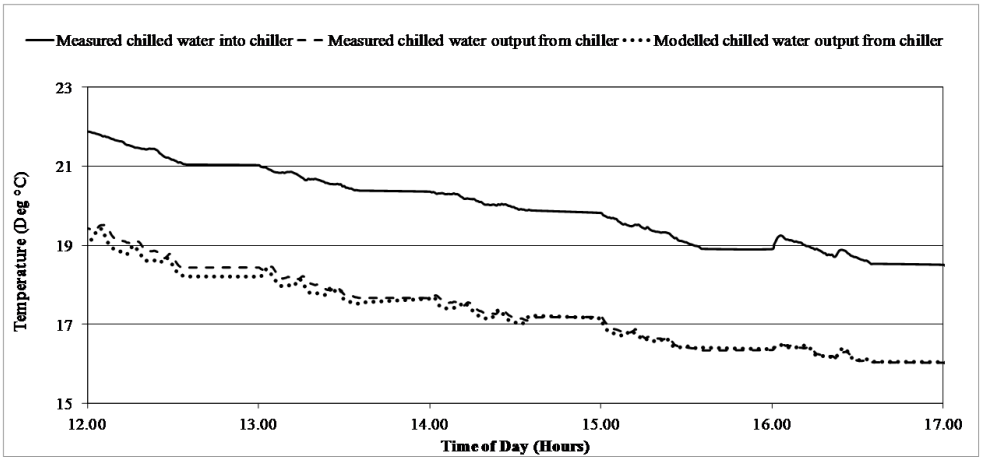

Fig. 3.8 - Measured *vs.* modelled chilled water data

Figure 3.9 shows how the modelled data (both the raw and smoothed data) compares to a theoretical ideal fit. The resulting correlation coefficient value between the modelled data and the ideal fit is of 0.995. It can be observed that the modelled dataset is most accurate for a specific range of working temperatures, and that at the extreme end of the modelled temperature range (where the least number of data points was available for calibration) a number of outliers are visible.

The accuracy of the model lies in its calibration process which is highly susceptible to the number (and range) of data points used to calibrate the model. The higher the number of data points used to calibrate the model the more accurate is the calibration process. Also, having a consistent number of data points over the whole range of working and non-working temperatures (including during specific time-periods such as cold-starts) aides in improving the accuracy of the calibration process. One limitation of this model is that the number of data points used for calibration was relatively limited and the model's accuracy therefore suffers from this fact. This does however not prevent the model from producing a reliable representation of the output of the absorption chiller.

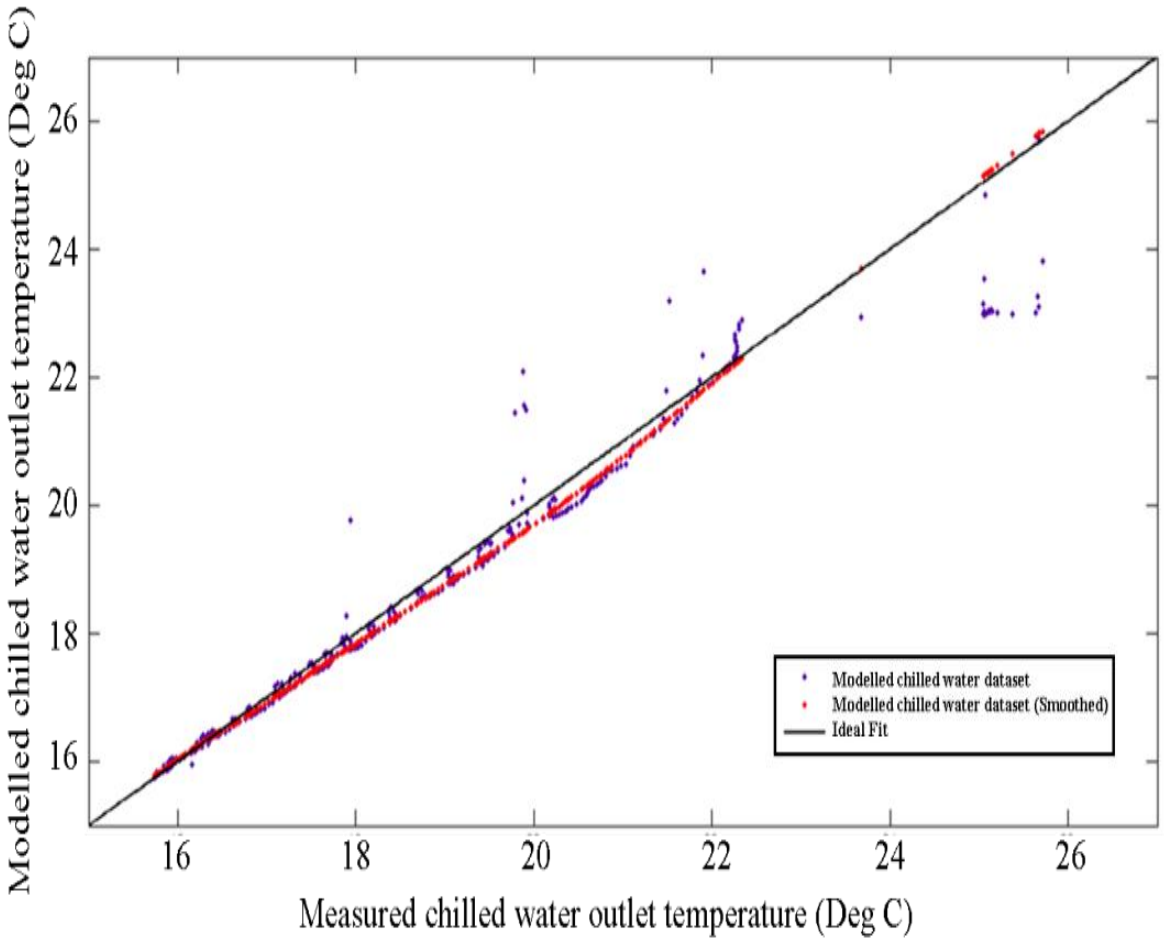

Fig. 3.9 - Modelled chilled water circuit outlet temperature data *vs.* ideal fit

Similarly, Figure 3.10 and Figure 3.11 show the modelled cooling and hot water outlet temperature profiles superimposed on the measured data for the same simulation period used in the case of the chilled water dataset.

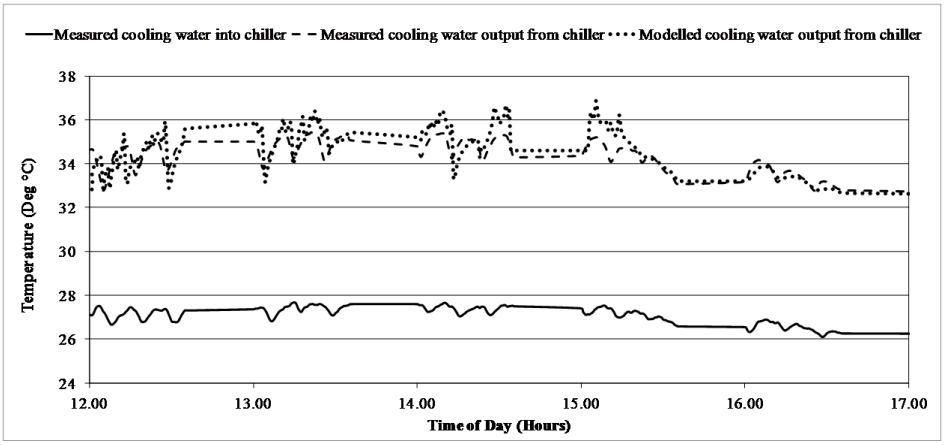

Fig. 3.10 - Measured *vs.* modelled cooling water datasets

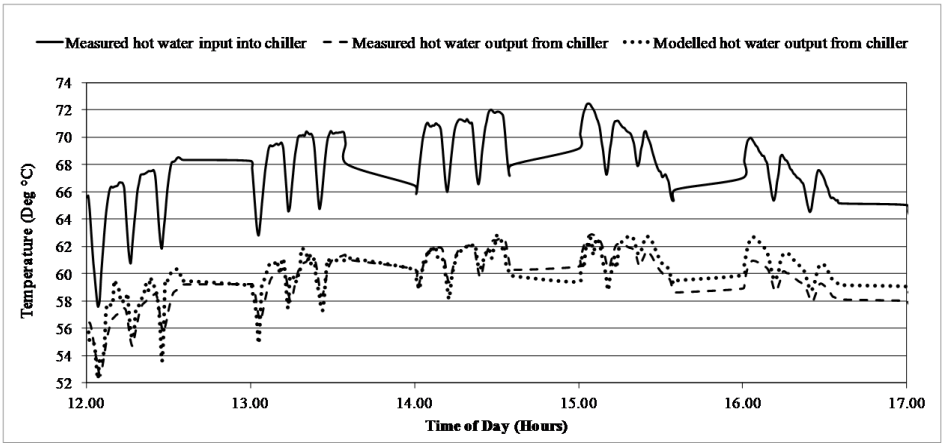

Fig. 3.11 - Measured *vs.* modelled hot water datasets

Both figures show good agreement between the measured and modelled datasets, although showing a slightly positive temperature bias when compared to the results obtained from the chilled water. In terms of the cooling water circuit temperatures, the maximum and mean error values between the modelled and measured datasets were calculated to be 2.19°C and 0.22°C respectively. The calculated standard deviation was 0.61°C. The hot water circuit temperatures showed a similar behaviour to the cooling water temperatures with the maximum and mean error values between the modelled and measured datasets being 2.81°C and 0.46°C respectively, whilst the

standard deviation was calculated to be 0.93°C.

In conclusion, the calibrated model delivers a good representation of the chiller behaviour and the modelled outputs compare favourably against results obtained from a more intrusive and less practical parametric identification involving physically dismantling and weighing the individual components of the chiller.

3.3.7 Use in plant networks

Inside an ESP-r plant network the absorption chiller component is connected via its 3 nodes to the other components of the system.

- Node *i*, the node representing the chilled water circuit is connected via the chilled water pump to a building's cooling circuit at a rated flow of 0.8 kg/s.

- Node *j*, the node representing the cooling water stream is connected to the cooling water pump where a rated flow 0.7 kg/s of constant temperature water (27°C) is supplied. Alternatively it can be connected to a cooling tower.

- Finally, Node *g*, the node representing the hot water circuit is connected to the hot water pump delivering a rated flow rate of 0.4 kg/s of hot water from a hot water source.

3.4 Variants in plant configuration

Two variations of the basic plant configuration (shown in Figure 3.2) were developed with a view to investigating their energy and environmental overall performance in Maltese buildings (this is discussed in Chapter 5). The variants developed were as follows.

3.4.1 Use of chilled water storage tank

The first modification to the basic plant configuration was the inclusion of a 0.3m^3 chilled water buffer tank added between the chiller and the cooling coils as shown in Figure 3.12.

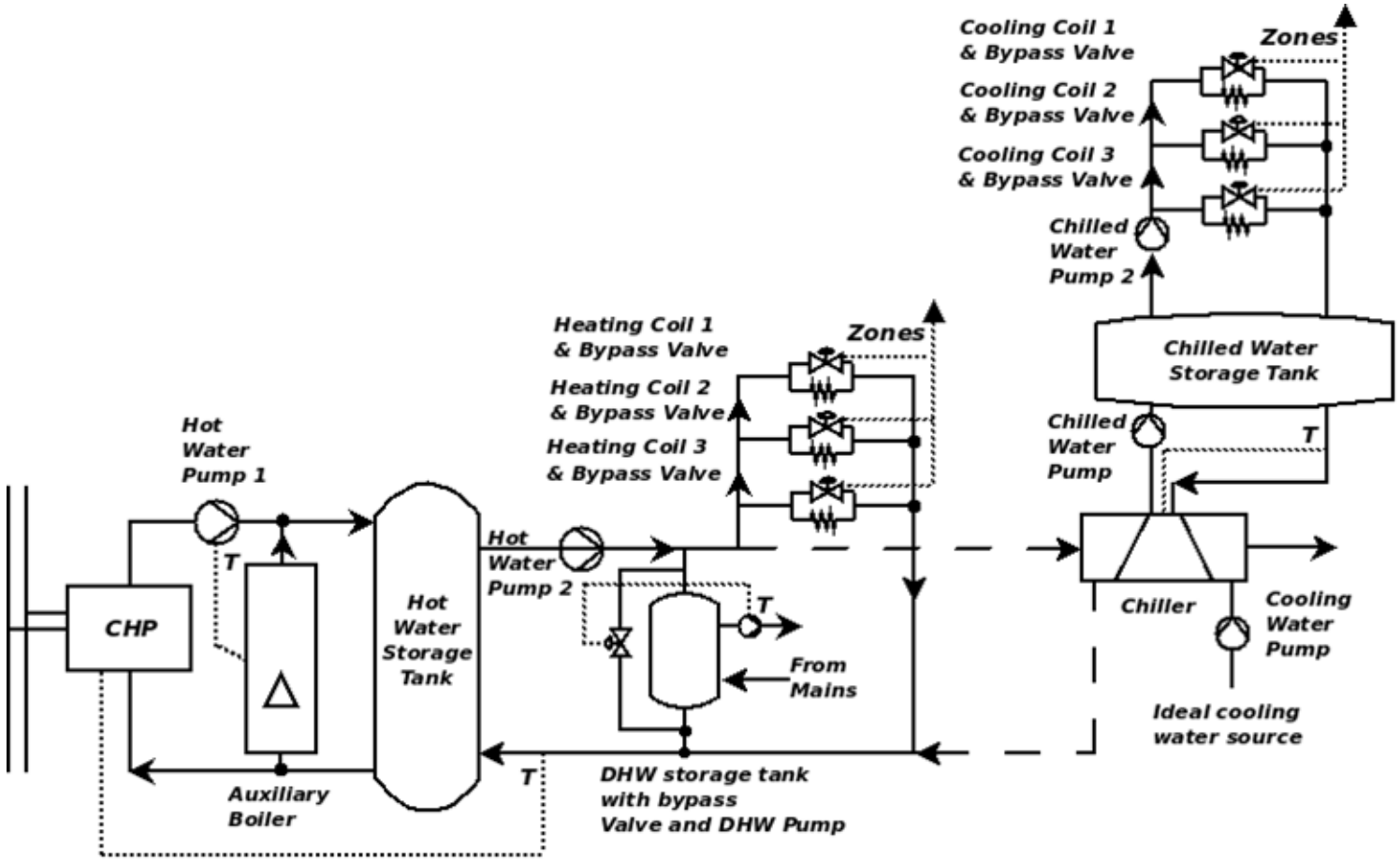

Fig. 3.12 - Micro-trigeneration plant with additional chilled water storage tank

The selected tank size is based on a short, web based market review showing what type of tank sizes are typically used for residential water storage [41]. The addition affects the performance of the micro-trigeneration plant during the summer season. The control strategy is in this case unaltered and is similar to that shown in Table 3.6.

3.4.2 Use of a SWH system in tandem with micro-trigeneration

The second modification to the plant configuration included the addition of a flat plate solar water heating (SWH) system on the return to the hot water storage tank as shown in Figure 3.13. The solar water heater, a 2.5m^2 flat plate, was optimised for maximum annual solar energy absorption for Maltese conditions, that is, south facing with a tilt of 45° as discussed by Borg *et al.* in [42].

The modelled flat plate SWH is a relatively small sized system, more apt for use by a single-family household rather than for multiple household as it is in this case, however whilst performing trial simulations it was observed that larger sized panels tend to have problems in summer due to the overheating of water. Since this in practice might result in potential damage being caused to the CHP unit, a conservatively sized SWH was used for this investigation. An alternative approach would have been to model multiple SWH systems in parallel, increasing the flow rate but limiting the increase in temperature across the setup. This setup was however not investigated further due to lack of time.

The modification affects the performance of the system throughout the whole year, although to varying degrees depending on the solar incident solar radiation. In Malta the average solar irradiation on a horizontal surface varies between roughly 2.5 kWh/m^2/day and 7.8 kWh/m^2/day, which is very similar to the radiation experienced in other Mediterranean countries such as Cyprus and Greece [42].

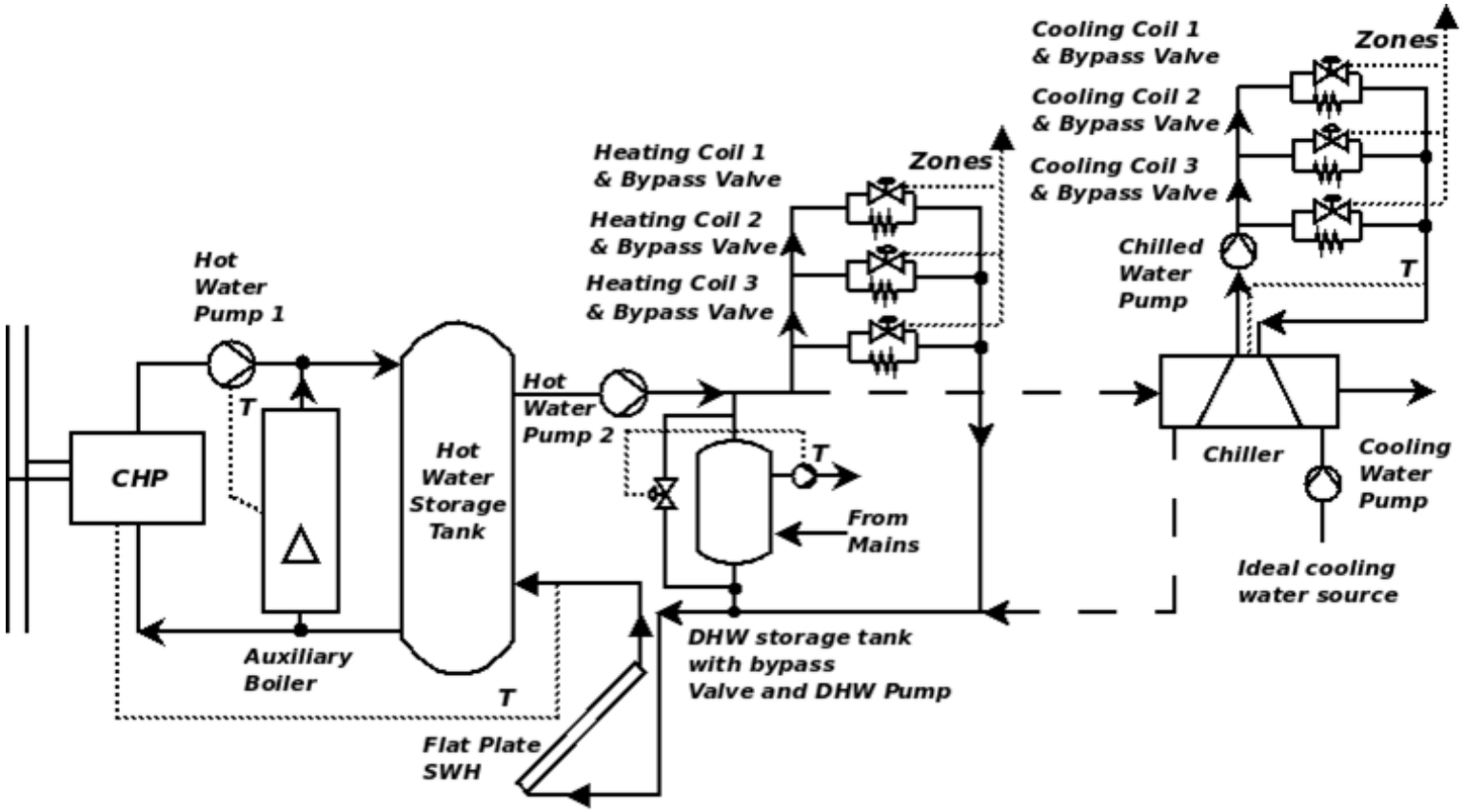

Fig. 3.13 - Micro-trigeneration plant with additional SWH system

3.5 Summary of Chapter 3

This chapter described the micro-trigeneration system, the basis of ESP-r plant components and networks, plant network design and the implementation of control: the strategies used to control the indoor temperature of each individual apartment in both the 3 household and the 6 household building were also presented and explained.

The core of this chapter outlined the development of a new generic model for a single-effect lithium bromide-water absorption chiller which, in contrast to most dynamic models that rely on complex modelling and calibration of the internal characteristics of the chiller, was developed in such a way as to enable its calibration as a single unit. Furthermore, whereas many other models require re-calibration of the internal components in order to represent different chiller types, the model presented in this research can be calibrated simply by measured data of the inlet and outlet temperatures of the three water circuits flowing in and out of the chiller. The model is therefore flexible and adaptable for calibration with other chiller data. Verification of the model indicated that the model provided a good approximation to the measured performance of the real chiller and its performance was very similar to that of another model. Finally, the integration of the model into an ESP-r trigeneration model and its variants was described.

3.6 Chapter References

[1] National Statistics Office (2007). "*Time Use-Survey 2002"* - National Statistics Office, Valletta, Malta.

[2] *"Decreto del Presidente della Republica recante norme per la progettazione, l'installazione, l'esercizio e la manutenzione degli impianti termici degli edifici ai fini del contenimento dei consumi di energia, in attuazione dell'art. 4, comma 4, della L. 9 gennaio 1991, n. 10"* - D.P.R. 412/93.

[3] Peeters, L., de Dear, R., Hensen, J.L.M. and D'haeseleer, W. "*Thermal comfort in residential buildings: Comfort values and scales for building energy simulation"* Applied Energy, 2009. 86: pgs. 772-780

[4] Fanger, P.O., "*Thermal comfort"*. 1970, New York, USA: McGraw-Hill

[5] ASHRAE, *"Chapter 9 - Thermal Comfort"* in *"The 2009 ASHRAE Handbook - Fundamentals"*, Mark Owen, Editor. 2009, American Society of Heating Refrigerating and Air Conditioning Engineers

[6] CIBSE, "*Guide A: Environmental design"*. 2006, London, UK: Chartered Institution of Building Services Engineers

[7] Oseland, N.A. "*A comparison of the predicted and reported thermal sensation vote in homes during winter and summer"* Energy and Buildings, 1994. 21: pgs. 45-54

[8] Humphreys, M. "*The influence of season and ambient temperature on human clothing behaviour"*, in "*Indoor climate"*, Danish Building Research, Editor. 1979: Copenhagen, Denmark

[9] "*Temperature records for the Maltese Islands"*. Online Database held at www.maltaweather.com [Accessed: 08/02/2011]; Available from: http://www.maltaweather.com/archives.shtml

[10] Clarke, J.A., "*Energy simulation in building design"*. 2nd Edition ed. 2001, Oxford: Reed Educational and Professional Publishing Ltd.

[11] Beausoleil-Morrison, I., Ferguson, A., D'haeseleer, W. and Kelly, N.J. (2007). "*Experimental Investigation of Residential Cogeneration Devices and Calibration of Annex 42 Models"* - A Report of Subtask B of FC+COGEN+SIM The Simulation of Building-Integrated Fuel Cell and Other Cogeneration Systems: Annex 42 of the International Energy Agency's

Conservation in Buildings and Community Systems Programme. International Energy Agency

[12] Baxi-SenerTec UK (2010). DACHS Mini-CHP - Online Brochure. [Accessed: 28/03/2011]; Available from: http://www.baxi-senertec.co.uk/documents/Sales_brochure_July_2010.pdf

[13] Baxi SenerTec Dachs UK Webpage (2010) [Accessed: 29/03/2011]; Available from: http://www.baxi.co.uk/products/DACHS.htm

[14] Hensen, J.L.M., (1991) "*On the thermal interaction of building structure and heating and ventilation system.*" Doctoral Thesis - Technische Universiteit Eindhoven, The Netherlands

[15] Fujii, T., Komatsu, T., Nishiguchi, A. and Matsushima, H. "*Dynamic simulation program with object-oriented formulation for absorption chillers (modelling, verification, and application to triple-effect absorption chiller)*" International Journal of Refrigeration 2010. 33: pgs. 259-268

[16] Beausoleil-Morrison, I., Mottillo, M., Brandon, R., Sears, P. and Ferguson, A. "*The simulation of a residential space-cooling system powered by the thermal output of a cogeneration system*" in *Proceedings of esim 2004*. Vancouver, Canada

[17] Mehrabian, M.A. and Shahbeik, A.E. "*Thermodynamic modelling of a single-effect LiBr–H_2O absorption refrigeration cycle*" Proc. IMechE, 2004. 219(Part E)

[18] Gordon, J.M. and Ng, K.C. "*A general thermodynamic model for absorption chiller: Theory and experiment*" Heat Recovery Systems and CHP, 1995. 15(1): pgs. 77-83

[19] Ng, K.C., Bong, T.Y., Chua, H.T. and Bao, H.L. "*Theoretical and experimental analysis of an absorption chiller*" International Journal of Refrigeration, 1993. 17(5): pgs. 351-358

[20] Grossman, G. and Zaltash, A. *"ABSIM - Modular Simulation of Absorption Systems"* International Journal of Refrigeration, 2001. 24: pgs. 531-543

[21] Jeong, S., Kang, B.H and Karngt, S.W. "*Dynamic simulation of an absorption heat pump for recovering low grade heat*" Applied Thermal Engineering, 1998. 18(1-2): pgs. 1-12

[22] Kohlenbach, P. and Ziegler, F. "*A dynamic simulation model for transient absorption chiller performance. Part II: Numerical results and experimental verification"* International Journal of Refrigeration, 2008. 31: pgs. 226 – 233

[23] Takagi, Y., Nakamaru, T. and Nishitani, Y. *"An Absorption chiller model for HVACSIM^{+}"*, in *IBPSA Conference 1999*. 1999: Kyoto, Japan

[24] Fu, D.G., Poncia G., and Lu, Z. "*Implementation of an object-oriented dynamic modelling library for absorption refrigeration systems"* Applied Thermal Engineering, 2006. 26: pgs. 217-225

[25] Kohlenbach, P. and Ziegler, F. *"A dynamic simulation model for transient absorption chiller performance. Part I: The model"* International Journal of Refrigeration, 2008. 31: pgs. 217-225

[26] Kim, B. and Park, J. "*Dynamic simulation of a single-effect ammonia-water absorption chiller"* International Journal of Refrigeration, 2007. 30: pgs. 535-545

[27] Shin, Y., Seo, J.A., Cho, H.W., Nam, S.C. and Jeong, J.H. *"Simulation of dynamics and control of a double-effect LiBr–H_2O absorption chiller"* Applied Thermal Engineering, 2009. 29: pgs. 2718-2725

[28] Nurzia, G., (2008) "*Design and simulation of solar absorption cooling systems."* Doctoral Thesis - Dipartimento di Ingegneria Industriale, Facoltà di Ingegneria, Università degli Studi di Bergamo, Italia

[29] *"TRNSYS - A TRaNsient SYstem Simulation Program"*, Version: 17.1 (June 2011), 2011, Solar Energy Laboratory, University of Wisconsin-Madison, USA

[30] Beausoleil-Morrison, I., Kelly, N.J., Ferguson, A., Griffith, B., Maréchal, F. and Weber A. (2007). "*Specifications for Modelling Fuel Cell and Combustion-Based Residential Cogeneration Devices within Whole-Building Simulation Programs"* - A Report of Subtask B of FC+COGEN+SIM The Simulation of Building-Integrated Fuel Cell and Other Cogeneration Systems: Annex 42 of the International Energy Agency's Conservation in Buildings and Community Systems Programme. International Energy Agency

[31] Kelly, N.J., (1998) "*Towards a design environment for building integrated energy systems: The Integration of electrical power flow modelling with*

building simulation." Doctoral Thesis - Department of Mechanical and Aerospace Engineering, University of Strathclyde, Glasgow, UK

[32] Aasem, E.O., (1993) "*Practical simulation of buildings and air-conditioning in the transient domain."* Doctoral Thesis - Department of Mechanical and Aerospace Engineering, University of Strathclyde, Glasgow, UK

[33] Kaita, Y., "*Thermodynamic properties of lithium bromide-water solutions at high temperatures"* International Journal of Refrigeration, 2001. 24: pgs. 374-390

[34] Klein, S.A., Radermacher, R. and Herold, K.E *"Chapter 6 - Single Effect Water/Lithium Bromide Systems"*, in *"Absorption Chillers and Heat Pumps"*. 1996, CRC Press: New York, USA

[35] Florides, G.A., Kalogirou, S.A., Tassou, S.A. and Wrobel, L.C. "*Design and construction of a LiBr-water absorption machine"* Energy Conversion and Management, 2003. 44: pgs. 2483-2508

[36] Volker, C. "*Sonnenklima Suninverse - Solar cooling product information and experience"* in *Derbi Conference*. 2009. Perpignan, France

[37] *SONNENKLIMA* package solution description - Online Brochure. [Accessed: 15/07/2010], Available from: http://www.solarcombiplus.eu/docs/D46_SonnenKlima_v02_English.pdf

[38] Kohlenbach, P., (2006) "*Solar cooling with absorption chillers: Control strategies and transient chiller performance."* Doctoral Thesis - Von der Fakultät III – Prozesswissenschaften, Technischen Universität Berlin, Germany

[39] Ferguson, A. and Kelly, N.J. (2007). "*Section III - A Generic Model Specification for Combustion-based Residential Cogeneration Devices"* in *"Specifications for Modelling Fuel Cell and Combustion-Based Residential Cogeneration Devices within Whole-Building Simulation Programs"* - A Report of Subtask B of FC+COGEN+SIM The Simulation of Building-Integrated Fuel Cell and Other Cogeneration Systems: Annex 42 of the International Energy Agency's Conservation in Buildings and Community Systems Programme. International Energy Agency

[40] Ferguson, A. and Kelly, N.J. "*Modelling Building-integrated Stirling CHP*

Systems" in *eSim 2006 The Canadian Building Simulation Conference*. 2006. Toronto, Canada

[41] Vaillant Webaite (2012). "*High performance unvented stainless steel cylinder range"* [Accessed: 20/06/2011]; Available from: http://www.vaillant.co.uk/stepone2/data/downloads/c9/42/00/uniSTOR.pdf

[42] Borg, S.P., Yousif, C. and Farrugia, R.N. "*Investigation of domestic solar water heaters installations in Malta"* in *Renewable Energies in Malta and Beyond*. 2005. Salina, Malta

CHAPTER 4
SIMULATION METHODOLOGY AND ANALYSIS METRICS

Having explained the different aspects of trigeneration and building demand, this chapter focuses on the methodology used to assess the performance of a residential micro-trigeneration system. In the first section of this chapter, the simulation methodology section, the different scenarios modelled to understand the influence of operating conditions (such as building size, building fabric etc.) on micro-trigeneration system performance are presented and explained. The second section, the analysis metrics section provides an explanation of the performance metrics used to compare the different scenarios and quantify the impact of different operating conditions on micro-trigeneration system performance.

4.1 Simulation methodology

4.1.1 Scenarios investigated

Table 4.1 lists the specific cases modelled using ESP-r and analysed in the next chapter. This was done using the datasets, profiles and plant/building configurations presented in the previous chapters. The results from these simulations will provide detailed information on the performance of different configurations of trigeneration system in current and future, low-carbon Maltese housing.

Each scenario is based primarily on:

- the type of building model used (i.e. 3 household building with 9 persons or 6 household building with 18 persons), and

- the type of plant configuration adopted (i.e. basic plant configuration, plant configuration with additional chilled water storage tank or plant configuration with additional solar water heater).

For each scenario the subscript term then indicates:

- the type of building fabric scenario (i.e. low efficiency fabric scenario or high efficiency fabric scenario), and

- the household appliances' electrical efficiency scenario (i.e. current efficiency electrical scenario or high efficiency electrical scenario) used in the simulation.

The various scenarios modelled enabled the effect of different operating conditions (such as building size, occupancy, building fabric and appliance electrical efficiency) have on micro-trigeneration system performance, to be assessed.

Table 4.1 - Scenarios investigated

Scenario Building fabric/Electrical efficiency	Type of building fabric scenario	Electrical efficiency scenario	Building type (Occupancy)	Type of plant configuration
$1_{Low/Current\ efficiency}$	Low efficiency fabric scenario	Current efficiency electrical scenario	3 Household building (9 Persons)	Basic plant configuration; Hot water storage tank size $0.3m^3$
$1_{Low/High\ efficiency}$		High efficiency electrical scenario		
$1_{High/Current\ efficiency}$	High efficiency fabric scenario	Current efficiency electrical scenario		
$1_{High/High\ efficiency}$		High efficiency electrical scenario		
$2_{Low/Current\ efficiency}$	Low efficiency fabric scenario	Current efficiency electrical scenario	6 Household building (18 Persons)	Basic plant configuration; Hot water storage tank size $0.5m^3$
$2_{Low/High\ efficiency}$		High efficiency electrical scenario		
$2_{High/Current\ efficiency}$	High efficiency fabric scenario	Current efficiency electrical scenario		
$2_{High/High\ efficiency}$		High efficiency electrical scenario		
$3_{High/Current\ efficiency}$	High efficiency fabric scenario	Current efficiency electrical scenario	6 Household building (18 Persons)	Basic plant configuration with additional $0.3m^3$ chilled water tank; Hot water storage tank size $0.5m^3$
$3_{High/High\ efficiency}$		High efficiency electrical scenario		
$4_{High/Current\ efficiency}$	High efficiency fabric scenario	Current efficiency electrical scenario	6 Household building (18 Persons)	Basic plant configuration with additional $2.5m^2$ flat plate SWH; Hot water storage tank size $0.5m^3$
$4_{High/High\ efficiency}$		High efficiency electrical scenario		
$5_{High/Current\ efficiency}$	High efficiency fabric scenario	Current efficiency electrical scenario	6 Household building (18 Persons)	Basic plant configuration; All cogenerated electricity was exported to the grid; Hot water storage tank size $0.5m^3$
$5_{High/High\ efficiency}$		High efficiency electrical scenario		

The different cases in Scenario 1 were used to investigate the effect of improving the building fabric and reducing the electrical demand on micro-trigeneration system performance. The building type used (including the associated occupancy and the thermal, electrical and DHW loads) was that of the 3 household building and the plant configuration used was the basic plant configuration shown in Figure 3.2. Scenario 2 had primarily the same scope as Scenario 1 that is, to study the impact of improving the building fabric and reducing the electrical demand on micro-

trigeneration system performance. However, the building type used was the 6 household building. Scenario 1 and 2 could be therefore compared to study the effect building size and occupancy have on micro-trigeneration system performance.

Whereas the first two scenarios investigated operating conditions which affect the demand side, Scenarios 3 and 4, examined in detail the effect changes in the plant configuration have on the system performance. Scenario 3 was used to investigate the use of a chilled water storage tank as a buffer between the absorption chiller and the cooling coils as shown in Figure 3.12. Scenario 4 was used to study the use of flat plate SWH system working in tandem with the micro-trigeneration system as shown in Figure 3.13. Given that the building type and the building fabric used for these scenarios were identical to the one used in Scenario 2_{High} (6 household building with high efficiency fabric), the individual cases in Scenario 2_{High} ($2_{High/Current\ efficiency}$ and $2_{High/High\ efficiency}$) served as the base case scenarios against which Scenarios 3 and 4 were compared.

Finally, Scenario 5 investigated the effect of exporting all the cogenerated electricity produced by the system to the grid, rather than using it to satisfy the building's own electrical demand and then exporting the excess to the grid, as done in all other scenarios. In this context, it is important to clarify that currently the only *Feed-in Tariff* (*FIT*) present in Malta is the one payable for *photovoltaic* produced electricity which is exported to the grid [1]. Any electricity used to satisfy own demand is metered for records through a second separate meter, but is not paid for. This results in a situation where people can opt to sell all their electricity generated and import electricity from the grid to cover for their own demand [2]. Depending on the difference between the electricity tariff and the *FIT*, and the type of user (the electricity tariff in Malta is based on tariff bands where the cost per unit of imported electricity becomes increasingly higher with increasing consumption) it may make more financial sense to sell the electricity produced rather than use it for own consumption. The *FIT* proposed in this research (and which is explained in much more detail in Section 4.2.3.1) works on a similar principle.

The building fabric, building size and occupancy, and plant configuration used for Scenario 5 is identical to the one used in Scenario 2_{High}.

4.1.1.1 Factoring for electricity grid improvements

Table 4.1 in the previous section covers almost all of the external parameters listed in Chapter 1. A parameter which was however not included in the table was the indirect effect of grid improvement and decarbonisation. An important aspect in gauging the energetic and environmental performance of a micro-trigeneration system is through comparison with the separate production of the equivalent quantity of heat and power. Changes and improvements in the electricity network have an important effect on micro-trigeneration system performance.

To simulate for grid improvement and decarbonisation, for each of the scenarios described in Table 4.1, the grid efficiency and the grid emission factor (used in calculating the energy required to produce the same energy products in separate generation and the associated emissions), were varied to represent different grid network improvements. A detailed explanation of how this was done is given in Section 4.2.1.4 and Section 4.2.2.2.

4.1.1.2 Factoring for varying LPG prices and electricity tariffs

In assessing the financial performance of a system, reference has to be made to the existing financial background. Whereas investment costs are generally fixed parameters set at the point of purchasing the equipment, running costs dictated predominantly by variable fuel prices (in this case LPG) and electricity tariffs can have an important effect on the financial feasibility of a system [3].

As with other studies [3, 4], where the sensitivity of a system to varying fuel prices and electricity tariffs was analysed, in this research for each of the technical scenarios described in Table 4.1 the electricity tariff and the LPG price used in the calculations were varied to represent different economic scenarios. A detailed explanation of how this was done is given in Section 4.2.3.1.

4.1.2 Weekly, monthly, seasonal and annual analysis

For each scenario listed in Table 4.1 a number of week-long simulations were performed for each of the three seasons considered, that is, the heating, cooling and the intermediate season. For reasons already discussed in Chapter 1 (mainly related to the temporal precision required in residential analysis [5-7]), simulations were run with a time resolution of 1 minute. In order to provide enough monthly variability, for both the heating and the cooling seasons, two separate week-long simulations were performed for each month. For the intermediate season only one week for each month was simulated (an explanation is given later in this section). The weeks used in the simulations are shown in Table 4.2.

Table 4.2 - Characteristic weeks investigated

Season	Week Investigated
Heating season	17th December - 23rd December
	24th December - 30th December
	8th January - 14th January
	15th January - 21st January
	5th February - 11th February
	21st February - 27th February
	5th March - 11th March
	12th March - 19th March
Cooling season	1st June - 7th June
	18th June - 24th June
	9th July - 15th July
	23rd July - 29th July
	9th August - 15th August
	20th August - 26th August
	3rd September - 9th September
	17th September - 23rd September
Intermediate season	10th April - 16th April
	10th May - 16th May
	10th October - 16th October
	10th November - 16th November
	10th December - 16th December

For each month, the results obtained from the two week-long simulations (one week

analysis in the case of the intermediate season) were then extrapolated to obtain monthly data for the individual scenarios. Aggregation of the monthly results produced the seasonal and eventually the annual results which can then be used to compare the different scenarios modelled.

An important aspect in such a type of modelling is the choice of characteristic weeks used for the analysis. Ortiga *et al*. in [8], propose a graphical method based on sub-diving the annual cumulative energy demand into a number of representative time periods to aid in selecting characteristic days for optimisation processes involving cogeneration and trigeneration models; they explain that as long as the selected days are chosen using this method, the number of representative days chosen to represent a whole year worth of data does not really influence the results obtained. The research in this thesis was however different as its objective was not to optimise a system but rather to use a combined deterministic/sensitivity analysis approach to compare different demand-supply scenarios. In this thesis therefore rather than the absolute results (which were still important), what was being sought was to understand the effect different operating conditions have on micro-trigeneration, by comparing the results to a base case scenario. As long as the same time periods were used to create the aggregated seasonal and annual performance metrics for the different scenarios, the selection of typical days was therefore less of an issue. Two separate week-long simulations per month were considered to be a reasonable representation of the diversity experienced over a month. In the case of the intermediate season the fact that the micro-trigeneration system supplied only hot water demand (which shows little climatic influence) during all the months of that season, justifies the use of only one week-long simulation for each month.

4.2 Analysis metrics

The type of analysis used to assess the different scenarios simulated relies on a *'traditional'* analysis of a project's energetic, environmental and economic performance. Using a combined deterministic approach and sensitivity analysis methodology as explained in Chapter 1, for each scenario listed in Table 4.1 a number of performance metrics from each category were used to assess that scenario.

In the deterministic approach, performance metrics for the micro-trigeneration system calculated for different scenarios were compared. Examples include the system's fuel consumption, the electrical performance of the system and the system's seasonal and annual overall efficiency. In the sensitivity analysis approach the performance metrics calculated for each scenario were subjected to a process where one parameter was varied over a reasonable range of possible values (an explanation as to how the range of values for each individual parameter was selected is given in the respective sections later in this chapter) to find the sensitivity of the scenario to that particular parameter. The *Primary Energy Savings* (*PES*), *Emission Savings – CO_2 savings* (*ES*) and metrics related to the financial aspects of the system are examples of such an analysis.

The data used to create these performance metrics was primarily derived from the raw ESP-r simulation time-series output, which was based on a 1-minute resolution format and included (amongst others) the air and water inlet and outlet temperatures and flow rates of all plant components, fuel consumption (in the case of the CHP unit), the internal temperature in the building zones and other internal parameters of the building such as the solar energy absorbed by each individual zone *etc*. Based on the type of analysis required this data was used, either:

- In its minute based format to obtain time-based profiles relating to the building internal conditions (*e.g.* the temperature profile of a particular zone during a particular time period) or the plant network (*e.g.* the micro-trigeneration system electrical output, the hot water circuit inlet temperature to the chiller over a particular time period *etc.*); or

- In time aggregated form to obtain system based parameters such as the CHP unit fuel consumption, the supplied thermal energy *etc*.

4.2.1 Energetic performance metrics

The performance indicators used to determine the energetic performance of the

micro-trigeneration system are those described by Dorer and Weber in their research [9]. Specifically these were the:

- supplied thermal energy (space heating, space cooling and DHW supply);
- electrical performance of the system (the net import, the net export and the net demand satisfied by micro-trigeneration system);
- micro-trigeneration system performance (fuel consumption, primary energy consumption and system efficiency); and the
- system's *primary energy savings* (*PES*).

Additionally, in this research the energetic analysis was broadened to include also the operational details of the CHP unit and the absorption chiller.

4.2.1.1 Supplied thermal energy

The total thermal energy supplied by the micro-trigeneration system includes the energy supplied to provide space heating, the energy supplied to provide space cooling and the energy supplied to heat water.

To calculate the energy supplied for space heating, E_{SH} in kWh, consider a period of time N minutes long during which space heating was being supplied to the individual zones inside the building. Assuming no substantial heat losses in the ventilation ducts, the space heating energy supplied during this time period can be assumed to be the total energy transferred from the hot water flowing in the 3 heating coils (HC) to the air flowing across the ventilation system, as defined in equation (4.1).

$$E_{SH} = \frac{c_{Water}}{60}\left(\sum_{n=1}^{N}[\dot{m}_{Water-HC1}(T_{In} - T_{Out}) + \dot{m}_{Water-HC2}(T_{In} - T_{Out}) + \dot{m}_{Water-HC3}(T_{In} - T_{Out})]_n\right) \quad - \quad (4.1)$$

Similarly, equation (4.2) defines E_{SC}, the energy supplied for space cooling in kWh,

which is the energy absorbed by the water flowing in the 3 cooling coils (CC) from the air flowing across the ventilation system.

$$E_{SC} = \frac{c_{Water}}{60}\left(\sum_{n=1}^{N}[\dot{m}_{Water-CC1}(T_{Out} - T_{In}) + \dot{m}_{Water-CC2}(T_{Out} - T_{In}) + \dot{m}_{Water-CC3}(T_{Out} - T_{In})]_n\right) \quad - (4.2)$$

T_{In} and T_{Out} are respectively the inlet and outlet temperature of the water flowing inside the coils. The water mass flow rates $\dot{m}_{Water}$ are defined in kg/s, whilst the specific heat capacity, c_{Water} in kJ/kgK. The energy supplied to provide hot water, E_{DHW} in kWh, was calculated using equation (4.3). T_{Feed} refers to inlet water temperature from the mains.

$$E_{DHW} = \frac{c_{Water}}{60}\sum_{n=1}^{N}\left(\dot{m}_{Water-DHW}(T_{Out} - T_{Feed})\right)_n \quad - (4.3)$$

The equations listed are in their general form, specific for a period of time of *N* minutes which can be equal to an hour, a day, week *etc*., depending on the type of aggregated analysis being conducted.

4.2.1.2 Calculating the electrical performance of the system

The electrical performance of the system was assessed by calculating the net import (from the grid), the net export (to the grid) and the net demand satisfied by micro-trigeneration system (*μTRIGEN*) over a specific period of time.

To obtain the electrical performance of the system, use was made of the electrical demand profiles created in Chapter 2. These were used in conjunction with the electrical output profile of the micro-trigeneration system to create net import/export electrical demand profiles for the whole building.

Considering the gross electrical power produced by the micro-trigeneration system over a specific period of time, in this case a day in August (shown in Figure 4.1), a net import/export electrical profile for the whole (in this case 6 households) building (shown in Figure 4.3) can be obtained by superimposing the electrical demand

profile for that same time period (shown in Figure 4.2).

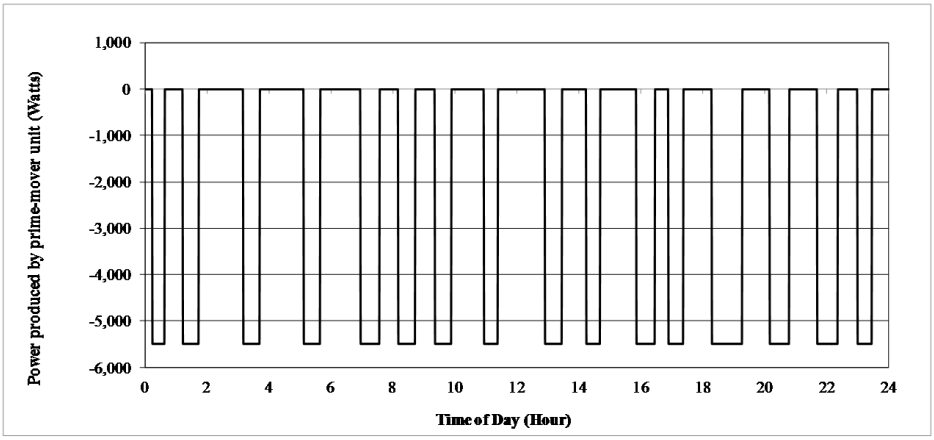

Fig. 4.1 - *μTRIGEN* system cogenerated electricity produced over a day in August

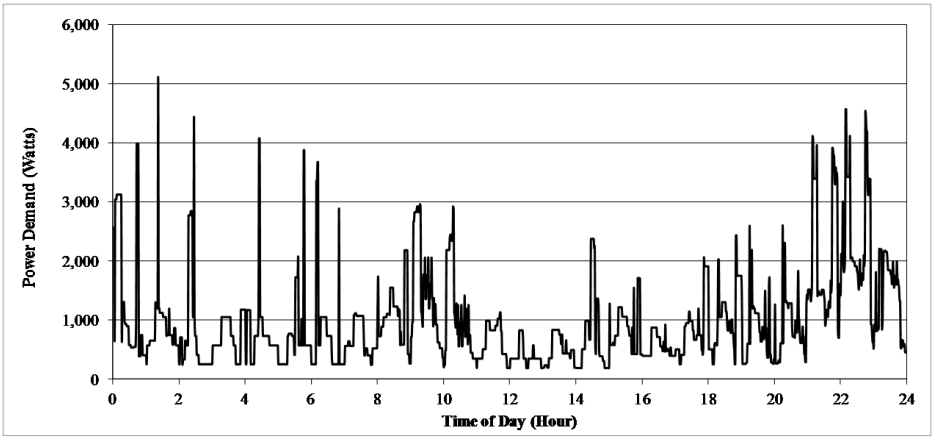

Fig. 4.2 - Electrical demand for a characteristic day in August for the 6 household building

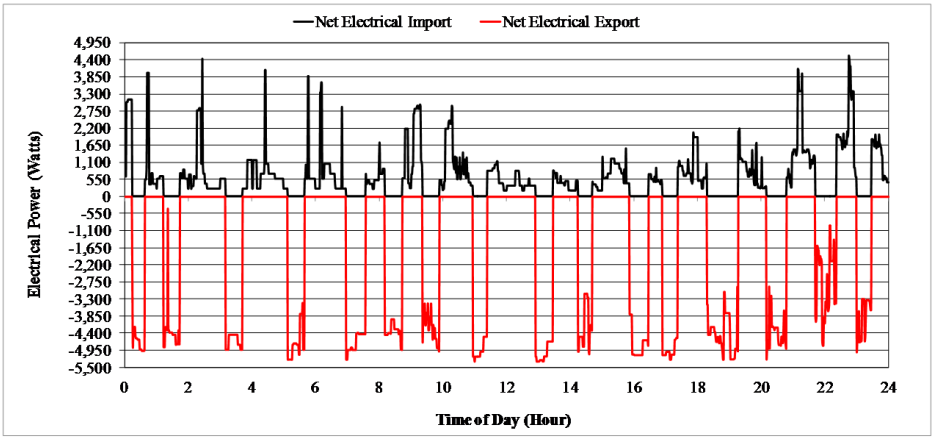

Fig. 4.3 - Resultant net import and export profile

Based on the data and profiles created the net electrical energy import ($E_{Net\ Import}$), the net electrical energy export ($E_{Net\ Export}$) and the net demand satisfied by the micro-trigeneration system ($E_{Net\ Demand\ \mu TRIGEN}$), all specified in kWh, could be calculated for any period of time *N* minutes (again depending on the type of aggregated analysis being done) using equations (4.4), (4.5) and (4.6) respectively.

For $E_{Net\ Import}$ equation (4.4)

$$E_{Net\ Import} = \frac{1}{60}\sum_{n=1}^{N}(Gross\ Elec.Demand_n - \mu TRIGEN\ Power\ Output_n)$$

If ($Gross\ Elec.\ Demand_n - \mu TRIGEN\ Power\ Output_n$) < *0, then*
(Gross Elec. Demand$_n$ – μTRIGEN Power Output$_n$) = 0

For $E_{Net\ Export}$ equation (4.5)

$$E_{Net\ Export} = \frac{1}{60}\sum_{n=1}^{N}(Gross\ Elec.Demand_n - \mu TRIGEN\ Power\ Output_n)$$

If (*Gross Elec. Demand$_n$ – μTRIGEN Power Output$_n$*) > *0, then*
(*Gross Elec. Demand$_n$ – μTRIGEN Power Output$_n$*) = *0*

For $E_{Net\ Demand\ \mu TRIGEN}$ equation (4.6)

$$E_{Net\ Demand\ \mu TRIGEN} = \frac{1}{60}\sum_{n=1}^{N}Gross\ Elec.Demand_n$$

Valid for *μTRIGEN Power Output$_n$ > 0; else if μTRIGEN Power Output$_n$ = 0, then*
$E_{Net\ Demand\ \mu TRIGEN}$ *= 0*
Also if *Gross Elec. Demand$_n$ > Max μTRIGEN Power Output$_n$, then*
Gross Elec. Demand$_n$ = Max μTRIGEN Power Output$_n$

The *Gross Elec. Demand$_n$* is the total electrical demand of the building (based on the electrical profiles created in Chapter 2 but excluding the electricity required to run the system's fans and pumps – not included in the analysis). The *μTRIGEN Power Output$_n$* is the electrical power output of the micro-trigeneration system.

4.2.1.3 Calculating the fuel consumption and the primary energy consumption

The total fuel consumption of the micro-trigeneration system, in kg, calculated over a period of *N* minutes was found by adding together equations (4.7) and (4.8), respectively the fuel consumed by the CHP unit and the auxiliary boiler. Fuel flow rates, $\dot{m}_{FUEL}$, are in kg/s.

$$\sum_{n=1}^{N}\left(\dot{m}_{FUEL(CHP)}\text{x } 60\ \right)_n \quad \text{- (4.7)}$$

$$\sum_{n=1}^{N}\left(\dot{m}_{FUEL(Aux)}\text{x } 60\right)_n \quad \text{- (4.8)}$$

The primary energy supplied to the micro-trigeneration system, $PE_{\mu TRIGEN}$, calculated in kWh, was then calculated using equation (4.9). The net calorific value of LPG (both the CHP unit and the auxiliary boiler are operated using LPG), C_{LPG}, was assumed equal to 46.15 MJ/kg [10].

$$PE_{\mu TRIGEN} = C_{LPG}\text{ x 60 x 0.278}\left(\sum_{n=1}^{N}\left(\left(\dot{m}_{FUEL(CHP)}\right)_n + \left(\dot{m}_{FUEL(Aux)}\right)_n\right)\right) \quad \text{- (4.9)}^{1}$$

4.2.1.4 Overall micro-trigeneration system efficiency

The efficiency of the micro-trigeneration system, $\eta_{\mu TRIGEN}$, was calculated using equation (4.10), defined by Dorer and Weber in [9]. The numerator represents the energy products (in kWh) produced by the micro-trigeneration system, whilst the denominator represents the primary energy consumed by the micro-trigeneration system over the same time period. The net export electrical energy in this case was considered to be an additional product as explained by Dorer and Weber in [9].

$$\eta_{\mu TRIGEN} = \frac{\left(E_{SH}+E_{SC}+E_{DHW}+E_{Net\ Demand\ \mu TRIGEN}+E_{Net\ Export}\right)100}{\left(PE_{\mu TRIGEN}\right)} \quad \text{- (4.10)}$$

4.2.1.5 Comparison with separate generation – the grid network efficiency

A problem associated with using equation (4.10) as a means to assess micro-

[1] 1 MJ = 0.278 kWh

trigeneration system performance is that, the equation does not discriminate between the different exergetic values of the energy products (thermal and electrical) produced by the unit [9, 11]. A more adequate method of comparison is to calculate the system's primary energy savings (*PES*) due to the system. This relies on comparing the primary energy consumption of the micro-trigeneration system and the primary energy consumption required to produce the same quantity and quality of products using separate generation. Equation (4.11) shows how the primary energy required to produce the same quantities of energy products assuming separate generation, $PE_{SEPARATE}$ in kWh, was calculated.

$$PE_{SEPARATE} = \frac{\left(\frac{E_{DHW}}{\eta_{Water}} + E_{Net\ Demand\ \mu TRIGEN} + E_{Net\ Export} + \frac{E_{SC}}{COP}\right)}{\eta_{Grid}} + \frac{E_{SH}}{\eta_{Gas\ Heater}} \quad \text{- (4.11)}$$

In this research, to simulate the separate production of energy commodities, it was assumed that in separate generation of energy commodities, the:

- *DHW* supply was supplied by an electric water heater having an electrical efficiency (including stand-by-losses), η_{Water}, of 85% [12];

- Space heating was supplied by an LPG heating system having an efficiency (including losses due to ancillaries), $\eta_{Gas\ Heater}$, of 85% [13]; and

- Space cooling was supplied by a vapour compression chiller with a Coefficient of Performance (COP) of 3 [13, 14].

The grid electrical efficiency based on actual electricity delivered (considering the actual energy going into the thermal stations in Malta and the actual electricity delivered at end-use), $\eta_{Grid,}$ was calculated as 25.5% [15].

Once both $PE_{\mu TRIGEN}$ and $PE_{SEPARATE}$ are known, the performance of the micro-trigeneration system can be assessed in terms of the *PES* of the system, calculated using equation (4.12), the official method defined in Directive 2004/8/EC to assess

cogeneration technologies [16].

$$PES = \frac{(PE_{SEPARATE} - PE_{\mu TRIGEN})100}{PE_{SEPARATE}} \quad \text{- (4.12)}$$

The higher the *PES*, the more '*energetically favourable*' is the system under investigation.

The grid electrical efficiency value, η_{Grid}, used in the calculation is very low compared to the typical European grid efficiency average of 40% [17]. Projects currently in progress in Malta, including a 200 MW_{el} interconnection with mainland Europe, are however expected to bring this value closer to the European average by the mid 2010s [18]. To simulate for such grid network improvements, and assess the sensitivity of the *PES* result obtained to the grid efficiency, the grid efficiency (η_{Grid}) value in equation (4.11) was varied between the current 25.5% and the European average of 40% at intervals of 2.5% to obtain different values of $PE_{SEPARATE}$. These were then used in equation (4.12) together with value of $PE_{\mu TRIGEN}$ to obtain the adjusted *PES* reflecting the new grid efficiency.

4.2.2 Environmental performance metrics

Similarly to the *PES*, the environmental assessment of the micro-trigeneration system was assessed by calculating the *Emission Savings – CO_2 Savings* (*ES*) of the system, which compares the carbon footprint of the micro-trigeneration system to the carbon footprint associated with producing the equivalent quantity and quality of energy commodities using separate generation.

4.2.2.1 Calculating the carbon footprint of the micro-trigeneration system

Since both the CHP unit and the auxiliary boiler are operated using LPG, the resulting emissions from the micro-trigeneration system in $kgCO_2$ was calculated using equation (4.13).

$$Emissions_{\mu TRIGEN} = e_{LPG} \text{ x } PE_{\mu TRIGEN} \quad \text{- (4.13)}$$

The emission factor of LPG, e_{LPG}, was in this case taken as 0.2495 $kgCO_2$ per kWh of primary energy consumed [19].

4.2.2.2 Comparison with separate generation – the grid network emission factor

The emissions due to separate generation, $Emissions_{SEPARATE}$, were calculated using equation (4.14).

$$Emissions_{SEPARATE} = e_{Grid}\left(\frac{E_{DHW}}{\eta_{Water}} + E_{Net\ Demand\ \mu TRIGEN} + E_{Net\ Export} + \frac{E_{SC}}{COP}\right) + e_{LPG}\left(\frac{E_{SH}}{\eta_{Gas\ Heater}}\right) \quad \text{- (4.14)}$$

Equation (4.14) is made up of two parts, the:

- Carbon footprint due to the grid electrically sourced energy products, which in separate generation would be satisfied by importing electricity from the grid; and the

- Emissions due to space heating which is operated directly on LPG.

Similarly to the procedure used to calculate the grid efficiency (η_{Grid}), e_{Grid} the emission factor of the electrical grid was calculated on the basis of the electricity actually delivered at end-use, that is, the figure includes all types of inefficiencies *e.g.* generation losses, distribution losses, unmetered losses *etc.* For the particular case of Malta this has been calculated at 1.088 $kgCO_2$ per kWh delivered [15]. The *Emission Savings* (*ES*) for the system was then calculated using equation (4.15) defined by Dorer and Weber in [9].

$$ES = \frac{(Emissions_{SEPARATE} - Emissions_{\mu TRIGEN})100}{Emissions_{SEPARATE}} \quad \text{- (4.15)}$$

In the same manner as the sensitivity of the *PES* to the grid efficiency was assessed using a range of grid efficiency values, the sensitivity of the *ES* result to the grid emission factor was assessed by varying the value of e_{Grid} in equation (4.14) between

the present 1.088 $kgCO_2$ per kWh delivered and a future 0.5 $kgCO_2$ per kWh delivered, reflecting the possible changes occurring in the near future in the Maltese electricity grid network. This was done at intervals of 0.1.

4.2.3 Economic performance metrics

Biezma and San Cristóbal in [20] explain by giving various examples present in literature that the economic analysis of a cogeneration system unit is usually done using investment criteria. Their research also discusses that although various criteria are available, the investment criteria typically used to accept or reject a cogeneration project are the *Net Present Value* (*NPV*), the *Internal Rate of Return* (*IRR*) and the *Payback Period* (*PP*). In this section an overview is given of the methods and equations utilised to financially assess the different scenarios.

4.2.3.1 Financial parameters used in modelling

In order to provide the input data required to define the investment criteria, two sets of data are required: the capital investment cost and the cash flow of the project (in this case of an individual scenario).

The former is a function of the initial cost to buy the equipment and can be simply considered as an investment cost related to the aggregated cost of procuring the different plant components. Table 4.3 show the *Investment Cost* (*I*) assumed for each scenario.

Table 4.3 - Investment costs for the different scenarios

Scenario	**Description**	**Approximate investment cost, *I* (Euros, €)**
1	CHP unit, absorption chiller and 0.3m^3 hot water storage tank	40,267
2	CHP unit, absorption chiller and 0.5m^3 hot water storage tank	40,457
3	CHP unit, absorption chiller, 0.5m^3 hot water storage tank and 0.3m^3 chilled water storage tank	41,057
4	CHP unit, absorption chiller, 0.5m^3 hot water storage tank and 2.5m^2flat plate SWH	40,857
5	CHP unit, absorption chiller and 0.5m^3 hot water storage tank	40,457

Costs are based on personal communications with the manufacturers and can only be considered as indicative as prices will vary depending on many factors, including supplier, taxation and freight.

The two most expensive plant components the CHP unit (5.5 kW_{el} Senertec Dachs IC Engine fed micro-CHP unit [21]) and the absorption chiller (the 10 kW_{th} SK SonnenKlima GmbH [22]) were identical for all scenarios and so the investment costs for the different scenarios were very similar. The only difference was associated with the additional cost of procuring the extra components constituting the different plant configurations. Not included in the costs are the ventilation system cost and the cost of the ancillary equipment, mainly pumps and fans: these were however identical for most scenarios. Although of an indicative nature the costs do nonetheless show the kind of cost magnitude such systems would entail and given that the research was aimed at producing comparative results between the different scenarios, the figures presented were enough to provide a reasonable indication of the effect different operating conditions have on the financial performance of micro-trigeneration in residential buildings.

The other set of data required to assess the investment criteria is the cash flow (*CF*) (or annual savings) of the project which is a more laborious calculation as it requires multiple calculations. As shown in equation (4.16) (an adaptation of the annual saving calculation proposed in [20]) the cash flow of a project includes not only the financial debits of the system due to the purchase of fuel, but also the revenues gained in exporting excess electricity to the grid and the saved cost from the net demand satisfied by the micro-trigeneration system.

$$CF = \left(E_{Net\ Export} \text{ x } FIT\right) + \left(E_{Total} \text{ x } Tariff\right) - \left(E_{Net\ Import} \text{ x } Tariff\right) - \left(E_{Net\ Export} + E_{Net\ Demand\ \mu TRIGEN}\right)MC - \left(Fuel_{\mu TRIGEN} - Fuel_{SEPERATE}\right)Cost\ of\ Fuel \quad \text{- (4.16)}$$

Table 4.4 describes each individual component making up the system's cash flow.

Table 4.4 - Explanation of the cash flow equation

Financial component	Explanation
$E_{Net\ Export}$ x FIT	**Revenue from net export sales:** A source of income is the sale of electricity to the grid at the agreed Feed-in Tariff (*FIT*). The monetary value of such a component is calculated by multiplying the net electricity exported to the grid by the applicable *FIT*.
E_{Total}x $Tariff$,where $E_{Total} = \frac{E_{DHW}}{\eta_{Water}} + \frac{E_{SC}}{COP} + E_{Net\ Demand\ \mu TRIGEN} + E_{Net\ Import}$	**Total invoiced electricity *without* trigeneration:** Assuming no micro-trigeneration system was present, E_{Total} includes the cost of all the electricity which would have otherwise been purchased through conventional separate generation sourced electricity, including the net imports.
$E_{Net\ Import}$ x $Tariff$	**Total invoiced electricity *with* trigeneration:** If a micro-trigeneration system is present only the net electrical imports need to be purchased through conventional separate generation sourced electricity. The net electrical imports have to be included as an extra additional cost which is not covered by the system.
$(E_{Net\ Export} + E_{Net\ Demand\ \mu TRIGEN})MC$	**Maintenance cost:** The financial value of such a cost is calculated by multiplying the electricity produced by the CHP Maintenance cost rate (*MC*) in € per kWh produced.
$(Fuel_{\mu TRIGEN} - Fuel_{SEPERATE})Cost\ of\ Fuel$	**Fuel purchasing costs:** Given that the fuel type is the same (LPG), the net cost of fuel purchased is calculated by deducting the amount of fuel which would have been used by the space heating in separate generation from the total fuel used by the micro-trigeneration system. The cost component is then calculated by multiplying the net amount of fuel used by the fuel cost.

Using the data obtained from the technical analysis of each individual scenario, the annualised cash flow can be calculated for each scenario. In calculating the cash flow of the different scenarios, reference is made to Section 4.1.1.2 were it was mentioned that to analyse the sensitivity of the different technical scenarios investigated to the financial backdrop in which the micro-trigeneration system was operating. It is clear from equation (4.16) that both the electricity tariff and LPG price can have a strong impact on the feasibility of a system. Moreover, compared to the *Investment Costs* which are predominately stable on the short-medium term, and the *Feed-in Tariff* which is also in many cases set for a long period of time, both the electricity tariff and fuel prices can be of a very variable nature. For this reason both the electricity tariff and LPG price were varied independently to create different economic conditions which enabled the assessment of the effect of these two parameters on the financial feasibility of the different scenarios investigated. In this context:

- Whilst keeping the price of LPG constant at the current price (1.187 € per kg), the electricity tariff used to calculate the cash flow of each individual scenario was varied between ± 50% of the current tariff (at different intervals: ± 10%, ± 25% and ± 50%) as shown in Table 4.5 [23]; and

- Whilst keeping the electricity tariff constant at the current tariff, the price of LPG was varied between the current high (1.187 € per kg +24%) and low (1.187 € per kg -14%) retail price in Malta, at different intervals.

Table 4.5 - Electricity tariff bands

Tariff band	Cumulative consumption (kWh)	-50% Current tariff (€ per kWh)	Current tariff (€ per kWh)	+50% Current tariff (€ per kWh)
1	0 - 2,000	0.0805	0.1610	0.2415
2	2,001 - 6,000	0.0865	0.1730	0.2595
3	6,001 - 10,000	0.0945	0.1890	0.2835
4	10,001 - 20,000	0.1800	0.3600	0.5400
5	20,001 & over	0.3100	0.6200	0.9300

Assuming an appropriate *Feed-in Tariff* was quite a problematic aspect. In most European countries the concept of a *FIT* is quite an established procedure. In Germany for example, *FIT* rates for micro-cogeneration have been established for quite some time and are specified in national legislation, based on whether the cogenerated electricity produced is exported (0.125 € per kWh) or used to satisfy the own demand (0.115 € per kWh) [24]. In certain cases these tariffs may also be augmented by other fiscal incentives such as grants on the investment costs and fuel tax exemptions. In Malta, so far the only experience with *FIT* is as explained earlier in Section 4.1.1, related to the production of electricity from domestic *photovoltaic* systems and which is paid at a rate of 0.25 € per kWh exported (guaranteed for 7 years) [1]. Again this *FIT* is (in some cases) augmented by a grant payable on the capital investment.

Assuming no other fiscal incentive (such as rebated fuel or investment grants) but the

FIT and considering the cost involved, a reasonable starting value for the *FIT* is of 0.50 € per kWh exported. The value is of course an arbitrary value chosen for the modelling carried out in this research, but may prove to be a starting iteration towards obtaining a legislated *FIT* for micro-CCHP in the course of future work.

The *Maintenance Cost* (*MC*) rate was assumed constant throughout the modelling process at a flat rate of 0.012 € per kWh produced [25].

The financial feasibility of each scenario under varying electricity tariffs and LPG prices was then measured using the *Present Worth*, the *Internal Rate of Return* and *Payback Period* investment criteria described in Section 4.2.3.2, Section 4.2.3.3 and Section 4.2.3.4.

4.2.3.2 Net present value - Present worth

The first investment criteria utilised was the Net Present Value of the project. The Net Present Value includes a number of methods which can be used to assess a project's feasibility [20]. In this thesis the *Present Worth* (*PW*) was chosen as the preferred method given that all other methods can actually be considered as derivatives of this method. The *PW* classifies whether a project is accepted or rejected on the basis of the calculated result being positive or negative. A project is accepted if the calculated *PW* is positive, conversely it is rejected if the *PW* is negative. Different projects are preferred between one another based on the highest *PW*. It is calculated over an expected project lifetime period of *Y* years using equation (4.17) presented in [20] by Biezma and San Cristóbal.

$$PW = -I + \sum_{y=1}^{Y} \left(\frac{CF}{(1+MARR)^{y}} \right) \quad \text{- (4.17)}$$

The expected lifetime of the project was assumed to be 25 years (expected lifetime is quoted in [21] at 80,000 hours, at an average of 3,000 hours per year) whilst the *Minimum Attractive Rate of Return* (*MARR*) was set at 6% as used in a similar project assessment discussed by Biezma and San Cristóbal in [20].

4.2.3.3 Internal rate of return

The second investment criteria used to assess the financial performance of a scenario was the *Internal Rate of Return* (*IRR*) calculated using equation (4.18) [20]. Contrary to what happens in calculating the *PW*, where the *Minimum Attractive Rate of Return* is fixed and the *PW* can therefore have either a positive or negative value (consequently determining the worthiness of a project), when calculating the *IRR*, the *Investment Rate* (*IR*) is varied until a value is found such that the *PW* is zero. A project is accepted if the calculated investment rate for the project is higher than the set *MARR*.

$$IRR = IR\ for\ PW = -I + \sum_{y=1}^{Y}\left(\frac{CF}{(1+IR)^{y}}\right) = 0 \quad \text{- (4.18)}$$

4.2.3.4 Payback period

The final investment criteria used, the simple *Payback Period* (*PP*) defined in equation (4.19) [20], is possibly the most important criteria for an investor as it gives an indication of the amount of time required to pay off the initial investment and start making profit.

$$PP = \frac{I}{CF} \quad \text{- (4.19)}$$

4.3 Summary of Chapter 4

This chapter has presented the different scenarios investigated together with the assessment methodology and associated performance metrics used to assess the value of the proposed scenarios.

By comparing different scenarios using a deterministic approach, the effect that different operating conditions (such as the building fabric, occupancy, building size, plant configuration) have on micro-trigeneration system performance can be quantified. The methodology also uses sensitivity analyses to demonstrate and quantify the effect of a number of other parameters (such as grid improvement and decarbonisation, electricity tariff, LPG price). The different scenarios and hence the different operating conditions being investigated are assessed on the basis of the

impact they have on the energetic, environmental and economic performance of the residentially modelled micro-trigeneration system. Based on the information obtained from the simulations performed, the effect of the different operating conditions on the modelled micro-trigeneration system can be assessed, with the scope of better understanding the interaction between the system and the surrounding environment.

Apart from the technical operating conditions which were discussed at length in Chapter 2 and Chapter 3 (*e.g.* reduced electrical demand due to the use of high efficiency appliance, reduced thermal due to high efficiency building fabric *etc*.), this chapter also introduces a number of other factors which have the potential of influencing micro-trigeneration system performance. These include indirect technical factors such as grid network improvements and decarbonisation. Finally, the economic factors which affect the financial viability and the financial metrics by which viability could be assessed of micro-trigeneration were discussed.

4.4 Chapter References

[1] *"Feed-in Tariffs (Electricty generated from solar photovoltaic installations)"* - Legal Notice 70 of 2011. Malta Resources Authority, Marsa, Malta

[2] Malta Resources Authority (2010). "*Feed-in Tariffs scheme 2011 - Information to stakeholders"* - Malta Resources Authority, Marsa, Malta. Online Presentation; [Accessed: 15/01/2012]; Available from: http://www.mra.org.mt/Downloads/licences/Energy%20Performance%20assessment,%20electricity%20and%20RES/FIT%20Scheme%202010%20-%20Information%20meeting.pdf

[3] Ren, H., Gao, W. and Ruan, Y. *"Optimal sizing for residential CHP system"* Applied Thermal Engineering, 2008. 28: pgs. 514-523

[4] Colonna, P. and Gabrielli, S. "*Industrial trigeneration using ammonia–water absorption refrigeration systems (AAR)"* Applied Thermal Engineering 2003. 23: pgs. 381-396

[5] Hawkes, A. and Leach, M. "*Impacts of temporal precision in optimising modelling of micro-Combined Heat and Power"* Energy, 2005. 30: pgs. 1759-1779

[6] Wright, A. and Firth, S. "*The nature of domestic electricity-loads and effects of time averaging on statistics and on-site generation calculations"* Applied Energy, 2007. 84(2007): pgs. 389-403

[7] Stokes, M., (2004) "*Removing barriers to embedded generation: a fine-grained load model to support low voltage network performance analysis."* Doctoral Thesis - Institute of Energy and Sustainable Development, De Montfort University, Leicester, UK

[8] Ortiga, J., Bruno, J.C. and Coronas, A. "*Selection of typical days for the characterisation of energy demand in cogeneration and trigeneration optimisation models for buildings"* Energy Conversion and Management, 2011. 52: pgs. 1934-1942

[9] Dorer, V. and Weber, A. (2007). *"Methodologies for the Performance Assessment of Residential Cogeneration Systems"* - A Report of Subtask C of FC+COGEN+SIM The Simulation of Building-Integrated Fuel Cell and Other Cogeneration Systems: Annex 42 of the International Energy Agency's

Conservation in Buildings and Community Systems Programme. International Energy Agency

[10] International Energy Agency, "*Energy Statistics Manual"*, ed. Claude Mandil. 2004, Paris, France: International Energy Agency

[11] Macchi, E., Campanari, S. and Silva, P. La Microcogenerazione a gas naturale, ed. Polipress. Vol. Scienza e tecnologia per l'energetica. 2005, Milano: Polipress

[12] DEFRA (2008). "*Policy Brief: Improving the energy performance of domestic heating and hot water systems"* - Volume in Series *"Market Transformation Programme"*. DEFRA, UK

[13] Angel, W.L., "*HVAC Design Sourcebook"*. 2011: McGraw-Hill Professional; 1st edition

[14] Fragiacomo, P., Arcuri, P. and Florio, G. *"A mixed integer programming model for optimal design of trigeneration in a hospital complex"* Energy 2007. 32 pgs. 1430-1447

[15] *"Enemalta Corporation Annual Report 2009 and Financial Statements 2008"* - Enemalta Corporation. Marsa, Malta. [Accessed: 10/09/2011]; Available from: http://www.enemalta.com.mt/enemaltastorage/images/files/annual%20reports/annual%20report%202009%20and%20financial%20statement%202008.pdf

[16] *"Directive 2004/8/EC of the European Parliament and of the Council of 11 February 2004 on the promotion of cogeneration based on a useful heat demand in the internal energy market and amending Directive 92/42/EEC"* - European Parliament and European Council

[17] *"Directive 2006/32/EC of the European Parliament and of the Council of 5 April 2006 on energy end-use efficiency and energy services"* - European Parliament and European Council

[18] Malta Resources Authority (2011). "*Malta 2nd National Energy Efficiency Action Plan"* - Malta Resources Authority, Marsa, Malta. [Accessed 17/12/2011]; Available from: http://ec.europa.eu/energy/efficiency/doc/mt_-_energy_efficiency_action_plan_en.pdf

[19] Herold, A. (2003). "*Comparison of CO_2 emission factors for fuels used in Greenhouse Gas Inventories and consequences for monitoring and reporting under the EC emissions trading scheme"* - ETC/ACC Technical Paper 2003/10. European Topic Centre on Air and Climate Change

[20] Biezma, M.V. and San Cristóbal, J.R. "*Investment criteria for the selection of cogeneration plants - A state of the art review"* Applied Thermal Engineering, 2006. 26(5-6): pgs. 583-588

[21] Baxi SenerTec Dachs UK Webpage (2010) [Accessed: 29/03/2011]; Available from: http://www.baxi.co.uk/products/DACHS.htm

[22] Volker, C. *"Sonnenklima Suninverse - Solar cooling product information and experience"* in *Derbi Conference*. 2009. Perpignan, France

[23] Enemalta Corporation (2010). "*Electricity Tariffs"*; [Accessed: 26/10/2011]; Available from: http://www.enemalta.com.mt/index.aspx?cat=2&art=5&art1=9

[24] Shaw, D. (2009). "*CHP comes of age"* - Online Presentation. [Accessed: 07/04/2012]; Available from: http://www.cibseashrae.org/presentations/Shaw0209.pdf

[25] Knight, I. and Ugursal, I. (2007). "*Residential Cogeneration Systems: A Review of the Current Technologies* - A Report of Subtask A of FC+COGEN+SIM The Simulation of Building-Integrated Fuel Cell and Other Cogeneration Systems: Annex 42 of the International Energy Agency's Conservation in Buildings and Community Systems Programme. International Energy Agency

CHAPTER 5
RESULTS AND DISCUSSION

This chapter presents the results obtained for the different scenarios modelled. As discussed in Chapter 4, for each modelled scenario the results obtained from the simulations of the trigeneration system serving a 3 and 6 household building were analysed in terms of their energetic, environmental and economic performance. Recalling that the aim of this thesis was to assess the performance of trigeneration in future Maltese housing, the effect of improving the building fabric and the electrical efficiency of household appliances have on the thermal and the electrical demands respectively is also examined in detail, as efficiency improvements have a significant effect on the viability and performance of trigeneration.

5.1 Effect on thermal demand of improving the building fabric

The first part of this chapter examines the effect of improving the building fabric on the thermal performance of the building, specifically the effect of improving the building fabric on thermal energy demand. In the analysis, two scenarios are investigated; Scenario 1 – the 3 household building and Scenario 2 – the 6 household building. For both scenarios two different building fabric cases were developed, a low efficiency fabric case (Scenario 1_{Low} and Scenario 2_{Low}) representing current Maltese housing and a high efficiency fabric case (Scenario 1_{High} and Scenario 2_{High}) representing future Maltese housing; these were used to analyse the effect of improving the building fabric on the heating and cooling load of the two buildings modelled. Inter-scenario comparisons were also undertaken, to examine the interaction between improving the building fabric and building size and occupancy.

In this first set of results presented, the annual amount of heating and cooling energy supplied to the two building models by the basic micro-trigeneration plant configuration (shown in Figure 3.2) are listed and discussed. In the case of the 3 household building the control scheme used is that shown in Table 3.5, whilst for the 6 household building the control scheme used is that shown in Table 3.6. Based on the data extracted from the four sets of simulations, equation (4.1) was used to calculate E_{SH} in kWh, the energy supplied for space heating, whilst equation (4.2) was used to calculate E_{SC} in kWh, the energy supplied for space cooling. These simulations quantify the effect of fabric improvements on building space heating and cooling thermal demand and are eventually used to quantify the effect building fabric has on the performance of a micro-trigeneration system.

5.1.1 Analysis of space conditioning energy requirements – Heating period

Table 5.1 lists the annual heating energy supplied for the four scenarios. As would be expected, the simulation results show that the heating load for the 6 household building is significantly higher than for the 3 household building. The load per household is however actually lower (825 kWh/household compared to 1,103 kWh/household in the low efficiency case and 536 kWh/household compared to 857 kWh/household in the high efficiency case), demonstrating that as housing density

increases so does energy-efficiency. In this specific case the larger amount of solar gains absorbed through the larger glazed area present in the 6 household building and the larger internal heat gains due to the higher number of occupants present, provide for a substantial reduction in space heating energy demand per household.

Table 5.1 - Annual heating energy supplied

Scenario$_{\text{Building fabric}}$	**Annual heating energy supplied E_{SH} (kWh) *per* Floor**			
	Ground Floor	**Middle Floor**	**Top Floor**	**Entire building**
1_{Low} (3 Household building - Low fabric)	1,234.5	1,044.2	1,032.6	3,311.2
1_{High} (3 Household building - High fabric)	1,137.1	740.9	692.9	2,570.9
Percentage difference between heating energy supplied 1_{Low} and 1_{High} (%)	-7.9	-29.1	-32.9	-22.4
2_{Low} (6 Household building - Low fabric)	2,093.4	1,361.8	1,492.2	4,947.1
2_{High} (3 Household building - High fabric)	1,698.9	718.7	796.3	3,213.1
Percentage difference between heating energy supplied 2_{Low} and 2_{High} (%)	-18.8	-47.2	-46.6	-35.1

The simulations also indicate that fabric improvements had a greater effect on the upper floors with only a minor impact on the ground floor. The main reason for this is that a significant pathway through which heat is lost in winter, and which is often overlooked in Maltese buildings is the flooring of the ground floor apartment. The *Technical Guidance - Conservation of Fuel, Energy and Natural Resources* [1] specifies that the maximum allowable U-Value through a ground floor is of 1.97 W/m^{2}K. The flooring for the ground floor based apartment used in this research was of 1.2 W/m^{2}K, which is already an improvement over the maximum allowable U-Value. It may therefore be the case that the guidance should be revised to account for such heat losses. In this context, Borg *et al*. [2] have discussed the improvement obtained in terms of reducing heat losses through the flooring of ground floor based apartment (in a Maltese building) through the laying of a carpet during winter.

Further, fabric improvements have a greater effect in the 6 household case compared to the smaller building. The reasons for this are that the two most efficient measures were the double glazing and the wall insulation. Given that the 6 household building

has a larger glazed and wall area than the 3 household building, improving the overall building fabric has the greatest effect in the larger building.

5.1.2 Analysis of space conditioning energy requirements – Cooling season

Table 5.2 shows the annual cooling energy supplied to different floors on an individual scenario basis.

Table 5.2 - Annual cooling energy supplied

Scenario$_{\text{Building fabric}}$	**Annual cooling energy supplied E_{SC} (kWh) *per* Floor**			
	Ground Floor	**Middle Floor**	**Top Floor**	**Entire building**
1_{Low} (3 Household building - Low fabric)	1,706.3	3,087.3	4,394.8	9,188.4
1_{High} (3 Household building - High fabric)	1,094.2	2,424.5	3,792.2	7,310.9
Percentage difference between heating energy supplied 1_{Low} and 1_{High} (%)	-35.9	-21.5	-13.7	-20.4
2_{Low} (6 Household building - Low fabric)	2,865.0	5,186.3	4,027.6	12,077.9
2_{High} (3 Household building - High fabric)	2,120.4	4,745.0	3,800.0	10,661.2
Percentage difference between heating energy supplied 2_{Low} and 2_{High} (%)	-26.0	-8.5	-5.7	-11.7

As expected given the smaller volume required to be cooled, the energy demand of the 3 household building was lower than the corresponding energy demands of the scenarios in the 6 household building. The load per household in this case is however higher in the 6 household building compared to the 3 household building (2,013 kWh/household compared to 1,531 kWh/household in the low efficiency case and 1,777 kWh/household compared to 1,218 kWh/household in the high efficiency case).

The reason for this is that, whereas in winter the higher heat gains (due to a larger glazed surface area and higher number to the number of occupants) act as a free source of heating which lowers the requirement for space heating, in summer the converse is true – the increase in heat gains results in a higher cooling demand per household. Further, the double glazed nature of the fabric used in the high efficiency case of the 6 household building (which offsets some of the energy savings made by improving the retention of internal heat gains) results in a situation where improving

the building fabric is most effective in the smaller building. An important modelling aspect during the cooling season is therefore to reduce solar gains through the addition of shading devices. Both building models results shown include the addition of external louvers shading approximately 70% of the buildings' glazed area.

In terms of the individual fabric improvement measures, simulations showed that the two most successful measures were the roof and wall insulation, with the former being the most important individual improvement given the high solar inclination during summer which renders roofs the main entry point of solar gains into buildings.

Finally, an important aspect is the fact that in both buildings, improving the building was most effective for the ground floor apartment. Explicitly this suggests that given their location (sheltered from direct sunlight by the floors above) lower located floors tend to benefit from improvements in the thermal envelope of the floors located above them. In this case the thicker (and more insulated) walls and roof serve as barrier to the flow of solar-based heat gains downwards towards the ground floor.

5.2 Effect of improving the electrical efficiency of appliances on residential electrical demand profiles

In Chapter 2 a method was presented whereby low-resolution electrical demand datasets can be used to create high-resolution demand profiles reflecting the effects of appliance energy-efficiency improvements in future years. Based on the aggregation of these individual appliance based profiles, a number of representative seasonal daily electrical demand profiles were modelled to represent the current and high efficiency electrical demand profiles of individual and aggregated households within the two buildings modelled.

A number of these profiles, specifically those for the characteristic days in February, May and August, for both the 3 household building used in Scenario 1 and the 6 household building used in Scenarios 2, 3, 4 and 5 were shown in Chapter 2. Table 5.3 summarises the key features of the demand profiles shown in Chapter 2, specifically those used to model the current and high electrical efficiency demand

profiles of the different floors in the 3 household building in Scenario 1. The key characteristics used to describe the profiles are the daily electrical energy consumption and the daily peak demand. Recalling from Chapter 2 which households were used to model the individual floors within the 3 household building, GF refers to the ground floor of the 3 household building (modelled using household 2A), MF refers to the middle floor (modelled using household 3B) and TF refers to the top floor (modelled using household 4B).

Table 5.3 - Key values obtained for the modelled demand profiles of the 3 household building - Scenario 1

Month	Value	Appliances' electrical efficiency	Floor (Household)			
			GF (2A)	MF (3B)	TF (4B)	Entire building
February	Daily peak demand (W)	Current Efficiency	2,134	2,219	2,597	4,013
		High Efficiency	2,005	1,972	2,129	4,027
		Percentage Difference	-6	-13	-22	0
	Daily electrical energy consumption (kWh)	Current Efficiency	3.53	6.92	9.84	20.29
		High Efficiency	2.59	5.22	7.27	15.08
		Percentage Difference	-36	-33	-35	-35
May	Daily peak demand (W)	Current Efficiency	2,048	2,276	2,590	6,331
		High Efficiency	2,055	2,655	2,240	6,026
		Percentage Difference	0	14	-16	-5
	Daily electrical energy consumption (kWh)	Current Efficiency	3.28	6.19	8.78	18.25
		High Efficiency	2.58	4.7	6.62	13.90
		Percentage Difference	-27	-32	-33	-31
August	Daily peak demand (W)	Current Efficiency	2,021	2,141	3,042	3,942
		High Efficiency	2,004	2,009	2,712	3,333
		Percentage Difference	-1	-7	-12	-18
	Daily electrical energy consumption (kWh)	Current Efficiency	2.29	4.45	6.95	13.69
		High Efficiency	1.68	3.36	5.07	10.11
		Percentage Difference	-36	-32	-37	-35

Additionally, Figure 5.1 shows the load duration curves for both the current and high electrical efficiency profiles described in the Table 5.3 for the month of February.

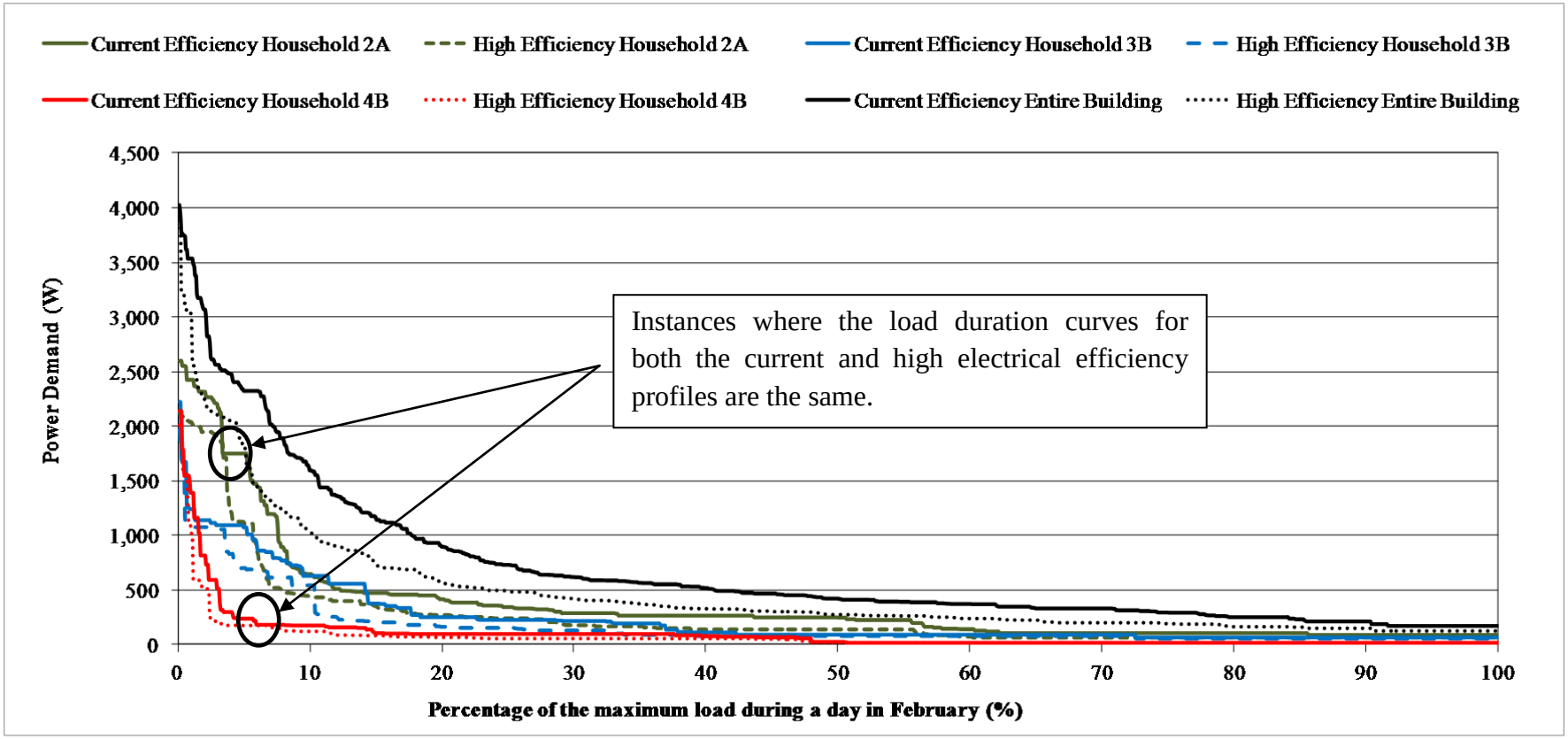

Fig. 5.1 - Load duration curves for the households in the 3 household building for a day in February

In terms of the daily electrical energy consumption, it can be observed that for all households and for the characteristic days shown, improving the energy-efficiency of electrical appliances results in an overall reduction in the range of 30% to 40%. As expected therefore, improving the energy-efficiency of appliances substantially reduces the electrical energy demand.

With regards to the daily peak demand however, although generally a reduction is observed, it can be seen that at this low level of aggregation (single household or small aggregation of households) the daily peak demand appears to be highly dependent on the time-of-use and the individual aggregation of individual appliance loads. For example, the results obtained for the daily peak demand in February show that, whereas increasing the electrical efficiency of appliances results in a reduction in the daily peak demand of each individual household, the aggregated daily peak demand for the entire building was slightly increased. Similarly for individual households the daily peak demand of household 3B was higher for the high electrical efficiency scenario compared to the current efficiency scenario. Likewise, in terms of the load duration curves, Figure 5.1 shows that although the average daily load decreases rather substantially, the variability inherent to this low level of aggregation results in a situation where even when using high electrical efficiency appliances, the instantaneous demand may be similar (if not higher) to that obtained with the 'low' efficiency appliances.

The results indicate that a changeover to more energy-efficient appliances may not always be successful in reducing the daily peak electrical demands of an individual household or a small aggregation of households; this also indicates that the daily peak demands are due to the coincidence of multiple loads rather than to individual large loads.

Table 5.4 shows the equivalent key features calculated for the electrical demand profiles modelled to represent the current and high electrical efficiency demand profiles of the different floors in the 6 household building used in scenarios 2, 3, 4 and 5. Recalling that in this case each floor was modelled to represent two

households, GF refers to the ground floor of the 6 household building (modelled using household 2A and 3A), MF refers to the middle floor (modelled using household 3B and 4A) and TF refers to the top floor (modelled using household 4B and 2B). Figure 5.2 shows the load duration curves for both the current and high electrical efficiency profiles described in the Table 5.4 for the month of February.

Table 5.4 - Key values obtained for the modelled demand profiles of the 6 household building - Scenarios 2, 3, 4 and 5

Month	Value	Appliances' electrical efficiency	Floor (Households)			
			GF (2A+3A)	MF (3B+4A)	TF (4B+2B)	Entire building
February	Daily peak demand (W)	Current Efficiency	3,057	3,971	3,121	6,742
		High Efficiency	2,227	3,227	3,265	6,286
		Percentage Difference	-37	-23	4	-7
	Daily electrical energy consumption (kWh)	Current Efficiency	7.23	14.90	11.04	11.04
		High Efficiency	5.11	10.97	8.19	8.19
		Percentage Difference	-42	-36	-35	-35
May	Daily peak demand (W)	Current Efficiency	2,541	4,599	4,228	7,367
		High Efficiency	2,158	4,064	3,960	8,031
		Percentage Difference	-18	-13	-7	8
	Daily electrical energy consumption (kWh)	Current Efficiency	7.85	14.58	10.88	10.88
		High Efficiency	5.86	11.00	8.38	8.38
		Percentage Difference	-34	-33	-30	-30
August	Daily peak demand (W)	Current Efficiency	2,247	3,878	3,322	5,118
		High Efficiency	2,153	3,295	2,764	4,778
		Percentage Difference	-4	-18	-20	-7
	Daily electrical energy consumption (kWh)	Current Efficiency	4.89	10.56	8.34	8.34
		High Efficiency	3.41	7.74	6.13	6.13
		Percentage Difference	-43	-37	-36	-36

The same conclusions can be drawn. Improving the energy-efficiency of electrical appliances leads to a reduction in the daily electrical energy consumption in the order of 30% to 40%, and the daily peak demand is more susceptible to individual aggregation of loads rather than individual high loads.

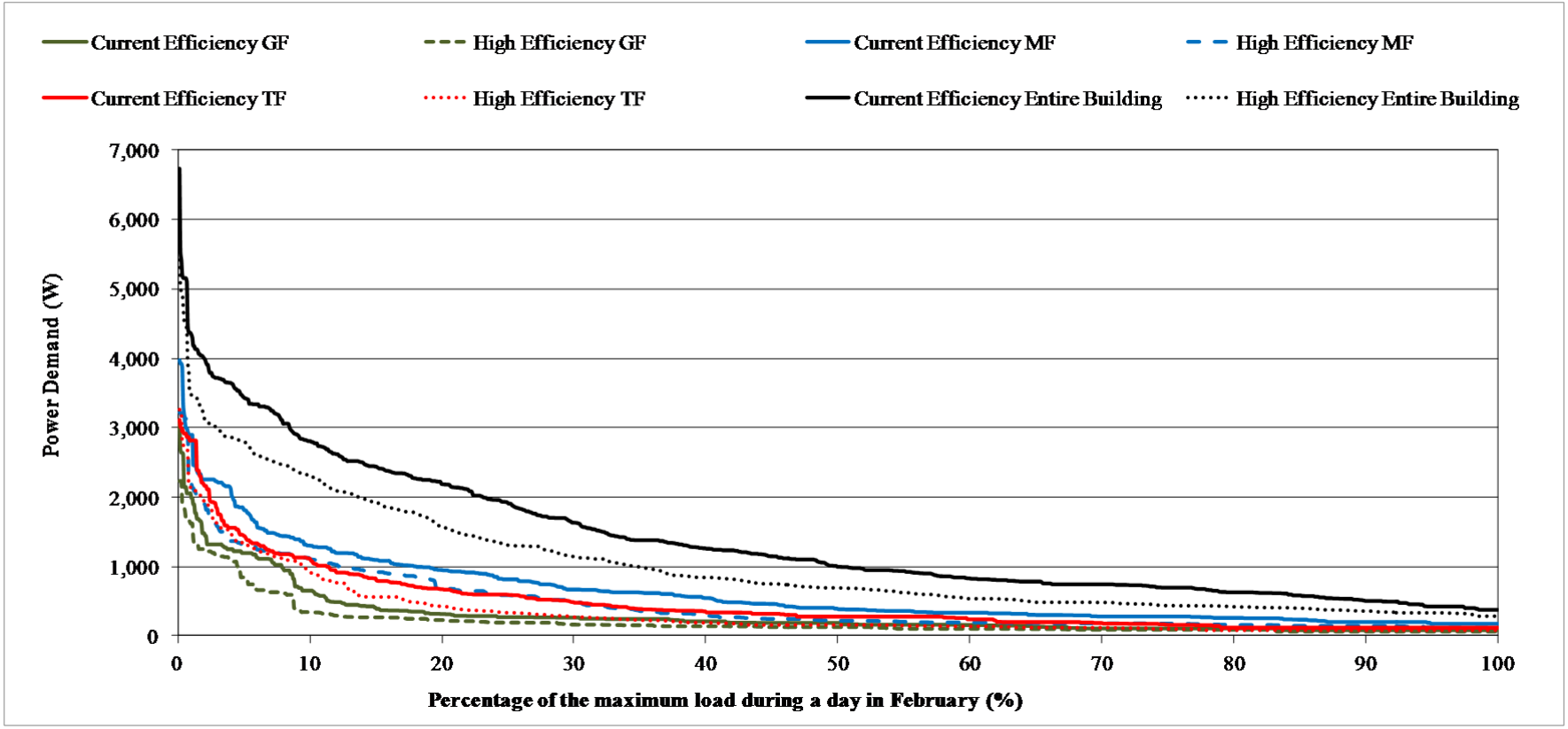

Fig. 5.2 - Load duration curves for the different floors in the 6 household building for a day in February

Finally, and this will be the discussed in more detail in later sections (Section 5.3.4 and Section 5.3.6), improving the electrical efficiency of appliances in a micro-trigeneration fed building, has an effect on the performance of the micro-trigeneration system simulated in each individual scenario.

In fact, excluding the effect of improving electrical efficiency on the internal heat gains emitted by the electrical appliances inside the buildings (which as discussed in Chapter 2 was negligible in this particular case), the resulting change in electrical demand changes the amount of electricity exported ($E_{Net\ Export}$), the amount of electricity imported ($E_{Net\ Export}$) and the net demand satisfied by the system ($E_{Net\ Demand\ \mu TRIGEN}$). Variations in these three quantities result in changes in the building's overall primary energy consumption and hence in the primary energy and annual CO_2 savings of each individual modelled scenario.

5.3 Micro-trigeneration system energetic performance metrics

5.3.1 CHP unit performance

5.3.1.1 Fuel consumption and operating hours

A first step in quantifying the energetic performance of a micro-trigeneration system for the various scenarios investigated is to analyse the operating hours and the fuel consumption of the CHP unit emerging from the simulations. Table 5.5 shows the seasonal and annual fuel consumption and operating hours of the CHP unit for the different scenarios modelled.

In the context of assessing the specific individual performance of the CHP unit, if (as discussed) the effect of reducing the electrical demand on the internal heat gains is negligible and the CHP is controlled via a thermal demand matching control philosophy (as it is in this case), the CHP unit specific thermal performance will be unaffected by the change in electrical demand. The subscript term differentiating each scenario into the current and high electrical efficiency scenarios is therefore not included as the results for both the current and high electrical efficiency scenarios are the same; the thermal performance of the system is independent of the electrical demand.

Table 5.5 - CHP unit fuel consumption and operating hours

Scenario **Building fabric**	**Scenario description**	**Total fuel consumption CHP unit Shoulder/Heating/Cooling/Annual (kg LPG)**	**Total CHP unit operating hours Shoulder/Heating/Cooling/Annual (Hours)**
1_{Low}	3 Household building with low efficiency building fabric; Basic plant configuration (0.3m^3 hot water tank)	599.9 / 816.3 / 1,591.7 / 3,007.9	390 / 536 / 1,041 / 1,967
1_{High}	3 Household building with high efficiency building fabric; Basic plant configuration (0.3m^3 hot water tank)	599.9 / 712.3 / 1,540.5 / 2,852.7	390 / 466 / 1,005 / 1,861
	Percentage difference between 1_{Low} and 1_{High} (%)	0.0 / -12.7 / -3.2 / -5.2	0.0 / -13.1 / -3.1 / -5.4
2_{Low}	6 Household building with low efficiency building fabric; Basic plant configuration (0.5m^3 hot water tank)	821.6 / 1,123.4 / 2,098.9 / 4,043.9	534 / 744 / 1,366 / 2,617
2_{High}	6 Household building with high efficiency building fabric; Basic plant configuration (0.5m^3 hot water tank)	821.6 / 915.7 / 2,020.8 / 3,758.1	534 / 601 / 1,319 / 2,444
	Percentage difference between 2_{Low} and 2_{High} (%)	0.0 / -18.5 / -3.7 / -7.1	0.0 / -19.2 / -3.4 / -6.5
3_{High}	6 Household building with high efficiency building fabric; Basic plant configuration (0.5m^3 hot water tank) with additional 0.3m^3 chilled water tank	821.6 / 915.7 / 2,308.6 / 4,045.3	534 / 601 / 1,508 / 2,632
	Percentage difference between 2_{High} and 3_{High} (%)	0.0 / 0.0 / 14.2 / 7.6	0.0 / 0.0 / 14.3 / 7.7
4_{High}	6 Household building with high efficiency building fabric; Basic plant configuration (0.5m^3 hot water tank) with additional 2.5m^2 flat plate SWH	764.8 / 910.9 / 1,991.5 / 3,667.3	497 / 597 / 1,297 / 2,382
	Percentage difference between 2_{High} and 4_{High} (%)	-6.9 / -0.5 / -1.4 / -2.4	-6.9 / -0.7 / -1.7 / -2.5
5_{High}	6 Household building with high efficiency building fabric; Basic plant configuration (0.5m^3 hot water tank). All electricity is exported	821.6 / 915.7 / 2,020.8 / 3,758.1	534 / 601 / 1,319 / 2,444
	Percentage difference between 2_{High} and 5_{High} (%)	0.0 / 0.0 / 0.0 / 0.0	0.0 / 0.0 / 0.0 / 0.0

In the table, the low and high efficiency fabric scenarios for the 3 household building (Scenario 1_{Low} and Scenario 1_{High}) and the 6 household building (Scenario 2_{Low} and Scenario 2_{High}) are compared between one another, whilst the remaining scenarios which include the scenarios with a modified plant configuration are compared with Scenario 2_{High}, which in this case is being used as the reference scenario.

As can be expected there is a direct correlation between the fuel consumption and the operating hours of the CHP unit. Both can be used to quantify how energy intensive a scenario is. The higher the values obtained for either criterion, the more energy intensive a specific case is.

Despite the fact that the shoulder months have the highest number of days (151 days compared to the 92 and 122 days of the heating and cooling seasons respectively), on a seasonal basis the absence of a space heating or cooling demand, resulted in the CHP unit operating for a very short time period: out of the possible 3,720 hours for the shoulder season, the average number of operating hours for all scenarios investigated was about 494 hours, resulting in an operating load factor of 13%. The average daily fuel consumption was of 5 kg of LPG. In comparison the CHP unit operated for 27% and 43% of the total time during the heating and cooling season respectively. The corresponding daily average fuel consumption for all scenarios for the heating and cooling season was *approx.* 10 and 16 kg of LPG respectively. The cooling season was as expected the most energy intensive season. This is an important consideration as it provides further evidence of how in warm climates reasonable operating load factors, which can make the system technically viable, can only be achieved if the micro-cogeneration system is complemented with the addition of thermally activated cooling device to provide cooling during summer.

Comparing the results obtained for the cases in Scenario 1 with those obtained for the case in Scenario 2, it can be observed that when the trigeneration system was connected to the larger 6 household building the resulting increase in thermal demand (heating, cooling and domestic hot water) resulted in an increase in operating hours and fuel consumption of the CHP unit of around 34%. This is also an

important aspect as it shows that in order to obtain high operating load factors, systems must be properly matched with the type of building. Oversizing a system will result in a low operating load factor and hence it is important that due consideration is given to this aspect.

With regards to the effect of improving the building fabric, it can be observed (by comparing the results obtained for the low and high efficiency building fabric cases for Scenario 1 and Scenario 2) that in general a refurbishment performed to bring the building fabric of a building up to specification with the *Technical Guidance - Conservation of Fuel, Energy and Natural Resources* [1] will result in an approximate reduction in fuel consumption and operating hours of around 6%. Improving the building fabric has therefore an adverse effect on the system as it reduces the operating load factor.

On a seasonal basis it can be seen that the largest reduction in both scenarios occurs for the heating season, mainly because the reduction in space heating energy in both scenarios is higher than the reduction in cooling demand.

In terms of different plant configurations, therefore considering only scenarios (Scenarios 2_{High}, 3_{High} and 4_{High}) where the thermal demand is the same (all exposed to the same type of conditions – 6 household building with high efficiency building fabric), the scenario with the highest number of operating hours and consequently the highest fuel consumption was Scenario 3_{High}, which includes an additional chilled water storage tank to the basic micro-trigeneration system plant configuration. Although as will be discussed in the next section, Section 5.3.1.2, the addition of a chilled water storage tank stabilizes the supply side (reducing the cycling 'On'/'Off' of both the CHP unit and chiller), the additional tank creates an extra thermal load in the form of storage heat gains. Compared to Scenario 2_{High} (the reference scenario), the addition of a chilled water storage tank accounts for a seasonal 14.3% and annual 7.7% increase in operating hours. The corresponding fuel consumption increase on a seasonal and annual basis was of 14.2% and 7.6% respectively.

The scenario with the lowest number of operating hours was Scenario 4_{High}, which includes an additional flat plate solar water heater to the basic plant configuration. The solar energy absorbed by the SWH offsets part of the heating energy supply which otherwise needs to be provided by the CHP. This results in a reduction in both the number of operating hours and fuel consumption. Although the effect was marginal (to reduce the increase in temperature across the SWH and prevent any damage being caused to the CHP unit the SWH selected was a small sized collector more suitable for a single family rather than a multi-family building), the results show the potential effect of adding other sources of distributed energy in the system.

5.3.1.2 Cycling 'On'/'Off'

When assessing the effect of different operating conditions on micro-trigeneration system performance, an important operational aspect which is often overlooked, is the CHP unit 'On'/'Off' cycling. Prime-movers especially those involving moving mechanical parts such as the internal combustion engine used in this case, have determined start-up and cooling down times. A constant high number of switching cycles is not ideal as the wear of the various components is accelerated. Table 5.6, tabulates the calculated seasonal and annual daily average number of 'On'/'Off' cycles together with the total seasonal and annual number of cycles for the different scenarios investigated. Operational behaviour is unaffected by the appliances' electrical efficiency.

- *Effect of improving building fabric*

The first part of the analysis focuses on the effect improving the building fabric has on the CHP unit 'On'/'Off' cycling. For both Scenarios 1 and 2, improving the building fabric results in an increase in the number of cycles during the heating season, and a decrease in a number of cycles during the cooling season.

To explain this result, recall that the CHP unit was controlled by an 'On'/'Off' controller with a 10°C dead band which switched the CHP unit 'On' below a lower limit of 65°C, and switched the unit 'Off' whenever the temperature surpassed the upper limit of 75°C.

Table 5.6 - CHP Unit switching cycles

Scenario **Building fabric**	**Scenario description**	**Daily average CHP unit cycling Shoulder/Heating/Cooling/Annual (No. of 'On'/'Off' cycles per day)**	**Total CHP unit 'On'/'Off' cycling Shoulder/Heating/Cooling/Annual (Total No. of cycles)**
1_{Low}	3 Household building with low efficiency building fabric; Basic plant configuration (0.3m^3 hot water tank)	7 / 11 / 20 / 12	1,057 / 1,037 / 2,461 / 4,554
1_{High}	3 Household building with high efficiency building fabric; Basic plant configuration (0.3m^3 hot water tank)	7 / 12 / 19 / 12	1,057 / 1,059 / 2,358 / 4,474
	Percentage difference between 1_{Low} and 1_{High} (%)		0.0 / 2.1 / -4.2 / -1.8
2_{Low}	6 Household building with low efficiency building fabric; Basic plant configuration (0.5m^3 hot water tank)	8 / 8 / 19 / 12	1,208 / 792 / 2,268 / 4,268
2_{High}	6 Household building with high efficiency building fabric; Basic plant configuration (0.5m^3 hot water tank)	8 / 10 / 18 / 12	1,208 / 893 / 2,204 / 4,304
	Percentage difference between 2_{Low} and 2_{High} (%)		0.0 / 12.7 / -2.8 / 0.9
3_{High}	6 Household building with high efficiency building fabric; Basic plant configuration and (0.5m^3 hot water tank) with additional 0.3m^3 chilled water tank	8 / 10 / 14 / 10	1,208 / 893 / 1,732 / 3,833
	Percentage difference between 2_{High} and 3_{High} (%)		0.0 / 0.0 / -21.4 / -10.9
4_{High}	6 Household building with high efficiency building fabric; Basic plant configuration (0.5m^3 hot water tank) with additional 2.5m^2 flat plate SWH	7 / 9 / 18 / 11	1,064 / 825 / 2,130 / 4,019
	Percentage difference between 2_{High} and 4_{High} (%)		-11.9 / -7.6 / -3.4 / -6.6
5_{High}	6 Household building with high efficiency building fabric; Basic plant configuration (0.5m^3 hot water tank). All electricity is exported	8 / 10 / 18 / 12	1,208 / 893 / 2,204 / 4,304
	Percentage difference between 2_{High} and 5_{High} (%)		0.0 / 0.0 / 0.0 / 0.0

Comparing Figure 5.3 and 5.4, respectively showing a typical CHP unit switching daily profile for the 6 household building with low efficiency fabric (Scenario 2_{Low}) and the 6 household building with high efficiency fabric (Scenario 2_{High}) for a day in February, it can be observed that for the same control scheme, a lower heating demand resulting from an improved building fabric requires the CHP unit to work for less hours, but with a slightly more intermittent behaviour.

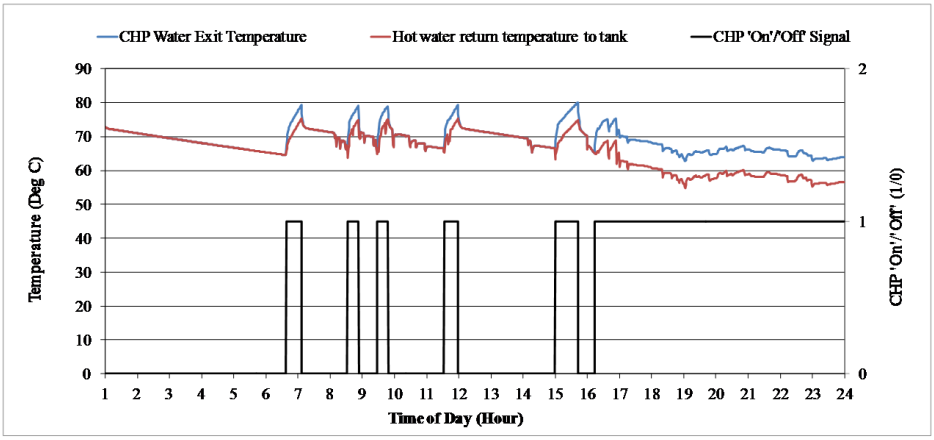

Fig. 5.3 - 'On'/'Off' Cycling during the heating season for the 6 household building with low efficiency fabric

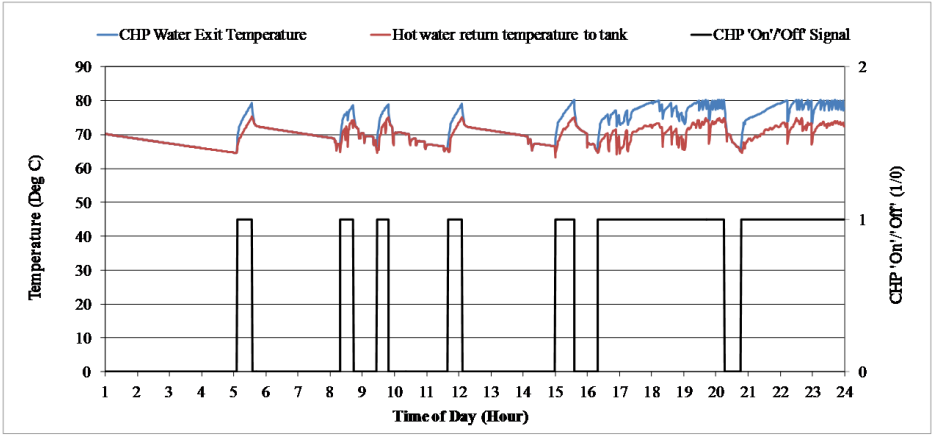

Fig. 5.4 - 'On'/'Off' Cycling during the heating season for the 6 household building with high efficiency fabric

After 16.00 Hours when the heating demand was at its maximum, the heat supplied by the CHP unit in the low efficiency fabric building closely matched the demand, with the hot water return temperature to the tank being continuously lower than the

set switching 'On' signal (65ºC) for the CHP. This resulted in the CHP operating continuously till 24.00 Hours. In the high efficiency fabric building intermittency very slightly increased. The difference in this case was of one single 'On'/'Off' cycle over a period of 24 hours; this trend was observed over the entirety of the simulations done for the heating season, resulting in a general reduction in the number of cycles, which is most evident in the percentage difference between Scenario 2_{High} and Scenario 2_{Low}.

During the cooling season the CHP unit was controlled in a similar fashion. It was however observed that during the cooling season improving the building fabric resulted in a marginal decrease in the number of CHP unit switching cycles. This was not observed for the entire simulations performed and as shown in Table 5.6 the difference in number of cycles between the low and high efficiency fabric cases for both the 3 and the 6 household building was marginal. One reason could be the fact that the lower number of operating hours experienced by the trigeneration feeding the high efficiency fabric buildings combined with a warmer outside temperature resulted in a situation where the hot water storage tank experienced less storage heat losses. Reducing the cooling demand effectively resulted in the CHP unit operating for fewer hours *but* with a more stable load behaviour.

The resulting overall effect of improving the building fabric on an annual basis was that the number of 'On'/'Off' cycles in the 3 household building (Scenario 1) marginally decreased whilst the number of cycles in the 6 household building (Scenario 2) marginally increased, therefore although the heating/cooling load changes significantly for the trigeneration system, the greater stability in temperatures in the improved fabric cases results in cycling remaining almost the same.

- *Effect of using different plant configurations*

Changing the plant configuration had a far more profound effect on cycling than lowering the thermal demand through improved fabric insulation. Compared to Scenario 2_{High} the addition of a chilled water storage tank in Scenario 3 reduced the

number of cycles during the cooling season from 2,204 to 1,732 cycles: a seasonal reduction of 21.4%. The addition of a solar water heater in Scenario 4, on the other hand, resulted in a reduction in the number of switching cycles for all three seasons. The SWH offsets part of the heating energy required to keep the temperature in the hot water storage tank between 65ºC and 75ºC, which therefore results in a lower number of switching cycles. A lower number of switching cycles of course has the (beneficial) effect of reducing the system's maintenance requirement.

5.3.2 Auxiliary boiler

In all three proposed plant configurations, the micro-trigeneration system included an auxiliary boiler to cater for periods of peak demands. Table 5.7 shows the resulting seasonal and annual auxiliary boiler fuel consumption for the different scenarios.

A first important conclusion that can be drawn, is that compared to the fuel consumption of the CHP unit, the fuel consumption of the auxiliary boiler was practically negligible for all scenarios. In fact in none of the scenarios investigated did the annual auxiliary boiler fuel consumption exceed 0.3% of the CHP unit annual fuel consumption, suggesting that the use of the auxiliary boiler was very sporadic, exclusively to cover for infrequent peak demands. During the simulation process, covering for such peak demands was essential in the process leading to the (integrity of the) mathematical iterative process used by the simulation tool to calculate the solution concentration of the weak and strong branch in the absorption chiller (Refer to Section 3.3.4.3) – value would diverge rather than converge. In real life covering for such short instances of peak demands may be superfluous rendering the auxiliary boiler unnecessary.

The only 'sizeable' change in auxiliary boiler fuel consumption was caused by the addition of the chilled water storage tank. The addition of a chilled water storage tank in Scenario 3_{High} results in an additional cooling demand which needs to be satisfied, resulting in the auxiliary boiler operating for a longer period of time to cover for a higher number of peak demands.

Table 5.7 - Auxiliary boiler fuel consumption

Scenario **Building fabric**	**Scenario description**	**Total auxiliary boiler fuel consumption** **Shoulder/Heating/Cooling/Annual** **(kg LPG)**
1_{Low}	3 Household building with low efficiency building fabric; Basic plant configuration and (0.3m^3 hot water tank)	2.1 / 2.6 / 2.4 / 7.0
1_{High}	3 Household building with high efficiency building fabric; Basic plant configuration (0.3m^3 hot water tank)	2.1 / 2.4 / 2.5 / 7.0
2_{Low}	6 Household building with low efficiency building fabric; Basic plant configuration and (0.5m^3 hot water tank)	3.5 / 3.0 / 3.4 / 10.0
2_{High}	6 Household building with high efficiency building fabric; Basic plant configuration (0.5m^3 hot water tank)	3.5 / 2.7 / 3.4 / 9.6
3_{High}	6 Household building with high efficiency building fabric; Basic plant configuration (0.5m^3 hot water tank) with additional 0.3m^3 chilled water tank	3.5 / 2.7 / 3.9 / 10.2
4_{High}	6 Household building with high efficiency building fabric; Basic plant configuration (0.5m^3 hot water tank) with additional 2.5m^2 flat plate SWH	3.6 / 2.7 / 3.4 / 9.7
5_{High}	6 Household building with high efficiency building fabric; Basic plant configuration (0.5m^3 hot water tank). All electricity is exported	3.5 / 2.7 / 3.4 / 9.6

5.3.3 Chiller's performance

As discussed, an important component in a micro-trigeneration system is the absorption chiller. Table 5.8 shows the chiller's total operational time for each scenario modelled.

Table 5.8 - Annual chiller operational time

Scenario **Building fabric**	**Annual chiller operational time** **Hours (Chiller seasonal operational load factor)**
1_{Low}	1,281 (43.8%)
1_{High}	1,034 (35.3%)
2_{Low}	1,772 (60.5%)
2_{High}	1,599 (54.6%)
3_{High}	1,706 (58.3%)
4_{High}	1,609 (54.9%)
5_{High}	1,599 (54.6%)

A lower space cooling demand due to improved building fabric as expected results in the chiller operating for a smaller number of hours. Reflecting the higher reduction in space cooling demand between the low and high building fabric efficiency cases for the 3 household building – Scenario 1 (20.4%), compared to the 6 household building – Scenario 2 (11.7%), the reduction in operating hours in Scenario 1 was of 19.3%, whilst that in Scenario 2 was of 9.1%.

In terms of building size and occupancy, connecting the micro-trigeneration system to the larger 6 household building results in an approximate increase in chiller operational time of around 38.3% in the low efficiency case (Scenario 2_{Low} compared to Scenario 1_{Low}) and 54.6% in the high efficiency case (Scenario 2_{High} compared to Scenario 1_{High}). The difference in operational time is again directly related to how effective improving the building fabric is in the two buildings. The larger glazed surface area and the higher internal gains due to the larger occupancy in the 6 household building offset part of the savings obtained through building fabric improvements resulting in a lower reduction in cooling demand compared to the 3 household building – hence the increase in the chiller's operational time.

Except for Scenario 3_{High}, the modelled changes in plant configuration did not affect the chiller, mainly because the chiller operating hours are exclusively a function of the cooling demand. The increase in number of operating hours in Scenario 3_{High}, the scenario with the additional chilled water storage was a direct result of the chiller's need to cover for additional thermal load caused by the storage thermal gains. The addition of the chilled water storage tank in Scenario 3_{High} does nonetheless improve on the stability of the chiller output cooling power as shown in Figure 5.5.

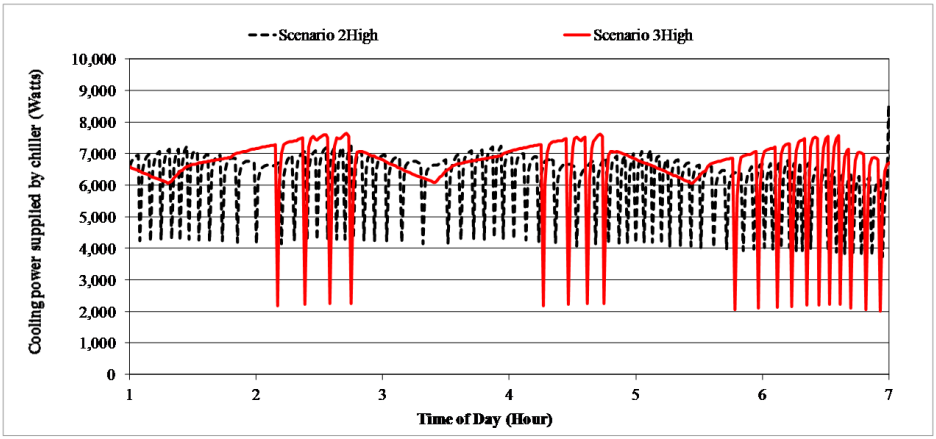

Fig. 5.5 - Chiller's cooling power output profile

Figure 5.5 shows how the addition of a chilled water tank stabilises the chiller's cooling power output profile over a 7 hour modelled period for a day in July. For comparative purposes the chiller output cooling power for the same period but for Scenario 2_{High} is shown in the background.

Combining these results with those obtained for the number of switching cycles (Section 5.3.1.2) it can be argued that, although the addition of a chilled water tank increases the system's fuel consumption (to cover for parasitic heat gains in the tank), the addition of a chilled water tank improves the operational behaviour of both the CHP unit and the absorption chiller by reducing the variability in operation. This is an important aspect which should be considered when selecting the appropriate plant system for a particular building.

5.3.4 Electrical performance of the micro-trigeneration system

Table 5.9 shows the annual electrical performance of the micro-trigeneration system (the gross electricity cogenerated by system, the net electrical imports, the net electrical exports and the net demand satisfied by the micro-trigeneration system) calculated for the different scenarios.

Table 5.9 - Annual micro-trigeneration system electrical performance

Scenario Building fabric/Electrical efficiency	**Gross electricity cogenerated by micro-trigeneration system (kWh)**	**Net imports** $E_{Net\ Import}$ **(kWh)**	**Net exports** $E_{Net\ Export}$ **(kWh)**	**Net demand satisfied by micro-trigeneration system** $E_{Net\ Demand\ \mu TRIGEN}$ **(kWh)**
$1_{Low/Current\ efficiency}$	10,702.5	3,977.1	9,301.5	1,401.0
$1_{Low/High\ efficiency}$	10,702.5	2,857.8	9,637.5	1,065.0
$1_{High/Current\ efficiency}$	10,175.4	4,076.0	8,873.3	1,302.1
$1_{High/High\ efficiency}$	10,175.5	2,932.4	9,185.1	990.4
$2_{Low/Current\ efficiency}$	14,461.2	7,349.9	10,781.1	3,680.2
$2_{Low/High\ efficiency}$	14,461.2	5,453.5	11,771.5	2,689.8
$2_{High/Current\ efficiency}$	13,401.0	7,716.6	10,079.5	3,321.5
$2_{High/High\ efficiency}$	13,401.0	5,676.5	10,930.0	2,471.0
$3_{High/Current\ efficiency}$	14,415.9	7,478.3	10,857.5	3,588.4
$3_{High/High\ efficiency}$	14,415.9	5,505.4	11,775.6	2,640.3
$4_{High/Current\ efficiency}$	13,036.3	7,730.9	9,735.6	3,300.7
$4_{High/High\ efficiency}$	13,036.3	5,707.7	10,620.1	2,416.1
$5_{High/Current\ efficiency}$	13,401.1	10,159.0	13,401.0	0.0
$5_{High/High\ efficiency}$	13,401.1	7,471.6	13,401.1	0.0

5.3.4.1 Effect of improving the building fabric on the electrical performance

As done in previous sections, the specific cases in Scenarios 1 and 2 were used to analyse the effect of improving the building fabric. The first important conclusion which can be drawn from the results obtained is that, the gross electricity cogenerated by the micro-trigeneration system depends exclusively on the number of operating hours of the system. Any reductions in thermal demand due to building fabric improvements will therefore lead to a reduction in the amount of cogenerated electricity. Also, since the change in internal heat gains due to a change in electrical demand is negligible, for the same building fabric, improving the electrical efficiency

of the household appliances does not change the electricity cogenerated by the micro-trigeneration system. Considering Scenario 1, improving the building fabric resulted in a reduction in gross electricity cogenerated by the micro-trigeneration system of approximately 5.0%. Likewise for Scenario 2 the reduction was of 7.3%.

This reduction in cogenerated electricity also results in a situation where, for the same electrical efficiency, improving the building fabric leads to higher electrical net imports, lower net exports and lower net demand satisfied by the micro-trigeneration system. Comparing the low and high fabric cases of the 3 household building for the current appliances' electrical efficiency (Scenarios $1_{\text{Low/Current efficiency}}$ and $1_{\text{High/Current efficiency}}$), the increase in net imports was of 2.5% whilst the decrease in net exports and net demand satisfied by the micro-trigeneration system were of 4.6% and 7.1% respectively. Likewise, comparing the low and high fabric cases of the 3 household building for future appliances' electrical efficiency (Scenarios $1_{\text{Low/High efficiency}}$ and $1_{\text{High/High efficiency}}$), the increase in net imports was of 2.6% whilst the decrease in net exports and net demand satisfied by the micro-trigeneration system were of 4.7% and 7.0% respectively. The individual cases in Scenario 2 show similar results.

5.3.4.2 Effect of improving the electrical efficiency on the electrical performance

As mentioned, improving the electrical efficiency of the household appliances does not alter the gross electricity cogenerated by the micro-trigeneration system, as this is related exclusively to the operating hours of the system.

Improving the electrical efficiency however results in a lower electrical demand, higher net exports, lower net imports and lower net demand satisfied by the micro-trigeneration system. Comparing the low and high electrical efficiency cases for the 3 household building with low efficiency fabric (Scenarios $1_{\text{Low/Current efficiency}}$ and $1_{\text{Low/High efficiency}}$), the increase in net exports was of 3.6% whilst the decrease in net imports and net demand satisfied by the micro-trigeneration system were of 28.1% and 24.0% respectively. Likewise, comparing the low and high electrical efficiency cases for the 3 household building with high efficiency fabric (Scenarios $1_{\text{High/Current efficiency}}$ and $1_{\text{High/High efficiency}}$), the increase in net exports was of 3.5% whilst the

decrease in net imports and net demand satisfied by the micro-trigeneration system were of 28.1% and 24.0% respectively. The same trend was observed when comparing the current and high electrical efficiency scenarios of all other scenarios.

5.3.4.3 Effect of different plant configurations on the electrical performance

What was discussed in section 5.3.4.1 regarding the effect of the building fabric on the system's electrical performance can be extended to analyse the effect of the different plant configurations; the higher the number of operating hours of the micro-trigeneration system the higher the amount of gross electricity cogenerated.

Compared to the current and high electrical efficiency cases of the 6 household building with high efficiency fabric (Scenarios $2_{\text{High/Current efficiency}}$ and $2_{\text{High/High efficiency}}$) – the reference scenarios for the different plant system configurations, the additional operating hours of the micro-trigeneration system with the additional chilled water tank used in Scenario 3_{High} resulted in the system producing a higher amount of cogenerated electricity. In both electrical efficiency cases (Scenario $3_{\text{High/Current efficiency}}$ and Scenario $3_{\text{High/High efficiency}}$), the electricity cogenerated by the system increased by 7.6%. The additional electricity cogenerated resulted in lower net imports[1], higher net exports[2] and higher net demand satisfied by the micro-trigeneration system[3].

Conversely, compared to Scenarios $2_{\text{High/Current efficiency}}$ and $2_{\text{High/High efficiency}}$, the reduction in operating hours of the micro-trigeneration system with the additional SWH used in Scenario 4_{High} resulted in the system producing a lower amount of cogenerated electricity. Compared to the equivalent scenarios in Scenario 2_{High}, the amount of electricity cogenerated in Scenario $4_{\text{High/Current efficiency}}$ and Scenario $4_{\text{High/ High efficiency}}$ decreased by 2.7%. The reduction in electricity cogenerated in this case

[1] 3.1% in Scenario $3_{\text{High/Current efficiency}}$ compared to Scenario $2_{\text{High/Current efficiency}}$ and 3.0% in Scenario $3_{\text{High/High efficiency}}$ compared to Scenario $2_{\text{High/High efficiency}}$.

[2] 7.7% in both Scenario $3_{\text{High/Current efficiency}}$ and Scenario $3_{\text{High/High efficiency}}$ compared to Scenario $2_{\text{High/Current efficiency}}$ and Scenario $2_{\text{High/High efficiency}}$.

[3] 8.0% in Scenario $3_{\text{High/Current efficiency}}$ compared to Scenario $2_{\text{High/Current efficiency}}$ and 6.9% in Scenario $3_{\text{High/High efficiency}}$ compared to Scenario $2_{\text{High/High efficiency}}$.

resulted in higher net imports[4], lower net exports[5] and lower net demand satisfied by the micro-trigeneration system[6].

5.3.5 Micro-trigeneration system primary energy consumption and efficiency

Table 5.10 shows the seasonal and annual micro-trigeneration system primary energy consumption and the correlated system efficiency. Given that the calculation of the micro-trigeneration system's primary energy consumption relies on multiplying the total fuel consumption by the net calorific value of the fuel (LPG), it is clear that the same trends and conclusions drawn for the operational hours and the fuel consumption can be extended to this case as well. Consequently:

- The highest primary energy consumption was during the cooling season when the operating load factor of the CHP unit was highest;

- Improving the building fabric reduces the primary energy consumption of the micro-trigeneration system;

- Adding a chilled water storage tank creates an extra thermal load which needs to be satisfied by the micro-trigeneration system operating for a longer number of hours, hence increasing the amount of primary energy consumed; and

- The addition of systems making use of renewable energy sources working in tandem with the micro-trigeneration system reduces the amount of primary energy consumed by the system.

[4] 0.2% in Scenario $4_{\text{High/Current efficiency}}$ compared to Scenario $2_{\text{High/Current efficiency}}$ and 0.6% in Scenario $4_{\text{High/High efficiency}}$ compared to Scenario $2_{\text{High/High efficiency}}$.

[5] 3.4% in Scenario $4_{\text{High/Current efficiency}}$ compared to Scenario $2_{\text{High/Current efficiency}}$ and 2.8% in Scenario $4_{\text{High/High efficiency}}$ compared to Scenario $2_{\text{High/High efficiency}}$.

[6] 0.63% in Scenario $4_{\text{High/Current efficiency}}$ compared to Scenario $2_{\text{High/Current efficiency}}$ and 2.2% in Scenario $4_{\text{High/High efficiency}}$ compared to Scenario $2_{\text{High/High efficiency}}$.

Table 5.10 - Micro-trigeneration system primary energy consumption and system efficiency

Scenario **Building fabric**	**Scenario description**	**Micro-trigeneration system primary energy consumption** **Shoulder/Heating/Cooling/Annual** $PE_{\mu TRIGEN}$ **(kWh)**	**Micro-trigeneration system efficiency** **Shoulder/Heating/Cooling/Annual** $\eta_{\mu TRIGEN}$ **(%)**
1_{Low}	3 Household building with low efficiency building fabric; Basic plant configuration (0.3m^3 hot water tank)	7,974 / 10,847 / 21,114 / 39,936	47.2 / 67.2 / 76.0 / 67.9
1_{High}	3 Household building with high efficiency building fabric; Basic plant configuration (0.3m^3 hot water tank)	7,974 / 9,467 / 20,437 / 37,878	47.2 / 65.3 / 68.6 / 63.3
2_{Low}	6 Household building with low efficiency building fabric; Basic plant configuration (0.5m^3 hot water tank)	10,929 / 14,920 / 27,847 / 53,696	55.7 / 74.0 / 78.7 / 72.7
2_{High}	6 Household building with high efficiency building fabric; Basic plant configuration (0.5m^3 hot water tank)	10,929 / 12,165 / 26,812 / 49,906	55.7 / 70.4 / 75.3 / 69.8
3_{High}	6 Household building with high efficiency building fabric; Basic plant configuration (0.5m^3 hot water tank) with additional 0.3m^3 chilled water tank	10,929 / 12,165 / 30,624 / 53,718	55.7 / 70.4 / 69.4 / 66.8
4_{High}	6 Household building with high efficiency building fabric; Basic plant configuration (0.5m^3 hot water tank) with additional 2.5m^2 flat plate SWH	10,179 / 12,102 / 26,425 / 48,705	57.9 / 70.6 / 76.1 / 70.8
5_{High}	6 Household building with high efficiency building fabric; Basic plant configuration (0.5m^3 hot water tank). All electricity is exported	10,929 / 12,165 / 26,812 / 49,906	55.7 / 70.4 / 75.3 / 69.8

Similarly to other operational characteristics, the primary energy consumption is dependent on the thermal demand of the building. In terms of primary energy consumption, the results for each scenario are therefore identical for both the current and high appliances' electrical efficiency.

An important conclusion which can be deduced from the table is that, there exists a strong correlation between the system efficiency and the operational load factor. Excluding the increase due to the parasitic load in the case of Scenario 3_{High}, (which accounts for the added chilled water storage tank) when the useful demand increases, the system efficiency increases. Annual system efficiencies for the different scenarios varied between a low of 63.3% for the 3 household building with high efficiency fabric to 72.7% for the 6 household building with low efficiency fabric, indicating that the higher the operational load factor, the higher the system efficiency.

For the same reasoning, on a seasonal basis, the proposed micro-trigeneration system displayed the highest seasonal efficiency during the cooling season when the operating load factor was highest and the lowest seasonal efficiency during the shoulder months when the operating load factor was lowest. In terms of operating conditions effecting system efficiency, it can be concluded that, for a fixed plant system size increasing the thermal demand (*e.g.* by increasing the occupancy of the building), increases the operating load factor which results in an increase in system efficiency. In contrast for a fixed plant system size, changes aimed at reducing the thermal demand, such as improving the building fabric, will result in lower system efficiencies.

In terms of the different plant configurations, the plant configuration with the highest annual system efficiency (*approx.* 71%) was the one used in Scenario 4_{High}, which includes the use of a solar water heater working in tandem with the micro-trigeneration system, whilst the lowest annual efficiency (66.8%) was the one used in Scenario 3_{High}, which includes the additional chilled water storage tank. In Scenario 4_{High} part of the primary energy consumption required was offset by the heating energy supplied by the solar water heater. This resulted in a lower micro-

trigeneration system primary energy consumption. In the latter case, given that part of the thermal load satisfied by the micro-trigeneration system was required to cover for storage heat gains which were not accounted for as a useful energy product, Scenario 3_{High} (although being the plant configuration with the highest number of operating hours) was the scenario with the lowest efficiency.

Two clarifications on the system efficiency which need to be mentioned are that:

- The system efficiency values reported in Table 5.10 for the different scenarios are the overall system efficiency and not the individual fuel efficiency values of the CHP unit (approximately 27% electrical efficiency, 65% thermal efficiency and 92% total fuel efficiency - reported in the CHP unit specs sheet [3]). As explained in Chapter 4 the system efficiency involves the calculation of all the energy products produced by the micro-trigeneration system divided by the total energy input and therefore includes the various inefficiencies of the different components (*e.g.* the CHP unit, the absorption chiller, storage heat losses *etc.*). In this context the calculated values for the system efficiency reported for the different scenarios show considerable agreement with the system efficiency values reported by Lin *et al.* in [4] and Khatri *et al.* in [5], who conducted experimental laboratory investigations on residential micro-trigeneration using a relatively similar plant setup; and

- Although the equation for system efficiency, (equation [4.10]) explicitly distinguishes between the net electrical demand satisfied by the micro-trigeneration system and the net exported electricity, the results for the different scenarios shown in Table 5.10 are not differentiated on the basis of their electrical efficiency. Since the gross electricity cogenerated by the system (which is equal to the aggregated contribution of the net export and the net demand satisfied by the system) is independent of the electrical demand (the effect on internal heat gains due to a change in electrical demand is negligible) and dependent only on the thermal demand, it follows that the

system efficiency is identical for both electrical efficiencies.

5.3.6 Energetic comparison with separate generation

5.3.6.1 Comparison assuming current grid network electrical efficiency

In Chapter 4, it was explained how the system efficiency is not an ideal way to evaluate the energetic performance of a micro-trigeneration system, and that measuring the performance of a micro-trigeneration system based on the primary energy savings, *PES*, was a much better way of assessment.

Table 5.11 shows the calculated annual primary energy consumed by the micro-trigeneration system, $PE_{\mu TRIGEN}$, the equivalent primary energy required to produce the same quality and quantity of energy products in separate generation, $PE_{SEPERATE}$, and the calculated system's *PES* for each investigated scenario.

When assessing primary energy savings Peacock and Newborough [6] explain that if the net electrical imports are not included in the calculation, residential electrical energy saving measures do not impact on the system's primary energy or emission savings unless the exported electricity and the net demand satisfied by the micro-trigeneration system are differentiated. A full analysis of the primary energy consumed by the micro-trigeneration in each modelled scenario therefore requires that the net electrical imports imported from the grid to cover for the balance in the building's electrical demand are included in the calculation. For this reason, each column in Table 5.11 is divided into two sub-categories: one showing the primary energy consumed by the micro-trigeneration (and the equivalent required in separate generation) when the net imports are excluded and the other showing the primary energy consumed when the net imports are included. In the former case only the net energy quantities produced by the micro-trigeneration system are taken into account. The same division is used in the calculation of the *annual PES*.

The grid efficiency, η_{Grid}, used in the calculation of $PE_{SEPERATE}$ was that described in Chapter 4, the electrical efficiency of the Maltese grid based on the actual electricity delivered; equal to 25.5% [7].

Table 5.11 - Micro-trigeneration primary energy comparison with separate generation and *PES*

Scenario Building fabric/Electrical Efficiency	**Scenario description**	***Annual*** $PE_{\mu TRIGEN}$ **(kWh)**		***Annual*** $PE_{SEPARATE}$ **(kWh)**		***Annual PES* (%)**	
		Excluding Net Imports	***Including Net Imports***	***Excluding Net Imports***	***Including Net Imports***	***Excluding Net Imports***	***Including Net Imports***
$1_{\text{Low/Current efficiency}}$	3 Household building with low efficiency building fabric; Basic plant configuration (0.3m^3 hot water tank). Appliances' current electrical efficiency.	39,936	55,532	75,978	91,574	47.4	39.4
$1_{\text{Low/High efficiency}}$	3 Household building with low efficiency building fabric; Basic plant configuration (0.3m^3 hot water tank). Appliances' high electrical efficiency.	39,936	51,143	75,978	87,187	47.4	41.3
$1_{\text{High/Current efficiency}}$	3 Household building with high efficiency building fabric; Basic plant configuration (0.3m^3 hot water tank). Appliances' current electrical efficiency.	37,878	53,863	70,585	86,569	46.3	37.8
$1_{\text{High/High efficiency}}$	3 Household building with high efficiency building fabric; Basic plant configuration (0.3m^3 hot water tank). Appliances' high electrical efficiency.	37,878	49,378	70,585	82,086	46.3	39.8
$2_{\text{Low/Current efficiency}}$	6 Household building with low efficiency building fabric; Basic plant configuration (0.5m^3 hot water tank). Appliances' current electrical efficiency.	53,696	82,519	113,362	142,185	52.6	42.0
$2_{\text{Low/High efficiency}}$	6 Household building with low efficiency building fabric; Basic plant configuration (0.5m^3 hot water tank). Appliances' high electrical efficiency.	53,696	75,082	113,362	134,748	52.6	44.3
$2_{\text{High/Current efficiency}}$	6 Household building with high efficiency building fabric; Basic plant configuration (0.5m^3 hot water tank). Appliances' current	49,906	80,167	105,324	135,585	52.6	40.9

	electrical efficiency.						
$2_{\text{High/High efficiency}}$	6 Household building with high efficiency building fabric; Basic plant configuration ($0.5m^3$ hot water tank). Appliances' high electrical efficiency.	49,906	72,167	105,324	127,584	52.6	43.4
$3_{\text{High/Current efficiency}}$	6 Household building with high efficiency building fabric; Basic plant configuration ($0.5m^3$ hot water tank) with additional $0.3m^3$ chilled water tank. Appliances' current electrical efficiency.	53,718	83,045	109,397	138,724	50.9	40.1
$3_{\text{High/High efficiency}}$	6 Household building with high efficiency building fabric; Basic plant configuration ($0.5m^3$ hot water tank) with additional $0.3m^3$ chilled water tank. Appliances' high electrical efficiency.	53,718	75,308	109,397	130,987	50.9	42.5
$4_{\text{High/Current efficiency}}$	6 Household building with high efficiency building fabric; Basic plant configuration ($0.5m^3$ hot water tank) with additional $2.5m^2$ flat plate SWH. Appliances' current electrical efficiency.	48,705	79,022	104,156	134,474	53.2	41.2
$4_{\text{High/High efficiency}}$	6 Household building with high efficiency building fabric; Basic plant configuration ($0.5m^3$ hot water tank) with additional $2.5m^2$ flat plate SWH. Appliances' high electrical efficiency.	48,705	71,088	104,156	126,540	53.2	43.8
$5_{\text{High/Current efficiency}}$	6 Household building with high efficiency building fabric; Basic plant configuration ($0.5m^3$ hot water tank). All electricity is exported Appliances' current electrical efficiency.	49,906	89,745	105,323	145,163	52.6	38.2
$5_{\text{High/High efficiency}}$	6 Household building with high efficiency building fabric; Basic plant configuration ($0.5m^3$ hot water tank). All electricity is exported. Appliances' high electrical efficiency.	49,906	79,206	105,323	134,624	52.6	41.2

The *PES* obtained for the different scenarios are all within a small range suggesting that the overall impact of the different operating conditions on the *PES* is low. From the results, certain trends can nonetheless be deduced:

- If the net imports are not included in the calculation and the effect of the change in electrical demand on the internal heat gains is negligible (as it is in this case), the thermal performance, the cogenerated electricity and hence the *PES* is the same for both appliances' electrical efficiency;

- At the current level of grid efficiency, including the net imports in the calculation significantly reduces the *PES*. Since in the appliances' high electrical efficiency case less net imports are required the highest *PES* is obtained for scenarios modelled using this level of electrical efficiency;

- Increasing the useful thermal load (*e.g.* when connecting the plant system to a larger building *etc.*) results in longer operating hours and hence in a higher *PES*;

- Improving the building fabric has a marginal negative effect on the system's *PES*. This negative effect is however compounded if the net electrical imports are included in the calculation of the *PES*;

- The addition of systems making use of renewable energy to offset part of the fuel consumption increases the system's *PES*. The plant system including the SWH (Scenario 4) is the plant configuration with the highest *PES*;

- The addition of a chilled water storage tank has a negative impact on the system's *PES* due to additional parasitic loads. The plant system used in Scenario 3 is the plant configuration with lowest *PES*; and

- Compared to using the cogenerated electricity for own demand, at the current level of grid efficiency, exporting all the cogenerated electricity and importing all the electricity from the grid (Scenario 5) results in a reduction in *PES*.

5.3.6.2 Effect of improving the grid network efficiency

So far the analysis performed has been based on a deterministic analysis, that is, in order to assess the effect of different operating conditions on the micro-trigeneration system, scenarios were compared to one another. In order to address the effect of grid improvement and decarbonisation, this section uses a sensitivity analysis approach to quantify the sensitivity of the system's *PES* to the grid efficiency, η_{Grid}.

Considering for example Scenario 1_{Low} (3 household building with low efficiency fabric), Figure 5.6 shows how the primary energy requirement (for both micro-trigeneration and separate generation) varies with an increase in grid efficiency. Plots show the effect, both when the net electrical imports are included (Inc.) and excluded (Exc.). Figure 5.6 shows how improvements carried out to increase the electrical efficiency of the grid would result in making separate generation more efficient, requiring less primary energy and consequently making the micro-trigeneration system less energetically advantageous. In this context it is important to remember that, whereas in separate generation increasing the electrical efficiency of the grid practically affects the entirety of the energy required to cover for the building's energy demand, only a small part of the electrical demand (the net electrical imports) will be affected when the building is fed by a micro-trigeneration system. Also, unless the net electrical imports are included, the primary energy required by the micro-trigeneration system is unaffected by the grid efficiency.

In terms of the *PES* the same reduction is experienced, as shown in Figure 5.7 for Scenario 1_{Low}. At the current grid efficiency, the calculated *PES* of Scenario 1_{Low} is of *approx.* 40% (47.4% if the net electrical imports are excluded and only the net performance of the micro-trigeneration system is considered). The negative sensitivity of the micro-trigeneration system's *PES* to improvements in the grid efficiency results in the micro-trigeneration system in Scenario 1_{Low} yielding a much lower *PES*, in the region of 20%. Also, with improving grid efficiency the different calculated *PES* (i.e. including and excluding net electrical imports) converge, because the difference in primary energy required to produce the additional net electrical imports diminishes.

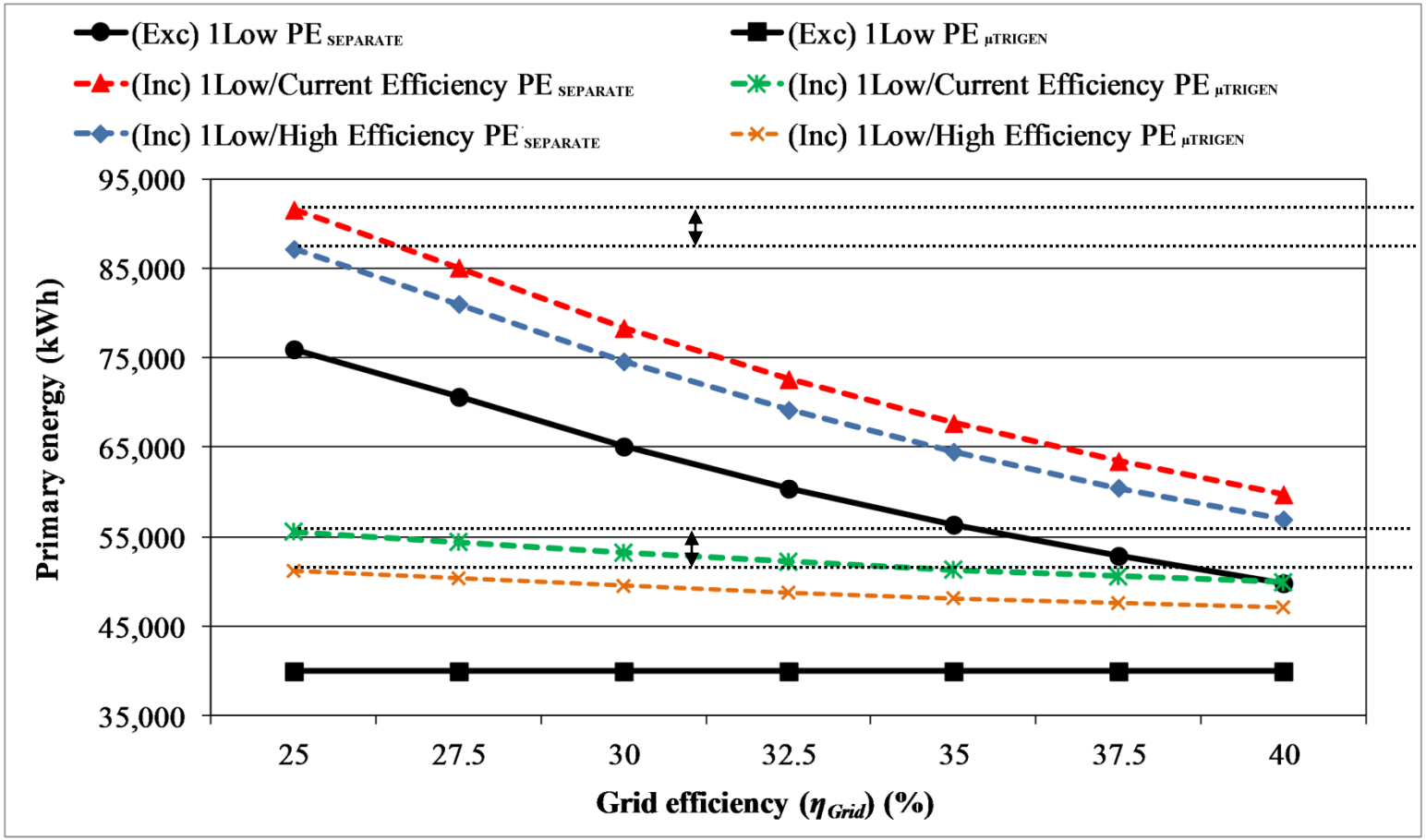

Fig. 5.6 - Sensitivity of $PE_{SEPARATE}$ and $PE_{\mu TRIGEN}$ to grid efficiency (η_{Grid}) (Scenario 1_{Low})

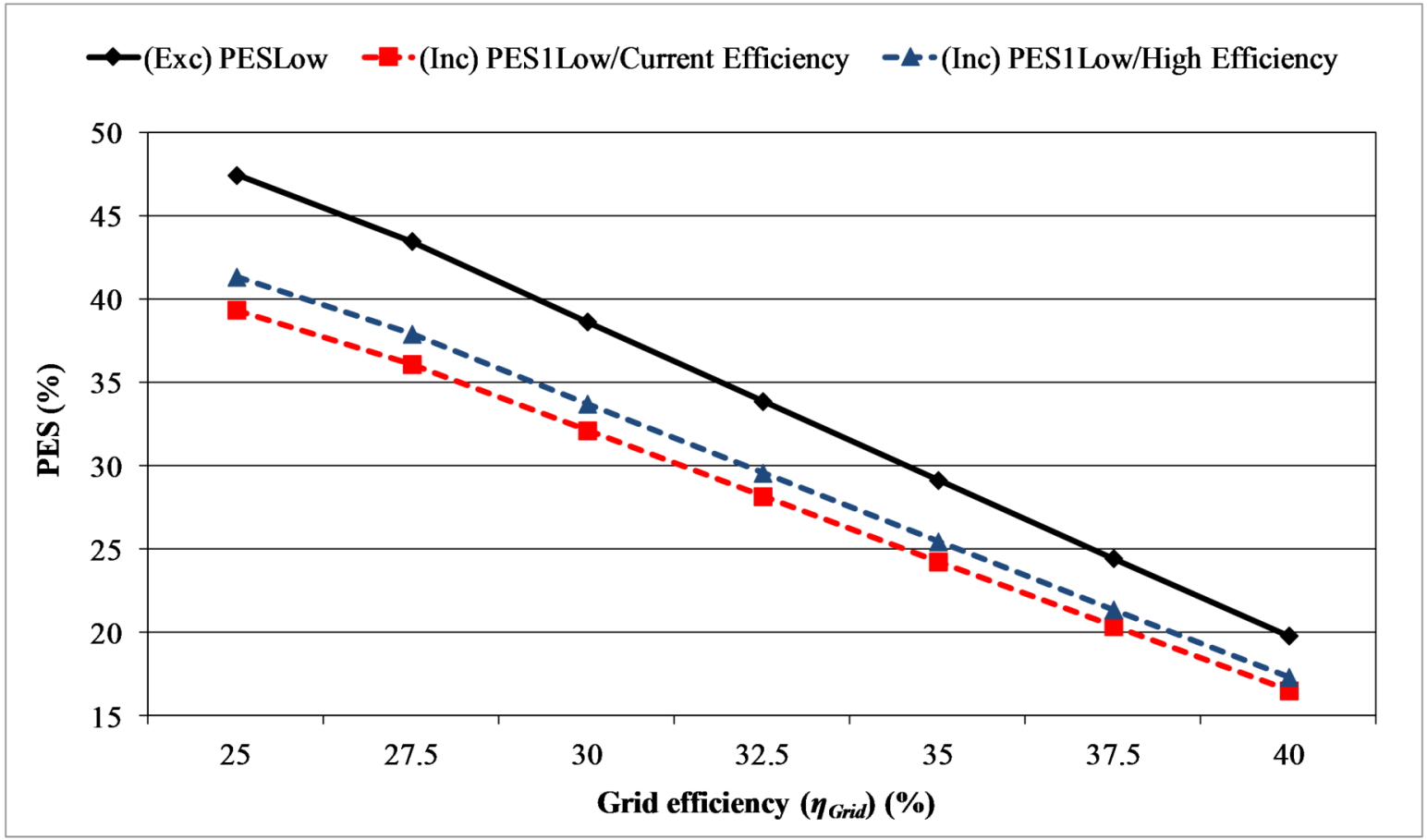

Fig. 5.7 - Sensitivity of *PES* to grid efficiency (η_{Grid}) (Scenario 1_{Low})

Similar results are obtained for all other scenarios.

This result yields an important conclusion. Micro-trigeneration systems operating in locations where the separate generation of energy products is very efficient, have limited capability of improving the overall energy-efficiency. From a Maltese perspective this is currently not the case as the grid network efficiency is currently very low. However with the improvements being implemented, which will yield a considerable increase in the grid's electrical efficiency, the technical edge a micro-trigeneration system currently has (in terms of its energy performance) on separate generation may be severely reduced or completely lost.

5.4 Micro-trigeneration system environmental performance metrics

The second part of the assessment process was to assess the micro-trigeneration system on the basis of its environmental performance metrics; the system's carbon footprint and comparison with separate generation.

5.4.1 Comparison assuming current grid network emission factor

Table 5.12 shows the annual micro-trigeneration system emissions, $Emissions_{\mu TRIGEN}$, the annual emissions emitted assuming the equivalent quantity and quality of energy products are produced by separate generation, $Emissions_{SEPARATE}$, and the annual CO_2 emissions savings of the system in comparison with separate generation. Similarly to Table 5.11, each column in Table 5.12 is divided into 2 headings, showing the emissions and savings if the net electrical imports are included or excluded. The grid emission factor, e_{Grid}, used in the calculation of $Emissions_{SEPARATE}$ was as described in Chapter 4, the emission factor of the Maltese grid based on the actual electricity delivered; equal to 1.088 kg/CO_2 per kWh [7].

In terms of absolute emissions emitted by the micro-trigeneration system under different operating conditions, the calculated values are a direct consequence of the operating hours and fuel consumption – the higher the operating hours, the higher the resulting fuel consumption and hence the emissions. Conclusions similar to the ones discussed for the primary energy consumption can therefore be deduced.

Table 5.12 - Micro-trigeneration emissions comparison with separate generation and *ES* (CO_2 Savings)

Scenario Building fabric/Electrical Efficiency	**Scenario description**	***Annual Emissions*$_{\mu TRIGEN}$ (kg CO_2)**		***Annual Emissions*$_{SEPARATE}$ (kg CO_2)**		***Annual ES* (% CO_2 Savings)**	
		Excluding Net Imports	***Including Net Imports***	***Excluding Net Imports***	***Including Net Imports***	***Excluding Net Imports***	***Including Net Imports***
$1_{Low/Current\ efficiency}$	3 Household building with low efficiency building fabric; Basic plant configuration (0.3m^3 hot water tank). Appliances' current electrical efficiency.	9,963	14,290	20,939	25,267	52.4	43.4
$1_{Low/High\ efficiency}$	3 Household building with low efficiency building fabric; Basic plant configuration (0.3m^3 hot water tank). Appliances' high electrical efficiency.	9,963	13,072	20,939	24,049	52.4	45.6
$1_{High/Current\ efficiency}$	3 Household building with high efficiency building fabric; Basic plant configuration (0.3m^3 hot water tank). Appliances' current electrical efficiency.	9,450	13,885	19,469	23,904	51.5	41.9
$1_{High/High\ efficiency}$	3 Household building with high efficiency building fabric; Basic plant configuration (0.3m^3 hot water tank). Appliances' high electrical efficiency.	9,450	12,640	19,469	22,660	51.5	44.2
$2_{Low/Current\ efficiency}$	6 Household building with low efficiency building fabric; Basic plant configuration (0.5m^3 hot water tank). Appliances' current electrical efficiency.	13,396	21,393	31,242	39,239	57.1	45.5
$2_{Low/High\ efficiency}$	6 Household building with low efficiency building fabric; Basic plant configuration (0.5m^3 hot water tank). Appliances' high electrical efficiency.	13,396	19,329	31,242	37,176	57.1	48.0
$2_{High/Current\ efficiency}$	6 Household building with high efficiency building fabric; Basic plant configuration (0.5m^3 hot water tank). Appliances' current	12,451	20,846	29,072	37,467	57.2	44.4

	electrical efficiency.						
$2_{\text{High/High efficiency}}$	6 Household building with high efficiency building fabric; Basic plant configuration ($0.5m^3$ hot water tank). Appliances' high electrical efficiency.	12,451	18,627	29,072	35,248	57.2	47.2
$3_{\text{High/Current efficiency}}$	6 Household building with high efficiency building fabric; Basic plant configuration ($0.5m^3$ hot water tank) with additional $0.3m^3$ chilled water tank. Appliances' current electrical efficiency.	13,402	21,538	30,200	38,337	55.6	43.8
$3_{\text{High/High efficiency}}$	6 Household building with high efficiency building fabric; Basic plant configuration ($0.5m^3$ hot water tank) with additional $0.3m^3$ chilled water tank. Appliances' high electrical efficiency.	13,402	19,391	30,200	36,190	55.6	46.4
$4_{\text{High/Current efficiency}}$	6 Household building with high efficiency building fabric; Basic plant configuration ($0.5m^3$ hot water tank) with additional $2.5m^2$ flat plate SWH. Appliances' current electrical efficiency.	12,151	20,562	28,749	37,160	57.7	44.7
$4_{\text{High/High efficiency}}$	6 Household building with high efficiency building fabric; Basic plant configuration ($0.5m^3$ hot water tank) with additional $2.5m^2$ flat plate SWH. Appliances' high electrical efficiency.	12,151	18,361	28,749	34,959	57.7	47.5
$5_{\text{High/Current efficiency}}$	6 Household building with high efficiency building fabric; Basic plant configuration ($0.5m^3$ hot water tank). All electricity is exported. Appliances' current electrical efficiency.	12,451	23,504	29,072	40,125	57.2	41.4
$5_{\text{High/High efficiency}}$	6 Household building with high efficiency building fabric; Basic plant configuration ($0.5m^3$ hot water tank). All electricity is exported. Appliances' high electrical efficiency.	12,451	20,580	29,072	35,266	57.2	44.7

The same conclusions discussed for the system's *PES* can be extended to the annual CO_2 savings (*ES*). Reducing the system's operational hours by reducing the useful thermal load (*e.g.* micro-trigeneration feeding a smaller building, lower occupancy *etc*.) results in a lower *ES*. Also, if the net electrical imports are included in the calculation of the annual CO_2 savings, reducing the thermal load by improving the building fabric results in a reduction in *ES*. Finally, decreasing the net electrical imports by improving the appliances' electrical efficiency increases the *ES*; otherwise if the net electrical imports are excluded from the calculation the annual *ES* is the same for both electrical efficiencies.

In terms of plant configuration, due to the parasitic thermal demand required to cover for energy losses of the additional chilled water tank, the plant system in Scenario 3_{High} has the lowest *ES* value. On the contrary the additional flat plate solar water heater, which offsets part of the CHP unit thermal load, renders the plant system used in Scenario 4_{High} the scenario with the highest *ES* value.

Finally exporting all the electricity and importing all the electricity from the grid results in a situation where although the annual CO_2 savings are the same if the net imports are not included (the cogenerated electricity in Scenario 2_{High} is similar to that in Scenario 5_{High}; the system therefore behaves in a similar fashion), if the net imports are included Scenario 5 becomes the scenario with the lowest *ES*.

5.4.2 Effect of improving the grid emission factor

To model the reduction in emitted CO_2 for varying degrees of grid network improvements, the grid emission factor was varied between the current value of 1.088 and a future 0.5 kg CO_2 per kWh delivered at end-use. Using the scenarios in Scenario 1_{Low} (3 household building with low efficiency fabric) as an example, Figure 5.8 shows how the emissions emitted by the micro-trigeneration and separate generation, $Emissions_{SEPARATE}$, vary with improving grid emission factor (e_{Grid}). As done with the primary energy savings both plots including and excluding the net electrical imports are shown. Figure 5.9 then shows how the *ES* varies with improving grid emission factor (e_{Grid}).

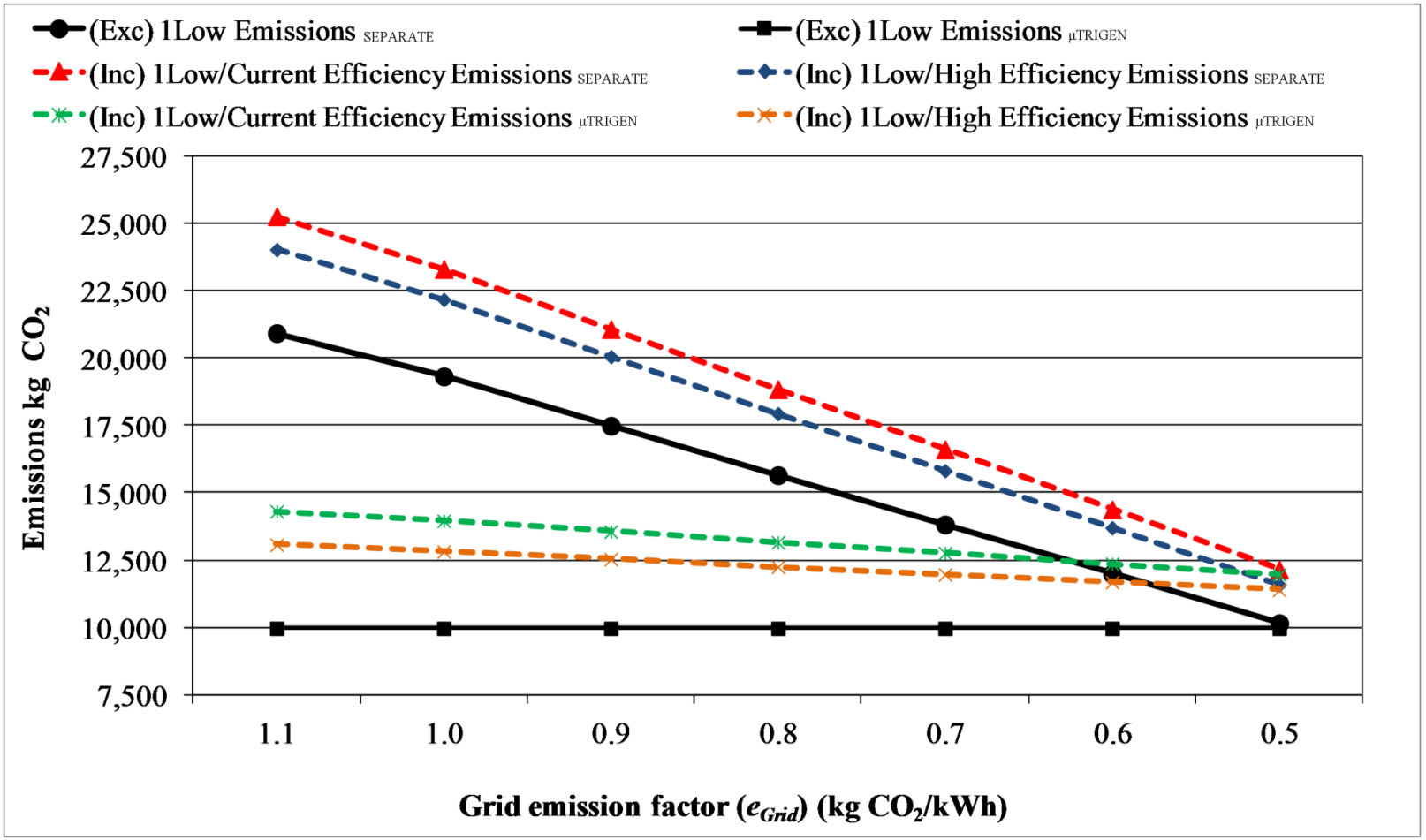

Fig. 5.8 - Sensitivity of $Emissions_{SEPARATE}$ and $Emissions_{\mu TRIGEN}$ to the grid emission factor (e_{Grid}) (Scenario 1_{Low})

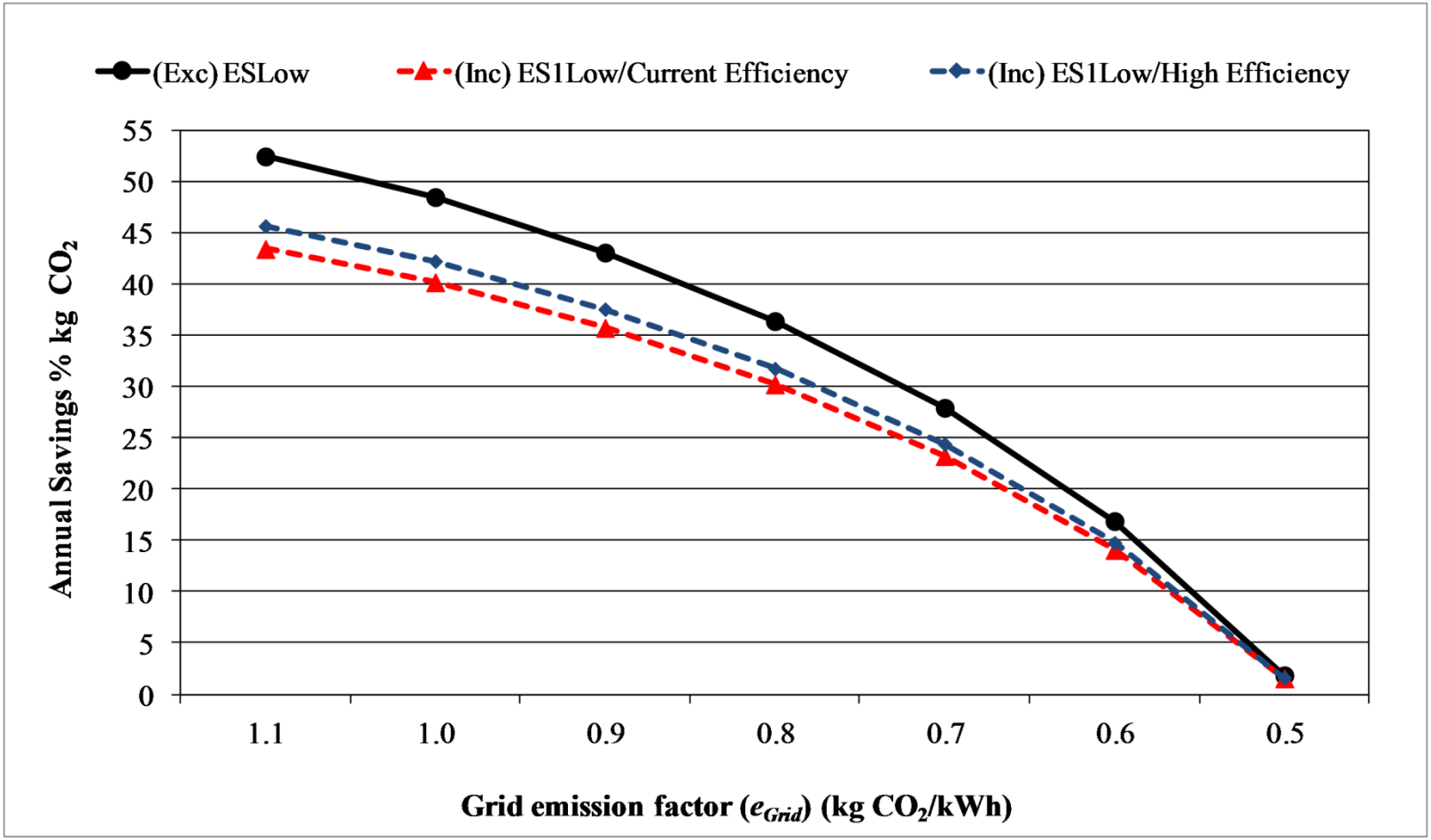

Fig. 5.9 - Sensitivity of annual *ES* (CO_2 savings) to the grid emission factor (e_{Grid}) (Scenario 1_{Low})

Similarly to the effect on $PE_{SEPARATE}$ and the system's *PES* caused by improving grid efficiency, improving the grid emission factor results in a reduction in emissions produced in separate generation, $Emissions_{SEPARATE}$, with a subsequent reduction in the micro-trigeneration system environmental advantage. In this case, considering a possible improvement in the grid emission factor of about 55% (from 1.088 to 0.5 kg CO_2 per kWh), it can be observed how the system's annual savings in Scenario 1_{Low} quickly drops to approximately 1.9% in both the current and high efficiency electrical cases. For other scenarios, such as Scenario 1_{High}, results indicate that although the extent of the reduction in annual savings is similar, (from 51.5% to -1%), a grid emission factor of 0.5 kg CO_2 per kWh yields a negative percentage of annual savings. This means that for the 3 household building, 0.5 kg of CO_2 per kWh appears to be the environmental limit beyond which the system loses any environmental advantage over using separate generation. Again from a Maltese perspective, this is currently not a problem as the grid network emission factor is well above this limit. However, when considering the development of a policy promoting micro-trigeneration in residential buildings this is an important aspect which must be taken into serious consideration as it might lead to an overestimation of the potential annual CO_2 savings which might be achieved.

Considering the case of 6 household building with low efficiency building fabric ($Scenario2_{Low}$) a similar behaviour can be observed. Figure 5.10 in fact shows that improving the grid emission factor from 1.088 to 0.5 kg CO_2 per kWh results in a drop in the system's annual CO_2 savings to approximately 6%. An important difference however is the fact that, whereas in the 3 household building the micro-trigeneration system's annual CO_2 savings are practically annulled, in the 6 household building the system's annual CO_2 savings are still relatively significant. This suggests that, although the same system plant size is being used for both buildings, the fact that the system is better matched with the demand in the larger building enables it to retain its environmental advantage vis-à-vis grid emission factor improvements.

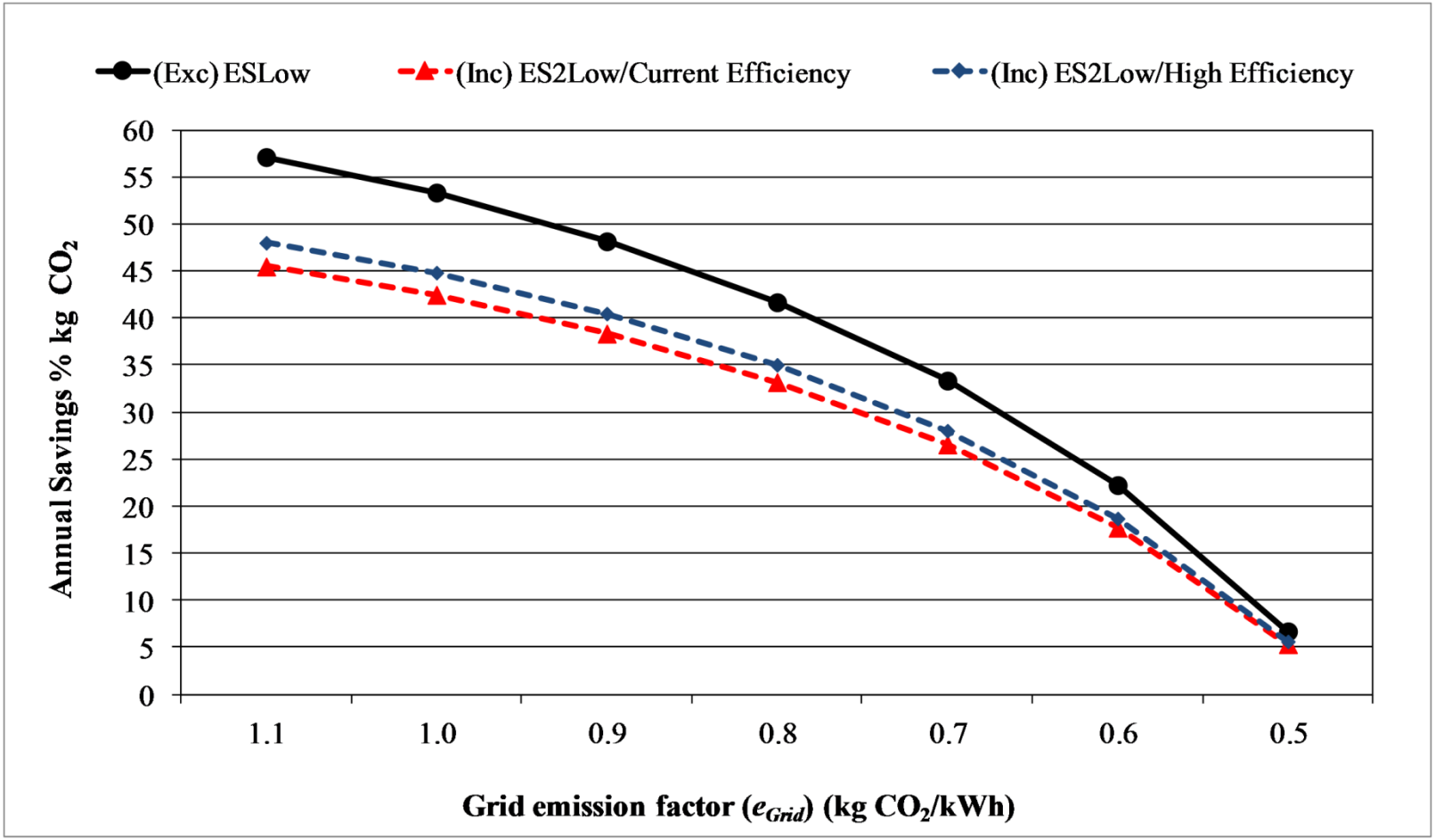

Fig. 5.10 - Sensitivity of annual *ES* (CO_2 savings) to the grid emission factor (e_{Grid}) (Scenario 2_{Low})

5.5 Micro-trigeneration system economic performance metrics

The third and final part of the assessment process involved assessing the economic performance of the micro-trigeneration system. As explained in Chapter 4 three criteria were used to financially assess the system's performance for each scenario: the ***present worth*** (*PW*), the ***internal rate of return*** (*IRR*) and the ***payback period*** (*PP*). Also, as discussed in Chapter 4 all three criteria were further analysed on the basis of two variable financial scenarios, that is:

- a scenario with a constant LPG price and variable electricity tariffs to assess the sensitivity of the system's financial viability to variable electricity tariffs (±50% of the current electricity tariffs[7]); and

- a scenario with a constant electricity tariff and variable LPG prices to assess the sensitivity of the system's financial viability to variable LPG prices (maximum and minimum current LPG prices[7]).

In both scenarios the assumed *Feed in Tariff* (*FIT*) was set at 0.50 € per kWh exported[7].

5.5.1 Present worth

5.5.1.1 Present worth assuming a variable electricity tariff scenario

Figure 5.11 shows the calculated *PW* of all scenarios for the 3 household building (Scenario 1) and the 6 household building (Scenario 2) for different electricity tariffs, and a constant LPG price of 1.187 € per kg. Given the value of the different energy products involved, throughout the economic analysis the scenarios were fully defined to include all differentiating aspects (*e.g.* type of building fabric, appliances' electrical efficiency *etc.*). Considering the magnitude of the *PW* as a measure of a project's financial feasibility, Figure 5.11 shows how the *present worth* of a project varies with varying electricity tariffs, for different building sizes and occupancies, building fabric efficiencies and appliances' electrical efficiencies.

[7] For details refer to Section 4.3.2.1 in Chapter 4.

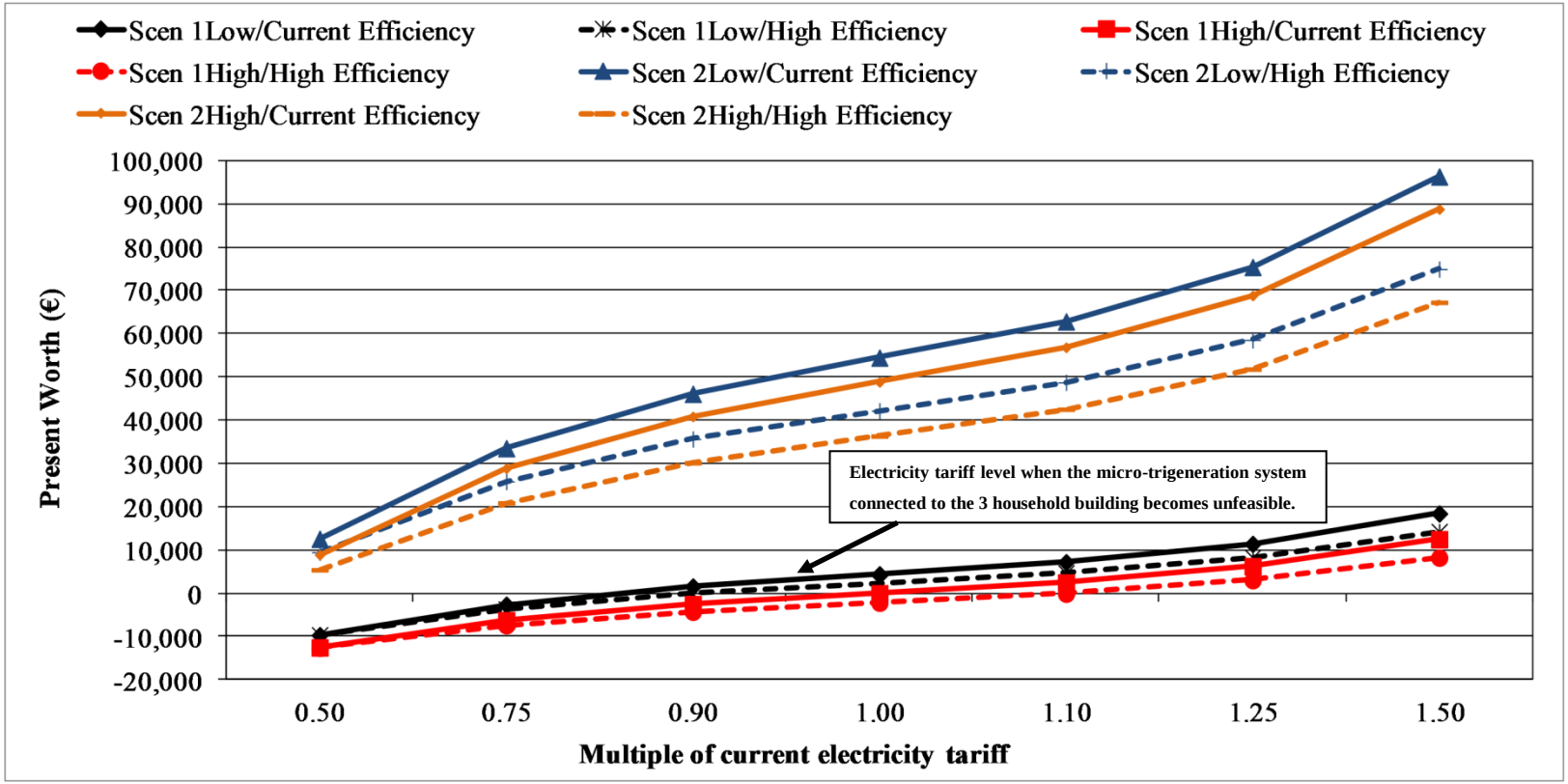

Fig. 5.11 - *PW* for Scenarios 1 and 2 for varying electricity tariffs

As electricity costs increase (relative to the LPG price) the financial advantage of the project increases. The higher the electricity tariff considered, the higher is the *PW* of the project. The rationale for this stems from the fact that the financial value of the cogenerated electricity used to satisfy the electrical demand of the households and hence offset imported electricity, is equivalent to the value of the imported electricity which has been offset. The higher the cost to import electricity, the more valuable is the cogenerated electricity used to satisfy the building's own energy demand.

Comparing the *PW* plots for the scenarios in the 3 household building with those in the 6 household building it can be observed how increasing the thermal demand (by increasing occupancy or connecting the micro-trigeneration system to a larger building), significantly increases the value of the project. At electricity tariffs lower than the current tariffs (*approx.* at a value of 0.95 times the current electricity tariff), the energy demand in the 3 household building results in a negative *PW* which renders the system financially unfeasible. The higher energy demand in the 6 household building, on the other hand, renders the scenarios feasible even at low electricity tariffs.

Comparing the scenarios for the different buildings also highlights the fact that the difference between the *PW* for the two sets of scenarios is sensitive to the electricity tariff. The difference between the two sets increases with increasing electricity tariffs.

Any measure aimed at reducing the energy demand of the building results in a decrease in the *PW* of the trigeneration system. Improving the electrical efficiency of appliances, hence reducing the electrical demand, results in a decrease in the project's *PW*. For both the 3 and the 6 household building scenarios it can be observed that the difference between the *PW* of the different appliances' electrical efficiency scenarios (current and high) increases substantially with increasing electricity tariffs, whilst the difference in *PW* between the different building fabric scenarios (low and high), stays reasonably constant throughout the entire range of electricity tariffs.

Given the different energy quantities of the two sets of scenarios for the 3 and 6 household buildings involved and the cost of the energy products, it can be observed that in the 3 household building scenarios the overall difference in *PW* is highest for the difference in fabric efficiency (for the same appliances' electrical efficiency), whilst in the 6 household building scenarios the overall difference in *PW* is highest for the difference in appliances' electrical efficiency (for the same building fabric). An explanation as to why this occurs necessarily has to take into consideration the cash flow (*CF*) of each scenario. Recall equation (4.16) in Chapter 4 describing how to calculate the cash flow for each individual scenario:

$$CF = \left(E_{Net\ Export} \text{ x } FIT\right) + \left(E_{Total} \text{ x } Tariff\right) - \left(E_{Net\ Import} \text{ x } Tariff\right) - \left(E_{Net\ Export} + E_{Net\ Demand\ \mu TRIGEN}\right)MC - \left(Fuel_{\mu TRIGEN} - Fuel_{SEPERATE}\right)Cost\ of\ Fuel$$

Excluding the net exports term ($E_{Net\ Export}$ x *FIT*), the annual maintenance cost term ([$E_{Net\ Export}$ + $E_{Net\ Demand\ \mu TRIGEN}$]*MC*) and the annual fuel costs term ([$Fuel_{\mu TRIGEN}$ – $Fuel_{SEPERATE}$]*Cost of Fuel*), which are constant and independent of the electricity tariff, the other two terms, the total invoiced electricity *without* trigeneration term (E_{Total} x *Tariff*) and the total invoiced electricity *with* trigeneration term ($E_{Net\ Import}$ x *Tariff*), are variable and dependent on the electricity tariff. In this context, Figure 5.12 shows the value of the individual terms making up the *CF* for the 6 household building with low efficiency fabric and current appliances' electrical efficiency (Scenario $2_{\text{Low/Current efficiency}}$).

It can be observed that the shape and magnitude of the resulting cash flow (solid black line) partly relies on terms which are dependent on the electricity tariff (i) and partly on terms which are independent of the electricity tariff (ii):

i. In the former case although the energy quantities calculated for E_{Total} and $E_{Net\ Import}$, are constant for a particular scenario, the varying electricity tariff dictates the magnitude and shape of the total invoiced electricity *without* trigeneration term and the total invoiced electricity *with* trigeneration term.

ii. In the latter case the magnitude of the remaining terms in the cash flow equation are, dependent on the energy quantity they represent multiplied by the assumed financial parameter (*e.g. FIT*), applicable for that specific term; both assumed constant for any given scenario.

For the same financial parameters, changes in an energy quantity due to (for example) a reduction in fuel consumption as a result of improving the building fabric, will lead to a different financial result for each term making up the *CF* of each scenario. For the different scenarios proposed therefore, the individual terms making up the *CF*, the resulting *CF* and eventually the *PW* reflect the aggregated effect of varying electricity tariffs, the energy quantities and the economic parameters assumed.

Considering (for example) the specific case of the current (Scenario $2_{\text{Low/Current efficiency}}$) and high (Scenario $2_{\text{Low/High efficiency}}$) appliances' electrical efficiency for the 6 household building with low efficiency fabric, Figure 5.13 compares the *CF* and its individual components for the two scenarios.

Recalling that for the same building fabric improving the electrical efficiency of appliances does not affect the thermal performance of the micro-trigeneration system (fuel consumption in unaltered), but results in an increase in net electrical exports and a decrease in net imports, it can be observed by comparing the plots obtained for Scenario $2_{\text{Low/Current efficiency}}$ and Scenario $2_{\text{Low/High efficiency}}$, that the individual terms making up the *CF* reflect these changes. Where an individual term is independent of the electricity tariff the change is constant throughout the electricity tariffs range.

In this case the aggregated effect of the different terms on the *CF* and the *PW* plot is that, as discussed, with improving household appliances' electrical efficiency, the *PW* of the project is reduced with a significant reduction occurring with increasing electricity tariffs.

A similar reasoning can be applied to all other cases.

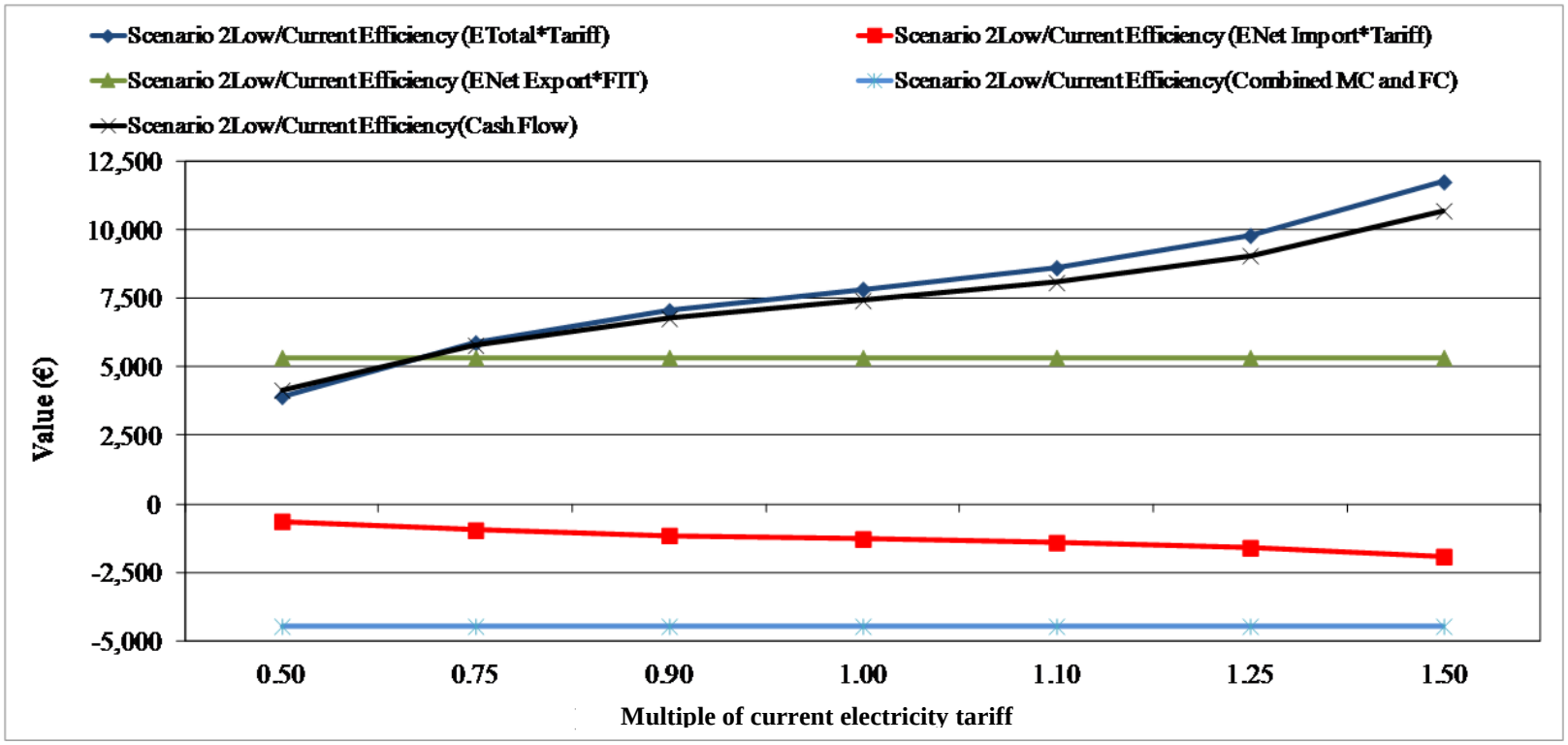

Fig. 5.12 - *CF* and *CF* component terms for Scenario $2_{\text{Low/Current efficiency}}$ for varying electricity tariffs

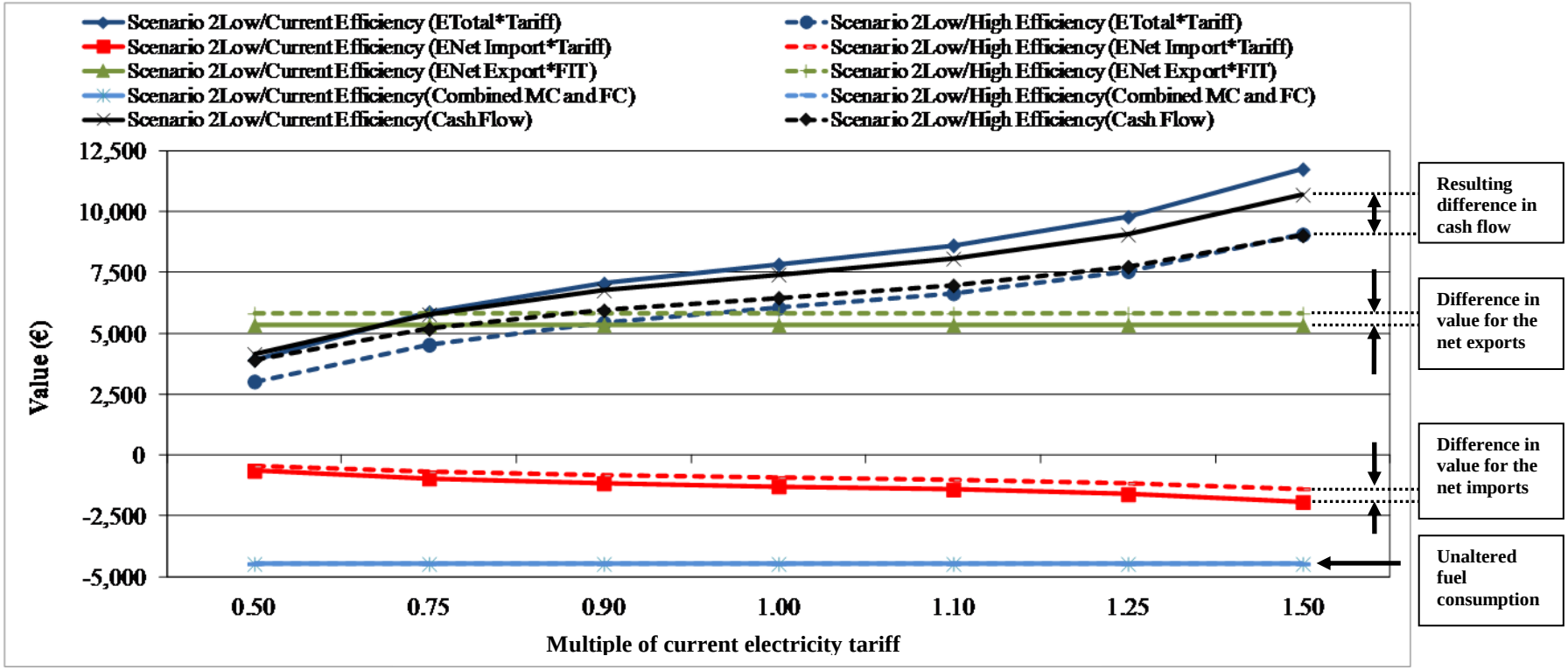

Fig. 5.13 - Difference in *CF* (and component terms) due to improvement in appliances' electrical efficiency

Having discussed the effect that changes in demand have on the *present worth* of a project, Figure 5.14 shows the effect the different plant configurations used to model Scenarios 3_{High} (additional chilled water tank) and 4_{High} (additional SWH) have on the *PW* of the project. For comparative purposes, also shown are the *PW* plots for the current and high electrical efficiency scenarios of the 6 household building with high efficiency fabric (Scenario $2_{High/Current\ efficiency}$ and Scenario $2_{High/High\ efficiency}$). The negligible difference in *PW* between the different scenarios suggests that that at these conditions (and for the selected financial parameters) the physical modifications effected in the plant configuration do not substantially affect the financial performance of the system. In real terms this means that, for the given conditions and the level of physical modifications effected, the financial aspect is not an important consideration when selecting the type of plant configuration.

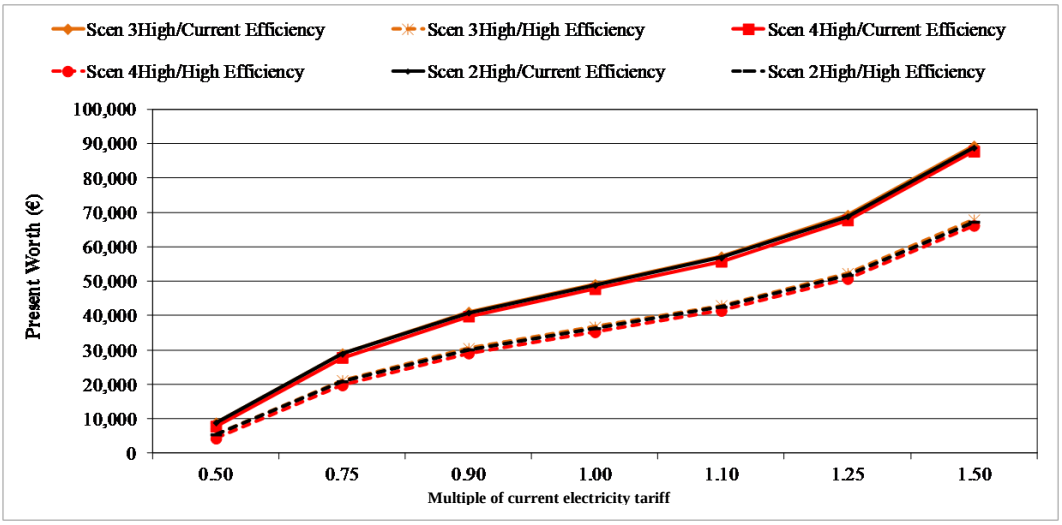

Fig. 5.14 - *PW* for scenarios with different plant configurations for varying electricity tariffs

Finally, whereas changing the plant configuration has no effect on the financial performance of the system, comparing the *PW* plots of the scenarios in Scenario 5_{High} with the corresponding ones in Scenario 2_{High} shows that the way the cogenerated electricity is used substantially alters the *PW* of a project. In Figure 5.15 the current and high efficiency scenarios of both Scenario groups 2_{High} and 5_{High} are shown.

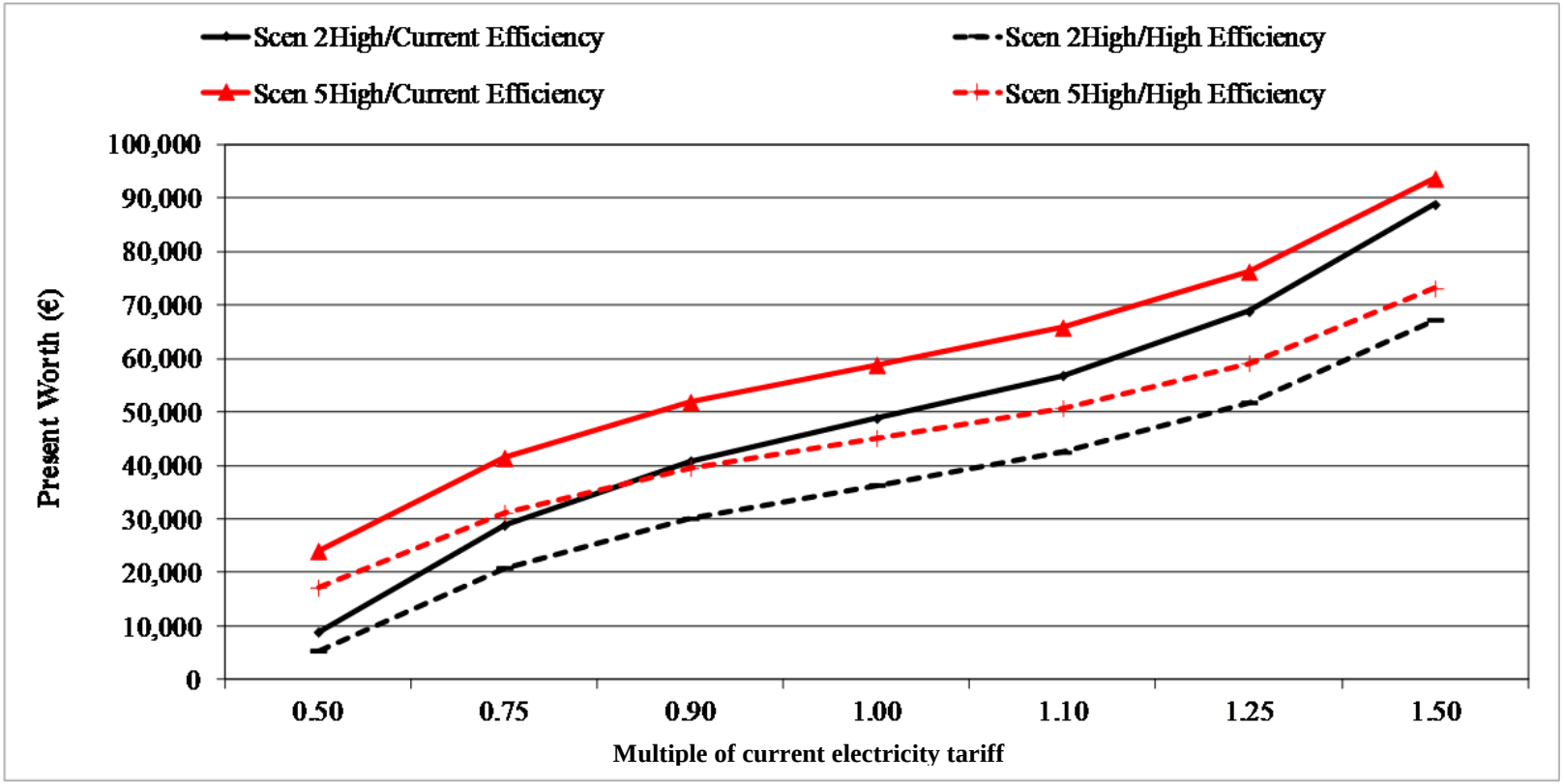

Fig. 5.15 - *PW* for Scenarios 2_{High} and 5_{High} for varying electricity tariffs

In the course of this chapter Scenario 5_{High} has been mentioned only sporadically in comparison to the other scenarios. As explained in Section 4.1.1, the reason for this is that the only difference between this scenario and the 6 household building with efficient building fabric (Scenario 2_{High}) was in the way the cogenerated electricity was used. Contrary to the other scenarios, in Scenario 5_{High} the electricity cogenerated by the micro-trigeneration system was not used to satisfy the building's own electrical demand with the excess being exported, but rather all the electricity cogenerated was exported to the grid. In terms of system operation, the system is unaffected. The system's financial value is however considerably affected, particularly if the price differential between the imported electricity and the *Feed in Tariff* is significant.

For the assumed *FIT*, at the low end of the electricity tariffs range when the cost of importing electricity from the grid is low, the calculated *PW* for Scenario $5_{High/Current\ efficiency}$ is about 2.7 times higher than the equivalent *PW* for Scenario $2_{High/Current\ efficiency}$. Similarly, the calculated *PW* for Scenario $5_{High/High\ efficiency}$ is 3.2 times higher than the equivalent *PW* for Scenario $2_{High/High\ efficiency}$. As the electricity tariff is increased, both ratios first drop to 1.2 times at the current electricity tariff and then to 1.1 times at the high end of the electricity tariffs range. For the assumed financial parameters therefore the results suggest that the projects would have a higher financial value if all the electricity is exported.

5.5.1.2 Present worth assuming a variable LPG price scenario

Having discussed the sensitivity of the *PW* of the proposed micro-trigeneration system to different operating conditions assuming varying electricity tariffs, this section examines the sensitivity of the system to different operating conditions assuming varying LPG prices. The electricity tariff in this case was assumed constant at the current tariff level. Figure 5.16 compares the *PW* plots for the cases in the 3 and the 6 household building (Scenarios 1 and 2 respectively) for varying LPG prices.

The first important consideration which arises from the plots is that contrary to its sensitivity to electricity tariffs which diminishes with lower electricity tariffs, the *PW*

of the system diminishes with increasing LPG prices. The plots however do show a similar financial sensitivity to the building's energy demand – the higher the useful energy demand the higher is the *PW* of a project. Measures aimed at reducing either the thermal demand (*e.g.* by improving the building fabric) or the electrical demand (*e.g.* by improving the electrical efficiency of appliances), therefore have a detrimental effect on the financial value of a project. Similarly, low operating load factors such as that experienced by the plant connected to the 3 household building (Scenario 1) tend to create a situation where the *PW* is very small, bordering on the negative with increasing LPG prices. In fact, at the current LPG price the system connected to the 3 household building is already almost at a break-even point.

On an individual building basis, in the case of the 6 household building the highest difference between the different scenarios is that due to the improvement of electrical efficiency of appliances. In the case of the 3 household building the highest difference between scenarios is that due to the improvement of the building fabric. The reason for this difference is once more the magnitude of the individual *CF* terms which reflect the changes in energetic performance due to the different scenarios.

Finally, considering that, as shown in Figure 5.17 for Scenario $2_{\text{Low/Current efficiency}}$, only one term in the cash flow equation is dependent on the assumed LPG price, the resulting *CF* and *PW* plots are both subject to a constant linear decrease reflecting the increasing fuel costs.

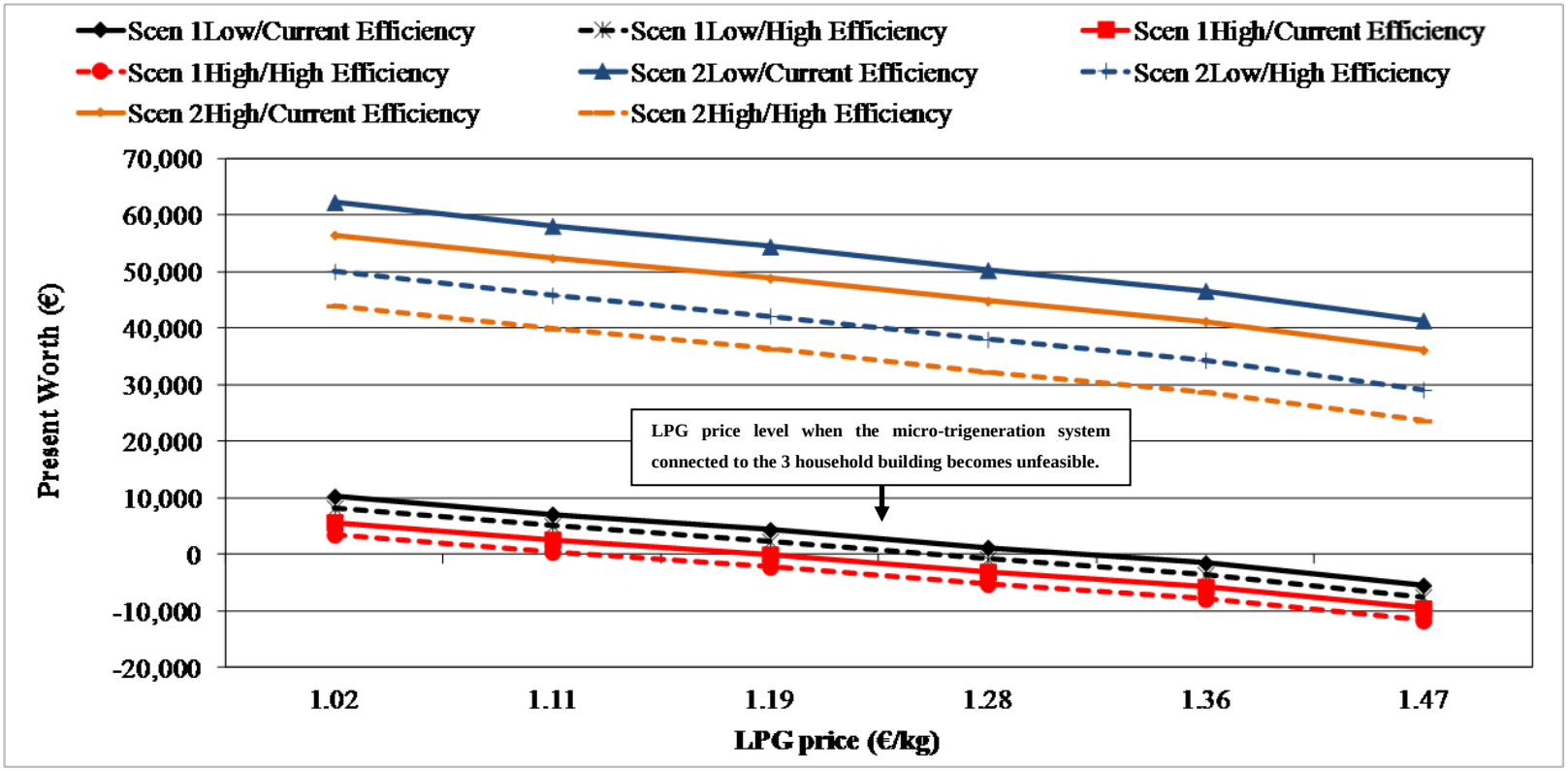

Fig. 5.16 - *PW* for Scenarios 1 and 2 for varying gas prices

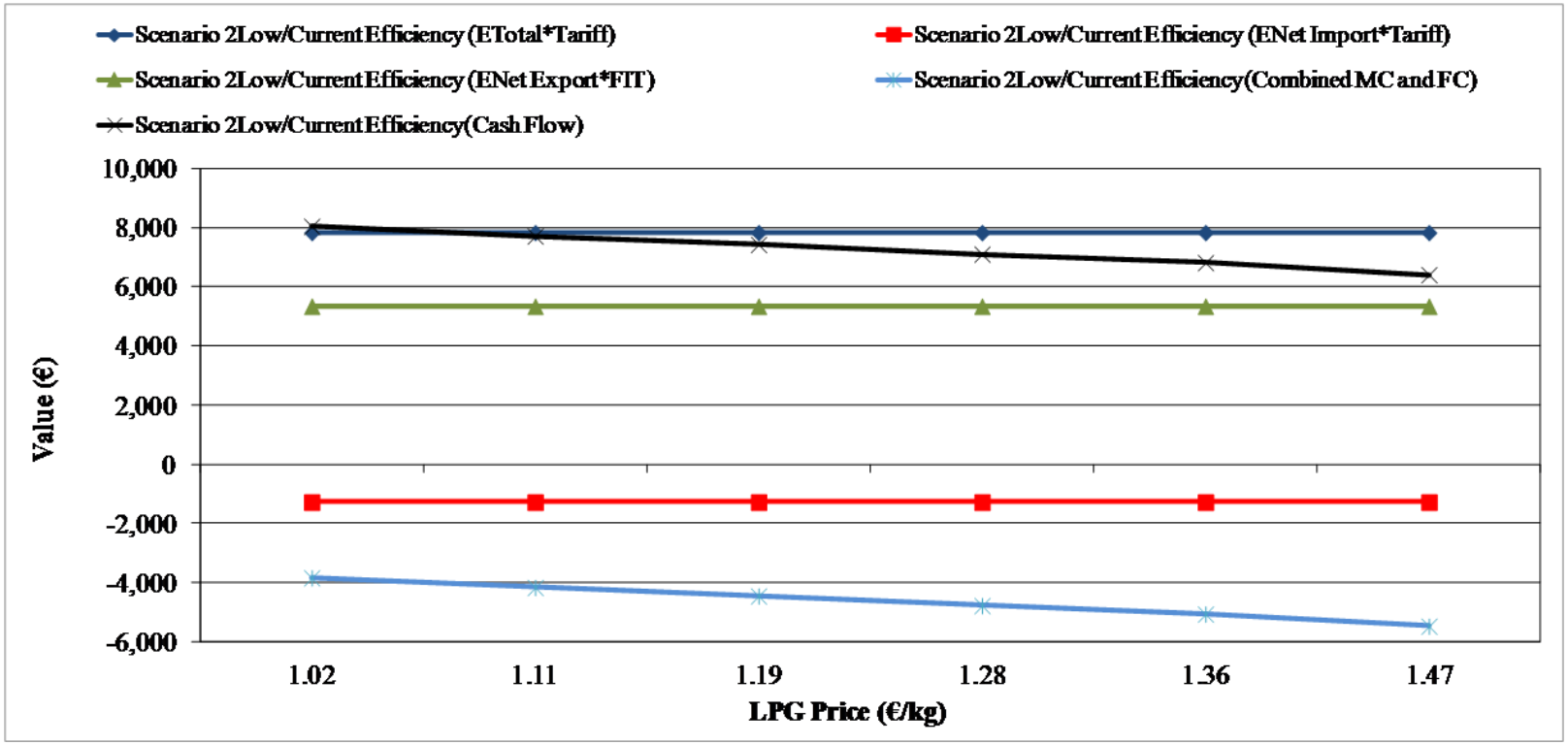

Fig. 5.17 - *CF* and *CF* component terms for Scenario $2_{\text{Low/Current efficiency}}$ for varying gas prices

Figures 5.18 and 5.19 shows how the different plant configurations used in scenario 3_{High} (additional chilled water tank) and Scenario 4_{High} (additional SWH) compare to the reference case – 6 household building with high efficiency fabric (Scenario 2_{High}).

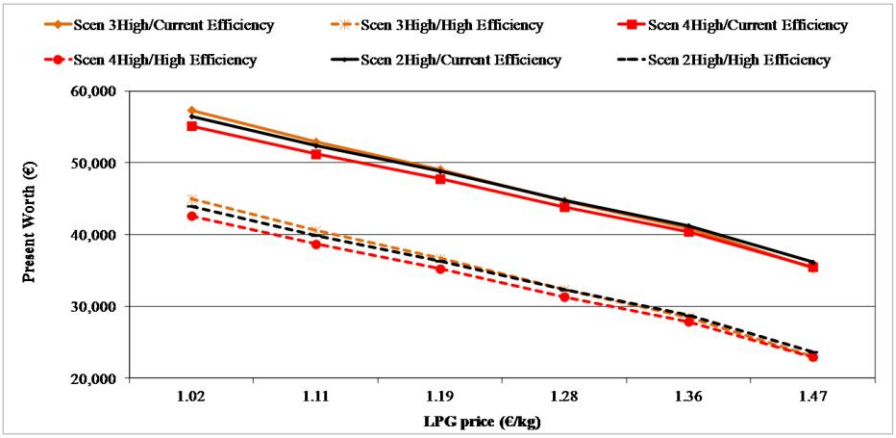

Fig. 5.18 - *PW* for scenarios with different plant configurations for varying gas prices

In terms of different plant configurations the difference between the various scenarios is negligible, although a slight divergence can be observed at the low end of the LPG prices range, where the fuel costs are lowest and the other terms of the *CF* equation (reflecting the electrical performance) are more significant in terms of their financial contribution to the overall *CF* and *PW* of the project.

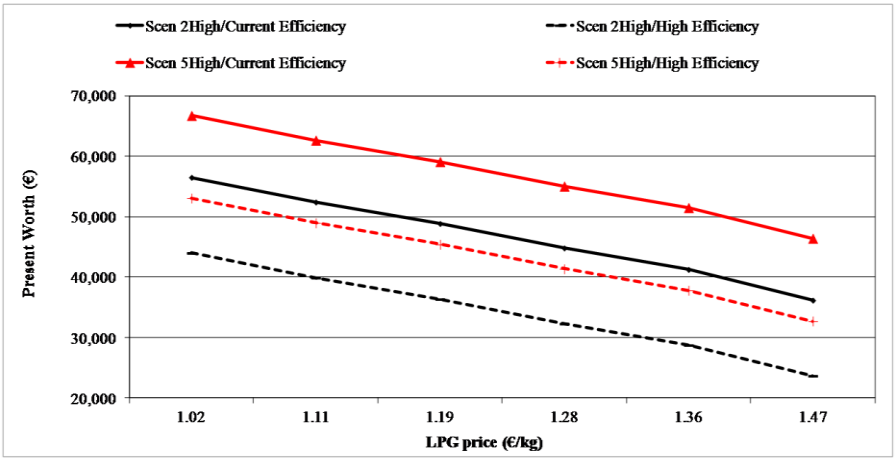

Fig. 5.19 - *PW* for Scenarios 2_{High} and 5_{High} for varying gas prices

For the assumed constant *FIT* and electricity tariffs (at current levels), Figure 5.19

shows that exporting all the cogenerated electricity and importing electricity from the grid is more financially remunerative throughout the modelled LPG prices range.

5.5.2 Internal rate of return and payback period

Given that both the internal rate of return (*IRR*) and the payback period (*PP*) are calculated using the cash flow as an equation parameter (equation [4.18] and equation [4.19] respectively), it is only logical to infer that both the *IRR* and *PP* are strongly correlated with the *PW* and the conclusions obtained for the different scenarios. For this reason in this section only the main plots will be shown as the trends obtained are similar to those obtained for the *PW*. Nonetheless, for the interested reader Appendix 'F' shows the additional plots not shown in this section.

5.5.2.1 Internal rate of return (IRR)

The *IRR* calculates the investment rate necessary for the present worth of a project to be zero and can hence be considered as a special case of the equation used to calculate the *PW*. It is assessed on the basis of a project being profitable if the calculated *IRR* is higher than the assumed minimum attractive rate of return (*MARR*).

Figure 5.20 and Figure 5.21 show the resulting *IRR* for all cases of the 3 (Scenario 1) and 6 (Scenario 2) household building scenarios (comparing building size and occupancy, building fabric and appliances' electrical efficiency scenarios), respectively for varying electricity tariffs and varying LPG prices. The same conclusions deduced for the *PW* for varying electricity tariffs and LPG prices can be extended to the *IRR* as well. In general reducing the energy demand leads to a lower financial value of the project with decreasing building size and occupancy, improving the electrical efficiency of household appliances and improving the building fabric all contributing to reducing the financial value of the project in different orders of magnitude, depending on the size of the project. In terms of different plant configuration, changing system configuration (assuming the effected changes) has a negligible effect on a project's financial value. Exporting the cogenerated electricity and using imported electricity renders the project more financially valuable.

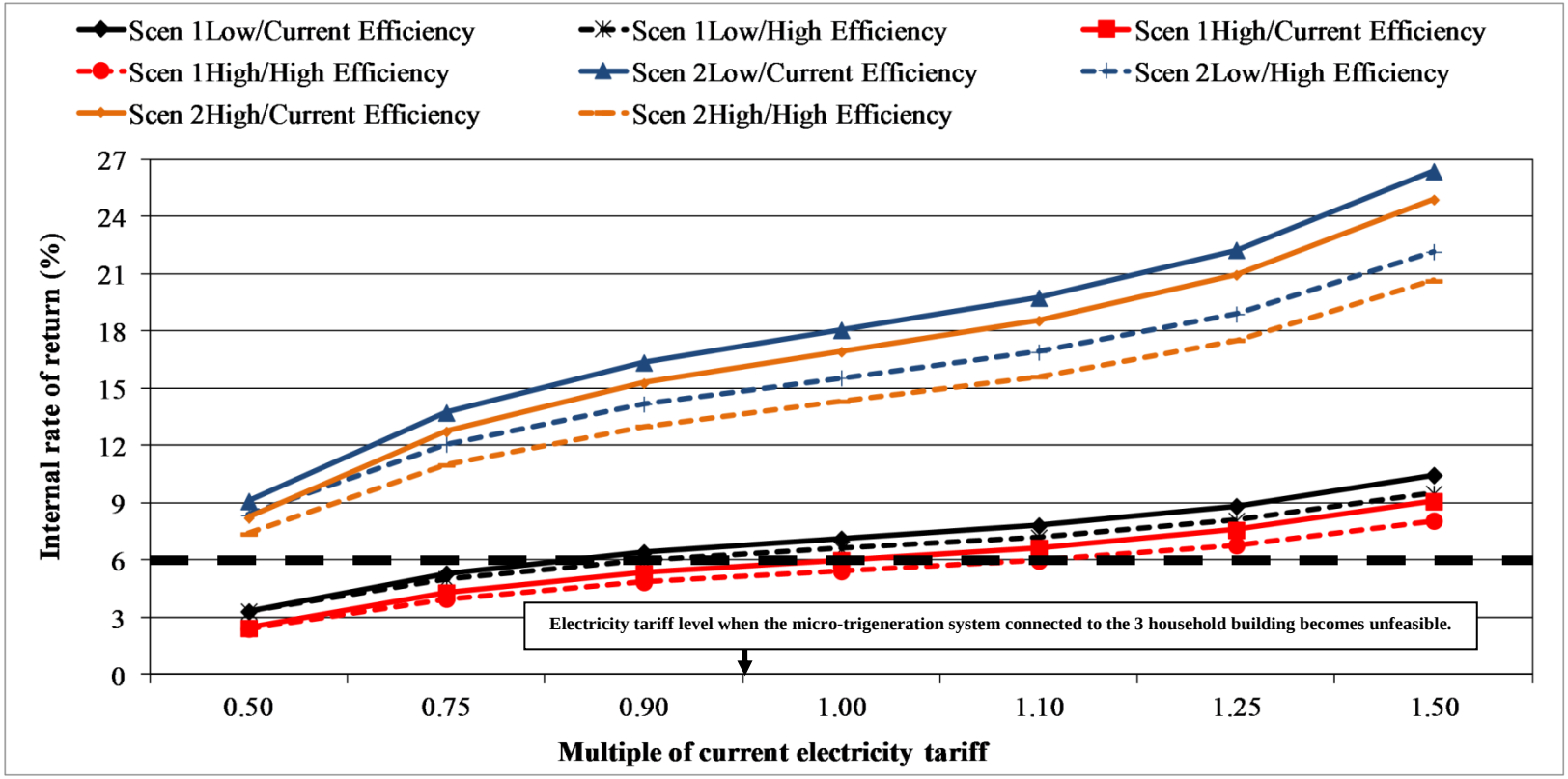

Fig. 5.20 - *IRR* for Scenarios 1 and 2 for varying electricity tariffs

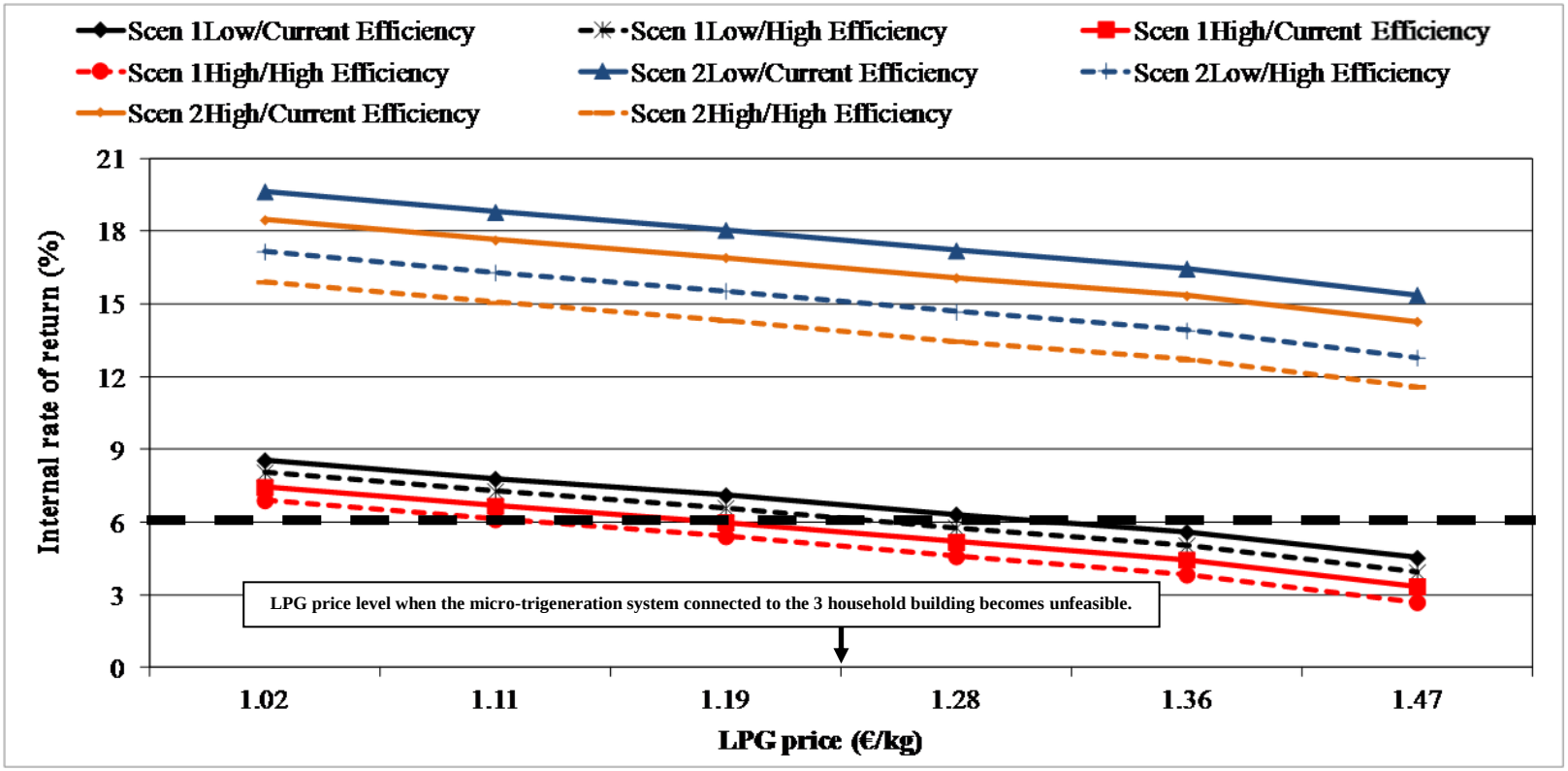

Fig. 5.21 - *IRR* for Scenarios 1 and 2 for varying gas prices

As explained, when assessing the *IRR* a project is only financially profitable if the calculated *IRR* is higher than the *MARR*. In this research, as explained in Chapter 4, an *MARR* of 6% (similar to the one used by Biezma and San Cristóbal in [8] for assessing a cogeneration project) was used. As can be seen from the 2 figures showing the different 3 and 6 household building scenarios, the *IRR* of the cases modelled to represent the 6 household building (Scenario 2) exceed the minimum threshold of 6% throughout the whole range of electricity tariffs and LPG prices range. Conversely, at the low end of the electricity tariffs range and at the high end of the LPG prices range, the calculated *IRR* for the different cases in Scenario 1, representing the 3 household building, are below the minimum threshold of 6%. For the 3 household building, this 6% *IRR* coincides with the same electricity tariff and LPG price thresholds calculated for the *PW*[8] to become negative. This suggests that beyond these electricity tariff and LPG price levels, the micro-trigeneration system feeding the 3 household building becomes financially not viable.

5.5.2.2 Payback period (PP)

The payback period is based on calculating the time required to obtain a return on the investment. The shorter the *PP* the more financially attractive is the system and consequently the scenario investigated. It is calculated as the inverse of the cash flow multiplied by the investment as shown in equation (4.19), and therefore contrary to the other two criteria, the relationship between the payback period and the *CF* is of an inversely proportional nature. The higher the cash flow (and eventually the higher the *PW* and the *IRR*) the shorter is the payback period of the system for the different scenarios.

Similarly to the previous sections, Figure 5.22 and Figure 5.23 show the resulting *PP* for all cases of the 3 (Scenario 1) and 6 (Scenario 2) household building scenarios (comparing building size and occupancy, building fabric and appliances' electrical efficiency scenarios), respectively for varying electricity tariffs and LPG prices.

[8] For the 3 household building scenarios, the *PW* becomes negative if (for the current average LPG price) the electricity tariff falls below 0.95 times the current electricity tariff or (at the current electricity tariff) the LPG price exceeds the current average LPG price of *approx.* 1.2 € per kg.

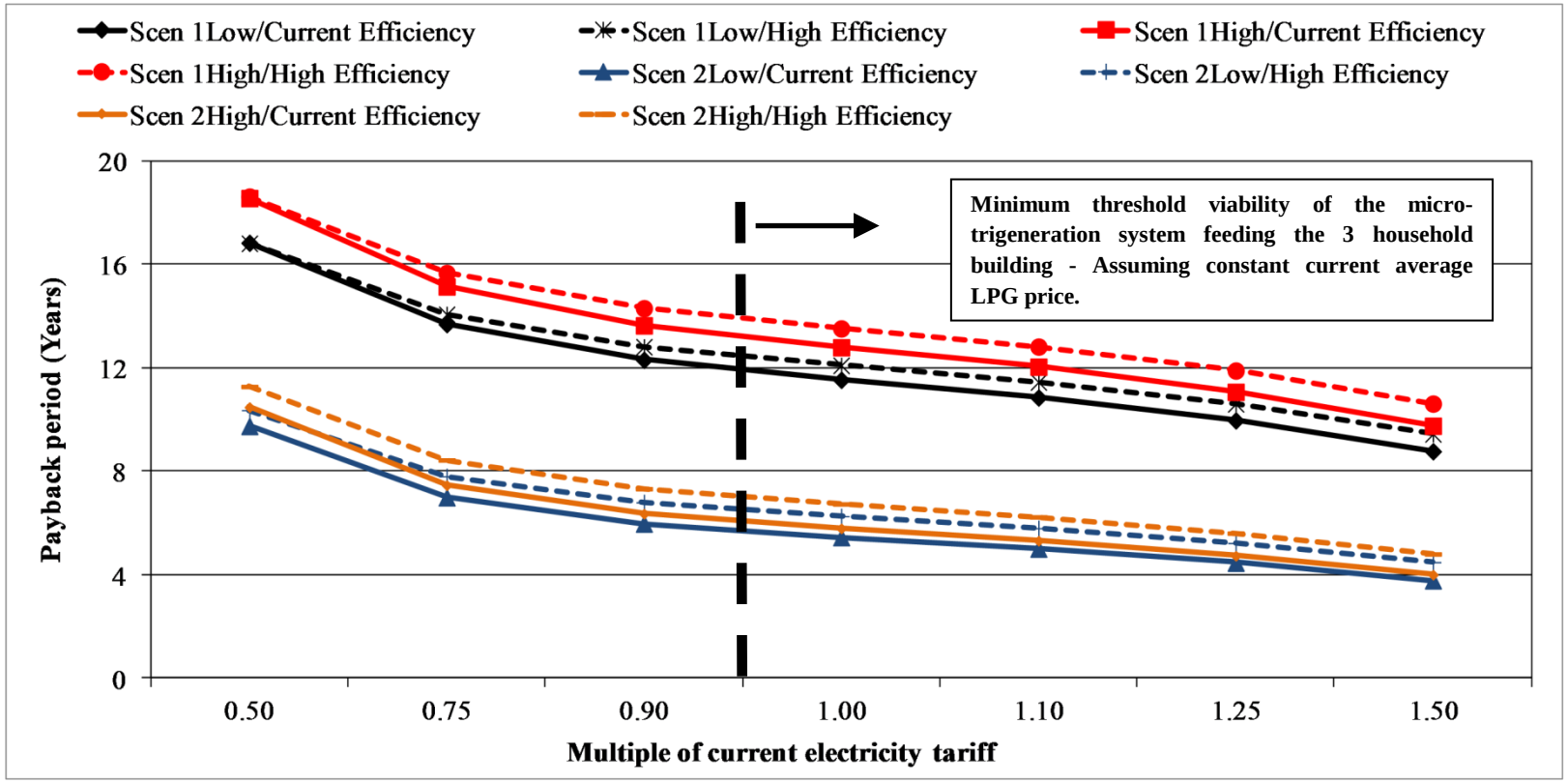

Fig. 5.22 - *PP* for Scenario groups 1 and 2 for varying electricity tariffs

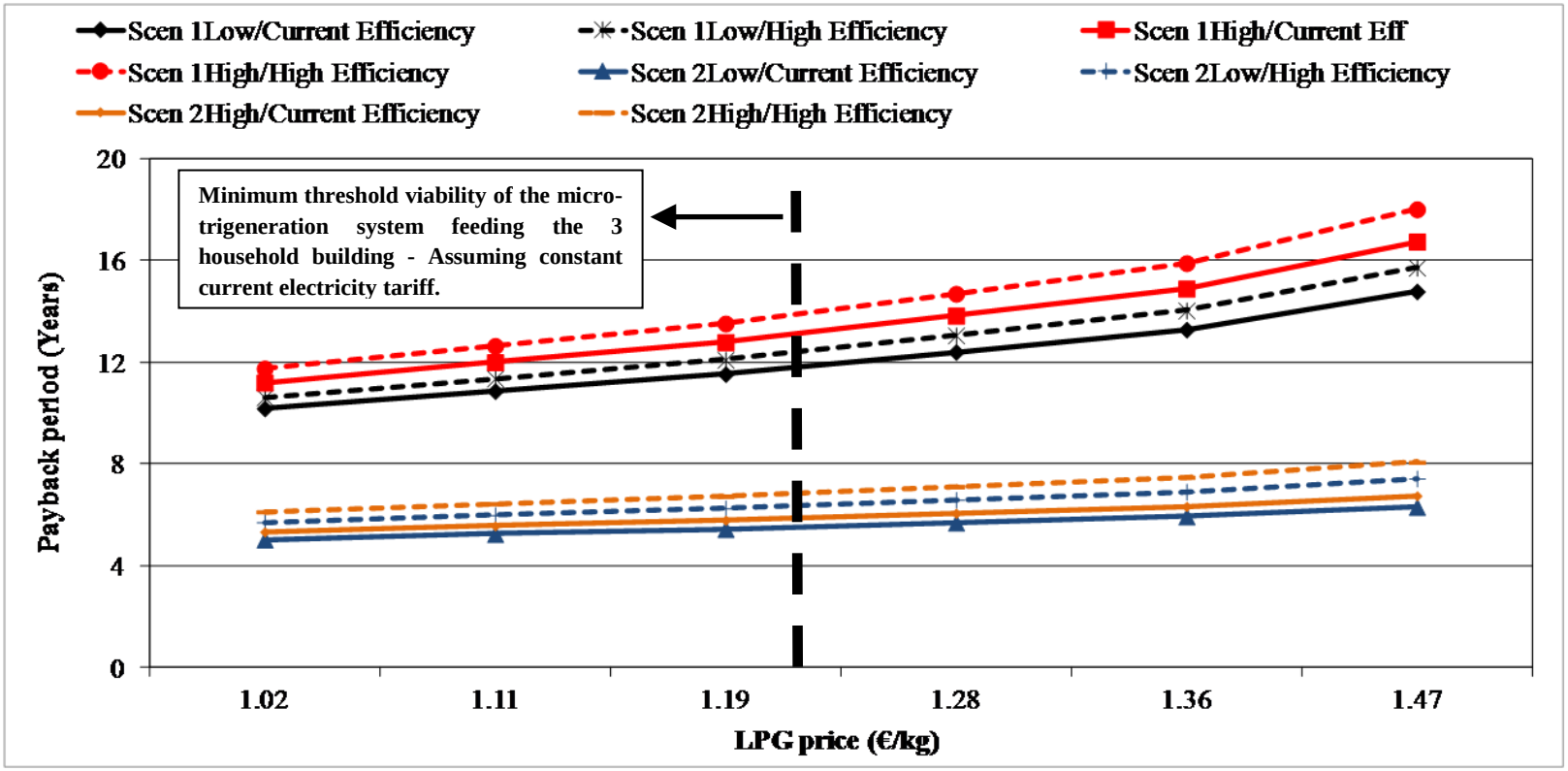

Fig. 5.23 - *PP* for Scenarios 1 and 2 for varying gas prices

Similarly to the *PW* and the *IRR*, it can be observed that with increasing electricity tariffs the resulting payback period improves, whilst for increasing LPG prices the resulting payback period deteriorates. For the variable electricity tariffs scenario, Figure 5.22 shows that, compared to the low end of the electricity tariffs range the payback period for all scenarios at the high end of the range is practically halved. Likewise, Figure 5.23 shows that, compared to the high end of the LPG prices range the payback period for all scenarios at the low end of the range is reduced by 33%.

Doubling the thermal load (by connecting the plant system to the 6 household building) leads to an approximate reduction of 50% in payback period. Similarly, for both financial scenarios and for both buildings, improving the building fabric and the electrical efficiency of appliances, results in a reduction in the financial feasibility of the system which in this case translates in an increase in the payback period.

Different plant configurations do not alter the expected payback period for the system, whilst exporting the cogenerated electricity and importing the entirety of the electrical demand results in a decrease in payback period.

Finally, specifically for the 3 household building an important aspect is the maximum payback period which might be expected for the electricity tariff and LPG gas price thresholds calculated using the *PW* and the *IRR*. For a fixed current LPG price, considering 0.95 times the current electricity tariff, as being the minimum electricity tariff below which the system would not be considered feasible for the 3 household building (due to a negative *PW* or *IRR* lower than 6%), the maximum payback period for the system in the 3 household building would be in the range of 12-14 years depending on the specifics of the individual case (such as building fabric, appliances' electrical efficiency *etc.*). Similarly, for a fixed current electricity tariff, considering 1.2 € per kg as being the maximum LPG price above which the system would not be considered feasible for the 3 household building, the maximum payback period for the system would be in the range of 12-14 years.

5.6 Integrated performance assessment

This section aims to bring together the results obtained for the different scenarios in a more integrated manner.

When comparing system performance using energetic, environmental and economic criteria different performance metrics criteria will yield different solutions as to which system or scenario is most feasible. Further, different performance will give contradictory results as to a system's value and feasibility.

To better illustrate this point, Table 5.13 summarises the system's response to the various external factors which were investigated during the course of this research. Based on the type of response, whether it is a negative or positive response (*e.g.* the increase or decrease in fuel consumption, higher or lower financial value, *etc*.) Table 5.13 is colour coded to distinguish the manner operational conditions affected the different performance criteria. Factors which positively affected a performance criterion are shaded in green, whilst those which negatively affected a performance criterion are shaded in red. Factors which did not affect (completely unrelated to the analysis) a performance criterion, or produced only a negligible change (related to the analysis but produced no significant change) are shaded in white and yellow respectively. It can be observed that the response of the system to the different external factors was not uniform and the best possible scenario is therefore dependent on the performance objective, be it maximising the energetic, environmental or financial performance.

Table 5.13 - Summary of micro-trigeneration system response to different operational conditions

Performance	*Energetic*							*Operational*	*Environmental*	*Financial*		
Operational Condition	***µTrigen fuel consumption***	***Effect on electrical performance***				***System efficiency ($\eta_{\mu TRIGEN}$)***	***Primary energy savings (PES)[9]***	***CHP Unit 'On'/'Off' Cycling***	***Emission savings (ES)[9]***	***Present worth (PW)***	***Internal rate of return (IRR)***	***Payback period (PP)***
		µTrigen cogenerated electricity	***Net imports***	***Net exports***	***Net demand satisfied by µTrigen***							
Building fabric improvement	Decreased (Improved)	Decreased (Deteriorated)	Increased (Deteriorated)	Decreased (Deteriorated)	Decreased (Deteriorated)	Decreased (Deteriorated)	Decreased (Deteriorated)	Variable (Depends on scenario)	Decreased (Deteriorated)	Decreased (Deteriorated)	Decreased (Deteriorated)	Increased (Deteriorated)
Increased building size and occupancy	Increased[10] (Deteriorated)	Increased (Improved)	Increased (Deteriorated)	Increased (Improved)	Increased (Improved)	Increased (Improved)	Increased (Improved)	Decreased (Improved)	Increased (Improved)	Increased (Improved)	Increased (Improved)	Decreased (Improved)
Addition of a chilled water storage tank	Increased (Deteriorated)	Increased (Improved)	Decreased (Improved)	Increased (Improved)	Increased (Improved)	Decreased (Deteriorated)	Decreased (Deteriorated)	Decreased (Improved)	Decreased (Deteriorated)	Negligible change	Negligible change	Negligible change
Appliances electrical efficiency improvement	Criterion not affected	Criterion not affected	Decreased (Improved)	Increased (Improved)	Decreased (Deteriorated)	Criterion not affected	Increased (Improved)	Criterion not affected	Increased (Improved)	Decreased (Deteriorated)	Decreased (Deteriorated)	Increased (Deteriorated)
Addition of SWH to the µTrigen system	Decreased (Improved)	Decreased (Deteriorated)	Increased (Deteriorated)	Decreased (Deteriorated)	Decreased (Deteriorated)	Increased (Improved)	Increased (Improved)	Decreased (Improved)	Increased (Improved)	Negligible change	Negligible change	Negligible change
Grid network improvement	Criterion not affected	Criterion not affected	Criterion not affected	Criterion not affected	Criterion not affected	Criterion not affected	Decreases (Deteriorated)	Criterion not affected	Decreases (Deteriorated)	Criterion not affected	Criterion not affected	Criterion not affected
All cogenerated electricity is exported	Criterion not affected	Criterion not affected	Increased (Deteriorated)	Increased (Improved)	Decreased (Deteriorated)	Criterion not affected	Decreases (Deteriorated)	Criterion not effected	Decreases (Deteriorated)	Increased (Improved)	Increased (Improved)	Decreased (Improved)
Increase in electricity tariff	Criterion not affected	Criterion not affected	Criterion not affected	Criterion not affected	Criterion not affected	Criterion not affected	Criterion not affected	Criterion not affected	Criterion not affected	Increased (Improved)	Increased (Improved)	Decreased (Improved)
Increase in LPG price	Criterion not affected	Criterion not affected	Criterion not affected	Criterion not affected	Criterion not affected	Criterion not affected	Criterion not affected	Criterion not affected	Criterion not affected	Decreased (Deteriorated)	Decreased (Deteriorated)	Increased (Deteriorated)

[9] Analysis of *PES* and *ES* includes the net electrical imports in the calculation.

[10] Fuel consumption increases if the entire building is considered - per household the micro-trigeneration system fuel consumption decreases.

Notwithstanding the diversity in response to the different criteria, certain conclusions on the way the various operational conditions affected the micro-trigeneration system integrated performance assessment can still be drawn:

- Apart from aspects related to a higher energy requirement (*e.g.* higher fuel consumption), for the same plant size, an increase in the useful thermal demand results in an improvement in the system's performance criteria. Considering the proposed system and the level of demand, the feasibility of such a system is heavily dependent on the magnitude of the demand which needs to be satisfied. Also, at this micro-level appropriate sizing and matching of demand-supply characteristics is particularly important, as by far increasing the thermal load is the single operating condition which mostly affects the system's performance.

- In general improving the building fabric resulted in a reduction in thermal demand which affected negatively all performance criteria, except for a reduction in fuel consumption. All other parameters including the most important and significant in assessing the micro-trigeneration system (the primary energy savings, the emission savings and the financial criteria) deteriorated with improving building fabric, although to a marginal extent compared to increasing the thermal demand by connecting to smaller sized buildings.

- Reducing the building's electrical demand by improving the electrical efficiency of household appliances did not affect the thermal performance of the micro-trigeneration system (*e.g.* fuel consumption, cycling, system efficiency *etc*.), although it did affect its electrical performance by changing how much of the cogenerated electricity was exported and how much was used to satisfy the buildings' own demand. Also in regards to electrical energy saving measures in household appliances and system performance criteria this thesis has shown that the assessment is two-fold – including and excluding net electrical imports. If net imports are excluded and only the net

performance of the micro-trigeneration system is considered, then both the primary energy and emission savings are not affected by improvements in the electrical efficiency of appliances. If net imports are included in the whole analysis then both primary energy and emission savings increase with improvements in the electrical efficiency of appliances. In terms of its financial performance the net imports are always included and especially with increasing electricity tariffs becomes an important aspect. Improving the electrical efficiency of appliances results in a decrease in the financial viability of the system.

- The plant configuration variations proposed (additional chilled water storage tank and flat plate solar water heater) did not impact significantly the micro-trigeneration system financial performance, mainly because in comparison with the cost of the CHP unit and the absorption chiller the cost of these modifications/additions was very small. Even though there were slight variations in terms of the financial performance (*PW*, *IRR* and *PP*) at the extreme ends of the assumed LPG price range, these variations were too small to be of any significance. The changes may become important for more conspicuous additions such as the use of a larger chilled water storage tank and solar water heater flat plate area, phase change storage and addition of other RES systems such as photovoltaics or micro-wind. Variations in plant configuration affected the system's energetic and environmental performance to a reasonable degree. The extent of these effects depended on the type of interaction which the proposed plant variation had with the system. For the same thermal load (same building size and fabric), the system's energetic and environmental performance improved when the plant modification resulted in a reduction in micro-trigeneration system fuel consumption (*e.g.* additional solar water heater), and deteriorated when the fuel consumption increased (*e.g.* additional chilled water storage tank).

- Based on observations made with respect to the micro-trigeneration system fuel consumption and the system's energetic and environmental performance

it can be deduced that reductions in micro-trigeneration system fuel consumption due to changes in the supply side (plant modifications) lead to an improved energetic and environmental performance. On the contrary, reductions in micro-trigeneration system fuel consumption due to changes in the demand side (reduction in thermal demand/operating hours) result in a lower system's energetic and environmental performance.

- Although from a thermal performance point of view, factors such as fuel consumption, cycling or system efficiency are not affected by how the cogenerated electricity is used, all three performance criteria are affected. Compared to a similar building and plant system scenario where the cogenerated electricity was used to cover for the building's own electrical demand and the surplus exported, exporting all the electricity and importing all the electricity from the grid at the current levels of grid efficiency and emission factor results in a decrease in both primary energy and emission savings. On the other hand, if the same principle adopted for the photovoltaic *FIT* in Malta is adopted in this case as well (*FIT* is applicable only to the exported electricity) for the selected financial parameters, that is, the *Feed in Tariff*, cost of fuel and the electricity tariff, exporting all the cogenerated electricity improves the financial feasibility of the system.

- For all scenarios, the financial performance of the system increases with increasing electricity tariffs and decreases with increasing LPG prices. The magnitude of this increase or decrease is however very dependent on the economic parameters selected.

- In general it was observed that the impact due to changing operating conditions was highest for the financial performance of the system, showing that the system's financial performance is very sensitive to changes in the selected operating conditions (and economic parameters).

- Finally, although grid network improvements and decarbonisation do not

directly affect the system's energetic and environmental performance, the reduction in energy demand required to produce the equivalent quantity and quality energy products severely affects the system's comparative performance to separate generation.

5.6.1 Maltese perspective (additional considerations)

From a Maltese perspective this research has shown that integrating micro-trigeneration in residential buildings has the potential to produce considerable primary energy and emission savings, even when included with other energy savings measures (*e.g.* improving the building fabric or improving the electrical efficiency of appliances *etc*.).

At the current levels of Maltese grid efficiency and emission factor, primary energy and emission savings for most scenarios are in the region of 40% and 45% respectively. These are considerable savings which leave little doubt that in selected Maltese dwellings, micro-trigeneration has the potential of becoming an important tool towards reducing overall energy demand and emissions, both prized objectives in the goal to reach the energy-efficiency targets set by the EU for 2020. An important fact which however must be considered is the planned improvement of the grid network. Rendering separate generation more efficient and less environmentally polluting will result in a considerable change in the energetic and environmental performance of the system. In fact, whereas at a high grid network electrical efficiency of 40%, a micro-trigeneration system will manage to retain a decent level of primary energy savings (higher than 15%), the rapid decrease observed with decreasing grid emission factor, will require different system planning considerations, including using cleaner prime-movers (*e.g.* hydrogen fed fuel cells) or CO_2 neutral fuels (*e.g.* biogas).

The system's financial viability substantially depends on the financing mechanism introduced. At the rate of 0.5 € per kWh exported and at the current LPG price and electricity tariff, the 6 household building, possibly the best suited building for the size of micro-trigeneration system investigated, has a payback period of about 6-7

years. Such a payback period would be very interesting from an investor point of view, especially when considering that the lifetime of the system is of about 25 years. For a complete study, however, other financing mechanisms (including capital costs grants, fuel tax breaks, extent of *FIT etc.*) need to be investigated before proceeding with a policy decision. In this regard this thesis provides the preparatory work required to arrive at such a policy decision.

5.7 Summary of Chapter 5

This chapter has presented and discussed the results obtained for the different scenarios investigated during this research.

The first part provided an analysis of how improving the building fabric and the electrical efficiency of appliances will affect the building's energy demand. Improving the electrical efficiency of household appliances had little effect on the thermal demand, mainly because the effect of changing electrical demand on internal heat gains due to appliances was in this case considered to be very small compared to the main thermal loads (heat loss or gain due to the heat transfer through the building fabric and ventilation). As expected efficiency improvements proved to be effective in reducing the electrical demand but this did not necessarily lead to a reduction in peak demands in individual households or small aggregation of households, primarily because instantaneous electrical demands at low levels of aggregation are more susceptible to aggregation of loads rather than individual high loads. This permits a certain degree of variability in the load profile which does not exclude peak demands from being higher in the high electrical efficiency case compared to the low efficiency case.

The second and main part of the chapter discussed the results obtained for the different micro-trigeneration system scenarios using three different assessment criteria: energetic, environmental and economic. In terms of improving building fabric, it was observed that this leads to a deterioration of the system's energetic, environmental and economic performance. Improving the building fabric results in a lower useful thermal demand which equates to a lower operating load factor of the

micro-trigeneration system. Conversely, increasing the useful thermal demand by connecting the plant system to a larger building leads to an improvement in the system's energetic, environmental and economic performance.

In terms of improving the electrical efficiency of appliances, although the thermal performance in this case is unaffected by the change in electrical demand, reducing the overall electrical demand of the building, thus including the net electrical imports results in an increase in the primary energy and emission savings. Conversely reducing the electrical demand, results in a decrease in the economic performance of the system.

On this micro-scale changes in plant configuration are primarily effective in changing the energetic and environmental performance of a system and are not so effective in improving the systems' economic performance, mainly because the cost of the modifications is small compared to the cost individual costs of the CHP unit and the absorption chiller. The comparative energetic and environmental results of the systems are heavily dependent on the alternate separate generation performance.

5.8 Chapter References

[1] *"Malta Building Regulations, Part F - Conservation of Fuel, Energy and natural Resources"* - (LN 238 of 2006). Building Regulations Office, Malta

[2] Borg, S.P., Kelly, N.J. and Rizzo, K. "*Modelling and simulating the effects of the use of insulated building fabric in a multi-story Maltese residential building"* in *Sustainable Energy 2012: The ISE Annual Conference*. 2012. Qawra, Malta

[3] Baxi-SenerTec UK (2010). DACHS Mini-CHP - Online Brochure. [Accessed: 28/03/2011]; Available from: http://www.baxi-senertec.co.uk/documents/Sales_brochure_July_2010.pdf

[4] Lin, L., Wang, Y., Al-Shemmeri, T., Ruxton, T., Turner, S., Zeng, S., Huang, J., He, Y. and Huang, X. *"An experimental investigation of a household size trigeneration"* Applied Thermal Engineering, 2007. 27: pgs. 576-585

[5] Khatri, K.K., Sharma, D., Soni, S.L. and Tanwar, D. *"Experimental investigation of CI engine operated Micro-Trigeneration system"* Applied Thermal Engineering, 2010. 30(11-12): pgs. 1505-1509

[6] Peacock, A.D. and Newborough, M. *"Effect of heat-saving measures on the CO_2 savings attributable to micro-combined heat and power (mCHP) systems in UK dwellings"* Energy, 2007. 33: pgs. 601-612

[7] *"Enemalta Corporation Annual Report 2009 and Financial Statements 2008"* - Enemalta Corporation. Marsa, Malta. [Accessed: 10/09/2011]; Available from: http://www.enemalta.com.mt/enemaltastorage/images/files/annual%20reports/annual%20report%202009%20and%20financial%20statement%202008.pdf

[8] Biezma, M.V. and San Cristóbal, J.R. "*Investment criteria for the selection of cogeneration plants - A state of the art review"* Applied Thermal Engineering, 2006. 26(5-6): pgs. 583-588

CHAPTER 6
CONCLUSION: OUTCOMES AND FUTURE WORK

6.1 Introduction

This final chapter concludes this research by giving an overview of the thesis, highlighting the main outcomes and making recommendations on possible future work which may be developed as a continuation to this thesis.

6.1.1 Overview of the thesis

This first section provides a short account of each individual chapter. It identifies the main work carried out and explains the objectives of each chapter.

Chapter 1 provides a review as how in warm climates micro-trigeneration could be developed as a tool to improve energy-efficiency in residential buildings. The chapter briefly explains the problems which have kept micro-cogeneration, and micro-trigeneration from reaching high market penetration rates and describes how existing literature on micro-trigeneration in residential buildings stops short from explaining how a system would respond to changes in its operational conditions. In this regard, this chapter explains the scope of this thesis and the methodology used to address the different research tasks. The scope of the thesis was two-fold:

i. Extend previous work done on micro-cogeneration in residential buildings to include a cooling aspect; and

ii. Make use of the building-plant models and demand data profiles developed to investigate how a residential micro-trigeneration system would perform under realistic dynamic operating conditions, subject to different operational scenarios.

In regards to the methodology, Chapter 1 explains that a combined deterministic and sensitivity analysis methodology making use of an integrated building-plant model built using the building simulation tool ESP-r, provided the most flexible and complete method to address the different research tasks of this thesis.

The second chapter, Chapter 2, explains the modelling process used to create the heat

and power demands of the building. These mainly include the modelling of the building environment (*e.g.* building geometry, fabric, shading *etc.*), the electrical demand, the internal heat gains and the domestic hot water profiles. The chapter also includes an analysis of how the various operating conditions being investigated (*e.g.* type of building fabric, building size and occupancy, appliances' energy-efficiency *etc.*) were factored in the modelling process.

Chapter 3 describes the micro-trigeneration plant developed using the building simulation tool ESP-r. The chapter makes specific reference to the basis of plant components and network design and the implementation of plant systems' control strategies. This chapter also outlines the development of a new generic dynamic model for a single-effect lithium bromide-water absorption chiller used extensively in the modelling and simulations performed.

Chapter 4 explains the type of scenarios investigated together with the assessment methodology and associated performance metrics used to assess the value of the proposed scenarios. Each particular scenario modelled was used to assess one of the individual operating conditions being investigated. Based on the data obtained from the simulations performed, the effect of the different operating conditions on the modelled micro-trigeneration system could be assessed.

Finally, Chapter 5 presents and discusses the results obtained for the different scenarios investigated in this research. The first part of the chapter is a general one and provides an analysis of how improving the building fabric and the electrical efficiency of appliances would affect the building's energy demand. The second part of the chapter discusses the results obtained for the different micro-trigeneration system scenarios using three different assessment criteria: energetic, environmental and economic.

6.2 Outcomes of the thesis

The outcomes of this thesis can be grouped in two categories. The first category describes outcomes obtained as a direct result of the modelling process. These

primarily include:

i. Improving the modelling of residential electrical loads by providing the means to generate high resolution electrical demand profiles including the effect of future energy-efficiency improvement measures. A method was developed whereby low-resolution electrical demand datasets can be used to create high-resolution demand data reflecting the effects of appliance energy-efficiency improvements. The method makes use of a three stage transformation process which first creates seasonal variations of individual monthly data, then converts the low-resolution hourly data into high-resolution minute data and finally projects the data into a high efficiency scenario reflecting improved appliance energy-efficiency.

ii. Characterisation of the thermal demand in a building through the modelling of the building characteristics and the internal heat gains. The research describes how, the characteristics of a typical Maltese multi-family residential building (including aspects such as building geometry, fabric, shading *etc*.) were modelled through the use of the building simulation tool ESP-r, and how the same building fabric and geometry were then modified to include for changes in operating conditions which could possibly impact micro-trigeneration system performance. With regards to the internal heat gains, a process leading to the modelling of high resolution internal heat gain profiles due to occupants and appliances was created by combining known occupancy and electrical demand profiles.

iii. Developing a detailed yet easy-to-calibrate model of an absorption chiller capable of capturing dynamic behaviour. The model developed in this research relies on a novel approach whereby, it can be easily calibrated as a single unit using measured data of the inlet and outlet temperatures of the three water circuits flowing in and out of the chiller, without the need for invasive measurements. The model which was built using a system of three control volumes each characterising the thermal mass corresponding to one of the water

circuits associated with the absorption chiller, specifically the chilled water, cooling water and hot water circuits can therefore be calibrated and adapted with ease for different chillers.

iv. Developing complex plant networks (representative of different micro-trigeneration plant configurations) using ESP-r. Each individual plant network was used extensively in the research to better understand how different plant configurations affect micro-trigeneration performance.

The second outcome category relates to the results on the performance characteristics obtained from the results of the different simulations performed. Chapter 5 goes into great detail in describing the individual results obtained; the following list therefore describes only the main key findings:

i. Compared to separate generation, micro-trigeneration has the potential of delivering advantageous energy and emission savings. This is especially true in countries or regions whose separate generation is neither very efficient nor clean. In the proposed scenarios the fossil fuel based micro-trigeneration system produced clear energy and emission savings with respect to procuring energy commodities by separate generation. Decarbonisation of the electricity grid will lead to the micro-trigeneration losing its energetic and environmental advantage.

ii. Improving the building fabric as expected reduces both the heating and cooling demand, although to a varying degree and depending on floor location. In terms of micro-trigeneration system performance, decreasing the useful thermal demand, equates to a lower operating load factor of the micro-trigeneration system which leads to a deterioration of the system's energetic, environmental and economic performance.

iii. Electrical efficiency improvements in household appliances proved to be effective in reducing the electrical energy consumption but may not necessarily effective in reducing peak demands in individual or small aggregation of

households. Instantaneous electrical demands at low levels of household aggregation are more susceptible to aggregation of individual loads rather than individual high loads. In terms of micro-trigeneration system performance, improving the electrical efficiency of household appliances (hence reducing the overall electrical demand of the building) leads to an improvement in the system's primary energy and annual CO_2 savings but in a reduction in the economic performance of the system.

iv. On such a micro-scale changes in plant configuration affect the energetic and environmental performance of the system but do not affect the systems' economic performance. Depending on the type of plant modification, system operation such as cycling 'On'/'Off' is severely affected.

v. Properly matching plant sizing with the building energy demand is very important. At low electricity tariffs or high fuel costs, oversizing a system may lead to the system's unfeasibility.

vi. The financial performance of the system is very sensitive to both the selected economic parameters (*FIT*, gas price, electricity tariff, capital cost *etc.*) and the level of changes in operating conditions modelled. In all scenarios general trends however were observed, where the financial performance of the system increased with increasing electricity tariffs and decreased with increasing LPG prices, although to varying degrees depending on the particular case for each scenario.

Some of the outcomes listed have already been described and published in peer reviewed papers [1-3].

6.3 Future work

Although this research provides an improvement to the existing knowledge on residential building modelling, especially in the context of micro-trigeneration, it can only be considered as a further step towards developing a complete understanding of

the subject. More work therefore needs to be done. This section suggests new avenues of research, not only in the specific context of micro-trigeneration in residential buildings, but also in a wider perspective of improving the modelling of building and plant systems components.

6.3.1 Additional scenarios

Although the selected operating conditions are representative of most of the operating conditions which might influence micro-trigeneration performance, additional conditions should also be investigated. Some of these have already been mentioned in the thesis itself. These include: using alternative CHP prime-movers, studying the effect on micro-trigeneration performance of micro-*RES* technologies which offset electrical demand (*e.g.* photovoltaics and micro-wind-turbines), the use of phase change materials in residential buildings, thermally activated cooling system operating with only a boiler and no CHP, and the use of multi-split systems.

An interesting development in residential buildings could also be the implementation of a building management system (*BMS*). As part of a series of measures aimed at improving the energy-efficiency in buildings, *BMS* might become an important tool given its capability of managing and optimizing mechanical and ventilation equipment, lighting and domestic appliances. Integrating a micro-trigeneration system within a building management system offers not only a challenge with respect to integrating the various system components, but also and especially, with respect to selecting the appropriate conditions and controls when the *BMS* should use simple mechanical (or even natural) ventilation over air conditioning. Such a system may also provide demand-supply management. This could completely change some of the characteristics obtained in this study. Modelling a micro-trigeneration system within a residential *BMS* would provide for an interesting research development.

6.3.2 Interaction between different operating conditions and the effect on micro-trigeneration

As discussed in Chapter 1, the primary scope of this research was to analyse the effect each individual operating condition had on micro-trigeneration. In practice

however, these operating conditions interact with one another creating complex supply-demand interactions with respect to their combined impact on micro-trigeneration performance. Complementary to the study could be the analysis of such interactions and their impact on micro-trigeneration performance.

6.3.3 Sensitivity to FIT and other financing mechanisms

In terms of its financial performance, this thesis has shown that the feasibility of a micro-trigeneration system is very sensitive to the selected economic parameters. Also, as discussed, the feasibility of a system heavily relies on the type of financing mechanism used.

In this thesis only one type of financing mechanism was investigated, however for a fully comprehensive study, more scenarios and permutations vis-à-vis grants on the capital costs, fuel tax rebate *etc*. are needed. Also, the sensitivity to the selected *FIT* is a very important parameter which should be thoroughly considered in any analysis leading to the establishment of the actual *FIT*.

6.3.4 Improving the modelling of high-resolution internal heat gains profiles

As discussed in Chapter 2, when modelling high-resolution internal heat gains due to appliances, an important difference compared to the modelling of the electrical demand, is the time delay effect. In this thesis it was assumed that most household appliances have a small thermal mass and that therefore this delay effect was negligible. However, in real life a household may possess a number of appliances whose thermal mass produces a noticeable time delay effect. An interesting starting point for future work is therefore to further develop this modelling method to include for appliances whose internal heat gain profiles are severely affected by this time delay effect. Moreover, contrary to this particular case, in future zero carbon or very low energy housing such a change may become significant, especially in the design of passive housing.

6.3.5 Improving the modelling of integrated building models

An important aspect in this research was the creation of a series of complex building-

plant models using the building simulation tool ESP-r. In the formulation of such models, the researcher must include for various aspects related to the full physical representation of the building-plant model, including the creation of electrical demand profiles, internal heat gains profiles, building characteristics, domestic hot water profiles, plant networks, plant controls *etc.* Including all these aspects drastically complicates the modelling process, especially when modelling at high temporal resolution. Improving the general integration of all these aspects within one single-tool is therefore an important task as it enables and facilitates the creation of detailed systems closely reflecting real-life situations.

6.3.6 Improving the absorption chiller dynamic model

Although the dynamic model of the absorption chiller modelled in this research already offers a good representation of the chiller behaviour, the accuracy of the model (and the calibration of the model to represent any other chiller) can be further improved if the model is calibrated using a larger dataset covering the whole range of working and non-working temperature ranges.

6.4 Concluding remark

This thesis has presented the main findings with regards to integrating micro-trigeneration in current and future energy-efficient buildings. It has also explored how different operating conditions will affect system performance. In doing so the research has managed not only to produce results in relation to the main research task but also to develop various tools which can be used in residential building modelling. Apart from the main findings in this thesis, it is hoped that future researchers will find these modelling tools useful in further improving and developing the current knowledge on energy performance in buildings.

6.5 Chapter References

[1] Borg, S.P. and Kelly, N.J. *"The effect of appliance energy efficiency improvements on domestic electric loads in European households"* Energy and Buildings, 2011. 43(9): pgs. 2240-2250

[2] Borg, S.P., Kelly, N.J. and Rizzo, K. *"Modelling and simulating the effects of the use of insulated building fabric in a multi-story Maltese residential building"* in *Sustainable Energy 2012: The ISE Annual Conference*. 2012. Qawra, Malta

[3] Borg, S.P. and Kelly, N.J. *"The development and calibration of a generic dynamic absorption chiller model"* Energy and Buildings, In Press, Accepted Manuscript. http://dx.doi.org/10.1016/j.bbr.2011.03.031

APPENDIX A

Equation factors for selected appliances calculated using the REMODECE Italian Datasets for use with equation (2.1) in Chapter 2. (Cont. Chapter 2)

Factors for use in equation (2.1) for dishwasher, calculated using the REMODECE Datasets [Results based on Italian dataset]

Normalised electrical energy consumption $e_{App(Dishwasher),Month(mo),Hour(ho)}$

$$e_{App(Dishwasher),Month(mo),Hour(ho)} = \left[\psi_{ho} + Amp_{ho} \sin\left(2\pi * \left(\frac{Month_{(mo)}}{12}\right) + \varphi_{ho}\right) + Rand(-\sigma_{STDEVho}, \sigma_{STDEVho})\right]$$

$Hour_{(ho)}$	Constant (ψ_{ho})	Amplitude (Amp_{ho})	Sine Phase (φ_{ho})	Standard Deviation ($\sigma_{STDEVho}$)
[0,1]	0.031	-0.048	-0.086	0.129
[1,2]	0.030	-0.043	0.037	0.129
[2,3]	0.026	-0.041	0.534	0.121
[3,4]	0.012	-0.023	0.957	0.100
[4,5]	0.017	-0.038	-0.193	0.121
[5,6]	0.017	-0.038	-0.193	0.121
[6,7]	0.050	0.029	-0.456	0.184
[7,8]	0.073	0.010	-0.415	0.164
[8,9]	0.079	0.047	-0.588	0.160
[9,10]	0.041	-0.042	-0.614	0.132
[10,11]	0.047	-0.053	-0.356	0.149
[11,12]	0.077	-0.045	-0.625	0.185
[12,13]	0.055	-0.065	-0.441	0.163
[13,14]	0.067	-0.075	-0.164	0.169
[14,15]	0.122	-0.032	-0.742	0.197
[15,16]	0.135	0.034	0.716	0.198
[16,17]	0.103	0.016	0.093	0.176
[17,18]	0.119	0.046	-0.154	0.211
[18,19]	0.100	-0.037	-1.809	0.212
[19,20]	0.065	-0.035	-0.273	0.163
[20,21]	0.109	-0.032	-0.336	0.183
[21,22]	0.170	-0.050	-1.220	0.215
[22,23]	0.139	-0.046	-1.533	0.203
[23,24]	0.071	-0.046	-0.177	0.167

Factors for use in equation (2.1) for electric oven, calculated using the REMODECE Datasets [Results based on Italian dataset]

Normalised electrical energy consumption $e_{App(Electric\ Oven),Month(mo),Hour(ho)}$

$$e_{App(Electric\ Oven),Month(mo),Hour(ho)} = \left[\psi_{ho} + Amp_{ho} \sin\left(2\pi * \left(\frac{Month_{(mo)}}{12}\right) + \varphi_{ho}\right) + Rand(-\sigma_{STDEVho}, \sigma_{STDEVho})\right]$$

$Hour_{(ho)}$	Constant (ψ_{ho})	Amplitude (Amp_{ho})	Sine Phase (φ_{ho})	Standard Deviation ($\sigma_{STDEVho}$)
[0,1]	0.000	0.000	0.000	0.000
[1,2]	0.031	0.131	0.540	0.218
[2,3]	0.000	0.000	0.000	0.000
[3,4]	0.000	0.000	0.000	0.000
[4,5]	0.000	0.000	0.000	0.000
[5,6]	0.000	0.000	0.000	0.000
[6,7]	0.044	0.085	1.396	0.218
[7,8]	0.044	0.085	1.396	0.218
[8,9]	0.054	0.140	0.578	0.241
[9,10]	0.058	0.149	0.874	0.229
[10,11]	0.115	0.297	0.794	0.333
[11,12]	0.097	0.270	0.548	0.295
[12,13]	0.106	0.231	0.529	0.267
[13,14]	0.103	0.152	0.434	0.251
[14,15]	0.061	0.187	0.606	0.236
[15,16]	0.085	0.181	0.141	0.275
[16,17]	0.101	0.046	-1.045	0.260
[17,18]	0.082	0.153	0.343	0.236
[18,19]	0.140	0.224	0.584	0.264
[19,20]	0.094	0.107	0.516	0.217
[20,21]	0.225	-0.297	1.386	0.300
[21,22]	0.267	-0.147	1.081	0.405
[22,23]	0.141	0.123	2.335	0.309
[23,24]	0.075	-0.058	2.540	0.240

Factors for use in equation (2.1) for lighting equipment, calculated using the REMODECE Datasets [Results based on Italian dataset]

Normalised electrical energy consumption $e_{App(Lights),Month(mo),Hour(ho)}$

$$e_{App(Lights),Month(mo),Hour(ho)} = \left[\psi_{ho} + Amp_{ho} \sin\left(2\pi * \left(\frac{Month_{(mo)}}{12}\right) + \varphi_{ho}\right) + Rand(-\sigma_{STDEVho}, \sigma_{STDEVho})\right]$$

$Hour_{(ho)}$	Constant (ψ_{ho})	Amplitude (Amp_{ho})	Sine Phase (φ_{ho})	Standard Deviation ($\sigma_{STDEVho}$)
[0,1]	0.041	-0.025	0.226	0.034
[1,2]	0.022	-0.006	-0.531	0.011
[2,3]	0.017	0.011	1.416	0.013
[3,4]	0.013	0.009	1.151	0.012
[4,5]	0.014	0.005	0.779	0.011
[5,6]	0.014	0.009	-0.297	0.014
[6,7]	0.019	0.012	-1.002	0.013
[7,8]	0.023	0.011	0.719	0.016
[8,9]	0.016	0.010	0.796	0.013
[9,10]	0.015	0.010	-0.178	0.011
[10,11]	0.015	0.010	-0.178	0.016
[11,12]	0.018	0.014	-0.268	0.014
[12,13]	0.009	0.008	0.174	0.008
[13,14]	0.012	0.008	0.308	0.010
[14,15]	0.011	0.008	0.245	0.008
[15,16]	0.019	0.008	0.087	0.012
[16,17]	0.027	0.004	0.070	0.016
[17,18]	0.016	0.015	0.811	0.016
[18,19]	0.014	0.011	0.843	0.011
[19,20]	0.014	0.005	0.868	0.009
[20,21]	0.019	0.002	-0.487	0.009
[21,22]	0.021	-0.005	0.644	0.008
[22,23]	0.018	-0.009	0.645	0.009
[23,24]	0.026	-0.016	0.291	0.018

Factors for use in equation (2.1) for microwave oven, calculated using the REMODECE Datasets [Results based on Italian dataset]

Normalised electrical energy consumption $e_{App(Microwave\ Oven),Month(mo),Hour(ho)}$

$$e_{App(MicrowaveOven),Month(mo),Hour(ho)} = \left[\psi_{ho} + Amp_{ho} \sin\left(2\pi * \left(\frac{Month_{(mo)}}{12}\right) + \varphi_{ho}\right) + Rand(-\sigma_{STDEVho}, \sigma_{STDEVho})\right]$$

$Hour_{(ho)}$	Constant (ψ_{ho})	Amplitude (Amp_{ho})	Sine Phase (φ_{ho})	Standard Deviation ($\sigma_{STDEVho}$)
[0,1]	0.037	0.024	-0.322	0.149
[1,2]	0.059	0.067	0.473	0.231
[2,3]	0.049	0.053	0.341	0.194
[3,4]	0.048	0.068	-0.136	0.220
[4,5]	0.058	0.043	0.107	0.212
[5,6]	0.061	0.010	1.475	0.180
[6,7]	0.099	0.057	0.190	0.200
[7,8]	0.088	-0.020	-1.396	0.174
[8,9]	0.129	0.027	-0.634	0.216
[9,10]	0.125	0.060	-1.331	0.227
[10,11]	0.050	0.044	-2.362	0.128
[11,12]	0.079	0.073	-1.271	0.188
[12,13]	0.110	0.036	-0.669	0.182
[13,14]	0.140	-0.099	-2.157	0.203
[14,15]	0.097	-0.064	-3.108	0.193
[15,16]	0.049	0.019	-3.879	0.128
[16,17]	0.043	0.026	-4.390	0.138
[17,18]	0.054	0.028	-3.889	0.152
[18,19]	0.036	-0.020	-3.105	0.119
[19,20]	0.027	-0.021	-2.857	0.114
[20,21]	0.074	0.027	-1.515	0.146
[21,22]	0.141	-0.046	-1.693	0.220
[22,23]	0.047	-0.018	-0.033	0.119
[23,24]	0.061	0.038	0.077	0.173

Factors for use in equation (2.1) for refrigerator, calculated using the REMODECE Datasets [Results based on Italian dataset]

Normalised electrical energy consumption $e_{App(Refrigerator),Month(mo),Hour(ho)}$

$$e_{App(Refrigerator),Month(mo),Hour(ho)} = \left[\psi_{ho} + Amp_{ho} \sin\left(2\pi * \left(\frac{Month_{(mo)}}{12}\right) + \varphi_{ho}\right) + Rand(-\sigma_{STDEVho}, \sigma_{STDEVho})\right]$$

$Hour_{(ho)}$	Constant (ψ_{ho})	Amplitude (Amp_{ho})	Sine Phase (φ_{ho})	Standard Deviation ($\sigma_{STDEVho}$)
[0,1]	0.264	-0.072	0.818	0.079
[1,2]	0.288	-0.071	0.540	0.069
[2,3]	0.263	-0.066	0.509	0.076
[3,4]	0.261	-0.046	0.085	0.047
[4,5]	0.257	-0.061	0.551	0.072
[5,6]	0.226	-0.037	0.029	0.045
[6,7]	0.264	-0.068	0.627	0.074
[7,8]	0.266	-0.059	0.417	0.071
[8,9]	0.217	-0.055	0.252	0.057
[9,10]	0.259	-0.059	0.699	0.075
[10,11]	0.272	-0.060	0.339	0.060
[11,12]	0.285	-0.059	0.783	0.080
[12,13]	0.270	-0.056	0.343	0.061
[13,14]	0.205	-0.052	0.589	0.065
[14,15]	0.263	-0.072	0.786	0.089
[15,16]	0.293	-0.073	1.019	0.070
[16,17]	0.258	-0.070	0.711	0.095
[17,18]	0.281	-0.058	0.636	0.059
[18,19]	0.207	-0.050	0.464	0.067
[19,20]	0.270	-0.055	0.685	0.066
[20,21]	0.270	-0.059	0.635	0.061
[21,22]	0.292	-0.068	0.534	0.071
[22,23]	0.230	-0.064	0.816	0.079
[23,24]	0.218	-0.068	1.020	0.086

Factors for use in equation (2.1) for TVs, IT and audiovisual equipment, calculated using the REMODECE Datasets [Results based on Italian dataset]

Normalised electrical energy consumption $e_{App(Television),Month(mo),Hour(ho)}$

$$e_{App(Television),Month(mo),Hour(ho)} = \left[\psi_{ho} + Amp_{ho} \sin\left(2\pi * \left(\frac{Month_{(mo)}}{12}\right) + \varphi_{ho}\right) + Rand(-\sigma_{STDEVho}, \sigma_{STDEVho})\right]$$

$Hour_{(ho)}$	Constant (ψ_{ho})	Amplitude (Amp_{ho})	Sine Phase (φ_{ho})	Standard Deviation ($\sigma_{STDEVho}$)
[0,1]	0.171	0.044	0.558	0.236
[1,2]	0.174	0.052	1.028	0.250
[2,3]	0.116	0.074	0.824	0.230
[3,4]	0.120	0.069	0.734	0.221
[4,5]	0.019	0.027	0.498	0.142
[5,6]	0.152	0.071	1.692	0.246
[6,7]	0.142	0.065	0.364	0.226
[7,8]	0.083	0.114	0.923	0.233
[8,9]	0.071	0.087	0.900	0.182
[9,10]	0.091	0.115	1.234	0.248
[10,11]	0.134	0.077	0.827	0.248
[11,12]	0.106	0.109	0.880	0.250
[12,13]	0.075	0.094	0.840	0.220
[13,14]	0.087	0.103	0.796	0.220
[14,15]	0.103	0.106	0.421	0.216
[15,16]	0.112	0.108	0.614	0.242
[16,17]	0.117	0.134	0.826	0.256
[17,18]	0.124	0.141	0.755	0.273
[18,19]	0.122	0.130	0.687	0.242
[19,20]	0.044	0.062	0.934	0.158
[20,21]	0.129	0.124	0.754	0.228
[21,22]	0.175	0.136	0.549	0.250
[22,23]	0.202	0.118	0.480	0.245
[23,24]	0.216	0.080	0.564	0.256

Factors for use in equation (2.1) for washing machine, calculated using the REMODECE Datasets [Results based on Italian dataset]

Normalised electrical energy consumption $e_{App(Washing\ machine),Month(mo),Hour(ho)}$

$$e_{App(Washing\ machine),Month(mo),Hour(ho)} = \left[\psi_{ho} + Amp_{ho} \sin\left(2\pi * \left(\frac{Month_{(mo)}}{12}\right) + \varphi_{ho}\right) + Rand(-\sigma_{STDEVho}, \sigma_{STDEVho})\right]$$

$Hour_{(ho)}$	Constant (ψ_{ho})	Amplitude (Amp_{ho})	Sine Phase (φ_{ho})	Standard Deviation ($\sigma_{STDEVho}$)
[0,1]	0.012	-0.007	-1.051	0.073
[1,2]	0.008	0.010	-0.537	0.076
[2,3]	0.007	0.005	-1.722	0.075
[3,4]	0.004	-0.009	-2.563	0.066
[4,5]	0.004	-0.009	-3.097	0.066
[5,6]	0.007	-0.011	-3.371	0.070
[6,7]	0.008	0.005	-3.854	0.070
[7,8]	0.023	0.010	-3.148	0.091
[8,9]	0.061	-0.022	-2.031	0.130
[9,10]	0.101	-0.019	-2.358	0.155
[10,11]	0.034	-0.010	-1.478	0.084
[11,12]	0.058	-0.014	-0.364	0.110
[12,13]	0.048	-0.021	-0.556	0.118
[13,14]	0.094	0.030	0.690	0.154
[14,15]	0.049	0.015	1.261	0.093
[15,16]	0.049	0.008	1.427	0.098
[16,17]	0.060	-0.014	2.838	0.131
[17,18]	0.052	0.000	1.717	0.107
[18,19]	0.036	-0.012	2.727	0.102
[19,20]	0.068	-0.030	3.190	0.139
[20,21]	0.029	-0.020	2.815	0.085
[21,22]	0.012	0.009	2.529	0.068
[22,23]	0.055	-0.022	2.321	0.135
[23,24]	0.035	-0.016	1.389	0.114

Factors for use in equation (2.1) for electric water heating equipment, calculated using the REMODECE Datasets [Results based on Italian dataset]

Normalised electrical energy consumption $e_{App(Water),Month(mo),Hour(ho)}$

$$e_{App(Water),Month(mo),Hour(ho)} = \left[\psi_{ho} + Amp_{ho} \sin\left(2\pi * \left(\frac{Month_{(mo)}}{12}\right) + \varphi_{ho}\right) + Rand(-\sigma_{STDEVho}, \sigma_{STDEVho})\right]$$

$Hour_{(ho)}$	Constant (ψ_{ho})	Amplitude (Amp_{ho})	Sine Phase (φ_{ho})	Standard Deviation ($\sigma_{STDEVho}$)
[0,1]	0.202	0.050	-0.072	0.122
[1,2]	0.157	0.043	1.355	0.116
[2,3]	0.185	-0.062	-1.081	0.144
[3,4]	0.148	-0.075	-0.681	0.129
[4,5]	0.138	-0.039	-0.053	0.119
[5,6]	0.219	-0.100	-1.128	0.197
[6,7]	0.154	-0.126	-1.281	0.216
[7,8]	0.243	-0.034	-1.530	0.211
[8,9]	0.308	0.146	0.346	0.171
[9,10]	0.220	0.109	0.940	0.127
[10,11]	0.214	0.103	0.588	0.128
[11,12]	0.163	0.104	-0.382	0.121
[12,13]	0.226	0.114	-0.137	0.121
[13,14]	0.267	0.169	0.020	0.152
[14,15]	0.162	0.109	0.211	0.103
[15,16]	0.174	0.137	-0.217	0.140
[16,17]	0.167	0.120	-0.595	0.132
[17,18]	0.199	0.066	-0.237	0.159
[18,19]	0.166	0.057	-0.196	0.147
[19,20]	0.210	0.119	-0.151	0.185
[20,21]	0.269	0.134	-0.207	0.184
[21,22]	0.219	0.125	-0.050	0.162
[22,23]	0.160	0.095	-0.215	0.134
[23,24]	0.158	0.108	-0.186	0.133

Factors for use in equation (2.1) for general consumption, calculated using the REMODECE Datasets [Results based on Italian dataset]

Normalised electrical energy consumption $e_{App(General\ Consumption),Month(mo),Hour(ho)}$

$$e_{App(General\ Conumption),Month(mo),Hour(ho)} = \left[\psi_{ho} + Amp_{ho} \sin\left(2\pi * \left(\frac{Month_{(mo)}}{12}\right) + \varphi_{ho}\right) + Rand(-\sigma_{STDEVho}, \sigma_{STDEVho})\right]$$

$Hour_{(ho)}$	Constant (ψ_{ho})	Amplitude (Amp_{ho})	Sine Phase (φ_{ho})	Standard Deviation ($\sigma_{STDEVho}$)
[0,1]	0.331	-0.062	0.870	0.202
[1,2]	0.304	-0.043	-0.116	0.192
[2,3]	0.308	-0.053	-0.422	0.190
[3,4]	0.282	-0.037	-0.225	0.155
[4,5]	0.304	-0.026	0.427	0.142
[5,6]	0.253	-0.041	1.328	0.140
[6,7]	0.145	-0.051	1.318	0.137
[7,8]	0.182	-0.044	1.426	0.174
[8,9]	0.256	0.064	-0.018	0.203
[9,10]	0.262	0.096	0.321	0.180
[10,11]	0.208	0.066	0.182	0.149
[11,12]	0.266	0.078	0.168	0.161
[12,13]	0.399	0.104	0.096	0.221
[13,14]	0.326	0.079	0.055	0.192
[14,15]	0.263	0.066	0.182	0.167
[15,16]	0.393	0.076	0.147	0.217
[16,17]	0.357	0.054	0.061	0.200
[17,18]	0.396	0.078	-0.046	0.217
[18,19]	0.327	0.100	-0.013	0.214
[19,20]	0.366	0.137	0.111	0.253
[20,21]	0.407	0.136	-0.130	0.230
[21,22]	0.363	0.105	-0.156	0.218
[22,23]	0.259	0.042	-0.660	0.160
[23,24]	0.312	0.034	-1.347	0.190

APPENDIX B

Electrical demand profiles (Cont. Chapter 2)

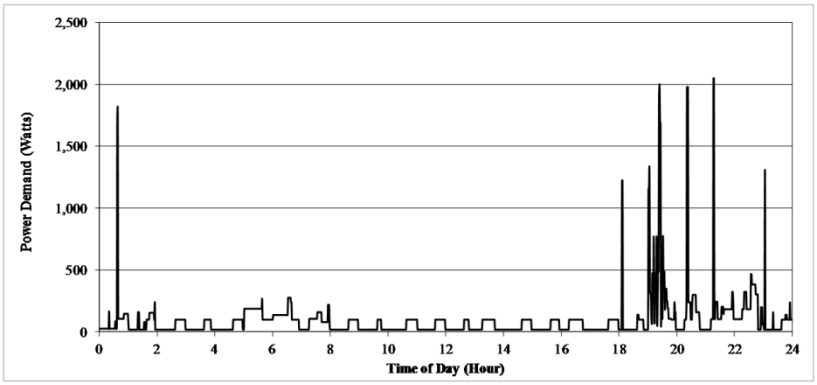

Fig. B1 - Current efficiency electrical demand profile for household 2A for a characteristic day in May – Ground floor 3 household building

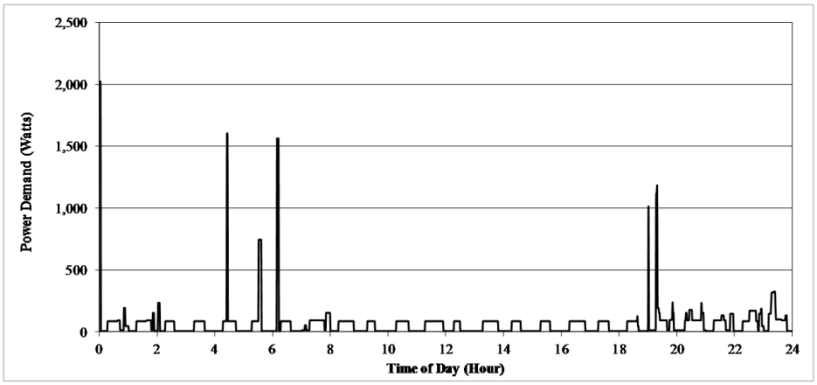

Fig. B2 - Current efficiency electrical demand profile for household 2A for a characteristic day in August – Ground floor 3 household building

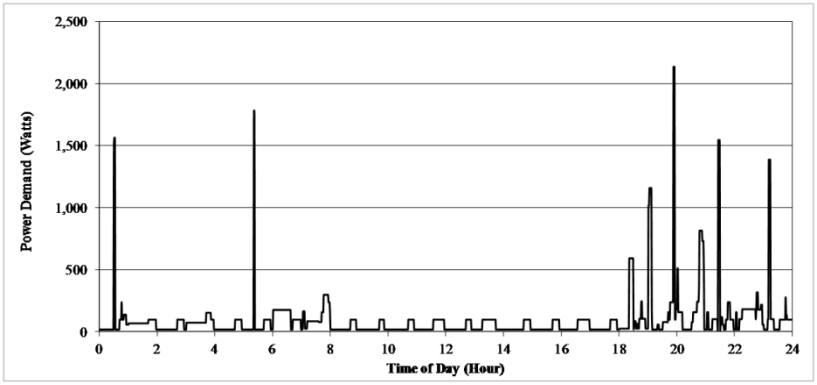

Fig. B3 - Current efficiency electrical demand profile for household 2A for a characteristic day in February – Ground floor 3 household building

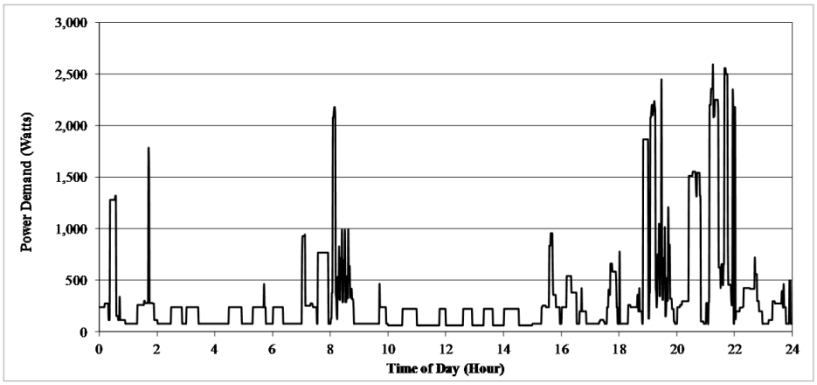

Fig. B4 - Current efficiency electrical demand profile for household 4B for a characteristic day in May – Top floor 3 household building

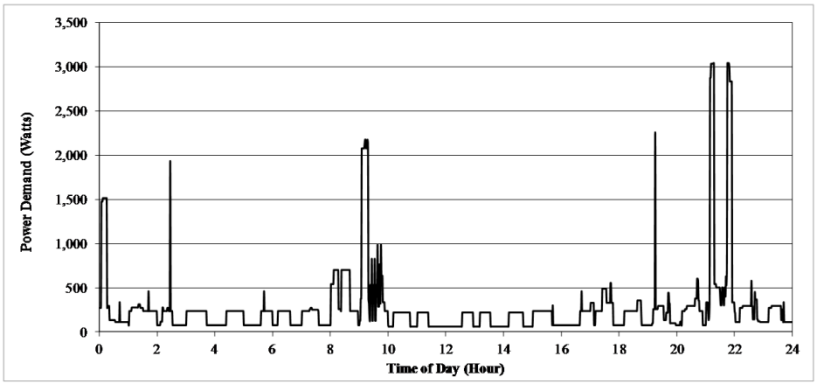

Fig. B5 - Current efficiency electrical demand profile for household 4B for a characteristic day in August – Top floor 3 household building

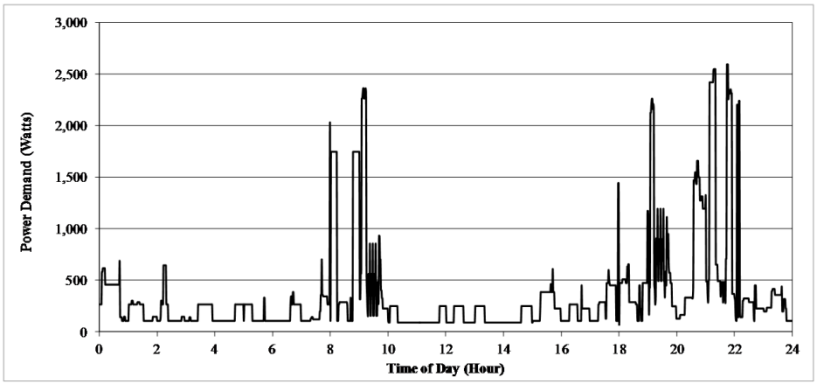

Fig. B6 - Current efficiency electrical demand profile for household 4B for a characteristic day in February – Top floor 3 household building

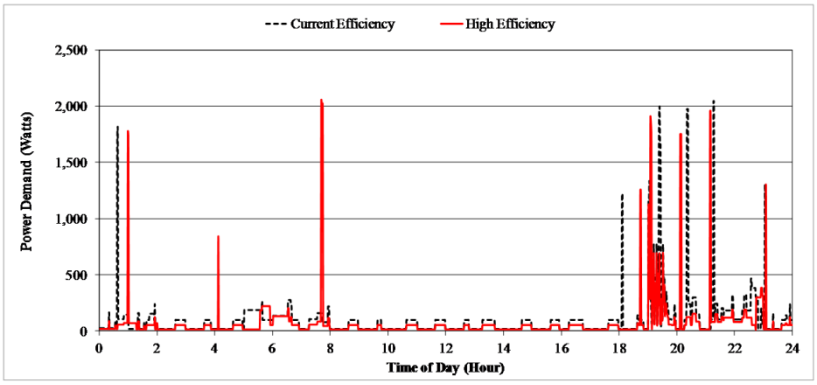

Fig. B7 - High efficiency electrical demand profile for household 2A for a characteristic day in May – Ground floor 3 household building

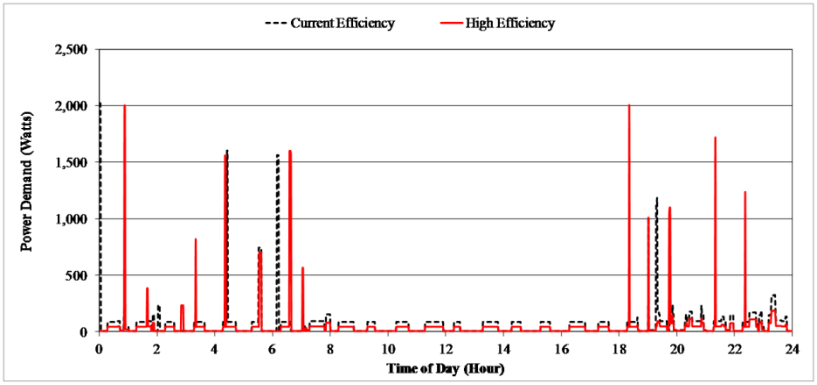

Fig. B8 - High efficiency electrical demand profile for household 2A for a characteristic day in August – Ground floor 3 household building

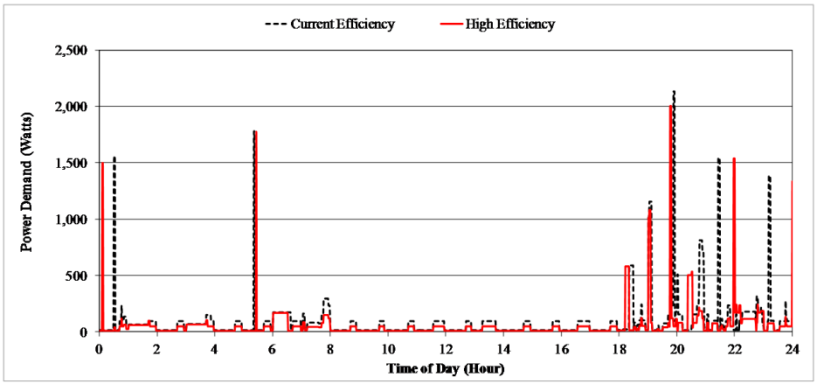

Fig. B9 - High efficiency electrical demand profile for household 2A for a characteristic day in February – Ground floor 3 household building

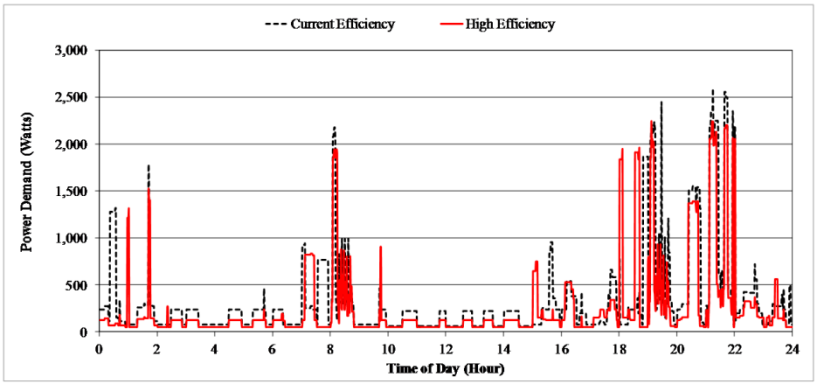

Fig. B10 - High efficiency electrical demand profile for household 4B for a characteristic day in May – Top floor 3 household building

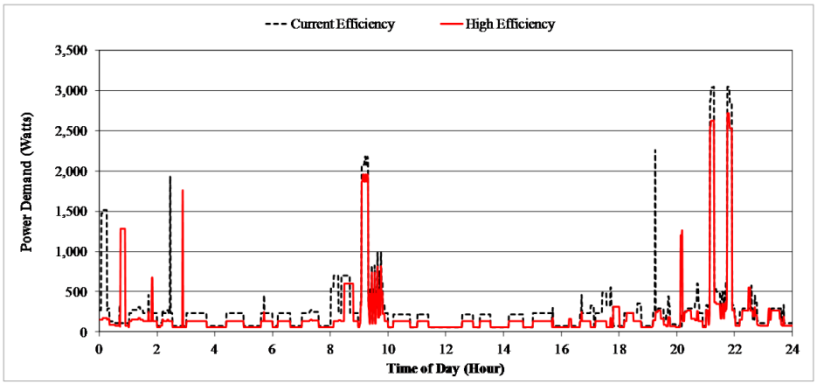

Fig. B11 - High efficiency electrical demand profile for household 4B for a characteristic day in August – Top floor 3 household building

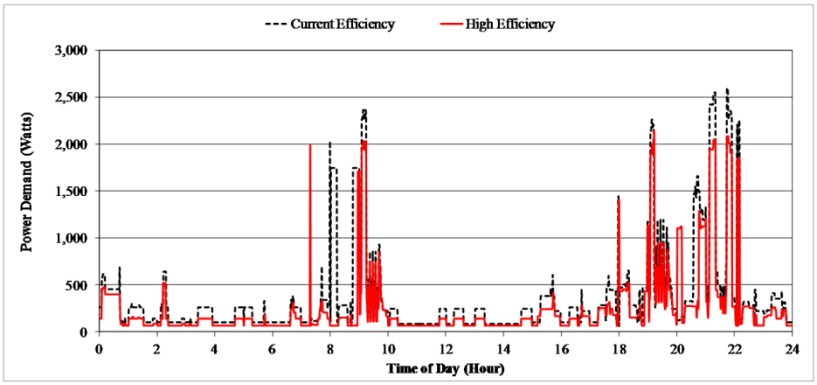

Fig. B12 - High efficiency electrical demand profile for household 4B for a characteristic day in February – Top floor 3 household building

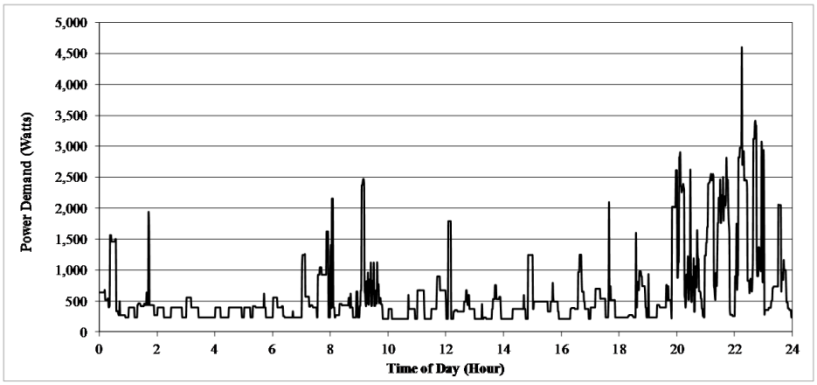

Fig. B13 - Current efficiency electrical demand profile for 2-household middle floor for a characteristic day in May – 6 household building

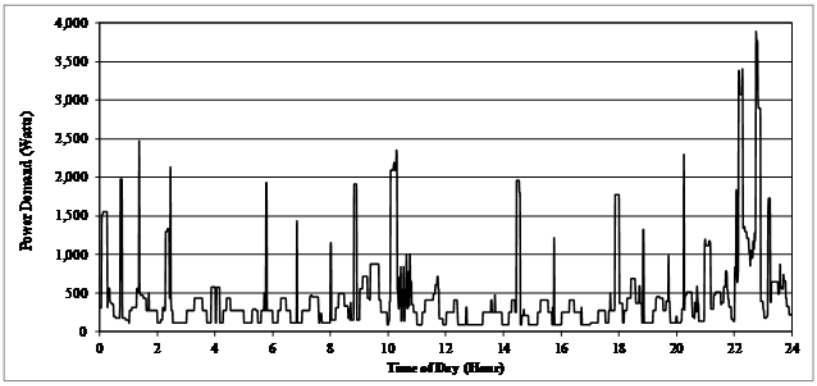

Fig. B14 - Current efficiency electrical demand profile for 2-household middle floor for a characteristic day in August – 6 household building

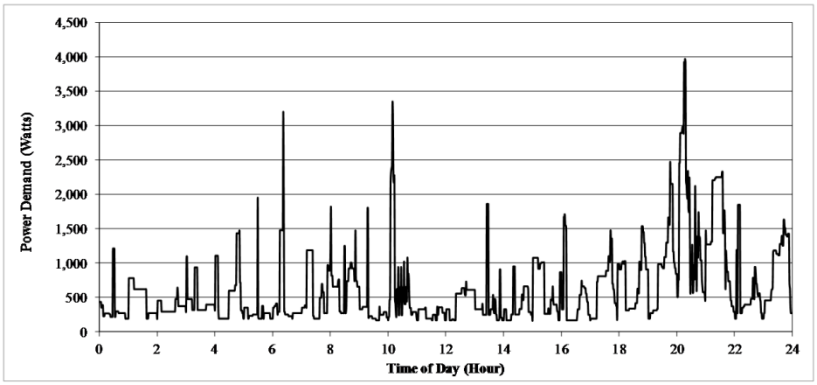

Fig. B15 - Current efficiency electrical demand profile for 2-household middle floor for a characteristic day in February – 6 household building

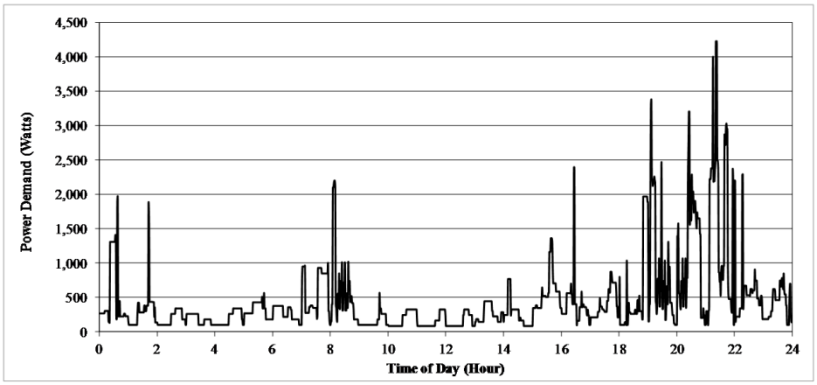

Fig. B16 - Current efficiency electrical demand profile for 2-household top floor for a characteristic day in May – 6 household building

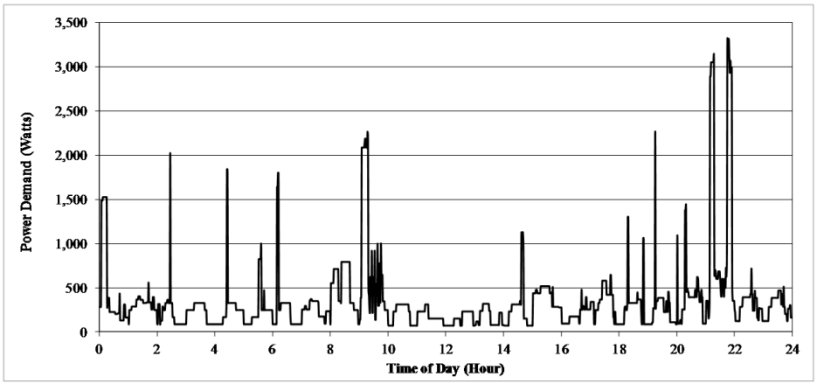

Fig. B17 - Current efficiency electrical demand profile for 2-household top floor for a characteristic day in August – 6 household building

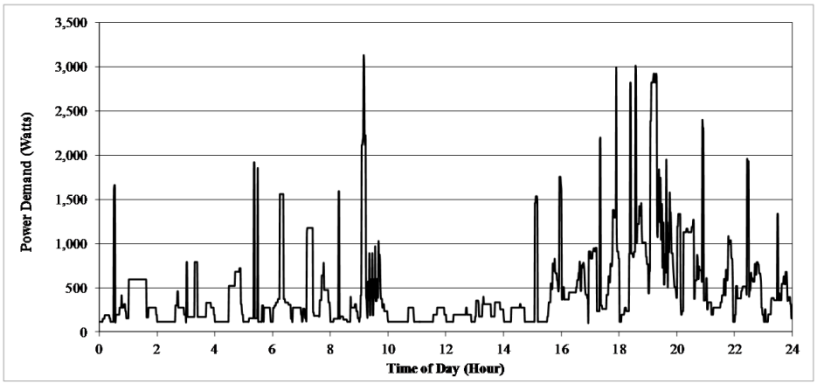

Fig. B18 - Current efficiency electrical demand profile for 2-household top floor for a characteristic day in February – 6 household building

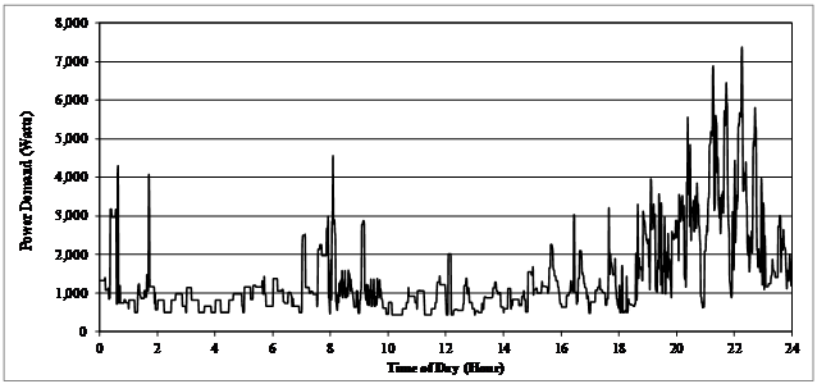

Fig. B19 - Current efficiency electrical demand profile for entire building for a characteristic day in May – 6 household building

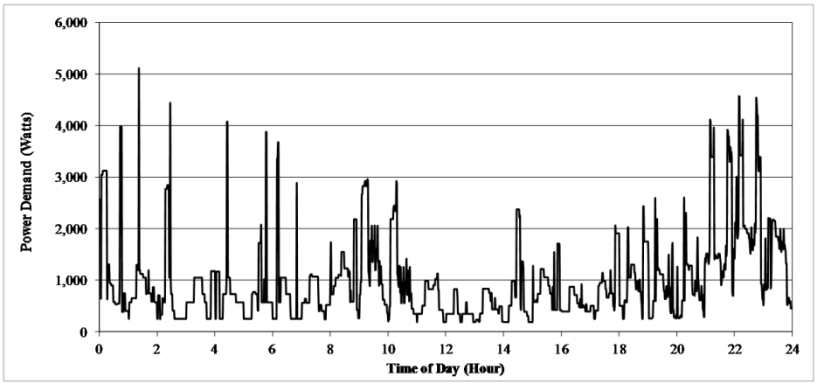

Fig. B20 - Current efficiency electrical demand profile for entire building for a characteristic day in August – 6 household building

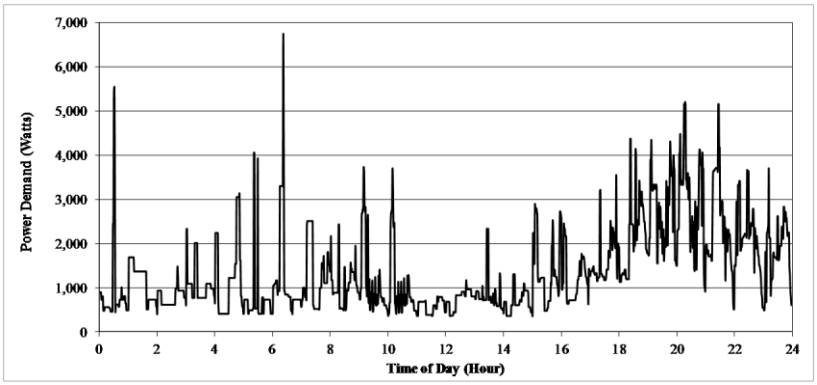

Fig. B21 - Current efficiency electrical demand profile for entire building for a characteristic day in February – 6 household building

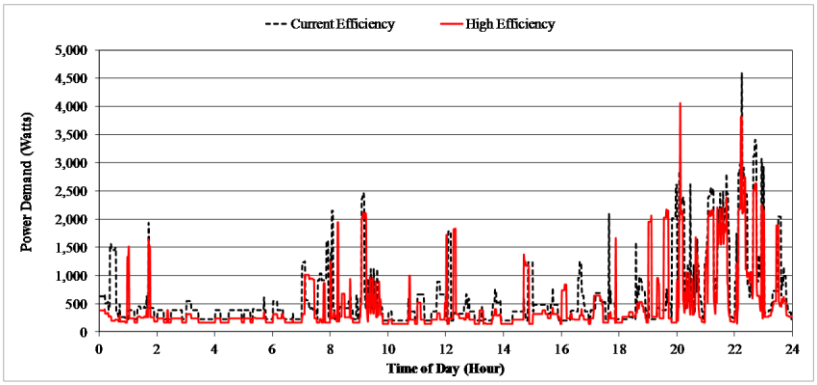

Fig. B22 - High efficiency electrical demand profile for 2-household middle floor for a characteristic day in May – 6 household building

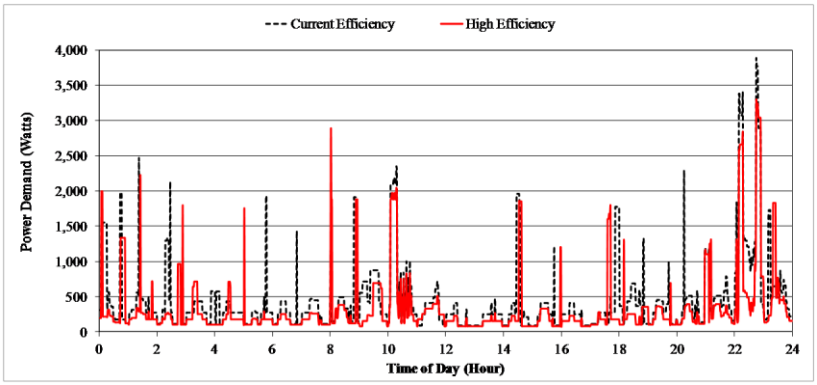

Fig. B23 - High efficiency electrical demand profile for 2-household middle floor for a characteristic day in August – 6 household building

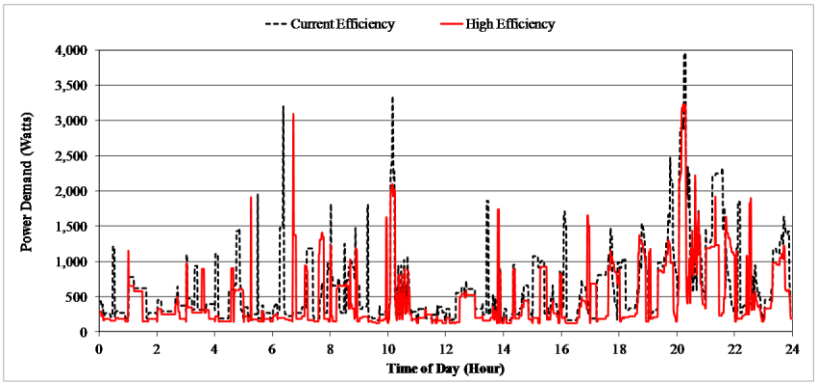

Fig. B24 - High efficiency electrical demand profile for 2-household middle floor for a characteristic day in February – 6 household building

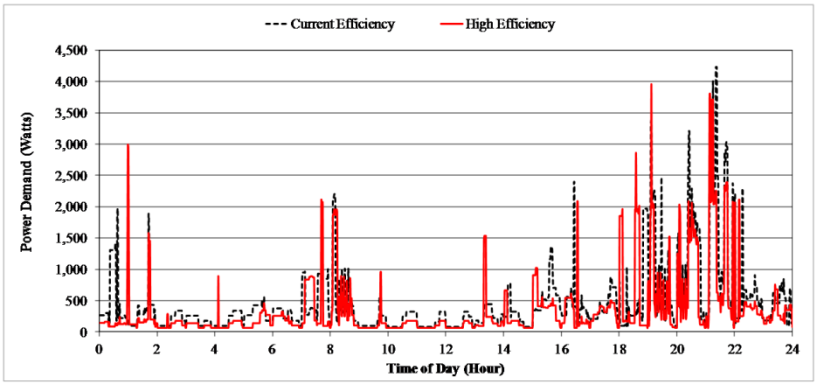

Fig. B25 - High efficiency electrical demand profile for 2-household top floor for a characteristic day in May – 6 household building

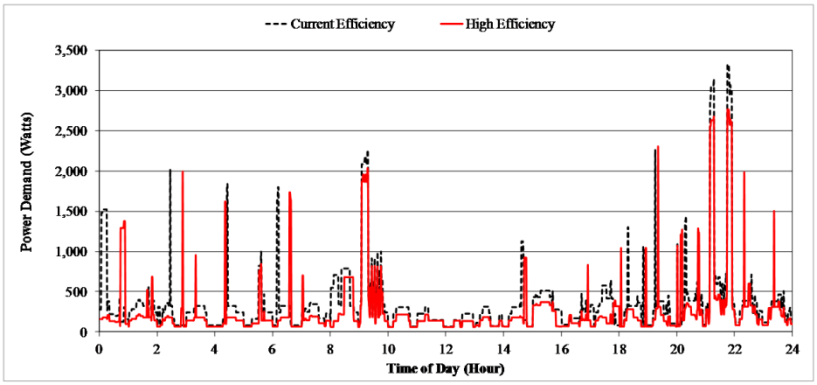

Fig. B26 - High efficiency electrical demand profile for 2-household top floor for a characteristic day in August – 6 household building

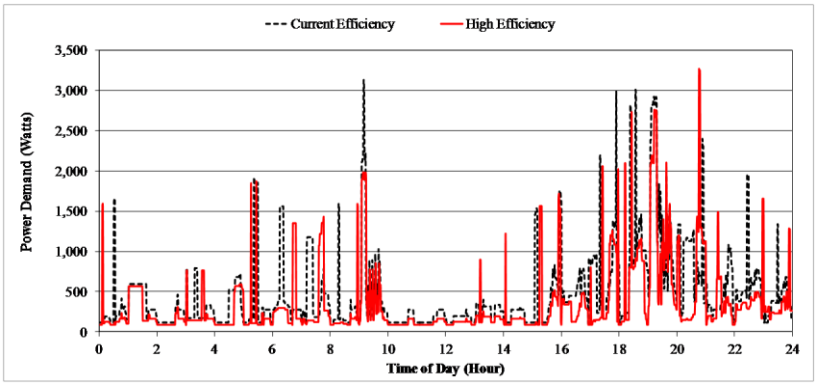

Fig. B27 - High efficiency electrical demand profile for 2-household top floor for a characteristic day in February – 6 household building

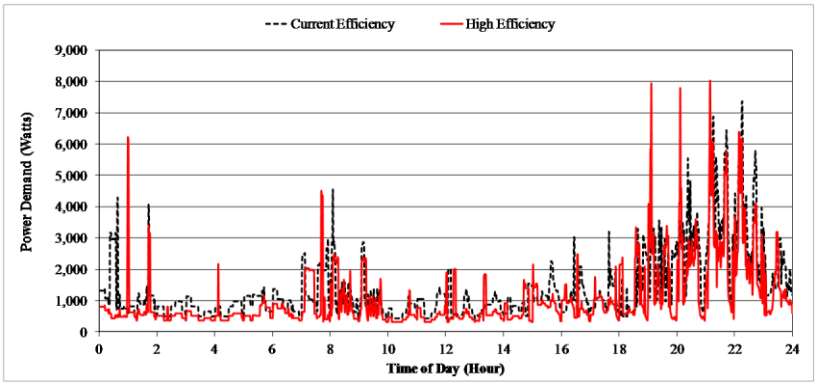

Fig. B28 - High efficiency electrical demand profile for entire building for a characteristic day in May – 6 household building

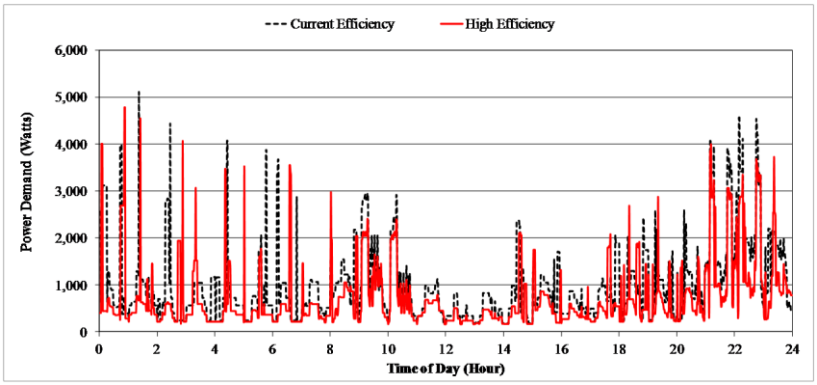

Fig. B29 - High efficiency electrical demand profile for entire building for a characteristic day in August – 6 household building

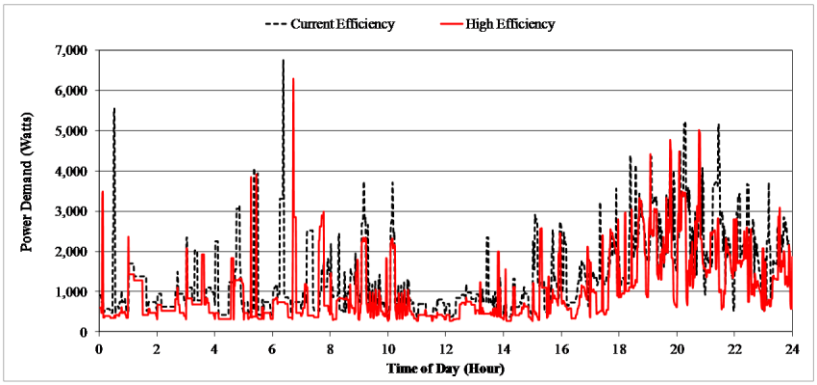

Fig. B30 - High efficiency electrical demand profile for entire building for a characteristic day in February – 6 household building

APPENDIX C

Characteristics of the main ESP-r plant components used in the modelling process

(Cont. Chapter 3)

Component ESP-r Database: Annex 42 model for ICE CHP systems

Name Assigned: CHP

Control Variable: Variable ('On' / 'Off')

Component Data:

5500.0	#1 System maximum power (W)
0.0000	#2 System minimum power (W)
80.000	#3 Maximum cooling water outlet temp (^{o}C)
2.0000	#4 Fuel type (1: liquid fuel, 2: gaseous mixture)
0.46150×10^{8}	#5 Liquid fuel heating value (J/kg):
	#6 to #19 not used
-1.0000	#20 Max rate of change in fuel flow (kg/s^{2})
-1.0000	#21 Max rate of change in power output (W/s)
53606.	#22 Power system thermal mass (J/K)
741.03	#23 Effective heat recovery UA coefficient (W/K)
13.748	#24 Effective heat loss UA coefficient (W/K)
1000.7	#25 Heat exchanger thermal mass (J/K)
90.000	#26 Start-up period duration (s)
1500.0	#27 Cool-down period duration (s)
2.0000	#28 Cool-down period mode (1: Mandatory, 2: optional)
-17.000	#29 Electric output at cool-down (W)
-17.000	#30 Net electrical output in standby mode (W)
5000.0	#31 Power output correlation minimum bound (W)
5500.0	#32 Power output correlation maximum bound (W)
60.000	#33 Cooling water temperature correlation minimum bound (^{o}C)
70.000	#34 Cooling water temperature correlation maximum bound (^{o}C)
0.0000	#35 Cooling water flow correlation minimum bound (kg/s)
100.00	#36 Cooling water flow correlation maximum bound (kg/s)
0.2700	#37 Performance map: Elec. efficiency correlation coeff. a0
0.0000	#38 Performance map: Elec. efficiency correlation coeff. a1
0.0000	#39 Performance map: Elec. efficiency correlation coeff. a2
0.0000	#40 Performance map: Elec. efficiency correlation coeff. a3
0.0000	#41 Performance map: Elec. efficiency correlation coeff. a4
0.0000	#42 Performance map: Elec. efficiency correlation coeff. a5
0.0000	#43 Performance map: Elec. efficiency correlation coeff. a6
0.0000	#44 Performance map: Elec. efficiency correlation coeff. a7
0.0000	#45 Performance map: Elec. efficiency correlation coeff. a8
0.0000	#46 Performance map: Elec. efficiency correlation coeff. a9
0.0000	#47 Performance map: Elec. efficiency correlation coeff. a10
0.0000	#48 Performance map: Elec. efficiency correlation coeff. a11

0.0000 #49 Performance map: Elec. efficiency correlation coeff. a12
0.0000 #50 Performance map: Elec. efficiency correlation coeff. a13
0.0000 #51 Performance map: Elec. efficiency correlation coeff. a14
0.0000 #52 Performance map: Elec. efficiency correlation coeff. a15
0.0000 #53 Performance map: Elec. efficiency correlation coeff. a16
0.0000 #54 Performance map: Elec. efficiency correlation coeff. a17
0.0000 #55 Performance map: Elec. efficiency correlation coeff. a18
0.0000 #56 Performance map: Elec. efficiency correlation coeff. a19
0.0000 #57 Performance map: Elec. efficiency correlation coeff. a20
0.0000 #58 Performance map: Elec. efficiency correlation coeff. a21
0.0000 #59 Performance map: Elec. efficiency correlation coeff. a22
0.0000 #60 Performance map: Elec. efficiency correlation coeff. a23
0.0000 #61 Performance map: Elec. efficiency correlation coeff. a24
0.0000 #62 Performance map: Elec. efficiency correlation coeff. a25
0.0000 #63 Performance map: Elec. efficiency correlation coeff. a26
0.6500 #64 Performance map: Thermal efficiency correlation coeff. b0
0.0000 #65 Performance map: Thermal efficiency correlation coeff. b1
0.0000 #66 Performance map: Thermal efficiency correlation coeff. b2
0.0000 #67 Performance map: Thermal efficiency correlation coeff. b3
0.0000 #68 Performance map: Thermal efficiency correlation coeff. b4
0.0000 #69 Performance map: Thermal efficiency correlation coeff. b5
0.0000 #70 Performance map: Thermal efficiency correlation coeff. b6
0.0000 #71 Performance map: Thermal efficiency correlation coeff. b7
0.0000 #72 Performance map: Thermal efficiency correlation coeff. b8
0.0000 #73 Performance map: Thermal efficiency correlation coeff. b9
0.0000 #74 Performance map: Thermal efficiency correlation coeff. b10
0.0000 #75 Performance map: Thermal efficiency correlation coeff. b11
0.0000 #76 Performance map: Thermal efficiency correlation coeff. b12
0.0000 #77 Performance map: Thermal efficiency correlation coeff. b13
0.0000 #78 Performance map: Thermal efficiency correlation coeff. b14
0.0000 #79 Performance map: Thermal efficiency correlation coeff. b15
0.0000 #80 Performance map: Thermal efficiency correlation coeff. b16
0.0000 #81 Performance map: Thermal efficiency correlation coeff. b17
0.0000 #82 Performance map: Thermal efficiency correlation coeff. b18
0.0000 #83 Performance map: Thermal efficiency correlation coeff. b19
0.0000 #84 Performance map: Thermal efficiency correlation coeff. b20
0.0000 #85 Performance map: Thermal efficiency correlation coeff. b21
0.0000 #86 Performance map: Thermal efficiency correlation coeff. b22
0.0000 #87 Performance map: Thermal efficiency correlation coeff. b23

0.0000	#88 Performance map: Thermal efficiency correlation coeff. b24
0.0000	#89 Performance map: Thermal efficiency correlation coeff. b25
0.0000	#90 Performance map: Thermal efficiency correlation coeff. b26
2.0000	#91 Cooling water loop: pump configuration (1= internal, 2= external)
0.5000	#92 Performance map: cooling water flow correlation coeff. c0
0.0000	#93 Performance map: cooling water flow correlation coeff. c1
0.0000	#94 Performance map: cooling water flow correlation coeff. c2
0.0000	#95 Performance map: cooling water flow correlation coeff. c3
0.0000	#96 Performance map: cooling water flow correlation coeff. c4
0.0000	#97 Performance map: cooling water flow correlation coeff. c5
0.0000	#98 Performance map: cooling water flow correlation coeff. c6
0.0000	#99 Performance map: cooling water flow correlation coeff. c7
0.0000	#100 Performance map: cooling water flow correlation coeff. c8
0.5000	#101 Performance map: Combustion air correlation coefficient d0 (kg/s)
0.5000	#102 Performance map: Combustion air correlation coefficient d1 (-)
0.5000	#103 Performance map: Combustion air correlation coefficient d2

Component ESP-r Database: Condensing boiler & ON/OFF control; 2 node model

Name Assigned: Auxiliary Boiler

Control Variable: Variable ('On' / 'Off')

Component Data:

50.000	#1 Component total mass (kg)
1000.0	#2 Mass weighted average specific heat (J/kgK)
0.30000×10^{-3}	#3 Full load gas firing rate if boiler on (m^3/s)
0.10000×10^{-1}	#4 Stand-by gas consumption relative to 1 (-)
0.35000×10^{8}	#5 Gas heating value at STP (J/m^3)
0.86000	#6 Full load water sided efficiency at Tc (-)
0.25000×10^{-2}	#7 Tangent of efficiency curve for Tj < Tc (1/K)
0.25000×10^{-3}	#8 Tangent of efficiency curve for Tj > Tc (1/K)
0.80000×10^{-2}	#9 Stand-by loss at Tj = Te relative to 1 (-)
0.41000×10^{-3}	#10 Tangent of stand-by loss curve (1/K)
1.0000	#11 Normalized start-stop loss (s)
95.000	#12 Upper boiler temperature limit (°C)

Component ESP-r Database: Variable Speed Domestic WCH Pump (kg/s); 1 node model

Name Assigned: Hot Water Pump 1

Control Variable: Fixed flow rate - 0.8 (kg/s)

Component Data:

5.0000	#1 Component total mass (kg)
2250.0	#2 Mass weighted average specific heat (J/kgK)
0.2000	#3 UA modulus from wall to environment (W/K)
150.00	#4 Rated total absorbed power (W)
1.0000	#5 Rated mass flow rate (kg/s)
0.7000	#6 Overall efficiency (-)

Component ESP-r Database: WCH Calorifier; 2 node model

Name Assigned: Calorifier for DHW supply

Control Variable: None

Component Data:

50.000	#1 Component total mass (kg)
4180.0	#2 Mass weighted average specific heat (J/kgK)
0.1000	#3 UA modulus (W/K)
5.0000	#4 Mass of encapsulated water in tubes (kg)
0.5000	#5 Coil internal heat transfer area (m^2)
10000.	#6 Coil internal heat transfer coefficient (W/m^2K)
8.0000	#7 Coil external heat transfer surface area (m^2)
600.00	#8 Coil external heat transfer coefficient (W/m^2K)

Component ESP-r Database: Variable Speed Domestic WCH Pump (kg/s); 1 node model

Name Assigned: DHW Pump

Control Variable: Variable flow rate defined by an external file

Component Data:

5.0000	#1 Component total mass (kg)
2250.0	#2 Mass weighted average specific heat (J/kgK)
0.2000	#3 UA modulus from wall to environment (W/K)
150.00	#4 Rated total absorbed power (W)
0.5000	#5 Rated mass flow rate (kg/s)
0.7000	#6 Overall efficiency (-)

Component ESP-r Database: Single Effect LiBr-Water Absorption Chiller; 3 node model

Name Assigned: Chiller

Control Variable: Variable (‘On’ / ‘Off’)

Component Data:

99.999	#1 Evaporator Total Mass (Fluids & Casing) (kg)
2743.2	#2 Mass weighted average specific heat of evaporator (J/kgK)
128.70	#3 Condensor/Absorber Total Mass (Fluids & Casing) (kg)
2160.9	#4 Mass weighted average specific heat of condenser and absorber (J/kgK)
66.607	#5 Generator Total Mass (kg)
1991.3	#6 Mass weighted average specific heat of generator (J/kgK)
0.6400	#7 Recovery heat exchanger effectiveness (-)
3.5000	#8 UA Modulus (W/K)
0.73500×10^{-1}	#9 p_{High} - High pressure curve coefficient (a0)
0.3429	#10 p_{High} - High pressure curve coefficient (a1)
8.0000	#11 Highest permissible high pressure (kPa)
4.0000	#12 Lowest permissible high pressure (kPa)
-0.13700×10^{-1}	#13 p_{low} - Low pressure curve coefficient (b0)
2.4020	#14 p_{low} - Low pressure curve coefficient (b1)
2.0000	#15 Highest permissible low pressure (kPa)
1.0000	#16 Lowest permissible low pressure (kPa)
40.000	#17 Working maximum outlet temp cooling water (°C)
42.000	#18 Working minimum outlet temp hot water (°C)
-6370.0	#19 CH_{Power} - Power function coefficient (c0)
304.90	#20 CH_{Power} - Power function coefficient (c1)
168.30	#21 CH_{Power} - Power function coefficient (c2)
-76.520	#22 CH_{Power} - Power function coefficient (c3)
2.5000	#23 Minimum chilled water temp protection (°C)
0.9000	#24 Circulation pump electrical efficiency (-)

Component ESP-r Database: Variable Speed Domestic WCH Pump (kg/s); 1 node model

Name Assigned: Cooling Water Pump

Control Variable: Fixed flow rate - 0.7 (kg/s)

Component Data:

5.0000	#1 Component total mass (kg)
2250.0	#2 Mass weighted average specific heat (J/kgK)
0.2000	#3 UA modulus from wall to environment (W/K)
150.00	#4 Rated total absorbed power (W)
1.0000	#5 Rated mass flow rate (kg/s)
0.7000	#6 Overall efficiency (-)

Component ESP-r Database: Variable Speed Domestic WCH Pump (kg/s); 1 node model

Name Assigned: Chilled Water Pump

Control Variable: Fixed flow rate - 0.8 (kg/s)

Component Data:

5.0000	#1 Component total mass (kg)
2250.0	#2 Mass weighted average specific heat (J/kgK)
0.2000	#3 UA modulus from wall to environment (W/K)
150.00	#4 Rated total absorbed power (W)
1.0000	#5 Rated mass flow rate (kg/s)
0.7000	#6 Overall efficiency (-)

Component ESP-r Database: Variable Speed Domestic WCH Pump (kg/s); 1 node model

Name Assigned: Hot Water Pump 2

Control Variable: Fixed flow rate - 0.8 (kg/s)

Component Data:

5.0000	#1 Component total mass (kg)
2250.0	#2 Mass weighted average specific heat (J/kgK)
0.2000	#3 UA modulus from wall to environment (W/K)
150.00	#4 Rated total absorbed power (W)
1.0000	#5 Rated mass flow rate (kg/s)
0.7000	#6 Overall efficiency (-)

Component ESP-r Database: Stratified tank with up to 100 layers; 2 node model

Name Assigned: Tank

Control Variable: None

Component Data:

0.3000	#1 Tank volume (m^3) (expanded to 0.5m^3 for the 6 households building)
1.5000	#2 Tank height (m)
-1.0000	#3 Tank perimeter (m; -1 if cylindrical)
1.5000	#4 Height of flow inlet 1 (m)
0.0000	#5 Height of flow outlet 1 (m)
0.0000	#6 Height of flow inlet 2 (m)
1.5000	#7 Height of flow outlet 2 (m)
0.1000	#8 Tank heat loss coefficient (W/m^2K)
0.0000	#9 Additional destratification conductivity (W/mK)
50.000	#10 Number of nodes
5.0000	#11 Internal time steps per simulation time step
20.000	#12 Initial temperature of tank (°C)

100.00 #13 Boiling temperature of fluid (°C)

APPENDIX D

Solving the partial differential equations

(Cont. Chapter 3)

One way to solve a partial differential equation is as mentioned by numeric approximation.

Considering the control volume *i* and its partial differential equation shown in (3.2), an explicit function can be obtained as shown in equation (D1) using a numerical approximation over a time period Δ*t*.

$$\frac{M_i \bar{c}_i (T_i^{t+\Delta t} - T_i^t)}{\Delta t} = (1-\alpha)\dot{m}_{chilled}^t c_{chilled}^t (T_{17}^t - T_i^t) + (1-\alpha)\mathrm{Q}_i^t \quad \text{- (D1)}$$

The value of α is in this case a value between 0 (fully explicit) and 1 (fully implicit).

Similarly for the control volume *i* an implicit function can be obtained as follows.

$$\frac{M_i \bar{c}_i (T_i^{t+\Delta t} - T_i^t)}{\Delta t} = (\alpha)\dot{m}_{chilled}^{t+\Delta t} c_{chilled}^{t+\Delta t} \left(T_{17}^{t+\Delta t} - T_i^{t+\Delta t}\right) + (\alpha)\mathrm{Q}_i^{t+\Delta t} \quad \text{- (D2)}$$

On adding and grouping the terms a '*Future term*' for the time period *t*+Δ*t* and the '*Present and known terms*' for the time period *t* are obtained on as shown in equation (D3).

For the *Future term:*

$$\left[-\alpha\left(\dot{m}_{chilled}^{t+\Delta t} c_{chilled}^{t+\Delta t}\right) - \frac{M_i \bar{c}_i}{\Delta t}\right] T_i^{t+\Delta t} + \alpha\left(\dot{m}_{chilled}^{t+\Delta t} c_{chilled}^{t+\Delta t}\right) T_{17}^{t+\Delta t} =$$

For the *Present and known terms:*

$$\left[(1-\alpha)(\dot{m}_{chilled}^t c_{chilled}^t) - \frac{M_i \bar{c}_i}{\Delta t}\right] T_i^t - (1-\alpha)(\dot{m}_{chilled}^t c_{chilled}^t) T_{17}^t - (\alpha)\mathrm{Q}_i^{t+\Delta t} - (1-\alpha)\mathrm{Q}_i^t \quad \text{- (D3)}$$

From equation (D3) the '*self coupling term*', the '*cross coupling term*' and the '*present and known terms*' coefficients are extracted and used in the solving process used by ESP-r.

The '*self coupling term*' is the coefficient in front of $T_i^{t+\Delta t}$, therefore:

$$\left[-\alpha\left(\dot{m}_{chilled}^{t+\Delta t}c_{chilled}^{t+\Delta t}\right)-\frac{M_i\bar{c}_i}{\Delta t}\right] \quad \text{- (D4)}$$

The '*cross coupling term*' is the term in front of $T_{17}^{t+\Delta t}$, therefore:

$$\alpha\left(\dot{m}_{chilled}^{t+\Delta t}c_{chilled}^{t+\Delta t}\right) \quad \text{- (D5)}$$

Finally the '*present and known terms*' is the entire term on the right hand side of equation (D3), therefore:

$$\left[(1-\alpha)(\dot{m}_{chilled}^{t}c_{chilled}^{t})-\frac{M_i\bar{c}_i}{\Delta t}\right]T_i^t-(1-\ \alpha)(\dot{m}_{chilled}^{t}c_{chilled}^{t})T_{17}^t-(\alpha)\mathrm{Q}_i^{t+\Delta t}-(1-\alpha)\mathrm{Q}_i^t \quad \text{- (D6)}$$

For the control volume *j* the process is similar. The terms shown in equation (D7), (D8) and (D9) are obtained for the '*self-coupling term*', the '*cross coupling term*' and the '*present and known terms*' respectively.

The '*self coupling term*' is defined in equation (D7):

$$\left[-\alpha\left(\dot{m}_{cooling}^{t+\Delta t}c_{cooling}^{t+\Delta t}\right)-\frac{M_j\bar{c}_j}{\Delta t}\right] \quad \text{- (D7)}$$

The '*cross coupling term*' is defined in equation (D8):

$$\alpha\left(\dot{m}_{cooling}^{t+\Delta t}c_{cooling}^{t+\Delta t}\right) \quad \text{- (D8)}$$

The '*present and known terms*' is defined in equation (D9):

$$\left[(1-\alpha)\left(\dot{m}_{cooling}^{t}c_{cooling}^{t}\right)-\frac{M_j\bar{c}_j}{\Delta t}\right]T_j^t-(1-\ \alpha)\left(\dot{m}_{cooling}^{t}c_{cooling}^{t}\right)T_{13}^t-(\alpha)\mathrm{Q}_j^{t+\Delta t}-(1-\alpha)\mathrm{Q}_j^t \quad \text{- (D9)}$$

Finally, for the control volume *g* the coefficients for the '*self-coupling term*', the '*cross coupling term*' and the '*present and known terms*' obtained using a similar process are shown in equation (D10), (D11) and (D12) respectively.

The '*self coupling term*' is defined in equation (D10):

$$\left[-\alpha\left(\dot{m}_{hot}^{t+\Delta t} c_{hot}^{t+\Delta t} + UA^{t+\Delta t}\right) - \frac{M_g \bar{c}_g}{\Delta t}\right] \quad \text{- (D10)}$$

The '*cross coupling term*' is defined in equation (D11):

$$\alpha\left(\dot{m}_{hot}^{t+\Delta t} c_{hot}^{t+\Delta t}\right) \quad \text{- (D11)}$$

The '*present and known terms*' is defined in equation (D12):

$$\left[(1-\alpha)(\dot{m}_{hot}^{t} c_{hot}^{t} + UA^{t}) - \frac{M_g \bar{c}_g}{\Delta t}\right] T_g^t$$
$$-(1-\alpha)(\dot{m}_{hot}^{t} c_{hot}^{t}) T_{11}^{t} - (\alpha)\mathrm{Q}_g^{t+\Delta t} - (1-\alpha)\mathrm{Q}_g^{t} - (\alpha) UA^{t+\Delta t} T_{env}^{t+\Delta t} - (1-\alpha) UA^{t} T_{env}^{t} \quad \text{- (D12)}$$

APPENDIX E

Absorption chiller plant component sub-routine code developed in ESP-r (Cont. Chapter 3) Actual code is in bold, comments are in normal font.

```
C ********** CMP73C **********************************************

C CMP73C simulates plant component IPCOMP with plant db code 730 i.e.
C 3 node (ISV=20) single-effect LiBr-water absorption chiller fed by hot water.
.
C The plant component simulates the performance of the three streams flowing
C into the chiller. The nodes represent respectively the thermal masses effected
C by the individual streams: Node 1 (i) represents the thermal mass effected
C by the chilled water stream, Node 2 (j) represents the thermal mass effected
C by the cooling water stream and, Node 3 (g) the thermal mass effected by
C the hot water stream.

C Matrix equation coefficients COUT (in order: self-coupling, cross-
C coupling, and present-time coefficients) for energy balance (ISTATS=1),
C 1st phase mass balance (ISTATS=2), or 2nd phase mass (ISTATS=3)

C  ADATA:  1 Evaporator total mass (kg)
C         2 Mass weighted average specific heat of evaporator (J/kgK)
C         3 Condenser and absorber total mass (kg)
C         4 Mass weighted average specific heat of condenser and absorber (J/kgK)
C         5 Generator total mass (kg)
C         6 Mass weighted average specific heat of generator (J/kgK)

C  BDATA:  1 Recovery heat exchanger effectiveness (-)
C         2 UA Modulus (W/K)
C         3 High pressure curve coefficient (a0)
C         4 High pressure curve coefficient (a1)
C         5 Highest permissible high pressure (kPa)
C         6 Lowest permissible high pressure (kPa)
C         7 Low pressure curve coefficient (b0)
C         8 Low pressure curve coefficient (b1)
C         9 Highest permissible low pressure (kPa)
C         10 Lowest permissible low pressure (kPa)
C         11 Working maximum outlet temperature cooling water (Deg C)
C         12 Working minimum outlet temperature hot water (Deg C)
C         13 Power function coefficient (d0)
C         14 Power function coefficient (d1)
C         15 Power function coefficient (d2)
C         16 Power function coefficient (d3)
```

```
C               17 Minimum chilled water temperature protection (Deg C)
C               18 Circulation pump electrical efficiency (-)

C  CDATA:  1 ON/OFF Control Signal (-)

C  PCDATF/P
C               1 Holds chiller actual ON/OFF state (-)

          SUBROUTINE CMP73C(IPCOMP,COUT,ISTATS)

#include "plant.h"
#include "building.h"

      COMMON/OUTIN/IUOUT,IUIN
      COMMON/SHOUT/ICOUT
      COMMON/TC/ITC,ICNT
      COMMON/TRACE/ITCF,ITRACE(MTRACE),IZNTRC(MCOM),ITU

      COMMON/SIMTIM/IHRP,IHRF,IDYP,IDYF,IDWP,IDWF,NSINC,ITS
      COMMON/Pctime/TIMSEC
      COMMON/PTIME/PTIMEP,PTIMEF
      COMMON/PCTC/TC(MPCOM)

      COMMON/PCEQU/IMPEXP,RATIMP
      COMMON/PITER/MAXITP,PERREL,PERTMP,PERFLX,PERMFL,itrclp,
     &         ICSV(MPNODE,MPVAR),CSVI(MPNODE,MPVAR)

      COMMON/C9/NPCOMP,NCI(MPCOM),CDATA(MPCOM,MMISCD)
      COMMON/C10/NPCON,IPC1(MPCON),IPN1(MPCON),IPCT(MPCON),
     &        IPC2(MPCON),IPN2(MPCON),PCONDR(MPCON),PCONSD(MPCON,2)

      COMMON/C12PS/NPCDAT(MPCOM,9),IPOFS1(MCOEFG),
     &        IPOFS2(MCOEFG,MPVAR)
      COMMON/PDBDT/ADATA(MPCOM,MADATA),BDATA(MPCOM,MBDATA)
      COMMON/PCVAL/CSVF(MPNODE,MPVAR),CSVP(MPNODE,MPVAR)
      COMMON/PCVAR/PCTF(MPCON),PCRF(MPCON),PUAF(MPNODE),
     &         PCQF(MPNODE),PCNTMF(MPCOM),
     &         PCTP(MPCON),PCRP(MPCON),PUAP(MPNODE),PCQP(MPNODE),
     &         PCNTMP(MPCOM)
```

```
      COMMON/PCOND/CONVAR(MPCON,MCONVR),ICONTP(MPCON),
     &          ICONDX(MPCOM,MNODEC,MPCONC)

      COMMON/PCDAT/PCDATF(MPCOM,MPCDAT),PCDATP(MPCOM,MPCDAT)
      COMMON/PCRES/QDATA(MPCOM),PCAOUT(MPCOM,MPCRES),napdat(mpcom)

      COMMON/WRNOFF/IWMOFF

      REAL       QDATA,PCAOUT
      INTEGER  napdat

      PARAMETER (SMALL=1.0E-15)
      REAL       COUT(MPCOE)
      Logical      closea
      character outs*124


C Values used throughout the calculations
      REALzmref, zmwk, zmst, f, XST, XWK,
     &          T1, T3, T4, T5, T7, T8, T10,
     &          h1, h2, h3, h4, h5, h7, h8, h10,
     &          zlPst, Pscst, GST, DST, COP,
     &          zlPwk, Pscwk, GWK, DWK, EEPump,
     &          rB, rE, rF, rG, rD, Wpump, ActPow,
     &          Phigh, Plow, ChPow


C Trace output
      IF(ITC.GT.0.AND.NSINC.GE.ITC.AND.NSINC.LE.ITCF.AND.
     &   ITRACE(37).NE.0) WRITE(ITU,*) 'Entering subroutine CMP73C'


C Check control data for relevant balance type
      IF(ISTATS.EQ.1.AND.
     &   (CDATA(IPCOMP,1).LT.0..OR.CDATA(IPCOMP,1).GT.1.)) THEN
       CALL DAYCLK(IDYP,PTIMEF,IUOUT)
       WRITE(outs,*) ' CMP73C: invalid control data for component ',
     &              IPCOMP,' : ',CDATA(IPCOMP,1)
       call edisp(iuout,outs)
```

```
      call edisp(iuout,' CMP73C: unresolvable error.')
      call epwait
      call epagend
      STOP
     END IF


C Initialize pointers to inter-connection(s) ICON, and node(s) INOD
C Chilled water inlet
      ICON1=ICONDX(IPCOMP,1,1)
C Cooling water inlet
      ICON2=ICONDX(IPCOMP,2,1)
C Hot water inlet
      ICON3=ICONDX(IPCOMP,3,1)
C Chilled water outlet
      INOD1=NPCDAT(IPCOMP,9)
C Cooling water outlet
      INOD2=NPCDAT(IPCOMP,9)+1
C Hot water outlet
      INOD3=NPCDAT(IPCOMP,9)+2


C Generate coefficients for energy balance equation
    IF(ISTATS.EQ.1) THEN

C The energy balance equations are partly based on work by Mehrabian
C M.A et al., "Thermodynamic Modelling of a single-effect lithium bromide-
C water absorption refrigeration cycle" 2005, Proc. IMechE, Vol.219 Part E,
C Journal of Process Mechanical Engineering

C Empirical calculations for cycle pressures and power were found using
C experimental data supplied by Edo Wiemken (Fraunhofer-Institut für
C Solare Energiesysteme ISE) and Martin Helm (Bavarian Centre for Applied
C Energy Research ZAE Bayern). Both datasets were based on measurements
C done on a Sonnenklima Sun Inverse 10kW rated absorption chiller.

C Index of numbering used throughout this sub-routine and the nomenclature used:

C Point 1 is the exit point of the weak solution from the absorber
```

C and the inlet point into the solution circulation pump.

C Point 2 is the exit point of the weak solution from the solution
C circulation pump and the inlet point into the solution recovery heat exchanger.

C Point 3 the exit point of the weak solution from the solution
C recovery heat exchanger and the inlet point into the generator.

C Point 4 is the exit point of the strong solution from the generator
C and the inlet point into the solution recovery heat exchanger.

C Point 5 is the exit point of the strong solution from the solution
C recovery heat exchanger and the inlet point into the solution expansion valve.

C Point 6 is the exit point of the strong solution from the solution
C expansion valve and the inlet point into the absorber.

C Point 7 is the exit point of the refrigerant from the generator
C and the inlet point into the condenser.

C Point 8 is the exit point of the refrigerant from the condenser
C and the inlet point into the expansion valve.

C Point 9 is the exit point of the refrigerant from the expansion
C valve and the inlet point into the evaporator.

C Point 10 is the exit point of the refrigerant from the evaporator
C and the inlet point into the absorber.

C Point 11 is the inlet point of the hot water in the generator.
C point 12 is the exit point of the hot water from the generator.

C Point 13 is the inlet point of the cooling water into the chiller.
C Point 16 is the exit point of the cooling water from the chiller.

C Point 17 is the inlet point of the chilled water into the evaporator
C Point 18 is the exit point of the chilled water from the evaporator.

C XST is the solution concentration (%) in the strong solution branch,

C downstream from the generator. (Assumption: XST=X4=X5=X6)

C XWK is the solution concentration (%) in the weak solution branch,
C upstream to the generator. (Assumption: XWK=X1=X2=X3)

C zmref is the mass flow rate (kg/s) of the refrigerant
C zmref=m7=m8=m9=m10
C zmwk is the mass flow rate (kg/s) inside the weak solution branch
C zmwk=m1=m2=m3
C zmst is the mass flow rate (kg/s) inside the strong solution branch
C zmst=m4=m5=m6

C First initialize UA modulus (for calculation of containment heat loss)

```
UA=BDATA(IPCOMP,2)
call eclose(PCNTMF(IPCOMP),-99.00,0.001,closea)
IF(closea) UA=0.
```

C Mark the points which will be used for further calculations and which
C therefore require first to be iterated.
C Outlet chilled water temperature

```
ICSV(INOD1,1)=1
CSVI(INOD1,1)=CSVF(INOD1,1)
```

C Outlet cooling water temperature

```
ICSV(INOD2,1)=1
CSVI(INOD2,1)=CSVF(INOD2,1)
```

C Outlet hot water temperature

```
ICSV(INOD3,1)=1
CSVI(INOD3,1)=CSVF(INOD3,1)
```

C Establish whether chiller is on or off (i.e. 1 or 0)

```
IONOFF=int(CDATA(IPCOMP,1))
```

C Anti-Freeze Protection - Conditional to ensure that chilled water outlet
C temperature does not go below freezing. Chiller shuts down when chilled
C water temperature falls below minimum temperature.

```
      IF(CSVF(INOD1,1).LE.BDATA(IPCOMP,17)) IONOFF=0


C Calculate the high pressure (Phigh) which is a function of hot water
C inlet temperature calculated empirically
C Phigh = a0*(Hot Water Inlet Temp) + a1
      Phigh = (BDATA(IPCOMP,3))*(CONVAR(ICON3,1)) + BDATA(IPCOMP,4)

C Limits of High Pressure
C Higher Limit
      If (Phigh.GE.BDATA(IPCOMP,5))Then
            Phigh=BDATA(IPCOMP,5)
      Else
            Phigh=Phigh
      End If
C Lower Limit
      If (Phigh.LE.BDATA(IPCOMP,6))Then
            Phigh=BDATA(IPCOMP,6)
      Else
            Phigh=Phigh
      End If


C Calculate the low pressure (Plow) which is a function of hot water
C inlet temperature calculated empirically
C Plow = b0*(Hot Water Inlet Temp) + b1
      Plow = (BDATA(IPCOMP,7))*(CONVAR(ICON3,1)) + BDATA(IPCOMP,8)

C Limits of Low Pressure
C Higher Limit
      If (Plow.GE.BDATA(IPCOMP,9))Then
            Plow=BDATA(IPCOMP,9)
      Else
            Plow=Plow
      End If
C Lower Limit
      If (Plow.LE.BDATA(IPCOMP,10))Then
            Plow=BDATA(IPCOMP,10)
      Else
```

```
            Plow=Plow
        End If


C Calculate the saturation temperatures T8 (DegC) and T10 (DegC) inside
C the condenser and evaporator respectively using the calculated
C saturation pressure (kPa) inside the two components. Calculations
C based on Revised Release on the IAPWS Industrial Formulation 1997
C for the Thermodynamic Properties of Water and Steam [International
C Association for the Properties of Water and Steam], 2007 - Chapter 8
C - Equations for Region 4. Valid for 0.6 < Psat (kPa) < 100

C Starting with T8
C Calculate rB
        rB=(Phigh/1000)**0.25
C Using rB, calculate constants rE, rF and rG
        rE=(rB**2)-(17.073846*rB)+(14.915109)
        rF=(1167.052415*rB**2)+(12020.8247*rB)-(4823.265376)
        rG=(405113.405442)-(724213.16703*rB**2)-(3232555.03223*rB)
C Using the Constants rE, rF and rG calculate rD
        rD=(2*rG)/((-rF)-(((rF**2)-(4*rE*rG))**0.5))
C Finally Calculate the Temperature in Deg C
        T8=(((650.175348 + rD)-((((650.175348 + rD)**2) -
     &  (4*(-0.238555 + (650.175348*rD))))**0.5))/2)-273.15


C For T10
C Calculate rB
        rB=(Plow/1000)**0.25
C Using rB, calculate constants rE, rF and rG
        rE=(rB**2)-(17.073846*rB)+(14.915109)
        rF=(1167.052415*rB**2)+(12020.8247*rB)-(4823.265376)
        rG=(405113.405442)-(724213.16703*rB**2)-(3232555.03223*rB)
C Using the Constants rE, rF and rG calculate rD
        rD=(2*rG)/((-rF)-(((rF**2)-(4*rE*rG))**0.5))
C Finally Calculate the Temperature in Deg C
        T10=(((650.175348 + rD)-((((650.175348 + rD)**2) -
     &  (4*(-0.238555 + (650.175348*rD))))**0.5))/2)-273.15
```

```
C Calculate T1 (DegC): T1 = ((T16-T13)/2)*1.275 + T13
C Approach temperature value (1.275) derived from Mehrabian M.A et al,
C "Thermodynamic Modelling of a single-effect lithium bromide-water
C absorption refrigeration cycle" 2005, Proc. IMechE, Vol.219 Part E
C Journal of Process Mechanical Engineering and reflects the difference
C due the approach point.
C For other absorption chillers this may be higher or lower.
      T1=((CSVF(INOD2,1)-CONVAR(ICON2,1))/2)*1.275 +
     &  CONVAR(ICON2,1)

C Set Maximum and Minimum Limits to T1
C These limits are set to ensure that T1 is iterable later on in the
C process leading to finding the concentration.
C Conditional to ensure that minimum T1 is higher than the cooling water
C inlet temperature.
      If(T1.LE.CONVAR(ICON2,1))Then
            T1 = CONVAR(ICON2,1)
      Else
            T1 = T1
      End If
C Conditional to ensure that maximum T1 is not higher than the working
C maximum cooling water outlet temperature.
      If(T1.GE.BDATA(IPCOMP,11))Then
            T1 = BDATA(IPCOMP,11)
      Else
            T1 = T1
      End If


C Calculate T4 (DegC): T4 = 0.95*T12.
C Approach temperature value (0.95) derived from Mehrabian M.A et al,
C "Thermodynamic Modelling of a single-effect lithium bromide-water
C absorption refrigeration cycle" 2005, Proc. IMechE, Vol.219 Part E
C Journal of Process Mechanical Engineering and reflects the difference
C due the approach point.
C For other absorption chillers this may be higher or lower.
      T4 = 0.95*CSVF(INOD3,1)
```

C Set Maximum and Minimum Limits to T4

C These limits are set to ensure that T1 is iterable later on in the

C process of finding the concentration.

C Conditional to ensure that maximum T4 is lower than the hot

C source highest temperature.

```
If(T4.GE.CONVAR(ICON3,1)) Then
        T4 = CONVAR(ICON3,1)
Else
        T4 = T4
End If
```

C Conditional to ensure that maximum T4 is not lower than the working

C minimum hot water outlet temperature.

```
If(T4.LE.BDATA(IPCOMP,12)) Then
        T4 = BDATA(IPCOMP,12)
Else
        T4 = T4
End If
```

C Calculate T5: T5 = T4 - EffRecHX*(T4-T2)

C But since T2=T1; (no change in temperature is assumed to occur in

C the pump) T5 = T4 - EffRecHX*(T4-T1)

```
T5=T4-(BDATA(IPCOMP,1))*(T4-T1)
```

C Calculate concentration of the strong solution leaving generator and

C entering the absorber. In order to find the concentration an iteration

C is performed whereby the known value of Phigh is compared with Pscst,

C the pressure calculated using an iteration based on known temperature

C and concentration value.

C Iteration based on finding the Dew Point Temperature (DST) [Kaita

C "Thermodynamic properties of lithium bromide and water solutions

C at high temperatures" 2001. International Journal of Refrigeration

C 24, 374-390] valid for LiBr concentrations between 40% < X < 65%; and

C Vapour Pressure Pscst [McNeely, L.A. 1979 "Thermodynamic Properties

C of Aqueous Solutions of Lithium Bromide" ASHRAE Trans., Vol.85, PT.1

C pgs 413-4381]. Start by assuming a concentration of XST=40

```
      XST=40

10    DST=-(9.133128) + (0.9439697*T4) - (7.32435E-05*(T4**2))
     &  -(0.4759724*(XST - 40)) - (2.882015E-03*(XST - 40)*(T4))
     &  -(1.55653E-05*(XST - 40)*(T4**2)) -
     &  (5.638571E-02*((XST - 40)**2)) -
     &  (1.345453E-04*((XST - 40)**2)*(T4)) +
     &  (1.992657E-06*((XST - 40)**2)*(T4**2)) +
     &  (1.108418E-03*((XST - 40)**3)) +
     &  (5.852133E-07*((XST - 40)**3)*(T4)) -
     &  (3.924205E-08*((XST - 40)**3)*(T4**2))

      zlPst =(7.05)-(1603.54)/(273.15 + DST)-
     &  (104095.5)/((273.15 + DST)**2)
      Pscst = 10**(zlPst)
      GST = Pscst-Phigh

      If(GST.GE.0.AND.GST.LE.0.005)Then
            XST=XST
      Else
            XST=XST+0.001
            GoTo 10
       End If
```

C Calculate concentration of the weak solution leaving absorber and
C entering the generator. In order to find the concentration an
C iteration is performed whereby the known value of Plow is compared
C with Pscwk, the pressure calculated using an iteration based on known
C temperature and concentration value.

C Iteration based on finding the Dew Point Temperature (DWK) [Kaita
C "Thermodynamic properties of lithium bromide and water solutions
C at high temperatures" 2001. International Journal of Refrigeration
C 24, 374-390] valid for LiBr concentrations between 40% < X < 65%; and
C Vapour Pressure Pscwk [McNeely, L.A. 1979 "Thermodynamic Properties
C of Aqueous Solutions of Lithium Bromide" ASHRAE Trans., Vol.85, PT.1
C pgs 413-434]. Start by assuming a concentration of XWK=40

```
      XWK=40

20    DWK=-(9.133128) + (0.9439697*T1) - (7.32435E-05*(T1**2))
     &  -(0.4759724*(XWK - 40)) - (0.002882015*(XWK - 40)*(T1))
     &  -(1.55653E-05*(XWK - 40)*(T1**2)) -
     &  (5.638571E-02*((XWK - 40)**2)) -
     &  (1.345453E-04*((XWK - 40)**2)*(T1)) +
     &  (1.992657E-06*((XWK - 40)**2)*(T1**2)) +
     &  (1.108418E-03*((XWK - 40)**3)) +
     &  (5.852133E-07*((XWK - 40)**3)*(T1)) -
     &  (3.924205E-08*((XWK - 40)**3)*(T1**2))

      zlPwk=(7.05)-(1603.54)/(273.15 + DWK)-
     &  (104095.5)/((273.15 + DWK)**2)
      Pscwk = 10**(zlPwk)
      GWK = Pscwk-Plow

       If(GWK.GE.0.AND.GWK.LE.0.005)Then
            XWK=XWK
      Else
            XWK=XWK+0.001
            GoTo 20
      End If
```

C Calculate Enthalpies (J/kg) at Point 8, exit from condenser assumed
C completely wet and Point 10, exit from evaporator assumed completely dry.
C Calculations performed using equations from Florides G.A. et al.,
C "Design and construction of a LiBr-water absorption machine" 2003,
C Energy Conversion and Management, 44, 2483-2508

C Enthalpy of Point 8 equivalent to hf at Tsat condenser (T8)

```
      h8=(-0.00125397*(T8)**2 + 1.88060937*(T8)
     &  + 2500.559
     &  + 0.00132635*(T8)**2 + 2.29983657*(T8) -
     &  2500.43063)*1000
```

C Enthalpy of Point 10 equivalent to hg at Tsat evaporator (T10)

```
      h10=(-0.00125397*(T10)**2 + 1.88060937*(T10)
```

```
     &      + 2500.559)*1000


C Refrigerating power (Watts) as a function of chilled water
C inlet temp (x)(Deg C), hot water inlet temp (y)(Deg C)
C and cooling water inlet temp (z)(Deg C)
C CHPow = f(x,y,z) = d0 + d1*x + d2*y + d3*z
C The empirical solution was found using a multiple regression
C technique for the experimental values
          IF(IONOFF.EQ.0) THEN
                CHPow = 0
          Else
                CHPow =  BDATA(IPCOMP,13) +
     &          (BDATA(IPCOMP,14))*(CONVAR(ICON1,1)) +
     &          (BDATA(IPCOMP,15))*(CONVAR(ICON3,1)) +
     &          (BDATA(IPCOMP,16))*(CONVAR(ICON2,1))
          End IF


C Calculate mass flow rate of refrigerant, zmref (kg/s)
C zmref = CHPower/(h10-h9)
C But, given there is no change in enthalpy in an expansion valve: h9=h8
C zmref = CHPower/(h10-h8)
          zmref= CHPow/(h10-h8)


C Calcualate the Circulation Ratio f
          f=XST/(XST-XWK)


C Calculate weak solution mass flow rate zmwk=m1=m2=m3 (kg/s)
          zmwk=zmref*f


C Calculate strong solution mass flow rate zmst=m4=m5=m6 (kg/s)
          zmst=zmwk-zmref


C Calculate enthalpies (J/kg) of point 1, 4 and 5
```

```
C Calculations performed using equations from Kaita. Y.,
C "Thermodynamic properties of lithium bromide and water solutions
C at high temperatures" 2001. International Journal of Refrigeration
C 24, 374-390
C Point 1 - Weak solution exit from absorber
      h1=((3.462023-0.02679895*XWK)*T1 +
     &    (0.5*T1**2)*(0.0013499-0.00000655*XWK) +
     &    (162.81-6.0418*XWK-0.0045348*XWK**2+0.0012053*XWK**3))
     &    *1000

C Point 4 - Strong solution exit from generator
      h4=((3.462023-0.02679895*XST)*T4 +
     &    (0.5*T4**2)*(0.0013499-0.00000655*XST) +
     &    (162.81-6.0418*XST-0.0045348*XST**2+0.0012053*XST**3))
     &    *1000

C Point 5 - Strong solution exit from recovery heat exchanger
      h5=((3.462023-0.02679895*XST)*T5 +
     &    (0.5*T5**2)*(0.0013499-0.00000655*XST) +
     &    (162.81-6.0418*XST-0.0045348*XST**2+0.0012053*XST**3))
     &    *1000


C Calculate work done by circulation pump (Wpump) (J/kg)
C through (P2-P1)/Denisty
      Wpump = (Phigh - Plow)*1000/
     &    (1145.36 + 470.84*(XWK/100) + 1374.79*(XWK/100)**2
     &    - (0.333393 + 0.571749*(XWK/100))*(273 + T1))


C Calculate h2 from: h2 = Wpump + h1
      h2 = Wpump + h1


C Electrical energy (Watts) required for pump = Wpump*zmwk/ElecEffPump
      IF(IONOFF.EQ.0) THEN
            EEPump=0
      Else
            EEPump=Wpump*zmwk/BDATA(IPCOMP,18)
```

```
      End If


C Calculate h3 (J/kg): h3=h2+(1-1/f)*(h4-h5)
      h3=h2+(1-(1/f))*(h4-h5)


C From h3 calculate T3 using Cpsol=(0.0976*X**2-37.512*X+3825.4)
C Calculations performed using equation from Florides G.A. et al,
C "Design and construction of a LiBr-water absorption machine" 2003,
C Energy Conversion and Management, 44, 2483-2508
      T3=h3/(0.0976*XWK**2-37.512*XWK+3825.4)


C Calculate temperature at point 7 (DegC)
      T7=0.5*(T4 + T3)


C Calculate Enthalpy at point 7 (J/kg) which is the value of the
C superheated steam evaluated at the saturation conditions of Point 8
C Calculations performed using equation from Florides G.A. et al,
C "Design and construction of a LiBr-water absorption machine" 2003,
C Energy Conversion and Management, 44, 2483-2508
      h7=(((0.00001*Phigh**2 -
     &    0.1193*Phigh + 2689
     &    - 32.508*log(Phigh)
     &    - 2513.2)/100)*(T7-T8)
     &    + 32.508*log(Phigh) + 2513.2)*1000


C This subsection enables the control of the absorption chiller
C through Node Qi. If Chiller is off then Qi is assumed to be zero,
C that is, there is no internal process going on in the evaporator and
C the chiller is not absorbing any heat. It is reasonably assumed that
C if the chiller is off than there is no internal process going on in
C either of the other components and therefore the external streams
C are not affected by the absorption chiller.

C The other streams are then controlled through node Qi
```

```
      IF(IONOFF.EQ.0) THEN
            Qi=0
      Else
C For Node 1 internal process Qi (NODE1) = zmref*(h9-h10)
C But, given there is no change in enthalpy in an expansion valve: h9=h8:
            Qi=zmref*(h8-h10)
      End If

      If (Qi.EQ.0)Then
            Qj=0
            Qg=0
      Else
C For Node 2 internal process Qj (NODE2)
C Qj=zmref*(h7-h8) + (zmref*h10 + zmst*h6 - zmwk*h1)
C But, given there is no change in enthalpy in an expansion valve: h6=h5:
            Qj=zmref*(h7-h8) + (zmref*h10 + zmst*h5 - zmwk*h1)
C For Node 3 internal process Qg (NODE3)
C Qg=zmwk*h3 - zmst*h4 - zmref*h7
            Qg=zmwk*h3 - zmst*h4 - zmref*h7
      End If


C Calculate COP
C COP = mchi*[(Cp @ T17)*T17 - (Cp @ T18)*T18] /
C mhot*[(Cp @ T11)*T11 - (Cp @ T12)*T12]
      IF(IONOFF.EQ.0) THEN
            COP=0
      Else
            COP= (PCONDR(ICON1)*CONVAR(ICON1,2)*
     &      (SHTFLD(3,CONVAR(ICON1,1))*CONVAR(ICON1,1)
     &      - SHTFLD(3,CSVF(INOD1,1))*CSVF(INOD1,1)))/
     &      (PCONDR(ICON3)*CONVAR(ICON3,2)*
     &      (SHTFLD(3,CONVAR(ICON3,1))*CONVAR(ICON3,1)
     &      - SHTFLD(3,CSVF(INOD3,1))*CSVF(INOD3,1)))
      End If


C Calculate Actual Refrigerant Power
      IF(IONOFF.EQ.0) THEN
```

```
            ActPow=0
        Else
            ActPow = PCONDR(ICON1)*CONVAR(ICON1,2)*
     &      (SHTFLD(3,CONVAR(ICON1,1))*CONVAR(ICON1,1)
     &      - SHTFLD(3,CSVF(INOD1,1))*CSVF(INOD1,1))
        End If


C Absorption chiller actual ON/OFF state
        PCDATF(IPCOMP,1)=IONOFF


C Establish heat capacity (J/K) of the thermal masses of Node 1, CW1,
C Node 2, CW2, and Node 3, CW3.
        CW1 = ADATA(IPCOMP,1)*ADATA(IPCOMP,2)
        CW2 = ADATA(IPCOMP,3)*ADATA(IPCOMP,4)
        CW3 = ADATA(IPCOMP,5)*ADATA(IPCOMP,6)


C Establish fluid heat capacity rates for the three stream flows (W/K)
C For chilled water stream
        C1=PCONDR(ICON1)*CONVAR(ICON1,2)*SHTFLD(3,CONVAR(ICON1,1))

C For cooling water stream
        C2=PCONDR(ICON2)*CONVAR(ICON2,2)*SHTFLD(3,CONVAR(ICON2,1))

C For hot water stream
        C3=PCONDR(ICON3)*CONVAR(ICON3,2)*SHTFLD(3,CONVAR(ICON3,1))


C Calculate Time Constant
        TC(IPCOMP)=AMAX1
     &  (CW1/AMAX1(Small,C1),CW2/AMAX1(Small,C2),
     &  CW3/AMAX1(Small,(C3+UA)))


C Set up implicit/explicit weighting factor ALPHA (1 = fully implicit)
        IF(IMPEXP.EQ.1) THEN
            ALPHA=1
```

```
ELSE IF(IMPEXP.EQ.2) THEN
        ALPHA=RATIMP
ELSE IF(IMPEXP.EQ.3) THEN
        IF(TIMSEC.GT.0.63*TC(IPCOMP)) THEN
                ALPHA=1
        ELSE
                ALPHA=RATIMP
        END IF
ELSE IF(IMPEXP.EQ.4) THEN
        CW1=0
        CW2=0
        CW3=0
        ALPHA=1
END IF
```

C Establish matrix equation self-coupling coefficients

C Node 1 chilled water

```
COUT(1)=ALPHA*(-C1)-CW1/TIMSEC
```

C Node 2 cooling water

```
COUT(2)=ALPHA*(-C2)-CW2/TIMSEC
```

C Node 3 Hot water

```
COUT(3)=ALPHA*(-C3-UA)-CW3/TIMSEC
```

C Establish matrix equation cross-coupling coefficients

C Node 1 chilled water

```
COUT(4)=ALPHA*(C1)
```

C Node 2 cooling water

```
COUT(5)=ALPHA*(C2)
```

C Node 3 hot water

```
COUT(6)=ALPHA*(C3)
```

C Establish matrix equation present and known terms coupling coefficients

```
C Node 1, thermal mass effected by chilled water
      COUT(7)=((1-ALPHA)*PCRP(ICON1)-CW1/TIMSEC)*CSVP(INOD1,1)
     &  -(1-Alpha)*(PCRP(ICON1))*(PCTP(ICON1))
     &  -ALPHA*Qi-(1-ALPHA)*PCQP(INOD1)

C Node 2 thermal mass effected by cooling water
      COUT(8)=((1-ALPHA)*PCRP(ICON2)-CW2/TIMSEC)*CSVP(INOD2,1)
     &  -(1-Alpha)*(PCRP(ICON2))*(PCTP(ICON2))
     &  -ALPHA*Qj-(1-ALPHA)*PCQP(INOD2)

C Node 3 thermal mass effected by hot water
      COUT(9)=((1-ALPHA)*(PCRP(ICON3) + PUAP(INOD3))-CW3/TIMSEC)
     &  *CSVP(INOD3,1)-(1-Alpha)*(PCRP(ICON3))*(PCTP(ICON3))
     &  -ALPHA*Qg-(1-ALPHA)*PCQP(INOD3)
     &  -ALPHA*UA*PCNTMF(IPCOMP)
     &  -(1-ALPHA)*PUAP(INOD3)*PCNTMP(IPCOMP)


C Store 'environment' future values
      PCTF(ICON1)=CONVAR(ICON1,1)
      PCTF(ICON2)=CONVAR(ICON2,1)
      PCTF(ICON3)=CONVAR(ICON3,1)
      PCRF(ICON1)=C1
      PCRF(ICON2)=C2
      PCRF(ICON3)=C3
      PCQF(INOD1)=Qi
      PCQF(INOD2)=Qj
      PCQF(INOD3)=Qg
      PUAF(INOD3)=UA


C Establish additional output variables
      napdat(ipcomp)=9
      PCAOUT(IPCOMP,1)=IONOFF
      PCAOUT(IPCOMP,2)=zmref
      PCAOUT(IPCOMP,3)=zmst
      PCAOUT(IPCOMP,4)=zmwk
      PCAOUT(IPCOMP,5)=Phigh
      PCAOUT(IPCOMP,6)=Plow
```

```
      PCAOUT(IPCOMP,7)=COP
      PCAOUT(IPCOMP,8)=EEPump
      PCAOUT(IPCOMP,9)=ActPow


C 1st Phase mass (i.e. water) balance coefficients
   Else IF (ISTATS.EQ.2) Then
      COUT(1)=1
      COUT(2)=1
      COUT(3)=1
      COUT(4)=-PCONDR(ICON1)
      COUT(5)=-PCONDR(ICON2)
      COUT(6)=-PCONDR(ICON3)
      COUT(7)=0
      COUT(8)=0
      COUT(9)=0


C 2nd Phase (i.e. air) balance coefficients
   Else IF (ISTATS.EQ.3) Then
      COUT(1)=1
      COUT(2)=1
      COUT(3)=1
      COUT(4)=0
      COUT(5)=0
      COUT(6)=0
      COUT(7)=0
      COUT(8)=0
      COUT(9)=0
   End If


C Trace output
     IF(ITC.GT.0.AND.NSINC.GE.ITC.AND.NSINC.LE.ITCF.AND.
    &  ITRACE(37).NE.0) THEN
      WRITE(ITU,*) ' Component      ',IPCOMP,':'
      WRITE(ITU,*) ' 3 node (ISV=20) Absorption Chiller & on/off'
      WRITE(ITU,*) ' control'
      WRITE(ITU,*) ' Matrix node(s) ',INOD1, INOD2, INOD3
```

```
      WRITE(ITU,*) ' Connection(s)  ',ICON1, ICON2, ICON3
      IF(ISTATS.EQ.1) THEN
        WRITE(ITU,*) ' CW1     = ',CW1,' (J/K)'
        WRITE(ITU,*) ' CW2     = ',CW2,' (J/K)'
        WRITE(ITU,*) ' CW3     = ',CW3,' (J/K)'
        WRITE(ITU,*) ' C1      = ',C1,' (W/K)'
        WRITE(ITU,*) ' C2      = ',C2,' (W/K)'
        WRITE(ITU,*) ' C3      = ',C3,' (W/K)'
        WRITE(ITU,*) ' TC      = ',TC(IPCOMP),' (s)'
        WRITE(ITU,*) ' ALPHA   = ',ALPHA,' (-)'
        WRITE(ITU,*) ' PCNTMF  = ',PCNTMF(IPCOMP),' (C)'
        WRITE(ITU,*) ' CDATA   = ',CDATA(IPCOMP,1)
        WRITE(ITU,*) ' IONOFF  = ',IONOFF,' (-)'
        WRITE(ITU,*) ' mref    = ',zmref,' (kg/s)'
        WRITE(ITU,*) ' mst     = ',zmst,' (kg/s)'
        WRITE(ITU,*) ' mwk     = ',zmwk,' (kg/s)'
        WRITE(ITU,*) ' Phigh   = ',Phigh,' (kPa)'
        WRITE(ITU,*) ' Plow    = ',Plow,' (kPa)'
        WRITE(ITU,*) ' COP = ',COP,' (-)'
        Write(ITU,*) ' Electrical Power Pump = ',EEPump,' Watts'
        Write(ITU,*) ' Actual Power = ',ActPow,' Watts'
      END IF
      WRITE(ITU,*) ' Matrix coefficients for ISTATS = ',ISTATS
      NITMS=9
      WRITE(ITU,*) (COUT(I),I=1,NITMS)
      IF(ITU.EQ.IUOUT) THEN
       IX1=(IPCOMP/4)*4
       IF(IX1.EQ.IPCOMP.OR.IPCOMP.EQ.NPCOMP) call epagew
      END IF
    END IF

    IF(ITC.GT.0.AND.NSINC.GE.ITC.AND.NSINC.LE.ITCF.AND.
   &   ITRACE(37).NE.0) WRITE(ITU,*) ' Leaving subroutine CMP73C'

    RETURN
    END
```

APPENDIX F

Micro-trigeneration system - Additional financial sensitivity charts.

(Cont. Chapter 5)

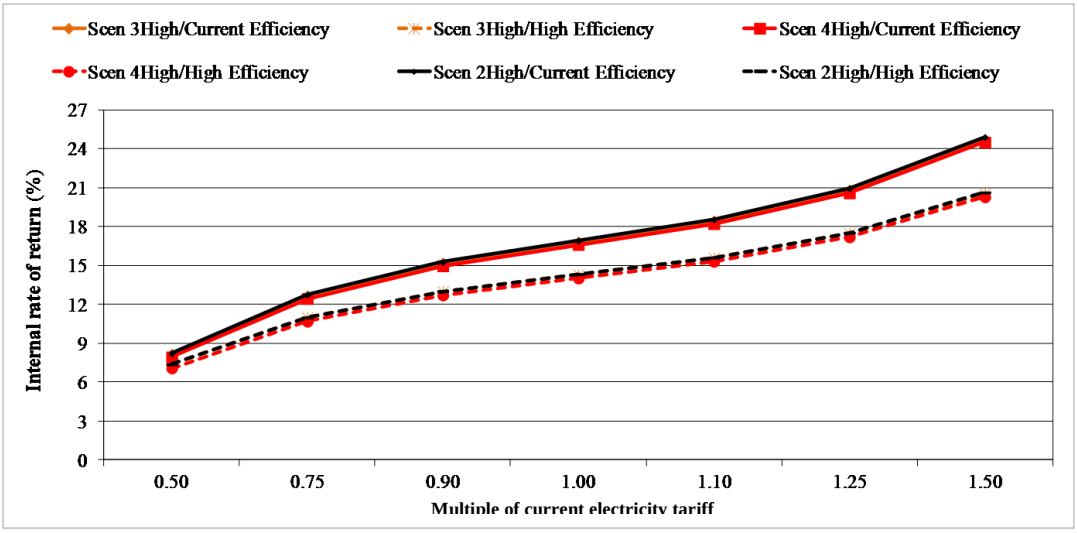

Fig. F.1 - *IRR* for scenarios with different plant configurations for varying electricity tariffs

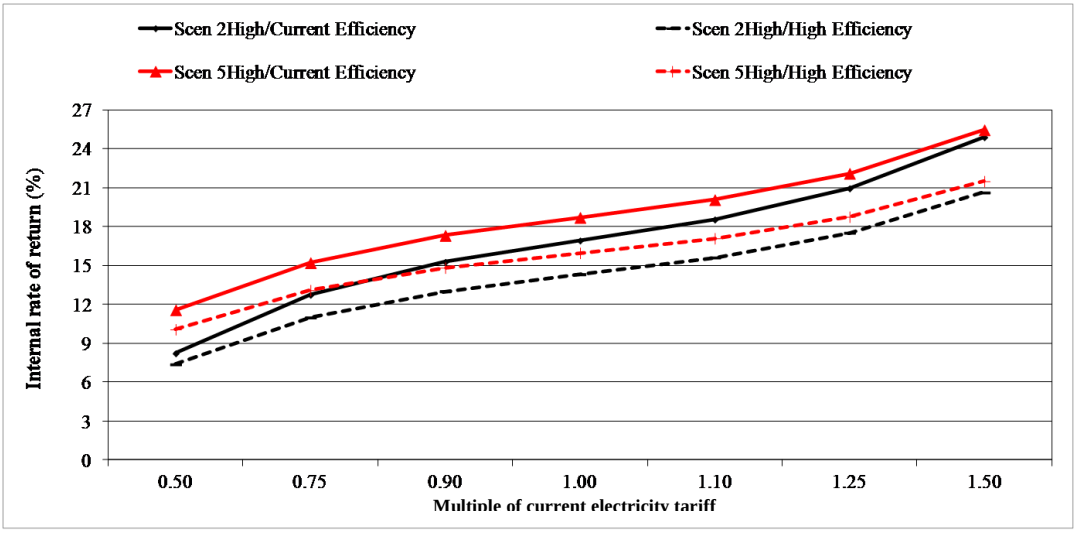

Fig. F.2 - *IRR* for Scenarios 2_{High} and 5_{High} for varying electricity tariffs

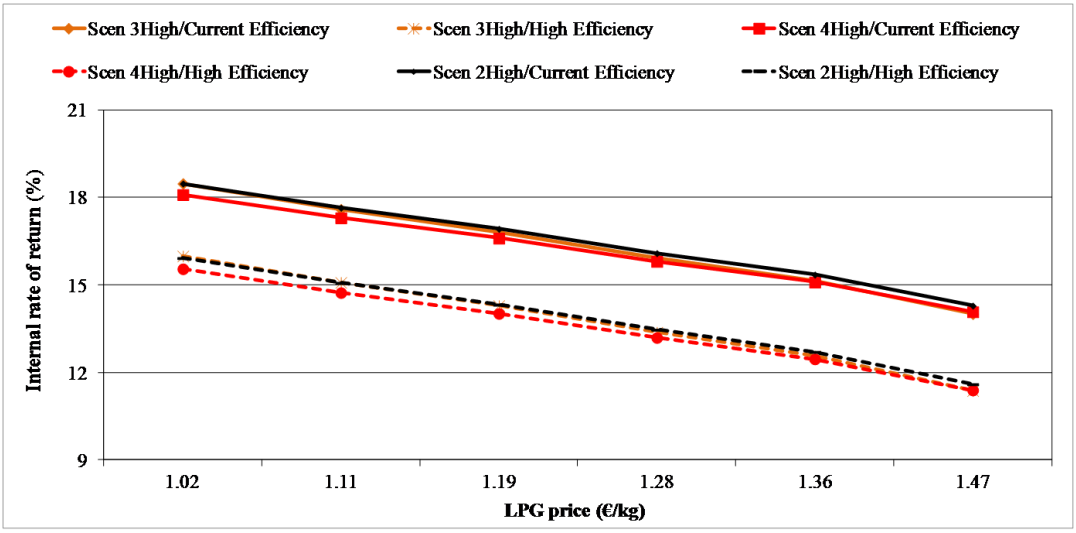

Fig. F.3 - *IRR* for scenarios with different plant configurations for varying gas prices

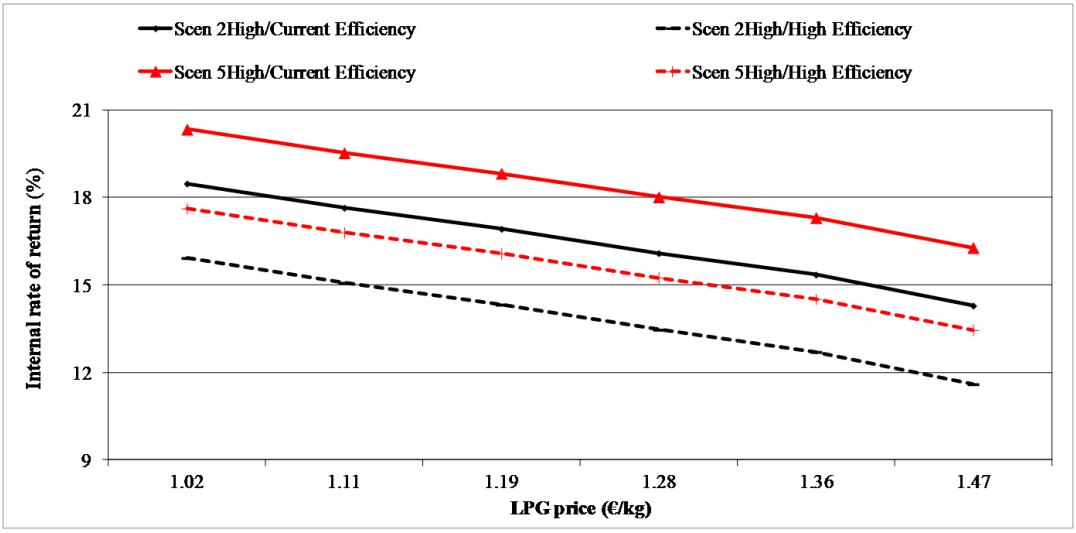

Fig. F.4 - *IRR* for Scenarios 2_{High} and 5_{High} for varying gas prices

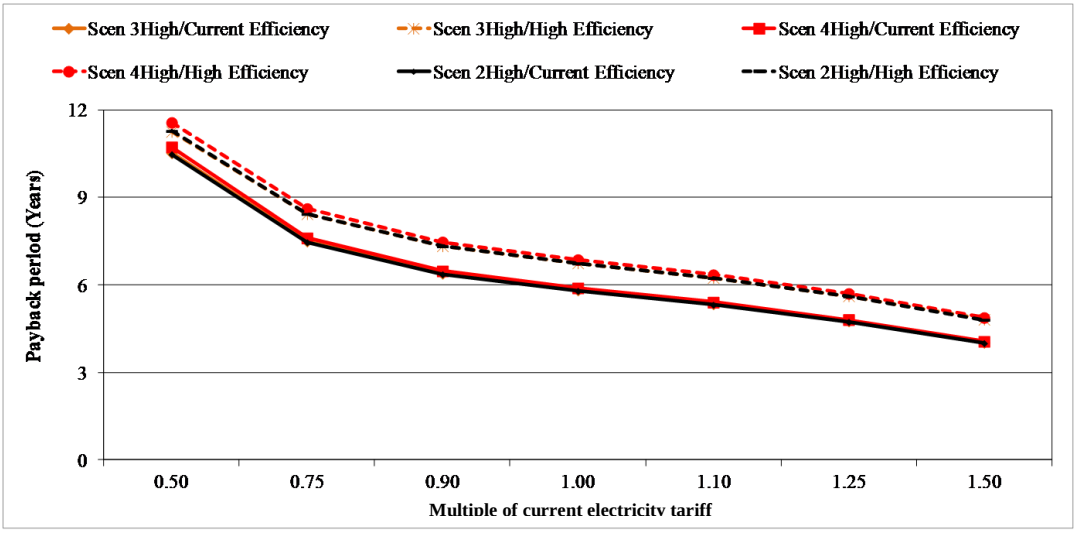

Fig. F.5 - *PP* for scenarios with different plant configurations for varying electricity tariffs

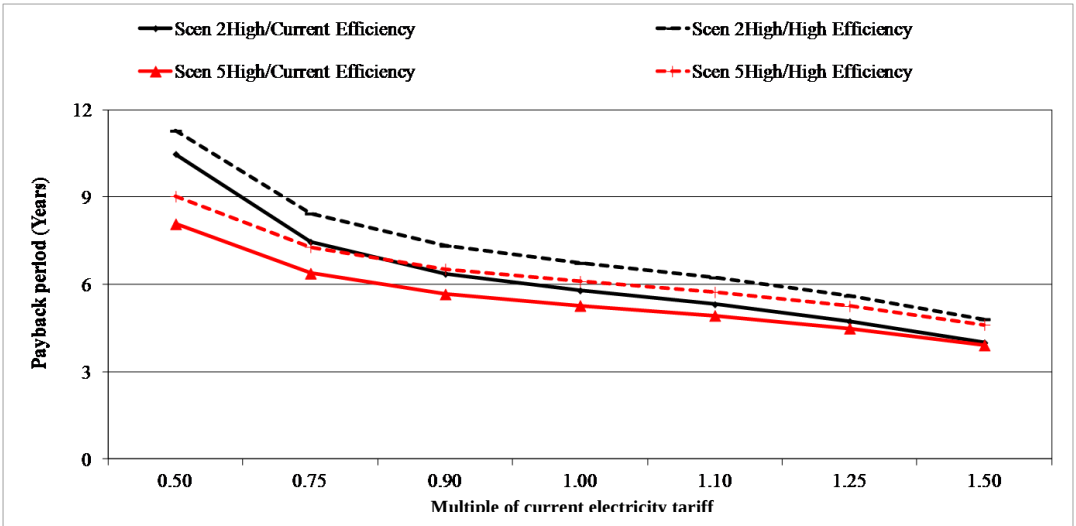

Fig. F.6 - *PP* for Scenarios 2_{High} and 5_{High} for varying electricity tariffs

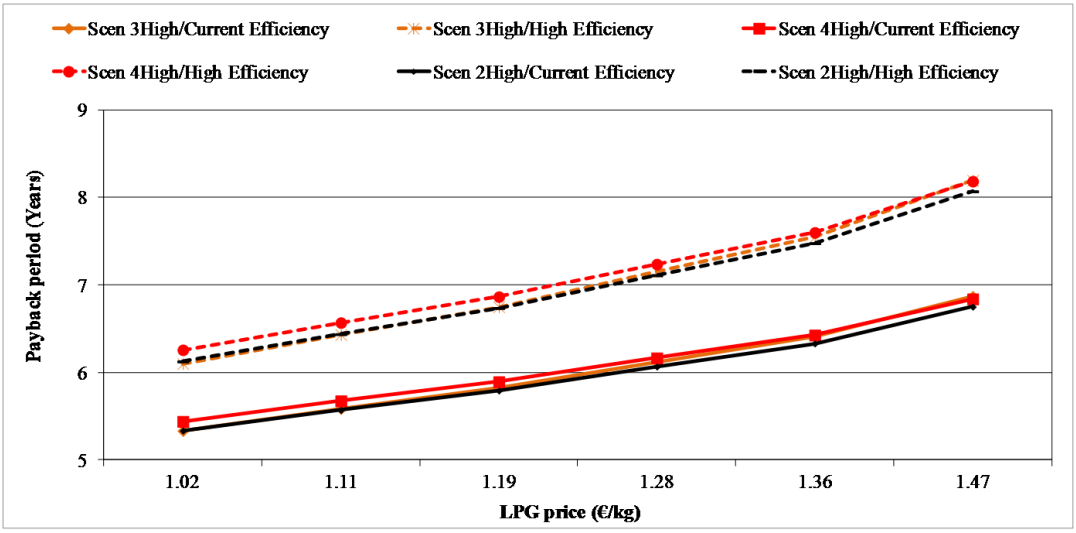

Fig. F.7 - *PP* for scenarios with different plant configurations for varying gas prices

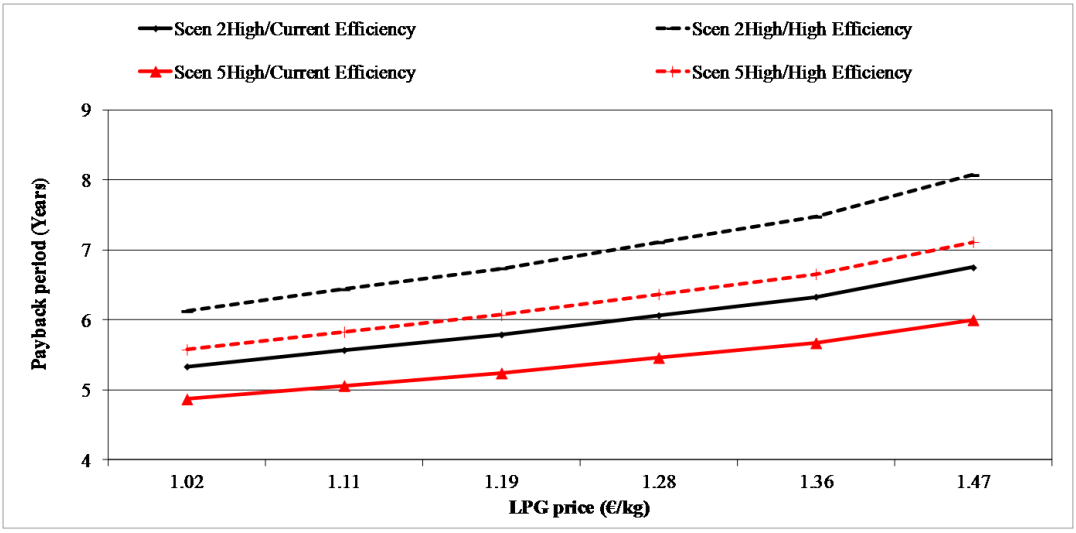

Fig. F.8 - *PP* for Scenarios 2_{High} and 5_{High} for varying gas prices